Bioengineering of Tendons using Controlled Spatiotemporal Release of Multiple Growth Factors and Concurrent Monitoring of Healing via Elasticity Mapping Ultrasonography

By

Adam Henry Biedrzycki

A dissertation submitted in partial fulfilment

Of the requirements for the degree of

Doctor of Philosophy

(Comparative Biomedical Sciences)

at the

UNIVERSITY OF WISCONSIN-MADISON

2015

Date of final oral examination: 12/16/2014

The dissertation is approved by the following members of the Final Oral Committee:

Mark D Markel, Professor, Medical Sciences
Peter Muir, Professor, Surgical Sciences
Troy Hornberger, Associate Professor, Comparative Biosciences
William L Murphy, Professor, Biomedical Engineering
Ray Vanderby Jr., Professor, Orthopedics and Rehabilitation

Abstract

Clinically effective treatments for tendon lacerations are equivocal and current protocols are associated with high levels of morbidity and re-injury. Injured tendons have limited self-healing capacity, due in part to poor vascularity and low metabolite supply. Furthermore, tendon-healing assessments are currently based on grey-scale echogenicity and appearance of organized tendon fibrils or scar tissue.

The aims of this research were to accelerate gain in mechanical strength and histological organization of tendon tissue after a partial tenotomy in a rabbit model, via the use of two growth factors (fibroblast growth factor (FGF) and vascular endothelial growth factor (VEGF)) released from suture material in a spatiotemporal fashion to coincide with the phases of tendon healing. In addition, we evaluated the effect of growth factor use on tendon vascularity via both histological assessment and microbubble contrast angiography (MCA). We also evaluated novel methods of monitoring tendon healing via the use of acoustoelastography (AE) and shear wave imaging (SWI).

The studies presented in this thesis demonstrate that FGF and VEGF were able to synergistically enhance the healing of tendon tissue using our suture material delivery platform. The use of our optimal suture group resulted in supra-physiological tensile strengths at a 4-week post surgical evaluation time point. This thesis provides evidence that in addition to superior mechanical properties, superior histological organization was

also attained. Superior healing was achieved with the addition of the angiogenic compounds and this angiogenic effect was identified successfully using MCA and histological evaluation techniques.

The use of AE and SWI was also correlated to structural and material properties of tendon, respectively, and these imaging modalities provided enhanced information in regard to the healing of the tendon tissue non-invasively.

In our 9-week post surgical long-term evaluation, we identified that the supra-physiological tensile strength values attained at the 4-week short term with our optimal growth factor group returned to baseline normal physiological values. The 9-week optimal growth factor group also demonstrated superior histological organization and a reduction in tendon cross sectional area. Thus, this thesis suggests that tendon healing mechanisms may mirror the remodeling process that occurs in bone. Further work is warranted, to provide supplementary evidence to support the idea of coupled remodeling in tendon tissue.

Acknowledgments

I am indebted to many individuals at the University of Wisconsin-Madison for their help and support during my time both as a resident in Large Animal Surgery and throughout the course of my PhD. In particular, I would like to express my gratitude to my advisor, Professor Mark D. Markel for being my mentor and friend throughout this time period; his dedication, support and assistance throughout my training and the various grant submissions to funding agencies have been paramount in the success I have achieved.

I would also like to express my gratitude to all the other members of my committee. Firstly, to Dr. Peter Muir for his guidance, insight and intellectual contributions to this work. To Dr. William Murphy and his entire laboratory for allowing me carry out all of my bench top studies in his facility and for permitting us to use their suture material delivery platform. To Dr. Troy Hornberger, for all his assistance and insight into the project. And finally, to Dr. Ray Vanderby Jr., for being so helpful and thoughtful in regard to all aspects of mechanical testing and tendon healing.

While working at the Wisconsin Institutes for Medical Research, I am indebted to Jae Sung Lee, who educated and guided me in the evaluation and growth of crystals on suture materials, in addition to Jim Molenda. Integral to this task was also Lance Rodenkirch at the Keck Imaging Center.

I want to thank all of the people in the Comparative Orthopaedic Research Laboratory. A special thank you to my good friend and colleague, Brett Nemke, who was such an integral part in budget mastering and keeping me on track and within the guidelines. The amount of support Brett contributed is greatly appreciated, in addition to all of the hunting trips on the side. To Yan Lu who assisted greatly with various aspects and to Vicki Kalscheur for her unwavering support in all matters histological. In addition, special thanks goes to all of the students who helped me with the surgeries and monitoring of all the rabbits, without whom this project would not have been successful; Carissa Sawyer, Alyssa White, Kelley Encinas and Sarah Rossmiller.

On the imaging side of the project, I wish to express my gratitude to Sabrina Brounts for her mentorship during my residency and her expertise on tendons and acoustoelastography for my PhD. In addition, Ryan DeWall, Jack Martin and Sarah Kohn for their assistance with the collection of imaging data. To Dr. Kenneth Waller for his help and analysis of the micro bubble contrast agent.

I wish to express my sincere indebtedness for the support, understanding, patience and love showered upon my by my fiancé, Jenna. It really would not have been possible for me to complete this work within the time frame without her help. And to my parents, Tadeusz and Barbara, and to my brother Olaf, for always encouraging me and supporting me throughout my education.

Finally, I sincerely appreciate the funding for this project provided by the AO Foundation, Zoetis, the American College of Veterinary Surgeons Foundation, the University of Wisconsin-Madison Companion Animal Fund, and the Comparative Orthopaedic Research Laboratory.

List of Figures

List of Tables

Table of Contents

Chapter I

Introduction

1.1 Significance

Tendon and ligamentous injuries are becoming increasingly more prevalent, with an estimated 50% of the 33 million musculoskeletal incidents occurring in the United States annually affecting the soft tissues, including tendons and ligaments.[1,2,3] Furthermore, ruptures of the Achilles tendon, the most frequent tendinous injury sustained, are on the increase due to improved athletic lifestyles. [4,5,6] In veterinary medicine, tendon injuries have been extensively studied in the dog[7] and in the horse.[8,10,11] Evidence in canine[7], equine[3-5] and human[11] models suggests that partial tears or ruptures may develop secondary to chronic overuse injuries, with the implication that acute injuries may be manifestations of accumulation of chronic damage. In equine tendon disorders, 43% of National Hunt horses demonstrated evidence of tendon disease[12] and 14.8% of all horses in flat racing in Japan in 1999 sustained an injury to the digital flexor tendons.[13]

Tendons are compositionally complex structures that function as important connections between the dynamic function of muscles and the static component of bones, a role that allows functional movement to occur.[1,2] They function as a stiffness buffer between the relatively high stiffness components of bone and the low stiffness of muscle. In addition, they function as energy stores and possess viscoelastic properties, which may help protect other musculoskeletal components from damage. Consequently, any injuries that occur to tendons result in disruption of the structure and function of this tissue, initiating substantial morbidity and discomfort for the patient.

It has been suggested that by 45 years of age, 1 in 10 people and 1 in 2 runners will suffer from some form of Achilles tendinopathy,[3] making this a high profile disease. Consequently, when utilizing animal models to simulate human injuries, studies must replicate similarities in pathogenesis of disease and take into account the anatomy of the structures involved, stages of healing and healing methods.

Injuries to the Achilles tendon can range from acute, often traumatic events, to chronic conditions resulting from overuse injuries, which can be preceded by degeneration.[4] Current treatment options post injury include both surgical and non-surgical therapies, with an accompanying variety of rehabilitation protocols.[5] However, at the culmination of the healing process, tendon rarely achieves functional equality to pre-injury conditions in regard to either biomechanical, histological or phenotypic conditions.[6] For optimum therapy therefore, a thorough understanding of the phases of healing is important when considering any interventional strategies.

The treatment of tendon injury may thus involve an attempt at direct repair[14] or a more conservative approach of non-surgical therapy, with or without the use of physiotherapy protocols.[15] Historically, restoration of tendon function following partial laceration or transection has focused on mechanical aspects, such as improvement of suture repair techniques or the enhancement of postoperative rehabilitation protocols. While these have led to marginal improvements in long-term outcome, functional restoration has not been reliably achieved and the long-term results have been highly unpredictable.[16] Postoperative morbidities include adhesion formation, re-rupture and

inadequate functional recovery.[17] The successful treatment of tendon lacerations therefore remains one of the most challenging problems in orthopaedic surgery. Although biologics, minimally invasive or percutaneous approaches and more aggressive rehabilitation protocols demonstrate some promise in enhancing the repair process, none have been widely accepted or thoroughly evaluated. The standard of care remains primary suture repair.[18] However, it is recognized that with flexor tendon injuries, a post-operative rupture rate of 3-17% can occur[19]. A similar post-operative rupture rate of 5.0% is reported for the Achilles tendon repair; the risk of rupture is double this figure if the patients are treated conservatively.[20] Furthermore, a large study identified that the majority of patients have not fully recovered 2 years after injury, regardless of method of treatment chosen.[21]

Injured tendons have limited self-healing capacity[22], due in part to relatively low vascularity, low metabolite supply and the functional characteristics of intact tendon are not typically recovered, even after several months of healing. Many attempts have been made to optimize the healing conditions of the flexor tendons on a bio-molecular level, mainly through modulation of different growth factors. The poor vascularity of the flexor tendons and the risk of tendon rupture after repair make the concept of augmenting the regeneration and resulting biomechanical strength of the tendon an inviting approach to facilitate functional repair.

The clinical implication is therefore that, while stability is critical for a successful repair, mobility of the repaired tendon is also important. These two treatment

protocols are antagonistic, and one is often sacrificed at the expense of the other. Improvement in the speed at which tendons regain strength therefore would permit early return to function and decrease long-term patient morbidity. Thus, a method which would permit a successful surgical tenorrhaphy with the resultant delivery of a concert of synergistically acting biologics resulting in the rapid acquisition of tensile strength and the restoration of normal tendon architecture would provide the cohesive link between repair and mobility of the injury site and is the main aim of investigation for this study.

One further challenge presents itself in the assessment of tendon strength and the introduction of rehabilitation methods. For large animal species such as humans and horses, there is a significant rate of re-rupture and further injury during the healing process following tendon repair.[10,23] Careful monitoring is required to minimize this risk, as tendon healing assessments are currently based on grey-scale echogenicity and appearance of organized tendon fibrils or scar tissue. These highly subjective assessments offer little information on which judgments of tendon strength can be determined and can lead to significant increases in patient morbidity if the assessments are incorrect.

Although magnetic resonance imaging (MRI) provides excellent anatomical tendinous information, it lacks any association to biomechanical data. Two potential investigative tools that could provide such estimates of tendon stiffness and strain include acoustoelastography (AE) and shear wave-imaging (SWI) technologies, which have been evaluated in both laboratory and clinical settings under constrained

conditions.[13-17] AE has been utilized in clinical studies evaluating normal and pathological patients, but data analyses were limited to small cohorts.[24] Recent studies have demonstrated validity for the SWI technology in rabbit tendon specimens evaluated post sacrifice[25], but also clinical applications as an imaging modality in horses.[26] However, the main foci of these studies were repeatability and reliability evaluations at single time points.[27] Therefore, these pilot trials were significantly limited in their scope as they lack correlation with any biomechanical data. A recent AE and SWI review article emphasized that available literature is currently sparse and more research is required, including longitudinal studies that monitor the progress of healing, as none currently exist.[28]

Due to the established importance of vascularity in tendon healing, an assessment of intra-tendinous angiogenesis is important. [29] Contrast enhanced Doppler ultrasonography is unable to image microcirculation due to its resolution limitations.[30] The use of micro bubble contrast agents (MCA's) as a perfusion marker has been extensively evaluated and MCA's have demonstrated significant differences in blood flow among human patients with normal tendons during exercise.[31] However, the significance of angiogenesis during healing and the link to biomechanical parameters, such as tendon stiffness, which could be evaluated with modalities such as AE and SWI, has never been determined. A critical appraisal of these modalities, as suggested in the current research proposal, would provide a significant foundation and reference on which to base future investigations. Such dynamic links would be of significant benefit to orthopaedic researchers, clinicians and patients.

References

1 **Pennisi, E.** Tending tender tendons. *Sci J* **295**, 1011-1011 (2002).

2 **Calve, S. et al**. Engineering of functional tendon. *Tissue Eng* **10**, 755-761 (2004).

3 **Butler, D. L., Juncosa, N. & Dressler, M. R.** Functional efficacy of tendon repair processes. *Annu. Rev. Biomed. Eng.* **6**, 303-329 (2004).

4 **Hess, G. W.** Achilles Tendon Rupture A Review of Etiology, Population, Anatomy, Risk Factors, and Injury Prevention. *Foot Ankle Spec* **3**, 29-32 (2010).

5 **Leppilahti, J., Puranen, J. & Orava, S.** Incidence of Achilles tendon rupture. *Acta Orthop* **67**, 277-279 (1996).

6 **Nyyssönen, T., Lüthje, P. & Kröger, H.** The increasing incidence and difference in sex distribution of Achilles tendon rupture in Finland in 1987–1999. *Scand J Surg* **97**, 272-275 (2008).

7 **Duffy Jr, F. J., Seiler, J. G., Gelberman, R. H. & Hergrueter, C. A.** Growth factors and canine flexor tendon healing: initial studies in uninjured and repair models. *J Hand Surg* **20**, 645-649 (1995).

8 **Docking, S., Daffy, J., van Schie, H. & Cook, J.** Tendon structure changes after maximal exercise in the Thoroughbred horse: Use of ultrasound tissue characterisation to detect in vivo tendon response. *Vet J* **194**, 338-342 (2012).

9 **Vergari, C. et al.** Axial speed of sound for the monitoring of injured equine tendons: A preliminary study. *J Biomech* **45**, 53-58 (2012).

10 **Patterson-Kane, J., Becker, D. & Rich, T.** The pathogenesis of tendon microdamage in athletes: the horse as a natural model for basic cellular research. *J Comp Pathol* **147**, 227-247 (2012).

11 **Krahe, M. A. & Berlet, G. C.** Achilles tendon ruptures, re rupture with revision surgery, tendinosis, and insertional disease. *Foot Ankle Clin* **14**, 247-275 (2009).

12 **Pickersgill, C., Marr, C. & Reid, S.** Repeatability of diagnostic ultrasonography in the assessment of the equine superficial digital flexor tendon. *Equine Vet J* **33**, 33-37 (2001).

13 **Kasashima, Y. et al.** Prevalence of superficial digital flexor tendonitis and suspensory desmitis in Japanese Thoroughbred flat racehorses in 1999. *Equine Vet J* **36**, 346-350 (2004).

14 **Strickland, J.** Management of acute flexor tendon injuries. *Orthop Clin North Am* **14**, 827-849 (1983).

15 **Seida, J. C. et al.** Systematic review: nonoperative and operative treatments for rotator cuff tears. *Ann Intern Med* **153**, 246-255 (2010).

16 **Strickland, J.** Flexor tendon surgery Part 2: Free tendon grafts and tenolysis. *J Hand Surg Br* **14**, 368-382 (1989).

17 **Taras, J., Gray, R. & Culp, R.** Complications of flexor tendon injuries. *Hand Clin* **10**, 93-109 (1994).

18 **Lynch, R. M.** Achilles tendon rupture: surgical versus non-surgical treatment. *Accid Emerg Nurs* **12**, 149-158 (2004).

19 **Elliot, D., Moiemen, N., Flemming, A., Harris, S. & Foster, A.** The rupture rate of acute flexor tendon repairs mobilized by the controlled active motion regimen. *J Hand Surg Br* **19**, 607-612 (1994).

20 **Khan, R. & Carey Smith, R. L.** Surgical interventions for treating acute Achilles tendon ruptures. *Cochrane Database Syst Rev* **9** (2010).

21 **Olsson, N. et al.** Major functional deficits persist 2 years after acute Achilles tendon rupture. *Knee Surg Sports Traumatol Arthrosc* **19**, 1385-1393 (2011).

22 **Yao, L., Bestwick, C., Bestwick, L., Maffulli, N. & Aspden, R.** Phenotypic drift in human tenocyte culture. *Tissue Eng* **12**, 1843-1849 (2006).

23 **Olsson, N. *et al.*** Stable Surgical Repair With Accelerated Rehabilitation Versus Nonsurgical Treatment for Acute Achilles Tendon Ruptures A Randomized Controlled Study. *Am J Sports Med* **12**, 2867-2876 (2013).

24 **De Zordo, T*. et al.*** Real-time sonoelastography: findings in patients with symptomatic achilles tendons and comparison to healthy volunteers. *Ultraschall in der Medizin-European Journal of Ultrasound* **31**, 394-400 (2010).

26 **Gehmert, S. et al**. Sonoelastography can be used to monitor the restoration of Achilles tendon elasticity after injury. *Ultraschall Med* **33**, 581 (2012).

27 **Lustgarten, M. et al.** Elastographic characteristics of the metacarpal tendons in horses without clinical evidence of tendon injury. *Vet Radiol Ultrasound* **55**, 92-101 (2014).

28 **Ooi, C., Malliaras, P., Schneider, M. & Connell, D.** “Soft, hard, or just right?” Applications and limitations of axial-strain sonoelastography and shear-wave elastography in the assessment of tendon injuries. *Skeletal Radiol* **43**, 1-12 (2014).

29 **Pufe, T., Petersen, W., Tillmann, B. & Mentlein, R.** The angiogenic peptide vascular endothelial growth factor is expressed in foetal and ruptured tendons. *Virchows Arch* **439**, 579-585 (2001).

30 **Ferrara, K. W*. et al.*** Evaluation of tumor angiogenesis with US: imaging, Doppler, and contrast agents. *Acad Radiol* **7**, 824-839 (2000).

31 **Pingel, J. et al.** The acute effects of exercise on the microvascular volume of Achilles tendons in healthy young subjects. *Clin Physiol Funct Imaging* **33**, 252-257 (2013).

1.2 Tendon Architecture

1.2.1 Tendon Embryology

Tendons and ligaments are structures of connective tissue whose embryological origins and formation are less well understood than other musculoskeletal counterparts such as bone or muscle. Although tendons and ligaments have a well-defined extracellular matrix, primarily composed of collagen, there are no specific embryological signaling components that define it. However, one defining characteristic of tendon and ligamentous tissue is their characteristic collagen and cellular orientation, with cells aligned parallel to the lines of force exerted along the structure.[1]

During embryogenesis, the early blastocyst layer termed the epiblast gives rise to the three germ layers of a triploblastic organism, the endoderm, ectoderm and mesoderm which forms in the third week during gastrulation.[2] The mesoderm itself can be further divided into several layers, including intermediate mesoderm, lateral plate mesoderm, axial mesoderm and paraxial mesoderm.[3,4] Paraxial mesoderm is organized into somatic compartments and by a sequence of morphological changes form sclerotome, myotome dermatome and syndetome regions which are responsible for the development of cartilage, muscles and bones and tendons.[3,4]

Until recently, the exact embryological origin of tendon and ligamentous tissue was unknown. The discovery of the syndetome provided the basis for further analysis

into tendon and ligament differentiation.[5] It is known that the scleraxis pathway, a member of the basic helix-loop-helix (bHLH) family, is involved in tendon differentiation signaling.[6] Scleraxis consists of two alpha helices, which are connected via a loop, and is involved in signaling in many musculoskeletal systems.[5] Activation of the scleraxis pathway is believed to occur via the activation of Ras/Raf/mitogen activated protein kinase/ERK kinase (MEK)/extracellular-signal-regulated kinase (ERK) cascade, which couples signals from cell surface receptors to transcription factors such as scleraxis.[7] It has been shown that ERK activity is required for proper activation of the scleraxis genes in the syndetome.[8]

Although tendons exist throughout the body, there appear to be differences in formation between the trunk and the appendicular limbs. Limb tendons originate from the lateral plate, while myogenic cells originate from the lateral part of the dermomyotome.[9] Limb tendons also tend to form in the dorsal and ventral areas of the limb, with areas of cartilage consolidation in the center, resembling the rudimentary structure of a normal limb. In addition, formation of tendon progenitor cells in the limb is independent of signaling from the myotome, whereby removal of this structure from the embryo leads to normal tendon formation and scleraxis expression. This situation is in direct contrast to trunk tendons, whereby loss of the myotome leads to loss of scleraxis expression.[10] From these studies, it is apparent that for trunk tendon formation, the myotome contains an as yet unidentified signal that is necessary for scleraxis expression in the syndetome of the trunk.

For both the trunk and limb tendons, the factors, which initiate scleraxis expression, are currently unknown.[1] FGF signaling via activation or blockade leads to an up regulation or inhibition of scleraxis in the sclerotome in chick embryos and therefore the FGF family would seem like a suitable candidate to activate scleraxis in the syndetome.[4] However, at the time of scleraxis initiation at approximately embryonic day 3 for the chick, the only known source of FGF is FGF-8, which is present in the axial ectodermal ridge (AER).[11] Given the distance between the AER and the syndetome, it is difficult to envisage how FGF-8 signaling could induce scleraxis transcription. The exact pathways are therefore unknown and require further study.

During further development, the tendon progenitor cells form tendon primordia, which are isolated groups of cells, develop into tendon tissue.[12] In the late limb period of tendon formation however, the presence of muscle is essential to complete the tendon formation.[1] In the absence of muscle, there is a progressive loss from proximal to distal of markers of tendon expression.[9] At this stage, it is suggested that FGF-4 signaling becomes important to ensure the maturation of the tendon structures.[13]

Although the presence of muscle at various time points seems critical to successful tendon formation, the same does not apply for cartilage. As tendons occur in close proximity to joints and the cartilaginous formation of bones, one would hypothesize that there is some coordination between cartilage and tendon formation. This has been shown not to be the case, as tendon formation occurs normally in the absence of cartilage differentiation in limbs of Sox5/Sox6 double mutant mice.[10] Despite

this finding and the fact that tendons eventually do connect to bones, the signals involved in tendinous insertion onto osseous structures are completely unknown.[1]

A similar embryonic pathway exists in the paradigm of ligaments, although the exact embryological origins have also not been established. In embryonic chicks at day 14, regions which develop into ligaments express scleraxis so this appears to be a common signaling pathway for a variety of musculoskeletal regions.[12] The tendon primordia that develop during early development are thought to contain the ligamentous precursors that are thought to be associated with joints.[14] In this case, due to the proximity of the ligamentous and joint structures, a further hypothesis is that the joint, or cartilaginous regions, could be involved as a signaling center to promote the differentiation of ligamentous tissue.[1] However, the signals involved in ligamentous formation are unknown so it is difficult to generate evidence to support such a hypothesis.

Wnt-14, which is involved in the formation of joints and synovial membrane, has been identified in the ligaments of fully developed and mature adult ligaments, and therefore there is the suggestion that it may play a role in the differentiation of ligamentous tissue.[15] A downstream gene of the Wnt-14 signaling pathway is growth differentiation factor-5 and 6 (GDF5/GDF6). Inactivation of these genes in mice results primarily in joint and cartilage defects, but there are also substantial defects in ligamentous structures.[16] In addition, GDF-5 deficient mice have altered tail and Achilles tendons supporting the role of the GDFs in tendon and ligamentous structures.[17,18]

Further evidence is provided by studies that show that ectopic supplementation of GDF5/6/7 results in ligamentous like structure formation.[19]

There are likely to be many further growth factor involved in tendon and ligament formation. For example, FGF-10, which is located in the joint interzone during chick limb development, favors the proliferation of mesenchymal cells in the region.[20] The roles of bone morphogenic proteins (BMPs) are also likely to play a role in ligament development. However, pathways linking Wnt signaling, BMPs and FGFs are as yet unidentified.

1.2.2 Tendon Cells

The vast majority of cells in mature, adult tendon tissue display thin layers of cytoplasm centered on a large, heterochromatic nucleus and have been termed “tenocytes” or “tendon fibroblasts”.[21] These may represent the quiescent or resting stage of tendons and may be involved in mechanosensing in conjunction with the ECM.[22] The more active cells, identified in immature or healing tendons, contain prominent nucleoli, rough endoplasmic reticula and Golgi apparatus, which produces collagen.[21] It has been well demonstrated that immature and developing tendon is hypercellular and as the aging process increases, there is a gradual reduction in cellularity,[23,24] thus supporting the notion of a relatively quiescent metabolic state of mature tendon. Thus, during the healing process, cells of a more active phenotype may be typically identified.

In support of the mechanosensing hypothesis of tenocytes, McNeilly demonstrated through cytoplasmic staining that tenocytes naturally form a three dimensional network of cells in contact between collagenous bundles by their long cytoplasmic processes.[25] Immunolabelling for connexin-43 in this case demonstrated the presence of gap junctions on the various cytoplasmic processes that support the hypothesis that there may be an involvement of these cells in load sensing and coordination of the response to tendon loading.[25]

In support of differing roles of cells throughout the tendon, several studies have identified a morphological and functional difference between surface cells of the tendon and those inside the core body. Khan's immunohistological studies described an outer layer of specialized fibroblasts and macrophage, termed epitenon, while those in the tendon core were a different population.[26] Each cell has also a specialized and individual response to injury. More recently, a stem cell population has also been identified in tendon, though their exact role has yet to be fully characterized. Bi et al. performed *in vitro* studies, which isolated a cell population from both human and murine sources that demonstrated increased adherence and the ability to produce daughter cells of several lineages and express tendon specific and stem cell specific markers.[27] These groups of cells were termed tendon stem cell/progenitor cells (TSPCs) and were shown to constitute 6% of the cultured tendon cell population *in vitro*. Using BrdU labeled cells *in vivo*, the authors were also able to demonstrate a similar percentage of

slow cycling cells, which they considered analogous to the TSPCs identified in cell culture experiments.

1.2.3 Extracellular Matrix

The extracellular matrix (ECM) of tendon consists chiefly of collagens and proteoglycans.[28] Collagen accounts for 65-80% of the dry mass of tendon, with elastin responsible for 1-2%. [29] Collagen is responsible for the tensile strength of tendon, while the proteoglycans provide the viscoelastic properties of the tendon.[30] Tendon is composed of a network of ECM containing tenoblasts and tenocytes, which account for 95% of the cellular elements of tendon and lie between the collagen fibers along the long axis of the tendon.[31] The major collagen in tendon is type I, accounting for 65-80% of the dry mass with elastin accounting for 2%.[32] Tenocytes synthesize collagen and all the components of the ECM and are active in energy generation, although the oxygen consumption by tendons and ligaments is 7.5 times lower than skeletal muscle.[33] This reduced metabolic rate results in slower healing after injury.[32] Tendon healing is a complex and highly regulated process corresponding with the initiation, sustainment and subsequent termination of a plethora of signaling molecules acting in highly organized concert.

1.2.4 Collagen

The major component of ECM collagen is type I, which is composed of two α_1 chains and one α_2 chain, arranged in a tight triple helix formation. While this remains the major collagen in adult tissues, a variety of other collagens are present and required during tenogenesis that are involved in the assembly of the final product.

In the developing chick embryo, it has been shown that heterotopic collagen types I/III are present in development.[34] Collagen type III is important in the initial fibril assembly process and has been associated with changes with the diameter of the fibrils.[35] It has been shown that collagen type III content is inversely proportional to diameter of a collagen fiber.[35] As development progresses, the collagen type III content in the central portion of the tendon decreases which is related to an increase in the fiber diameter. At the time of hatching, collagen type III is confined to the sheath around the tendon.[34] This form of recycling or replacement of collagen type III by collagen type I during embryogenesis may be related to healing pathways in adult tissue, as subsequently described. During healing of tendons, collagen type III is initially deposited which is later supplanted by collagen type I, providing significant parallels between the two processes. The collagen type III helices formed during repair are associated with smaller diameter and immature fibrils as previously mentioned.

A group of collagens knows as the fibril associated collagens with interrupted triple helices, or FACITs, are present and usually localized to the surface of fibrils.[36]

Such FACITs include collagen types XII and XIV, which are structurally similar homotrimers, composed of two collagenous domains (COL1 and COL2) and three non-collagenous domains (NC1-3).[37] Collagen type XII forms a bridge between the fibril and the matrix components of decrorin and fibronectin whereas collagen type XIV has been shown to be important in linear fibrillar growth.[38,39] Furthermore, fibril assembly is subject to further modulation by various small leucine rich proteins (SLRPs) such as biglycan (Class I SLRP), lumican and fibromodulin (Class II SLRPs).[40]

An important component in regard to the function of tendon tissue is that the collagen molecules with fibrils undergo covalent intra and intermolecular cross linking, catalyzed by the enzyme lysl oxidase (LOX) and the degree of cross linking increases as development progresses.[41] It is believed that SLRPs may regulate the intermolecular cross linking of collagen, activating as either co-receptor for LOX and promoting oxidation of appropriate lysine residues, or via steric hindrance of inappropriate lysine residues to ensure correct cross linkage of collagen molecules.[40]

1.2.5 Elastin

Of further interest is the composition of elastin in various tendon and ligament locations. For example, the Achilles tendon is mainly composed of collagen with only a small contribution from elastin. However, the nuchal ligament in herbivores can contain up to 83% elastin.[32] Elastic fibrillogenesis is therefore a process where fibrillin containing microfibrils are released into the ECM and are thought to serve as a

framework for the subsequent deposition of elastin onto the structures.[33] The microfibril-associated glycoproteins (MAGPs) fibulin-5 and emilin-1 have been shown to also form part of the structural framework and form part of the network establishing a link between microfibrils and elastin.[34]

1.2.6 Fibrillogenesis

Tendon tissue is primarily composed of collagen and when mature, is of low cellularity. Therefore, once tendon primordia have formed, the production of collagen and the expression of tendon extracellular matrix (ECM) must occur in order to be functional. Histological analysis has demonstrated the ordered presence of rows of tenocytes separated by bundles of collagen fibers under microscopy. However it has also been shown from developmental studies that the arrangement of tenocytes into organized rows occurs prior to collagen fibrillogenesis.[42] This implies that cell orientation dictates ECM orientation. However, the signaling molecule(s) that are responsible for the linear arrangement of tenocytes are unidentified and it remains a mystery why tenocytes would choose to arrange themselves in parallel layers.[1]

Once the tenocytes are arranged in rows the process of fibrillogenesis is initiated, which can be under the control of the Smad pathway and associated signaling cascades or mechanosensory pathways.[43] This is believed to occur in three overlapping phases; the assembly phase, linear growth and lateral growth.

During the assembly phase, collagen molecules are assembled in close proximity to the tendinous fibroblasts and form immature collagenous fibrils in a process termed collagen fibrillogenesis.[39] The packaging, vectorial arrangement and secretion of the procollagen molecules in a spatially orientated fashion are a prerequisite of successful fibril deposition. Collagen is formed in narrow channels, which extend from the perinuclear Golgi region to an opening at the cell surface.[39,44] The secretory vesicles of collagen fuse with the plasma membrane of the tenocyte and release the contents into the pericellular region. However, it is highly likely that integrin and other signaling and anchoring molecules on the cell surface interact with the newly secreted collagen in order to maintain close proximity and orientation of the fibril.[44] Once secreted these structures have a D-periodicity of 10-30 μm with tapered ends, which are either long α chains or short β chains, which are important for the second and third stages of linear and lateral growth described later.[44] At this stage, the collagen molecules are neither straight nor rigid, but rather they are semi flexible providing some plasticity to the structure.[39,44]

During the second period of formation, immature fibrils are assembled end to end, to form long structures in a process termed linear growth, which provides elongation of the tendon or ligament and this growth is restricted to the region of the tapered ends.[39,44] During this stage, the fibrils exhibit centrosymmetricity in that there is a polarization between the carboxylic acid terminus and the amino group on the molecules.[39] Linear growth in this phase results in a D-periodicity of 82-170 μm.[39] In the third period, termed lateral growth, fibrils associate with each other laterally which

results in an increase in the diameter of the fibril.[39] In this phase, growth is no longer restricted to the tapered ends and can occur throughout the molecule. Once these large diameter fibrils are formed, they coalesce together and are ordered into fibers, contributing the to hierarchical organization of tendon tissues (**Figure 1.2.6A**).

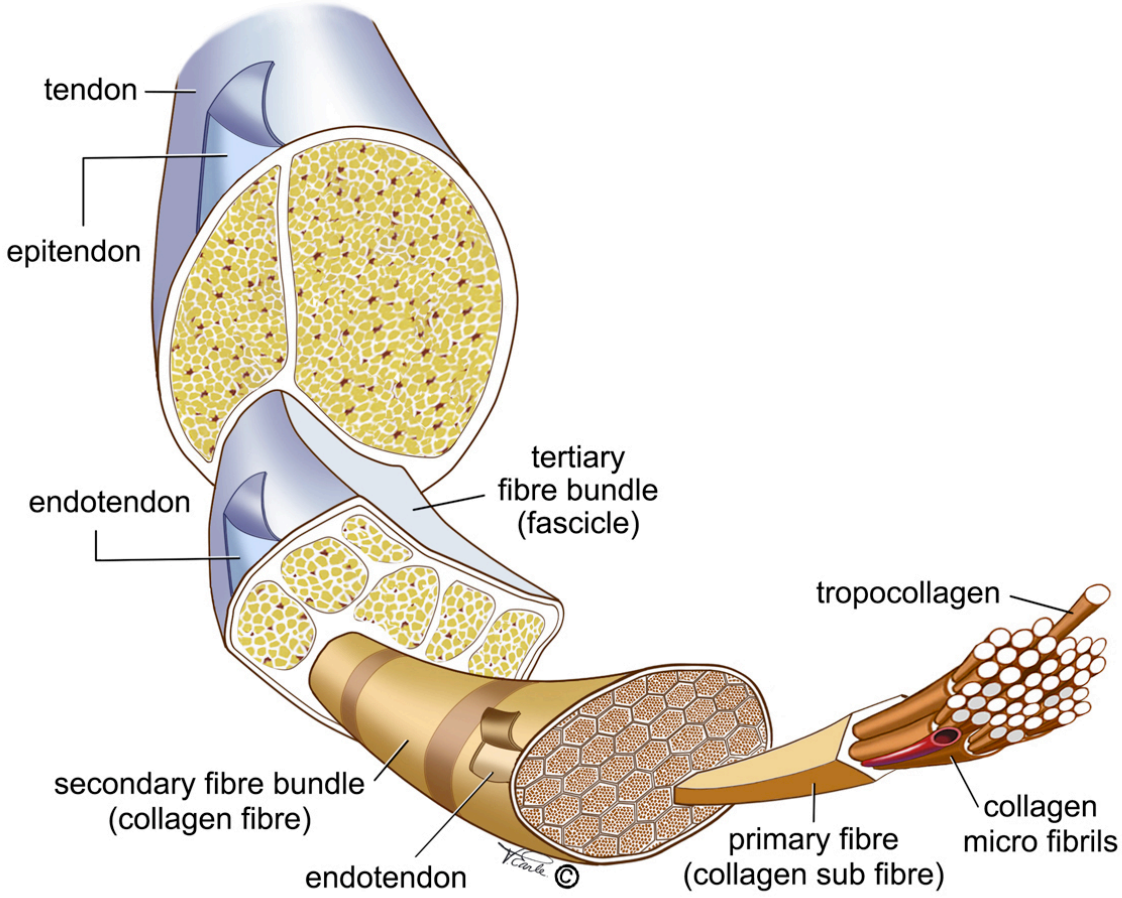

Figure 1.2.6A Hierarchical organization of tendons. Three polypeptide chains combine to form a helical tropocollagen molecule. Five tropocollagen molecules assemble to form a microfibril and the aggregation of microfibrils form fibrils. Fibrils then are grouped into fibers, fibers are bundled together into fiber bundles and fiber bundles are grouped into fascicles. A thin layer of loose connective tissue (endotenon) encases the fascicles and/or fiber bundles. Surrounding the tendon as a whole is a further sheet of connective tissue (epitenon), which is continuous with the endotenon. Reproduced from Internet Source.[45]

1.2.7 Tendon Types

Tendons are of two major types, chiefly based on the presence or absence of a covering sheath being either intrasynovial or extrasynovial. Intrasynovial tendons have bilayer membranes containing synovial fluid, such as the flexor tendons of the hand or portions of the digital flexor tendons of the horse. Tendon sheath fluid assays have demonstrated hyaluronic acid and protein concentrations similar to those identified in joint fluid. Therefore, the tendon sheath fluid is believed to serve similar functions as joint fluid, such as gliding and nutrition of tendon tissue and cells.[46]

An extrasynovial tendon, such as the Achilles tendon, has no such synovial membrane, but is covered by a thin layer of loose connective tissue termed the paratenon.[47] Intrasynovial and extrasynovial tendons have been shown to heal via differing mechanisms, the implication being that the synovial sheath is the critical determinant in selecting the healing pathway, both of which are discussed in more detail in later sections.

1.2.8 Tendon Vasculature

Several studies have been performed which characterized the various source of blood flow to tendon tissue. Those tendons, which lie within synovial sheaths, much like cells of the cartilaginous layer in joints, receive a substantial portion of nutrients via synovial fluid bathing.[46] In addition for the tendon however, there is an additional blood

supply from segmental vessels. For those tendons without the protection of a synovial sheath, the majority of blood is supplied via the osseotendinous and myotendinous junctions, in addition to perforating vessels traversing the mesotenon and paratenon.[48]

The Achilles tendon has been the focus of a substantial portion of work regarding tendon vasculature supply.[49] Injection studies performed in cadaver sections described a network of evenly distributed vessels in the paratenon, from which vessels ran centrally towards the tendon via branches in the mesotenon.[50] Further investigation into the blood supply of the Achilles via angiographic testing, light microscopy and histological analyses have identified three primary areas for tendon nourishment; the musculotendinous junction, the osseotendinous junction and the paratenon.[51] The vessels in the epitenon are chiefly derived proximally from the musculotendinous branches of the gastrocnemius and distally from vessels in the calcaneus. The vessels coursing through the paratenon are thought to be derived from the main arteries of the distal limb, including the cranial and caudal tibial arteries, the saphenous artery, the popliteal artery and the sural arteries. There is believed to be an anastomosing network between the paratenon supply and the osseous and myotendinous blood supply, which ramifies in the mesotenon.[52]

References

1 **Tozer S. & Duprez D.** Tendon and ligament: development, repair and disease. *Birth Defects Res., Part C* **75**, 226-236 (2005)

2 **Henkels., J.A. & Zamir, E.A.** A Novel Biomimetic Model for Studying Mechanics of Embryonic Morphogenesis and Differentiation, ASME Summer Bioengineering Conference *Am Soc Bio Eng,* 431-432 (2010).

3 **Salingcarnboriboon, R. et al.** Establishment of tendon-derived cell lines exhibiting pluripotent mesenchymal stem cell-like property. *Exp Cell Res* **287**, 289-300 (2003).

4 **Brent, A.E. & Tabin, C.J.** Developmental regulation of somite derivatives: muscle, cartilage and tendon. *Curr Opin Genet Devel* **12**, 548-557 (2002).

5 **Pryce, B.A. et al.** Generation of transgenic tendon reporters, ScxGFP and ScxAP, using regulatory elements of the scleraxis gene. *Dev Dynam* **236***,* 1677-1682 (2007).

6 **Léjard, V. et al.** Scleraxis and NFATc regulate the expression of the pro-α1 (I) collagen gene in tendon fibroblasts. *J Biol Chem* **282**,17665-17675 (2007).

7 **Chang, F. et al.** Signal transduction mediated by the Ras/Raf/MEK/ERK pathway from cytokine receptors to transcription factors: potential targeting for therapeutic intervention. *Leuk Lymphoma* **17**,1263-1293 (2003).

8 **Brent, A.E. & Tabin, C.J.** FGF acts directly on the somitic tendon progenitors through the Ets transcription factors Pea3 and Erm to regulate scleraxis expression. *Dev Biol* **131**, 3885-3896 (2004).

9 **Chevallier, A., Kieny, M. & Mauger, A.** Limb-somite relationship: origin of the limb musculature. *J Embryol Exp Morph* **41**, 245-258 (1977).

10 **Brent, A.E., Braun, T. & Tabin, C.J.** Genetic analysis of interactions between the somitic muscle, cartilage and tendon cell lineages during mouse development. *Dev Biol* **132**, 515-528 (2005).

11 **Crossley, P.H. et al.** Roles for FGF8 in the induction, initiation, and maintenance of chick limb development. *Cell* **84**,127-136 (1996).

12 **Schweitzer, R. et al.** Analysis of the tendon cell fate using Scleraxis, a specific marker for tendons and ligaments. *Dev Biol* **128**, 3855-3866 (2001).

13 **Edom□Vovard, F. & Duprez, D.** Signals regulating tendon formation during chick embryonic development. *Dev Dynam* **229**, 449-457 (2004).

14 **Kardon, G.** Muscle and tendon morphogenesis in the avian hind limb. *Dev Biol* **125**, 4019-4032 (1998).

15 **Hartmann, C. & Tabin, C.J.** Wnt-14 plays a pivotal role in inducing synovial joint formation in the developing appendicular skeleton. *Cell* **104**, 341-351 (2001).

16 **Storm, E.E. et al.** Limb alterations in brachypodism mice due to mutations in a new member of the TGFb-superfamily. *Nature* **368**, 639-642 (1994).

17 **Clark, R.T. et al.** GDF-5 deficiency in mice leads to disruption of tail tendon form and function. *Connect Tissue Res* **42**, 175-186 (2001).

18 **Mikic, B. et al:** GDF□5 deficiency in mice alters the ultrastructure, mechanical properties and composition of the Achilles tendon. *J Orthop Res* **19**, 365-371 (2001).

19 **Wolfman, N.M. et al.** Ectopic induction of tendon and ligament in rats by growth and differentiation factors 5, 6, and 7, members of the TGF-beta gene family. *J Clin Invest* **100,** 321-330 (1997).

20 **Lovinescu, I., Koyama, E. & Pacifici, M.** Roles of FGF-10 on the development of diathrodial limb joints. *Pa Dent J* **103**, 5-9 (2002).

21 **Ippolito, E. et al.** Morphological, immunochemical, and biochemical study of rabbit achilles tendon at various ages. *J Bone Joint Surg* **62**, 583-598 (1980).

22 **Donnelly, E., Ascenzi, M. G., & Farnum, C.** Primary cilia are highly oriented with respect to collagen direction and long axis of extensor tendon. *J Orthop Res*, **28**, 77-82 (2010).

23 **Holmes, I.** Variations in tendon cell morphology with animal, site and age. *J Anat* **108**, 305-310 (1971).

24 **Moore, M. J. & De Beaux, A.** A quantitative ultrastructural study of rat tendon from birth to maturity. *J Anat* **153**,163-166 (1987).

25 **McNeilly, C. M., Banes, A. J., Benjamin, M., & Ralphs, J. R.** Tendon cells in vivo form a three dimensional network of cell processes linked by gap junctions. *J Anat* **189**, 593-597 (1996).

26 **Khan, R. J., Fick, D., Keogh, A., Crawford, J., Brammar, T., & Parker, M:** Treatment of acute Achilles tendon ruptures: A meta-analysis of randomized, controlled trials. *J Bone Joint Surg* **87**, 2202-2210 (2005).

27 **Bi, Y. et al.** Identification of tendon stem/progenitor cells and the role of the extracellular matrix in their niche. *Nature Med* **13**, 1219-1227 (2007).

28 **Kjær, M.** Role of extracellular matrix in adaptation of tendon and skeletal muscle to mechanical loading. *Physiol Rev* **84**, 649-698 (2004).

29 **Kannus, P.** Structure of the tendon connective tissue. *Scand J Med Sci Spor* **10**, 312-320 (2004).

30 **Puxkandl, R. et al.** Viscoelastic properties of collagen: synchrotron radiation investigations and structural model. Philos Trans R Soc Lond B Biol Sci **357**, 191-197 (2002).

31 **Kannus, P., Jozsa, L. & Jarvinnen, M.** Basic science of tendons. In: Garrett WE Jr, Speer KP, Kirkendall DT, editors. Principles and practice of orthopaedic sports medicine. Philadelphia: Lippincott Williams and Wilkins, 21–37 (2000).

32 **O'Brien, M.** Structure and metabolism of tendons. *Scand J Med Sci Spor* **7**, 55-61 (1997).

33 **Vailas, A. et al**. Physical activity and hypophysectomy on the aerobic capacity of ligaments and tendons. *J Appl Physiol Respir Environ Exerc Physiol* **44**, 542-546 (1978).

34 **Birk, D. & Mayne, R.** Localization of collagen types I, III and V during tendon development. Changes in collagen types I and III are correlated with changes in fibril diameter. *Europ J Cell Biol* **72**, 352-361 (1997).

35 **Liu, X. et al.** Type III collagen is crucial for collagen I fibrillogenesis and for normal cardiovascular development. *Proc Nat Acad Sci* **94**,1852-1856 (1997).

36 **Walchli, C. et al.** Tissue-specific expression of the fibril-associated collagens XII and XIV. *J Cell Sci* **107**, 669-681 (1994).

37 **Shaw, L.M. & Olsen, B.R.** FACIT collagens: diverse molecular bridges in extracellular matrices. *Trends Biochem Sci* **16**,191-194 (1991).

38 **Font, B. et al.** Characterization of the interactions of type XII collagen with two small proteoglycans from fetal bovine tendon, decorin and fibromodulin. *Matrix Biol* **15**, 341-348 (1996).

39 **Zhang, G. et al.** Development of tendon structure and function: regulation of collagen fibrillogenesis. *J Musculoskelet Neuronal Interact* **5**, 5-21 (2005).

40 **Kalamajski, S. & Oldberg, Å.** The role of small leucine-rich proteoglycans in collagen fibrillogenesis. *Matrix Biol* **29**, 248-253 (2010).

41 **Siegel, R.C., Pinnell, S.R. & Martin, G.R.** Cross-linking of collagen and elastin. Properties of lysyl oxidase. *Biochem* **9,** 4486-4492 (1970).

42 **Benjamin, M. & Ralphs, J.** The cell and developmental biology of tendons and ligaments. *Internat Rev Cytol* **196**, 85-130 (2000).

43 **Yang, G., Crawford, R.C. & Wang, J.H.** Proliferation and collagen production of human patellar tendon fibroblasts in response to cyclic uniaxial stretching in serum-free conditions. *J Biomech* **37**,1543-1550 (2004).

44 **Zhang, G. et al:** Decorin regulates assembly of collagen fibrils and acquisition of biomechanical properties during tendon development. *J Cell Biochem* **98**, 1436-1449 (2006).

45 http://ubcmedicalart.wordpress.com/gallery-2/structure-of-tendons/, accessed 10 October 2014

46 **Hagberg, L., Heinegård, D. & Ohlsson, K.** The contents of macromolecule solutes in flexor tendon sheath fluid and their relation to synovial fluid: a quantitative analysis. *J Hand Surg Br* **17**, 167-171 (1992).

47 **O'Brien, M.** The anatomy of the Achilles tendon. *Foot Ankle Clin* **10**, 225-238 (2005).

48 **Mayer, L.** *The Physiological Method of Tendon Transplantation: Historical. Anatomy and Physiology of Tendons. I*. 1916

49 **Fenwick, S.A., Hazleman, B. L. & Riley, G. P.** The vasculature and its role in the damaged and healing tendon. *Arthritis Res* **4**, 252-260 (2002).

50 **Carr, A. J. & Norris, S. H.** The blood supply of the calcaneal tendon. J *Bone Joint Surg Br* **71**, 100-101 (1989).

51 **Ahmed, I. M., Lagopoulos, M., McConnell, P., Soames, R. W. & Sefton, G. K.** Blood supply of the Achilles tendon. *J Orthop Res* **16**, 591-596 (1998).

52 **Kannus, P.** Structure of the tendon connective tissue. *Scand J Med Sci Spor* **10**, 312-320 (2000).

1.3 Anatomy of the Achilles Tendon

The Achilles tendon is considered to be the largest diameter and tendon with the highest tensile strength in humans. It is formed by the fusion of the soleus and gastrocnemius muscles.[1] As the fibers from these muscles merge, their orientation is proximal-distal in relation to the limb. However, there is a spiral component to the Achilles tendon with lateral spiraling as the Achilles courses distally to its osseous insertion on the calcaneus.

The tendon inserts on the caudal, or posterior, aspect of the calcaneus. The distal portion of the tendon is separated from the calcaneus by the retrocalcaneal bursa, which serves to protect the structure during dorsiflexion.[2] Immunohistochemical staining for collagen type II and histology with toluidine blue has demonstrated that there are interlocking regions of calcified fibrocartilagenous zones in addition to bone at the enthesis of the human Achilles tendon.[3] Fibrocartilage in such context is predominantly identified in regions where tendons are subjected to compression.[4]

A thick layer of paratenon, deep to which is the epitenon layer containing the vascular membrane, covers the Achilles tendon.[5] Juxtaposed between these two layers is a microfilm layer of fluid, which imparts a certain similarity between this tendon and true intrasynovial tendons.

1.3.1 Mechanical Properties of Tendon

The majority of our knowledge of the mechanical properties of tendons relies on material testing of ex vivo samples in a materials testing machine.[6] These data permit the generation of information relating to the structural properties of a tendon (ultimate tensile strength, stiffness) and the material properties of the tendon (stress, strain and Young's modulus). This system requires the stretching of the specimen by an external force with concurrent monitoring of the deformation and the applied force, thus mimicking the natural mechanisms of tendon loading.[7] From such data, a force deformation plot can be generated, which relates stiffness (n/mm) to energy (J). In an elongation to failure curve (force-deformation), which is a reflection of the structural properties of the individual specimen, four classic regions have been identified through which tendon properties are exerted. Region I represents the toe, or the initial region of the curve in which the natural crimp of tendons is elongated, but there is no further fiber stretching.[6] In the linear region II, stiffness remains constant as a function of elongation and thus forms a linear function. In this region, the fibers are stretched. Tendons operating in this region remain elastic and return to their original length upon relaxation. Region II ends when the fibers are stretched beyond their elastic limit and results in failure. The initial point of failure is the initiation of region III and represents the start of the plastic region; tendons no longer return to their original length upon relaxation but are permanently elongated. As region III proceeds, further fiber disruption occurs, until the ultimate failure occurs, which represents region IV (**Figure 1.3.1A**).

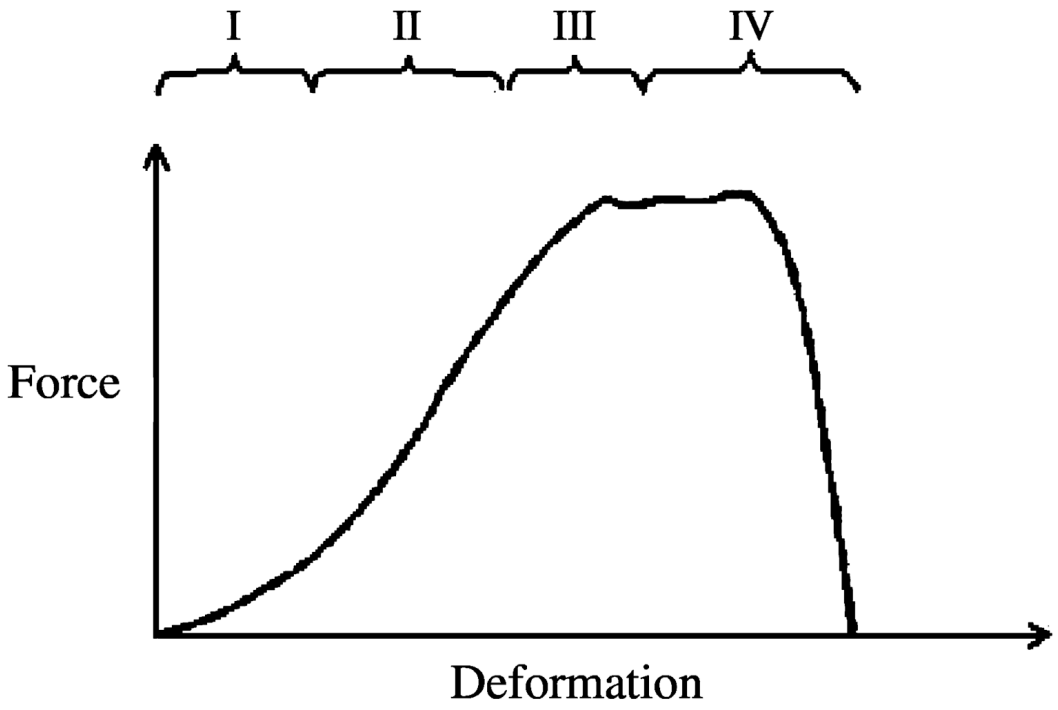

Figure 1.3.1A. Sketch of a typical force-elongation curve for a tendon pulled to failure. The tendon progresses through the toe region, with elimination of fiber crimp (region I), the linear, elastic region of fiber stretching (region II), the plastic failure region (region III) and finally the region of complete fiber rupture (region IV). Adapted from Maganaris et al.[8]

To normalize for size and interspecies dimensional differences the force deformation curve is normalized.[6] Force is normalized to stress by incorporation of the tendon cross sectional area and deformation is normalized to strain by consideration of the original length of the tendon, resulting in a stress-strain curve, which reflects the intrinsic material properties of the specimen.[9] Strain is calculated via dividing the change in tendon length by the original length. However, during the tendon lengthening procedure, the original cross sectional area becomes reduced as a result of the lengthening. Stress measurements are therefore complicated by the assumptions of uniform cross sectional area, which may vary throughout the tendon, in addition to

assuming a constant cross sectional area during lengthening, when a reduction truly occurs.

Reported properties from such curves thus include Young's Modulus (MPa), ultimate Stress (MPa), ultimate strain (%), and toughness (J/kg). Typical values reported for tendons include 1-2 GPa for Young's Modulus[10], 50-125 MPa for ultimate stress, 13-32% strain at failure for bone-tendon models and 5-16% for tendon mid-substance values[11,12] and 1,000 -45,000 J/kg for toughness.[6]

Several factors can influence the mechanical properties of tendons. Disuse of muscular tissue and concurrently, tendons, results in increased collagen turnover and a reduction in the cross linkages, which decreases glycosaminoglycan and water content. In addition, there is an increase in the non-uniform orientation of the collagen fibrils, which ultimately results in a reduction of the inherent intrinsic properties of the material.[13] The opposite effect is achieved with physical activity and exercise, resulting in an improvement in the material properties.

Anatomical site is also an important consideration in regard to tendon properties, as the loads experienced by the Achilles tendon on the posterior aspect, tend to represent the highest strains experienced in comparison to those tendons on the anterior surface during extension of the limb. Not only is the degree of strain sustained critical, but the rate the strain is applied is important also, due to the viscoelastic nature of tendons. It has also been reported that the human Achilles tendons exhibits strain

rate sensitivity similar to other human tendons and has material properties similar to other tendon sites.[14] This occurs despite the higher *in vivo* loading rates the tendon experiences. The authors of one paper commented that is unknown why the Achilles tendon fails to adapt to the high *in vivo* stresses, but that the failure of adaption leaves the tendon at an increased risk of injury, which may explain the high incidence of injuries to this tendon.[14] Furthermore, While most tendons experience peak stresses below 30 MPa, the human Achilles tendon experiences peak stress around 67 MPa.[10] As previously mentioned, the elastin content, most notably of the nuchal ligament can also affect the material properties of the tendinous and ligamentous structures. The elastin content varies throughout different anatomical locations.

1.3.2 Rabbit Achilles Tendon Anatomy

The rabbit is often used in Achilles tendon research due to its availability and that the size of the Achilles tendon structure enables straightforward mechanical testing and histological analyses.[15] There are several key anatomical differences however between human and rabbit Achilles tendon anatomy. In humans, the lateral and medial gastrocnemius musculotendinous units fuse at 23% of their proximal-distal course, resulting in a large Achilles tendon of approximately 200 mm in length.[15] This contrasts significantly with the rabbit, in which the medial and lateral gastrocnemius tendons remain separate for 93% of their overall length (**Figures 1.3.2A and 1.3.2B**).[15] In the rabbit, a true Achilles tendon exists for only the distal 7%, or for the final 3 mm proximal

to the calcaneal insertion.[15] As such, studies that document transection of the Achilles tendon often fail to specify the exact anatomical name for the area, which has been transected, making comparisons between studies extremely difficult.[15]

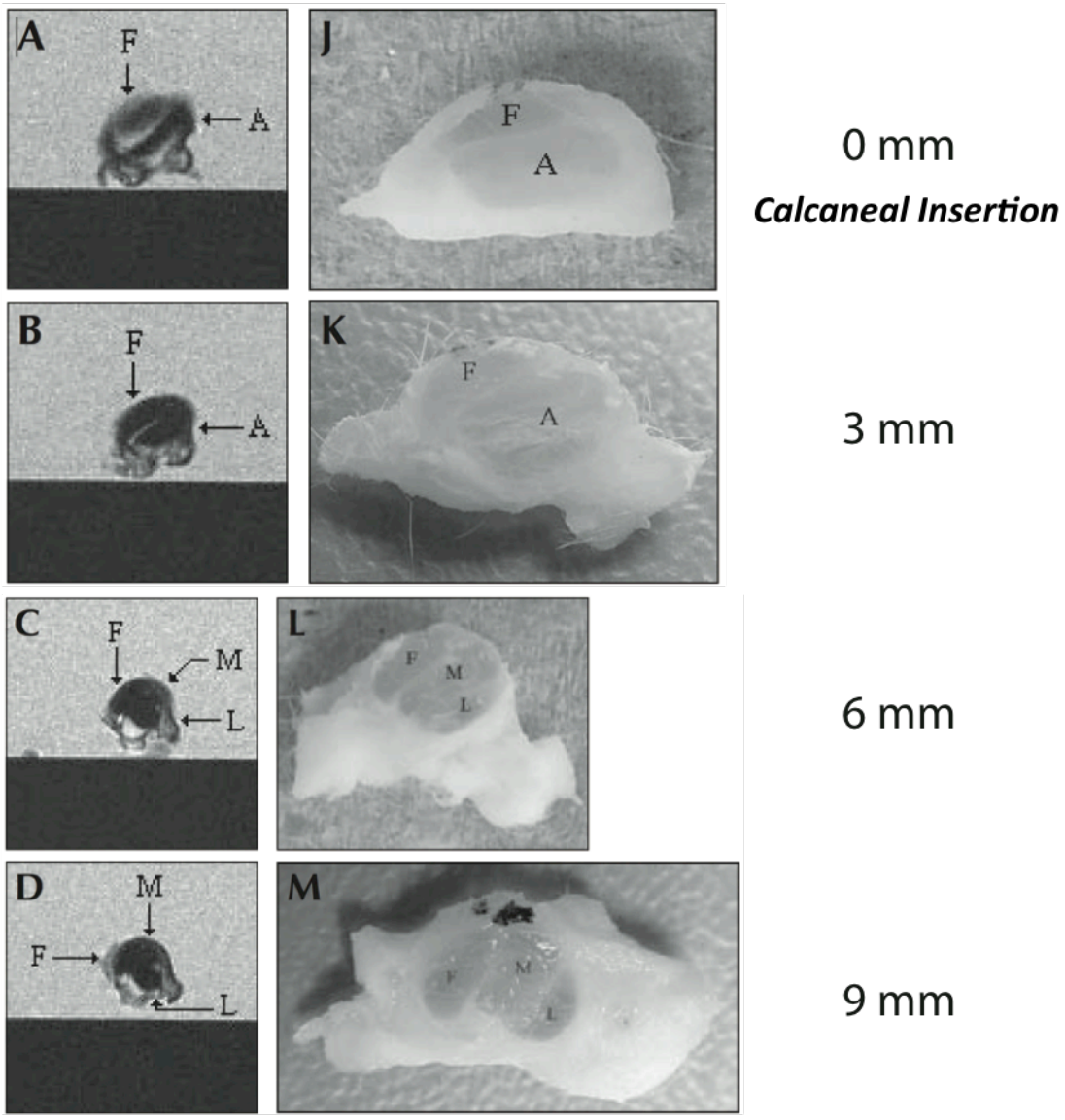

Figure 1.3.2A. Axial Proton Density Magnetic Resonance Images (**left panels**) and axial gross anatomy sections (**right panels**) of the rabbit calcaneus–Achilles tendon–gastrocnemius–soleus complex. **F**, flexor digitorum superficialis tendon; **M**, medial gastrocnemius tendon; **L**, lateral gastrocnemius tendon; **A**, Achilles tendon. Scale on the far right indicates distances in a proximal direction from the calcaneus. Reproduced from Doherty et al.[15]

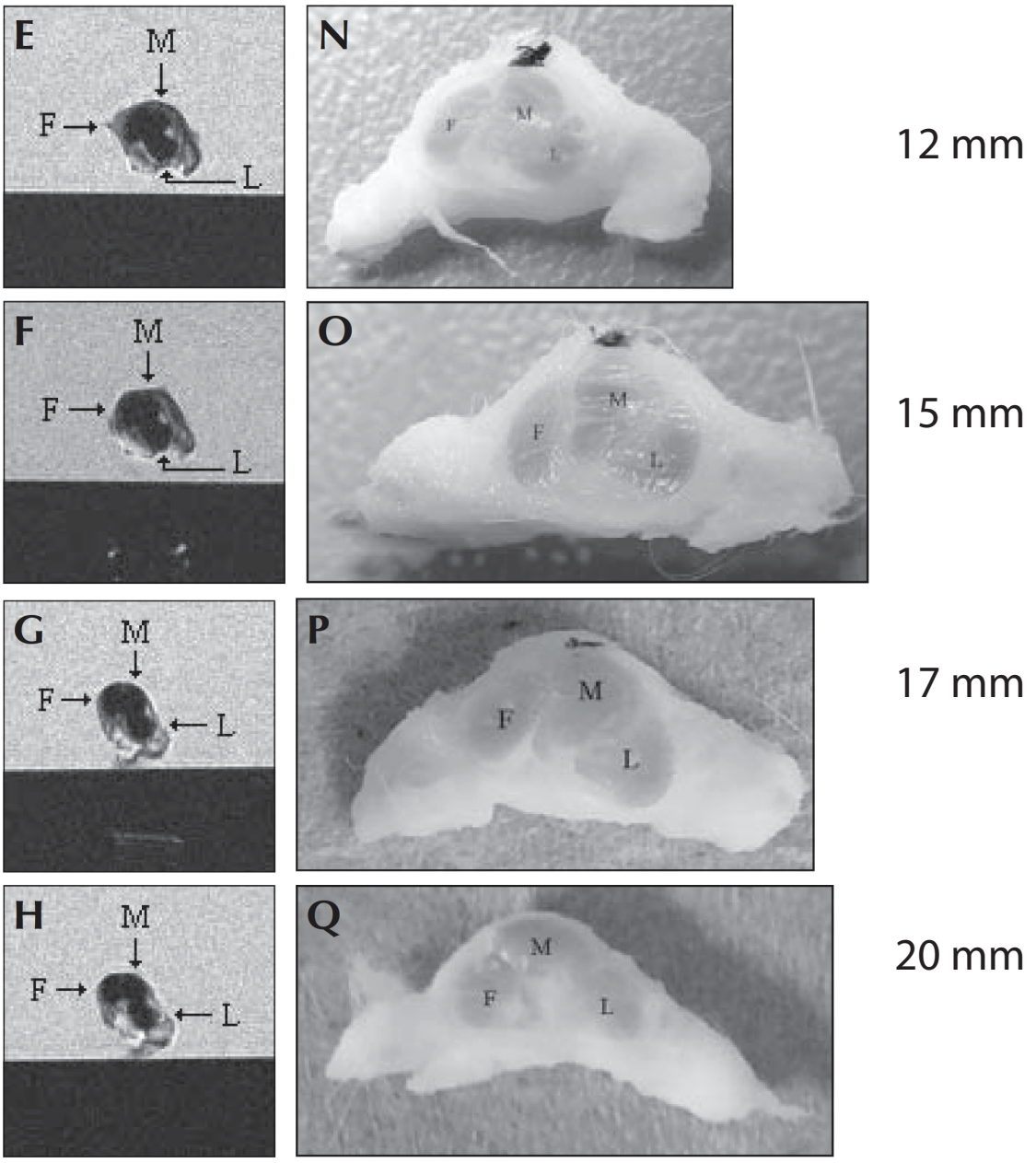

Figure 1.3.2B. Axial Proton Density Magnetic Resonance Images (**left panels**) and axial gross anatomy sections (**right panels**) of the rabbit calcaneus–Achilles tendon–gastrocnemius–soleus complex. **F**, flexor digitorum superficialis tendon; **M**, medial gastrocnemius tendon; **L**, lateral gastrocnemius tendon; **A**, Achilles tendon. Scale on the far right indicates distances in a proximal direction from the calcaneus. Reproduced from Doherty et al.[15]

References

1 **Cummins, E.J. & Anson, B.J.** The structure of the calcaneal tendon (of Achilles) in relation to orthopedic surgery, with additional observations on the plantaris muscle. *Surg, Gyn Obst **83***, 107-116 (1946).

2 **Rufai, A., Ralphs, J.R. & Benjamin, M.** Structure and histopathology of the insertional region of the human Achilles tendon. *J Orthop Res* **13**, 585-593 (1995).

3 **Milz, S., Rufai, A., Buettner, A., Putz, R., Ralphs, J. R., & Benjamin, M.** Three□dimensional reconstructions of the Achilles tendon insertion in man. *J Anat **200***, 145-152 (2002).

4 **Benjamin, M. & Ralphs, J.R.** Fibrocartilage in tendons and ligaments—an adaptation to compressive load. *J Anat* **193**, 481-494 (1998).

5 **Nisbet, N.W.** Anatomy of the calcaneal tendon of the rabbit. *J Bone Joint Surg Br* **42**, 360-366 (1960).

6 **Maganaris, C.N. & Paul, J.P.** In vivo human tendon mechanical properties. *J Physiol* **521**, 307-313 (1999).

7 **Shadwick, R.E.** Elastic energy storage in tendons: mechanical differences related to function and age. *J Appl Physiol* **68,** 1033-1040 (1990).

8 **Maganaris, C.N., Narici, M.V. & Reeves, N.D.** In vivo human tendon mechanical properties: effect of resistance training in old age. *J Musculoskelet Neuronal Interact* **4**, 204-208 (2004).

9 **Viidik, A.** Tensile strength properties of Achilles tendon systems in trained and untrained rabbits. *Acta Orthop* **40**, 261-272 (1969).

10 **Ker, R.F., Alexander, R.McN. & Bennett, M.B.** Why are mammalian tendons so thick? *J Zool* **216**, 309–324 (1988).

11 **Haut, T.L. & Haut, R.C.** The state of tissue hydration determines the strain-rate-sensitive stiffness of human patellar tendon. *J Biomech* **30**, 79-81 (1997).

12 **Nakagawa, Y., Hayashi, K., Yamamoto, N. & Nagashima, K.** Age-related changes in biomechanical properties of the Achilles tendon in rabbits. *Europ J App Physiol Occup Physiol* **73**, 7-10 (1996).

13 **Yasuda, K. & Hayashi, K.** Changes in biomechanical properties of tendons and ligaments from joint disuse. *Osteoarthr Cartilage* **7**, 122-129 (1999).

14 **Wren, T.A., Yerby, S.A., Beaupré, G.S. & Carter, D.R.** Mechanical properties of the human Achilles tendon. *Clin Biomech* **16**, 245-251 (2001).

15 **Doherty, G.P. et al.** Comparative anatomy of rabbit and human Achilles tendons with magnetic resonance and ultrasound imaging. *Comp Med* **56**, 68-74 (2006).

1.4 Tendon Healing

The archetypally regarded hypothesis has been that tendon and ligamentous fibrillogenesis during repair post injury is related to fibrillogenesis during embryonic development. Tendon healing occurs through two, linked pathways, the intrinsic pathway associated with the proliferation of epitenon, endotenon and tenocytes, or via extrinsic mechanism, which is invasion via cells form the synovia or surrounding sheath.[1] The involvement of these two systems occurs throughout the phases of tendon healing described. It has been demonstrated that extrinsic tenoblasts can initiate the repair process by proliferation and migration, without relying on changes in vascularity or formation of adhesions for support.[2]

The majority of studies into tendon healing have been performed on transected animal tendons or ruptured human tendons. In essence, the response to injury in tendons occurs in three overlapping time periods; an inflammatory phase, a proliferative or repair phase and finally a remodeling or maturation phase (**Figure 1.4A**).[3,4]

1.4.1 Inflammatory Phase

During the inflammatory phase, erythrocytes and inflammatory cells, particularly neutrophils, enter the site of injury in the resulting hematoma, with platelet activation and the invasion of cells that form a granuloma.[5] After the initial 24-hour period, monocytes and macrophages become the predominate cell type resulting in the release

of chemotactic and vasoactive factors and the phagocytosis of necrotic material.[5] The exact sequence of appearance of inflammatory cells in traumatized tendon tissues has been poorly studied.[6] Accumulation of inflammatory cells is dependent on mitogenesis of resident inflammatory cells, or recruitment from the vascular system. Neutrophils, which are one of the first inflammatory cells to arrive at the site of injury, in addition to their role in phagocytosis, release cytokines that may attract monocytes and promote their differentiation into macrophages and stimulate resident macrophages.[6] These activated macrophages, which predominate in the inflammatory phase, are then able to release growth factors that can induce ECM formation and stimulate fibroblasts, tenoblasts and stem cells to proliferate.[5] This phase typically occurs up to 7 days post injury in humans, but is only present until days 3-4 in the rabbit.

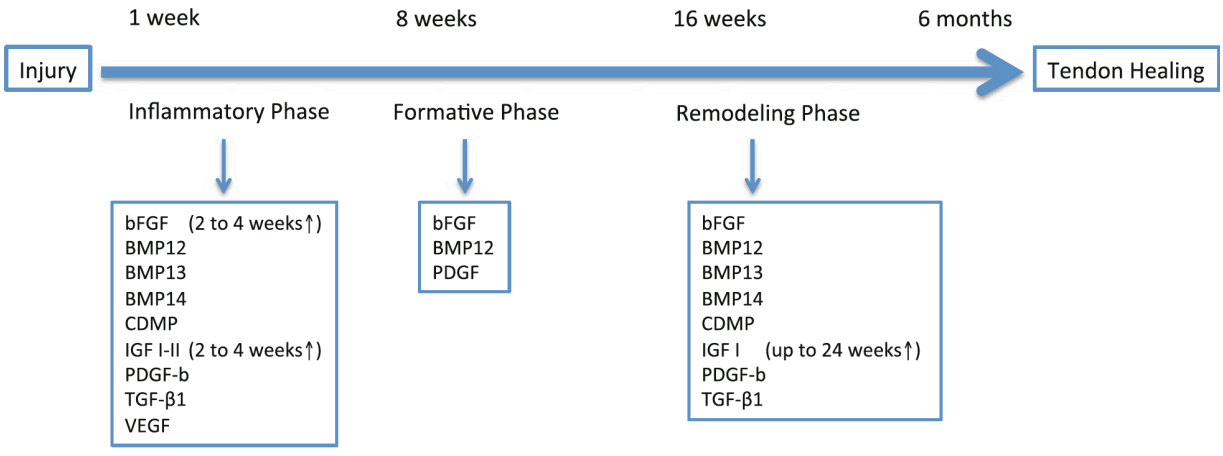

Figure 1.4A Representation of the phases of tendon healing. The timescale provided is representative of human phases of repair. From Muller et al.[3]

1.4.2 Proliferative Phase

Following a few days post injury, the formative, or proliferative phase begins (**Figure 1.4A**). This is characterized by the migration of tenocytes into the wound with the initiation of collagen type III synthesis.[7] This phase lasts for several weeks in both humans and rabbits, during which time the concentrations of water and glycosaminoglycan's (GAGs) remains elevated. Recruited and migrated fibroblasts in the granulation tissue primarily produce collagen type III that gradually permits the increase in mechanical strength of the repair. Furthermore, mechanical loading of the tissue results in elastic deformation, which permits mechanical signaling to influence this period of tendon healing via the ECM. It is at this stage that the region of repair reaches its largest size and this large cross sectional area compensates for tissue's material weakness in the region.[7] ECM formation requires the removal of granulation tissue laid down in the inflammatory phase, via the formation of collagen and elastin fibers, which are then saturated with proteoglycans and glycoproteins.

1.4.3 Maturation Phase

The final period involved in tendon healing include a consolidation or maturation stage (**Figure 1.4A**), which are part of a remodeling phase, initiated between days 36-42 in the rabbit.[8] At approximately 3-4 weeks post injury, epitenon fibroblasts further contribute to the repair process via migration and proliferation.[9] The epitenon fibroblasts

are the initial cell type to synthesize collagen, which are later followed by endotenon fibroblasts, which migrate over the severed ends of tendon stumps.[10]

These processes of tendon healing result in a change in the size and shape of the tendon tissue. As such, there is a decrease in cellularity, resulting in a change of phenotype from cellular to fibrous, with an increase in the production of collagen, predominately type I and GAGs. Biomechanical forces play a significant role in the alignment of tenocytes and collagen, according to the lines of stress. The collagen type III laid down in the proliferative phase is gradually resorbed and replaced with collagen type I, which results in superior organization and permits the cross linking of the hydroxypyridinium residues, enhancing biomechanical strength.[11] As a result of improved histological organization, the cross sectional area reduces which results in increased material properties, identified by an increase in tensile strength per unit of cross sectional area (stress).[11]

1.4.4 Intrinsic and Extrinsic Repair

While these three phases summarize the broad timescales of tendon healing, healing may also occur concurrently through two other, linked pathways, the intrinsic pathway associated with the proliferation of epitenon, endotenon and tenocytes, or via an extrinsic mechanism, which is invasion via cells form the synovia or surrounding sheath.[12] The involvement of these two systems occurs throughout the three phases of tendon healing described. It has been demonstrated that extrinsic epitenon tenoblasts,

can initiate the repair process by proliferation and migration, without relying on changes in vascularity or formation of adhesions for support.[13]

This intrinsic repair via internal tenocytes has been shown to secrete larger and more mature collagen in comparison to extrinsic epitenon cells.[14] Nevertheless, the type and degree of trauma, presence of a synovial sheath and mechanical stress exerted may influence the contribution of a specific cell type and mechanism in regard to healing pathway However, it is widely regarded that intrinsic healing results in improved biomechanics and fewer complications in comparison to extrinsic repair, which is primarily associated with scar tissue and adhesion formation.[9] It is also important to understand these types of repair may vary according to anatomical location, as extrinsic healing has been shown to predominate in rotator cuff repairs.[15]

The quality and organization of newly deposited collagen into the site of injury has a similar appearance to native tendon tissue.[16] Proteolytic degradation of collagen fibers is an important component for the remodeling phase in the formation of uniform tendon bundles. [10] It is uncertain whether newly formed fibrils can be bonded together with the existing collagen in the healing matrix or if new collagen that spans the gap must be formed.

It has been noted that as tendon regenerates, areas of translucency appear juxtaposed to the site of injury. It has been proposed that the translucency develops as a result of liberation of intact collagen fibril segments from the area, allowing them to be

reincorporated into the regenerating tendon.[10] Due to this translucency, this area often complicates the demarcation between intact and damaged tendon during tendon repair procedures.[17] During the formative phase of the intrinsic process, there is an increase in opacity of the region of tendon injury that can be observed. It has been proposed therefore that this intrinsic tendon repair is more of a connective tissue remodeling process, with the recycling of collagen fibrils phagocytized by macrophages, rather than a synthetic process of de novo collagen production.[17] The formative phase corresponds to the chemotactic signaling of fibroblasts, via signaling molecules including the macrophage induced production of fibronectin matrix and the fibroblastic deposition of collagen into the region. At the conclusion of this formative phase, the recovery of tendon opacity occurs.

Suturing techniques of tendons have therefore evolved to include large margins on either side of the tendon gap to avoid weakening of the area, which occurs during the healing process, represented by the area of translucency.[10] As the tendon is repaired, there is a gradual transference of tension from tendon ends, which can be repaired utilizing suture material, to the newly synthesized tissue. Such mechano-transduction factors are important in modulating signals via the ECM and are likely to play a role in both embryogenesis of tendon tissue and repair, as tension influences cell orientation, promotes collagen synthesis and aids in fibrillar remodeling.[18]

There are a series of significant parallels between tendon and ligamentous formation during embryogenesis and therefore similar repair pathways may also exist. A

more thorough understanding of these processes may lead to future advancements in the methods and modalities currently employed to treat injuries of these structures. The overlapping phases that dominate the repair process of the rabbit Achilles tendon include the inflammatory, proliferative and remodeling phase, which are supported by both intrinsic and extrinsic repair mechanisms, as previously described. It is important to note that the contribution of each pathway (intrinsic vs. extrinsic) and the timing and duration of each phase are species and location dependent and their importance and contribution will vary depending on the technique chosen to repair any damaged tendon tissue.

1.4.5 Discrete Plasticity

The capacity of tendons to heal depends on the type of injury, its duration and location.[19] Tendon overuse is a common problem in sport and work settings.[20] The act of repeated overloading can lead to sequelae such as tendinosis and tendinitis which may be manifestations of micro-tearing of collagen fibrils, which subsequently weaken the tendon and can lead to rupture. As such, the healing of fully ruptured tendons is relatively poor. Although healing times for sub rupture overextensions are shorter than complete ruptures, the rate of healing remains sub-optimal.[21] Tendon healing is a complex and highly regulated process corresponding with the initiation, support and subsequent termination of a variety of signally molecules acting in highly organized fashion as previously described.

For a prolonged period of research into tendon healing, it was believed that during the overloading of a tendinous structure, microscopic damage occurred which resulted in the dissociation of collagen fibrils into their subfibrillar components.[22] However, recent studies have identified that functionally cross-linked collagen fibrils undergo a more complex series of breakdown events.[23] A phenomenon whereby in contrast to the uniform loss of cohesion historically reported, fibrils were observed to exhibit plastic deformation via a molecular denaturation mechanism that were repeated at discrete locations several hundred nanometers along the length of the collagen fibril and were in areas of concentrated, denatured collagen.[23,24] The authors who identified this discrete plasticity form of denaturation determined that as tendons were subjected to increasing overload, the linear density of the nano-scaled kinks increased and they termed this model of tensile-overload induced strain damage discrete plasticity. In this type of damage, the collagen molecules uncoil and as such are then in a stable, denatured state.[25] This discrete plasticity is a distinct form of damage, which is different from the classical interpretation of tendon injury, which occurs during fatigue loading, where tendons exhibited kinked fiber deformations with widening of the inter fiber space.[26,27] This process of discrete plasticity is therefore considerably different from the classical model described.[26]

When single, triple helix collagen type I monomers are exposed to saline solution at body temperature, they become unstable and denature, essentially forming random coils.[28] However, when arranged as a fibril, the proximity of neighboring molecules

imparts conformational stability of the collagen molecule and thus imparts thermal stability in a form of stabilization known as polymer-in-a box constraint.[29] Discrete plasticity is a mode of fibrillar damage that occurs on the nanometer scale whereby collagen fibrils undergo discrete kinks, which results in a stable fibril **(Figure 1.4.5A)**.

The fibril is not a weak spot where total rupture subsequently occurs. As further overuse occurs, new discrete zones of plasticity develop resulting in an increase in the number of kinks.[25] The development of multiple kink sites is distinct from what was termed micro unfolding, which is an unfolding of the collagen molecule during which local regions of the collagen helix denature temporarily before refolding.[30,31]

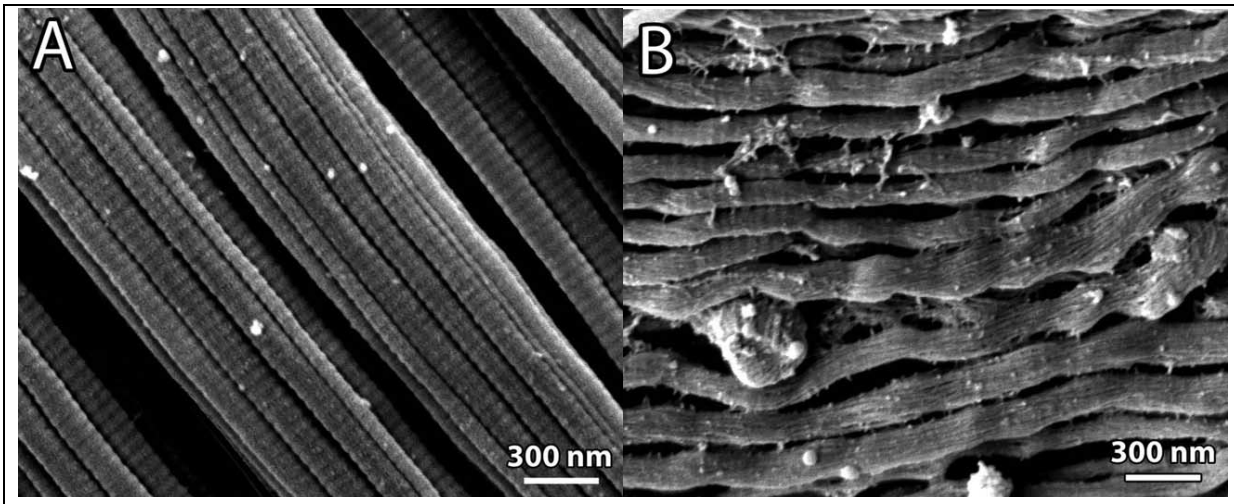

Figure 1.4.5A. **A:** Scanning electron micrographs of unloaded, control tendons which contained only native, undamaged fibrils. **B:** Highly kinked fibrils, characteristic of discrete plasticity, were found in overloaded tendons. Despite the kinking and partial loss of D-banding, note that the fibrils seem to be solid, having retained most of their substance. From Veres et al.[25]

1.4.6 Macrophages and Tendon Healing

The role of macrophages during wound healing has been heavily investigated and continues to evolve as further studies are conducted. Activated macrophages of different phenotypes are classified into M1 macrophages, which are classically activated and function primarily as immune effector cell with an inflammatory phenotype, and M2 macrophages, which are alternatively activated and considered anti-inflammatory.[6,32] Four different subtypes of M2 macrophages exist and have different functions, including regulation of immunity, maintenance of tolerance and tissue repair (**Figure 1.4.6A**).[33]

The heterogeneity and plasticity of macrophage populations allow them to play multiple, often complementary roles during tissue inflammation and healing. For example, M1 macrophages, characterized by the expression of CD68 and CD80, are mainly present in circulation and migrate to injured tissue to remove necrotic debris by phagocytosis. They are induced to differentiate when there is recognition of pathogen-associated molecular patterns (PAMPs), peptidoglycan, intracellular proteins and nucleic acids in addition to the T cell cytokine interferon gamma (IFN-γ).[34] They therefore exhibit a mainly phagocytic phenotype and antigen processing activity in addition to being a rich source of pro-inflammatory cytokines. M2 macrophages, characterized by CD68 and CD163 expression, are not involved in phagocytosis[35] but are involved in myogenic cell expression in rat skeletal muscle injury.[36,37] Furthermore, they are activated by a variety of stimuli including IL-4 and Il-13 and demonstrate a

phenotype that has been reported as being important in the promotion of wound healing and tissue remodeling in addition to resolving inflammation in injured tissue.[38]

In a rat Achilles tendon injury model, it was demonstrated that following the initial accumulation of neutrophils post injury, M1, followed by M2 macrophages arrived at the site.[6] While neutrophils and M1 macrophages peak at 24 hours post injury where populations increase by 46 and 18-fold respectively, the increase in M2 cells did not occur until day 3.[6] Neutrophils and M1 macrophage numbers returned to baselines values at 7 and 14 days post injury respectively.[6] Furthermore, it is well known that macrophages are a potent source of growth factors and cytokines, which stimulate angiogenesis, tenocyte proliferation and inflammatory cell recruitment, which all constitute part of the inflammatory phase of tendon healing.[39] It has been suggested that the rapidly invading neutrophils and M1 macrophages produce interleukin-1 (IL-1) and tumor necrosis factor (TNF), which inhibit fibroblast proliferation and stimulate extracellular matrix breakdown and that these factors are primarily released during injury.[6] With the recruitment of M2 macrophage, growth factors and cytokines stimulate fibroblasts and promote ECM synthesis but inhibit ECM degradation.[6]

As our knowledge of macrophages has increased, our understanding of macrophage polarization in healing has also increased in complexity. It is now clear that there are a broader range of signals that induce distinct macrophage phenotypes than the traditional M1/M2 classification permits. As previously stated, IL-4/IL-13 signaling was thought to be critical for differentiation of the M2 phenotype. However, the

existence of M2-like characteristics in macrophages has been identified in the absence of this type of signaling.[40] Furthermore, the co-stimulation of M1 macrophages with adenosine, activating the adenosine A_{2A} receptor and activation of Toll like receptors (TLR's), results in a phenotypic switch of the M1 phenotype into an M2d phenotype **(Figure 1.4.6A).**[41]

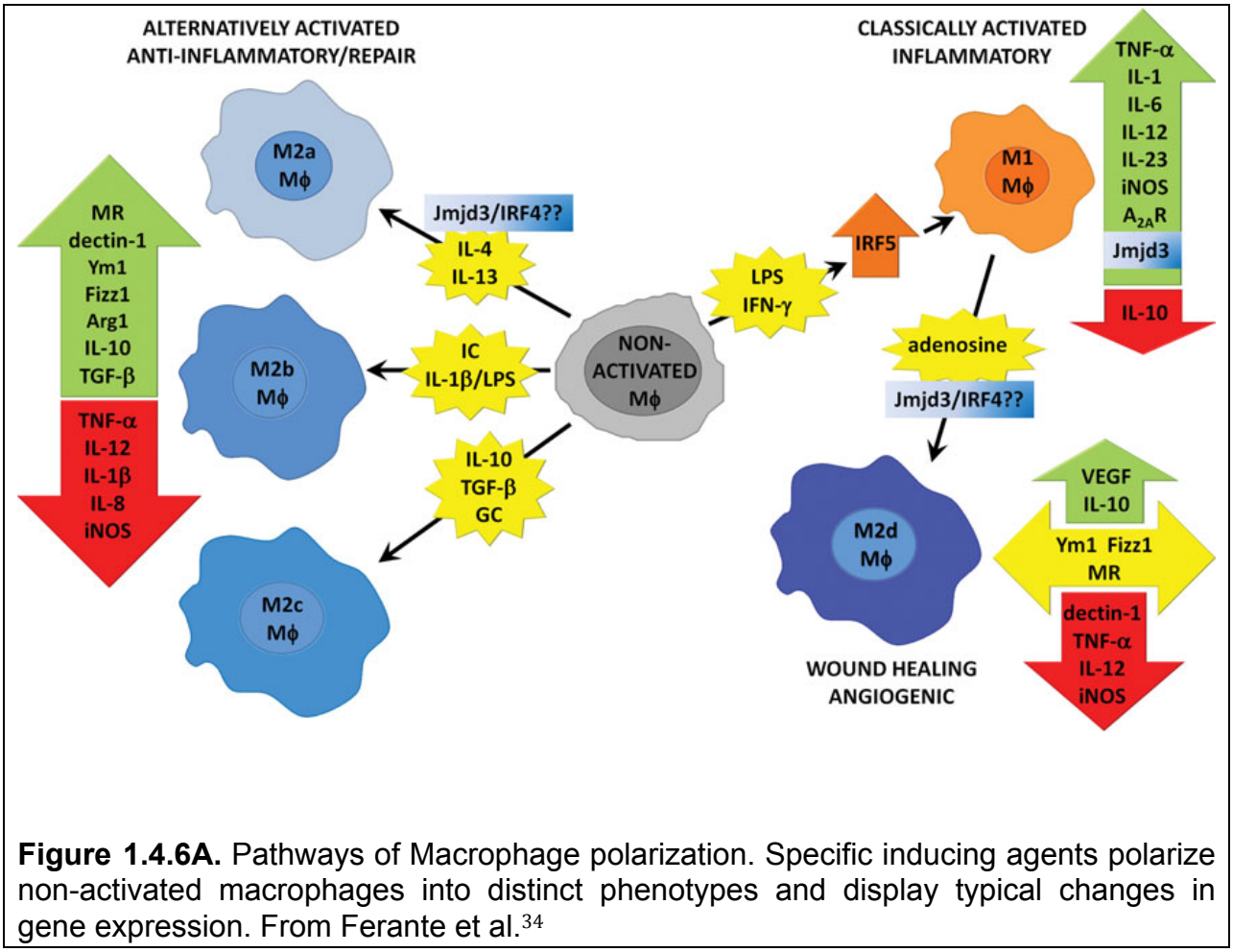

Figure 1.4.6A. Pathways of Macrophage polarization. Specific inducing agents polarize non-activated macrophages into distinct phenotypes and display typical changes in gene expression. From Ferante et al.[34]

A more complete understanding of the spatiotemporal changes in signaling molecules during tendon healing and the effects of macrophage plasticity are required **(Figure 1.4.6B).** However, it is feasible that the initial type of macrophage during tendon injury is representative of the M1 phenotype when clearance of damaged material is crucial. The heterogeneity of macrophages may therefore result in a change of phenotype and the resultant crosstalk between macrophage subtypes may result in the enhanced differentiation or recruitment of an M2 subclass during the later stages of wound healing in order to further direct tissue formation.[40]

1.4.7 Macrophage Collagen Interaction

There is a paucity of information regarding the interaction between macrophages and collagen fibrils.[25] The ECM plays a role in mechano-sensing and through integrin anchoring onto resident cells, can transmit tensile strains which are subsequently interpreted by the cells permitting a response.[42] Although there have been several studies which document macrophage phagocytizing and removing the extracellular matrix in areas of damage, the signaling and transduction pathways involved are unknown.[47,43,44] Macrophages are therefore an attractive cell to study as a primary collagen damage sensing cell as they are able to release a variety of matrix metalloproteinase enzymes and cathepsin in addition to possessing the ability to phagocytize collagen fibril fragments.[45,46]

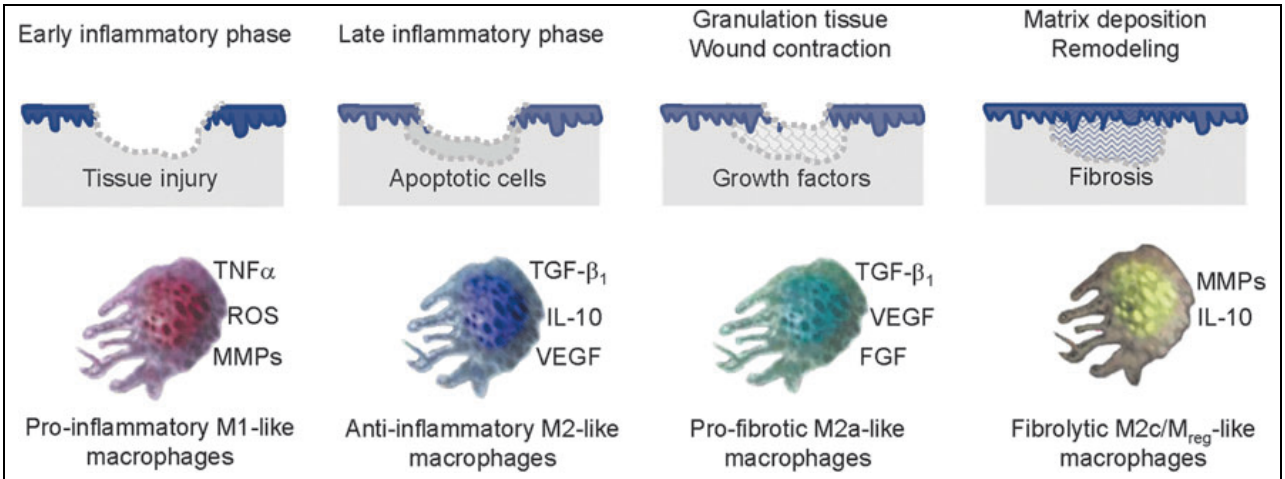

Figure 1.4.6B. Functional macrophage phenotypes proposed to be induced at different stages of normal tissue repair: **(1)** pro-inflammatory M1-like macrophages are induced by necrotic cells and/or infection in early inflammation (days 1–5 after wounding) and produce pro-inflammatory cytokines, proteases, and reactive oxygen species (ROS) to support host defense; **(2)** anti-inflammatory M2- like macrophages are induced on phagocytosis of apoptotic cells, which abundantly populate the wound tissue in the late inflammatory phase, around day 5 after wounding. They synthesize mediators that dampen inflammation (interleukin [IL]-10) and lay the foundation for new tissue formation **(3)** pro-fibrotic M2-like macrophages promote the granulation tissue formation and wound contraction by producing growth factors and extracellular matrix persisting in the wound milieu to day 10 after wounding; and **(4)** fibrolytic M2c/M reg-like macrophages may be induced in the ischemic scar milieu to secrete proteases and promote tissue remodeling without re-inducing inflammation due to simultaneous secretion of regulatory IL-10. From Sindrilau et al.[47]

Of particular interest is the heterogeneity in morphology of the macrophages membrane identified during attachment to damaged and intact collagen fibrils. The three morphologies identified; smooth, blebed and ruffled, have previously been characterized and represent indices of cellular activation.[25,48] In particular, the ruffled membrane morphology was associated with the greatest phagocytic activity.[25] The area on the kinked fibrils had a moth-eaten appearance indicative of degradation by enzymes **(Figure 1.4.6C)**. The study by Veres et al. also identified the expression of MMP-1 and

MMP-9 in these cell types and surrounding milieu. MMP-1 is an efficient cleaver of triple helical type I collagen, but a poor cleaver of denatured collagen.[49] MMP-9 is an efficient cleaver of denatured collagen, but not helical collagen.[50] When cultured on intact fibrils, the macrophage-like U937 cells secrete similar amounts of MMP-1 and MMP-9. However, when they are centered over areas of discrete plasticity, significantly less free MMP-9 is secreted into the medium, which may indicate that it is bound to the damaged collagen fibrils. These macrophage-like cells are able to detect and respond to the presence of collagen fibrils with discrete plasticity.[25] In this context, one cannot help draw the parallel between ruffled macrophage resulting in the release of proteolytic enzymes to cleave denatured collagen and osteoclastic resorption, via the release of protons, of mineralized bone matrix, an attractive paradigm considering both cell types have a common myeloid/monocyte precursor.

Further support for the ruffled membrane macrophage behavior occurred in studies utilizing the U937 macrophage-like cell line and collagen fibrils displaying discrete plasticity noted a difference in the morphological behavior of these cells when exposed to damaged collagen and intact collagen.[25] While centered on areas of discrete plasticity, macrophages demonstrate a ruffled membrane morphology, with evidence of enhanced spreading and attachment **(Figure 1.4.6C).** They tended to form clusters of smooth, flattened sheets in undamaged tissue; such a morphology was not encountered in areas of discrete plasticity. The ruffled macrophages were shown to degrade collagen fibrils specifically in areas of discrete plasticity.

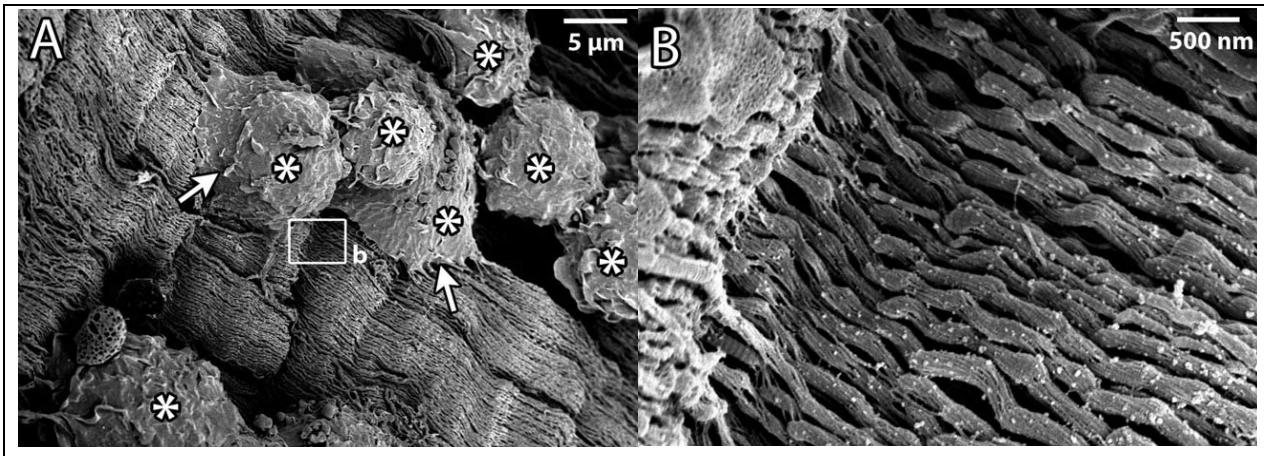

Figure 1.4.6C. The macrophage-like U937 cells found on collagen fibrils with strain-induced discrete plasticity are morphologically distinct from those found on undamaged fibrils. The cells showed a greater uniformity, being mostly of the ruffled type (* in **A**) and had acquired a dome-shape, increasing their contact area with the damaged fibrils (arrows in A). **B:** A magnified view of the boxed location in (A) shows the structure of the discrete plasticity fibril array that formed the substrate for these cells. From Veres et al. [25]

This leads to the conclusion that overstretching of tendons results in local uncoiling (denaturation)[24] and discrete plasticity is recognized by macrophages, enabling them to identify damaged collagen matrix and initiate phagocytosis of denatured collagen.[25] Therefore, there appears to be a critical role for macrophages in tendon healing, which is supported by studies that have identified that macrophage suppression results in a decrease in collagen type III deposition and decrease in myofibroblast recruitment at the injury site and this has negative consequences in terms of biomechanical repair strength.[51]

While there is evidence to suggest macrophages are crucial to recognizing and initiating the phagocytosis of areas of discrete plasticity, there is no current link into how this phenomenon may direct the activation and proliferation of fibroblasts, the cells of

repair in the tendon. Of significant interest from the Veres study is the presence of secreted matrix, produced via the ruffled macrophage, next to areas of discrete plasticity.[25] The matrix in this case is suspected to be fibronectin. Fibronectin is known to aid fibroblasts in the identification process of damaged collagen.[25] Furthermore, fibronectin deposits are known to be secreted at sites of ligament and tendon injury including ruptures.[52,53] It is also interesting to note that the binding of fibronectin to collagen is increased when that collagen is denatured.[54] Thus fibronectin may be an efficient tag for the identification of damaged fibrils. In order to repair fibrils that have suffered strain induced discrete plasticity, their denatured collagen content is required to be phagocytized. The area of damage can subsequently be recognized by macrophages that can remove denatured collagen fibrils and secrete the fibronectin in the fibrillar void. Following this collagenolysis, fibroblasts are able to locate regions of fibrillar void due to the presence of fibronectin. Soluble fibronectin is also a chemoattractant for fibroblasts, highlighting the multiple potential roles of this compound.[55] Once fibroblasts attach to the site of damage, they are able to secrete collagen to replace the damaged tissue and complete the repair process.

As previously suggested, ECM remodeling is also a critical process that occurs during development and tissue repair.[56] There is a significant amount of evidence that has demonstrated the deposition of fibronectin is a prerequisite for the deposition of collagen type I.[57,58] For example, in the absence of fibronectin, collagen type I is not deposited into the ECM, despite the presence of soluble collagen.[59] In addition it has been demonstrated that fibronectin stabilizes collagen type I matrix fibrils and reduces

the amount of collagen endocytosis by phagocytic cells, highlighting the importance of fibronectin in regulating the remodeling of both collagen fibrils and the ECM during tendon repair. [56]

In conclusion, there is evidence that discrete plasticity, or the stable denatured state of collagen fibrils, which occurs during tendon overloading, may be equivalent to micro-damage sustained in bone. As described, these areas of discrete plasticity are targeted by macrophages (the proposed osteoclastic equivalent cell of tendon), which release enzymes to removed denatured collagen and secrete fibronectin, a matrix that provided chemotaxis for fibroblasts to enter the area and secrete collagen and thus repair the damaged tendon. Further study is required in order to better ascertain the link between discrete plasticity, macrophage differentiation and fibroblastic recruitment in this form of proposed tendon repair.

References

1 **Carpenter, J.E. et al.** The effects of overuse combined with intrinsic or extrinsic alterations in an animal model of rotator cuff tendinosis. *Am J Sport Med* **26**, 801-807 (1998).

2 **Gelberman, R.H. et al.** Flexor tendon repair. *J Orthop Res* **4**, 119-128 (1986).

3 **Muller, S.A. et al.** Tendon healing: an overview of physiology, biology, and pathology of tendon healing and systematic review of state of the art in tendon bioengineering. *Knee Surg Sports Traumatol Arthrosc*, 1-9 (2013).

4 **Woo, S.L-Y. et al.** Injury and repair of ligaments and tendons. *Ann Rev Biomed Eng* **2**, 83-118 (2000).

5 **Sharma., P. & Maffulli, N.** Biology of tendon injury: healing, modeling and remodeling. *J Musculoskelet Neuronal Interact* **6**,181-190 (2006).

6 **Marsolais, D., Cŏté, C.H. & Frenette, J.** Neutrophils and macrophages accumulate sequentially following Achilles tendon injury. *J Orthop Res* **19**, 1203-1209 (2001).

7 **Voleti, P.B., Buckley, M.R. & Soslowsky, L.J.** Tendon healing: repair and regeneration. *Ann Rev Biomed Eng* **14**, 47-71 (2012).

8 **Riley, G.P. et al:** Matrix metalloproteinase activities and their relationship with collagen remodelling in tendon pathology. *Matrix Biol* **21**,185-195 (2002).

9 **Manske, P.R., Lesker, P.A.** Histologic Evidence of Intrinsic Flexor Tendon Repair in Various Experimental Animals An In Vitro Study. *Clin Orthop Rel Res* **182**, 297-304 (1984).

10 **Ingraham, J.M., Hauck, R.M. & Ehrlich, H.P.** Is the tendon embryogenesis process resurrected during tendon healing? *Plast Recon Surg* **112**, 844-854 (2003).

11 **Kato, Y.P. et al.** Mechanical properties of collagen fibres: a comparison of reconstituted and rat tail tendon fibres. *Biomat* **10**, 38-42 (1989).

12 **Carpenter, J.E. et al.** The effects of overuse combined with intrinsic or extrinsic alterations in an animal model of rotator cuff tendinosis. *Am J Sport Med* **26**, 801-807 (1998).

13 **Gelberman, R.H. et al.** Flexor tendon repair. *J Orthop Res* **4**,119-128 (1986).

14 **Fujita,M., Hukuda, S. & Doida, Y.** Experimental study of intrinsic healing of the flexor tendon: collagen synthesis of the cultured flexor tendon cells of the canine. *Nihon Seikeigeka Gakkai zasshi* **66**, 326-333 (1992).

15 **Uhthoff, H.K. & Sarkar, K.** Surgical repair of rotator cuff ruptures. The importance of the subacromial bursa. *J Bone Joint Surg Br* **73**, 399-401 (1991).

16 **Schneider, L. & Hunter, J.** Flexor tendons-late reconstruction. *Operat Hand Surg* ***2***, 1898-1893 (1999).

17 **Ehrlich, H.P. et al.** Dynamic changes appearing in collagen fibers during intrinsic tendon repair. *Ann Plast Surg* **54**, 201-206 (2005).

18 **Banes, A. & Qi, J.** Modulation of cell intrinsic strain to control matrix synthesis, secretion, organization and remodeling, in, *Vol Google Patents,* (2004).

19 **Peltz, C.D. et al.** Exercise following a short immobilization period is detrimental to tendon properties and joint mechanics in a rat rotator cuff injury model. *J Orthop Res* **28**, 841-845 (2010).

20 **Arnoczky, S.P., Lavagnino, M. & Egerbacher, M.** The mechanobiological aetiopathogenesis of tendinopathy: is it the over□stimulation or the under□ stimulation of tendon cells? *Int J Exp Pathol* **88**, 217-226 (2007).

21 **Smith, R.K. & Goodship, A.E.** Tendon and Ligament physiology: responses to exercise and training. *Equine Exercise Physiology: The Science of Exercise in the Athletic Horse*,**106** (2008).

22 **Knörzer, E. et al.** New aspects of the etiology of tendon rupture. *Arch Orthop Traumat Surg* **105**, 113-120 (1986).

23 **Veres, S.P. & Lee, J.M.** Designed to fail: a novel mode of collagen fibril disruption and its relevance to tissue toughness. *Biophys* **102**, 2876-2884 (2012).

24 **Veres, S.P., Harrison, J.M. & Lee, J.M.** Mechanically overloading collagen fibrils uncoils collagen molecules, placing them in a stable, denatured state. *Matrix Biol* **33**, 54-59 (2013).

25 **Veres, S.P., Brennan□Pierce, E.P. & Lee, J.M.** Macrophage□like U937 cells recognize collagen fibrils with strain□induced discrete plasticity damage. *J Biomed Mat Res A*, (2014).

26 **Fung, D.T. et al.** Early response to tendon fatigue damage accumulation in a novel in vivo model. *Biomech* **43**, 274-279 (2010).

27 **Fung, D.T. et al.** Second harmonic generation imaging and Fourier transform spectral analysis reveal damage in fatigue-loaded tendons. *Ann Biomed Eng* **38**, 1741-1751 (2010).

28 **Leikina, E. et al.** Type I collagen is thermally unstable at body temperature. *Proc Nat Acad Sci* **99**, 1314-1318 (2002).

29 **Miles, C.A. & Ghelashvili, M.** Polymer-in-a-box mechanism for the thermal stabilization of collagen molecules in fibers. *Biophys* **76**, 3243-3252 (1999).

30 **Kadler, K.E., Hojima, Y. & Prockop, D.** Assembly of type I collagen fibrils de novo. Between 37 and 41 degrees C the process is limited by micro-unfolding of monomers. *Biol Chem* **263**, 10517-10523 (1988).

31 **Kadler, K. et al.** Collagen fibril formation. *Biochem* **316**, 1-11 (1996).

32 **Dakin, S.G. et al.** Macrophage sub-populations and the lipoxin A4 receptor implicate active inflammation during equine tendon repair. *PloS one* 7:e32333 (2012).

33 **Millar, N.L. et al.** Inflammation is present in early human tendinopathy. *Am J Sport Med **38***, 2085-2091 (2010).

34 **Ferrante, C.J. & Leibovich, S.J.** Regulation of macrophage polarization and wound healing. *Adv Wound Care* **1**,10-16, (2012).

35 **McLennan, I.S.** Resident macrophages (ED2-and ED3-positive) do not phagocytose degenerating rat skeletal muscle fibres. *Cell Tissue Res* **272**,193-196 (1993).

36 **Massimino, M. et al.** ED2+ macrophages increase selectively myoblast proliferation in muscle cultures. *Biochem Biophys Res Comm* **235**, 754-759 (1997).

37 **Murray, P.J. & Wynn, T.A.** Protective and pathogenic functions of macrophage subsets. *Nature Rev Immunol* **11**, 723-737 (2011).

38 **Martinez, F.O., Helming, L. & Gordon, S.** Alternative activation of macrophages: an immunologic functional perspective. *Ann Rev Immunol* **27**, 451-483 (2009).

39 **Ding, A.H., Nathan, C.F. & Stuehr, D.J.** Release of reactive nitrogen intermediates and reactive oxygen intermediates from mouse peritoneal

macrophages. Comparison of activating cytokines and evidence for independent production. *Immunol* **141**, 2407-2412 (1988).

40 **Daley, J.M. et al.** The phenotype of murine wound macrophages. *J Leuk Biol* **87**, 59-67 (2010).

41 **Grinberg, S. et al.** Suppression of PLCβ2 by Endotoxin Plays a Role in the Adenosine A 2A Receptor-Mediated Switch of Macrophages from an Inflammatory to an Angiogenic Phenotype. *Am J Pathol* **175**, 2439-2453 (2009).

42 **Arnoczky, S.P., Lavagnino, M. & Egerbacher, M.** The mechanobiological aetiopathogenesis of tendinopathy: is it the over□stimulation or the under□ stimulation of tendon cells? *Int J Exp Pathol* **88**, 217-226 (2007).

43 **Li, S. et al.** Macrophage depletion impairs corneal wound healing after autologous transplantation in mice. *PloS one,* 8:e61799 (2013).

44 **Li, F. et al.** Cell shape regulates collagen type I expression in human tendon fibroblasts. *Cell Mot Cytoskelet* **65**, 332-341 (2008).

45 **Vérollet, C. et al.** Extracellular proteolysis in macrophage migration: losing grip for a breakthrough. *Europ J Immunol* **41**, 2805-2813 (2011).

46 **Svoboda, E. & Deporter, D.** Phagocytosis of exogenous collagen by cultured murine fibroblasts and macrophages: A quantitative electron microscopic comparison. *J Ultrastruct Res* **72**, 169-173 (1980).

47 **Sindrilaru, A. & Scharffetter-Kochanek, K.** Disclosure of the Culprits: Macrophages—Versatile Regulators of Wound Healing. *Adv Wound Care* **2**, 357-368 (2013).

48 **Finch, G. et al.** Surface morphology and functional studies of human alveolar macrophages from cigarette smokers and nonsmokers. J *Reticuloendoth Soc* **32**, 1-23 (1982)

49 **Knäuper, V. et al.** Cellular mechanisms for human procollagenase-3 (MMP-13) activation Evidence that MT1-MMP (MMP-14) and gelatinase a (MMP-2) are able to generate active enzyme. *Biol Chem* **271**, 17124-17131 (1996).

50 **Riley, G.P. et al.** Matrix metalloproteinase activities and their relationship with collagen remodelling in tendon pathology. *Matrix Biol* **21**, 185-195 (2002).

51 **Chamberlain, C.S. et al.** The influence of macrophage depletion on ligament healing. *Connect Tissue Res* **52**, 203-211 (2011).

52 **Amiel, D. et al.** Fibronectin in healing flexor tendons subjected to immobilization or early controlled passive motion. *Matrix* **11**, 184-189 (1991).

53 **Neurath, M.** Expression of tenascin, laminin and fibronectin following traumatic rupture of the anterior cruciate ligament. *Zeitschrift fur Orthopadie und ihre Grenzgebiete* **131**, 168-172 (1992).

54 **Rucklidge, G.J., Riddoch, G.I. & Robins, S.P.** Immunocytochemical staining of rat tissues with antibodies to denatured type I collagen: a technique for localizing areas of collagen degradation. *Coll Rel Res* **6**, 41-49 (1986).

55 **Rennard, S.I. et al.** Production of fibronectin by the human alveolar macrophage: mechanism for the recruitment of fibroblasts to sites of tissue injury in interstitial lung diseases. *Proc Nat Acad Sci* **78**, 7147-7151 (1981).

56 **Shi, Y. et al.** Regulation of apoptosis during development: input from the extracellular matrix (review). *Int J Molec Med* **2**, 273-355 (1998).

57 **Sottile, J. & Hocking, D.C.** Fibronectin polymerization regulates the composition and stability of extracellular matrix fibrils and cell-matrix adhesions. *Molec Biol Cell* **13**, 3546-3559 (2002).

58 **Sottile, J. et al.** Fibronectin-dependent collagen I deposition modulates the cell response to fibronectin. *Am J Physiol Cell Physiol* **293**, C1934-C1946 (2007).

59 **Velling, T. et al.** Polymerization of type I and III collagens is dependent on fibronectin and enhanced by integrins α11β1and α2β1. *Biol Chem* **277**, 37377-37381 (2002).

1.5 Tendon Healing Interventions

1.5.1 Genes and Tendon Healing

Although there is a high incidence of injuries to the Achilles tendon sustained during exercise, there is an incomplete understanding in regard to the mechanisms, which may lead to tendon disruption. Some studies have identified the role that genetics may play in increasing susceptibility to Achilles tendon injury. The identification of the link between the ABO blood group genes and Achilles tendon pathology led researchers to consider other genetic candidates located on chromosome 9 (9q32-q34) which are closely linked to the ABO gene [1] Two genes, which encode for ECM tendon components, are the tenascin-c gene and the col5A1 gene.[2]

The COL5A1 gene encodes for a component of collagen type V, the pro alpha 1(V) collagen chain. Although minor amounts of collagen type V are found in tendons, they do tendon to form heterotypic fibers with collagen type I.[3] Based on the role collagen type V plays in the cornea, there is speculation that collagen type V may function as a regulator of fibrillogenesis in tendons via the modulation of fibril growth.[4]

The role of collagen type V was investigated in the rabbit patellar tendon, where Dressler identified an age-dependent increase in type V content coupled with a decrease in fibril diameter and biomechanical properties of the tendon.[5] Although such studies provide evidence to support the role of collagen type V genes in Achilles

tendinopathy, there are none that provide a conclusive link.

Another candidate gene in close proximity to COL5A1 is the tenascin-c gene.[6] The role of tenascin-c is coupled to the regulatory function of the ECM, thus there may be an important role in cell-matrix communication and interaction.[7] Classically, tenascin-c is associated in high concentration in regions responsible for the transmission of mechanical force, such as the myotendinous or osseotendinous junctions.[6] Jarvinen et al demonstrated that the expression of the tenascin-c gene is regulated in a dose dependent manner by mechanical loading in tendons[8], thus a possible conclusion from this is that it plays a role in mechano-sensing and may be responsible for the remodeling of tendon tissue in response to loading.

Although COL5A1 and tenascin-c genes have been associated with Achilles tendon injuries, further research is required to elucidate the role other candidate genes may have in this heterotopic condition.[9]

1.5.2 Growth Factors in Tendon Healing

A growth factor definition has classically been used in the sense that it a substance, which can cause growth, proliferation or differentiation of a target cell and is usually a protein. As such, growth factors are implied to have positive or anabolic effects. Cytokine, which is a term with no specific implications in regard to function, can encompass proteins which have anabolic and catabolic effects, which are both essential

in wound healing.[10] As previously described, wound healing is a complex process involving several overlapping stages that include inflammation, the formation of granulation tissue and ECM remodeling.[11]

Numerous growth factors have been identified in wound healing.[12] Despite research into healing, few studies have been performed which comment on the time of the appearance of growth factors in the different phases of tendon healing.[13] However, growth factors may be produced by cells in the area of injury, by cells involved in the repair process, or may be delivered via the blood. The blood components that are released at the site of injury produce a clot with the activation of the clotting cascade and the resulting matrix forms a scaffold for the influx of inflammatory cells. Platelet degranulation occurs in the area of damage, releasing growth factors from alpha granules such as epidermal growth factor, (EGF), platelet derived growth factor (PDGF), transforming growth factor beta (TGF-β) and vascular endothelial growth factor (VEGF).[14] IL-1 along with PDGF is important chemotactic agents for the arrival of neutrophils to the site of injury.[15] With the assistance of TGF-β, monocytes are encourage to differentiate into macrophages that augment the inflammatory response and can stimulate both catabolic and anabolic pathways.[13] Furthermore, they initiate the formation of granulation tissue and are a further source for growth factor release such as fibroblast growth factor (FGF).

The final product of wound healing is a scar and the construction of this tissue is the result of complex interaction of signals that coordinate cellular processes.[16] The bioactive agents released in this context may act by paracrine, autocrine or endocrine pathways and can bind to ECM proteins or cellular receptors to initiate a cascade of molecular events.

The culmination of the growth factor-receptor interaction is the binding of transcription factors to gene promoters that modulate cellular function.[17] One of the major influences on the proliferation of fibroblasts, a significant cellular component of repaired tendinous tissue, is FGF.[18]

1.5.3 Fibroblast Growth Factor (FGF)

The FGF family comprises 23 members, part of the heparin binding growth factor family. FGF has been shown to demonstrate angiogenicity, via the up regulation of VEGF and mitogenic effects in many mesenchymal cells, such as fibroblasts.[19,20] It has also been shown to stimulate the production of urokinase plasminogen activator (uPA), a protease required for neovascularization.[21] FGF acts on high affinity FGF receptors (FGFR), of which four have been identified. These receptors are primarily tyrosine kinase transmembrane proteins.

FGF-2 or basic FGF (bFGF) is a single chain polypeptide of 146 amino acids, which has a significant impact on wound healing, playing critical roles in granulation tissue formation, re-epithelization and tissue remodeling.[12] In addition, FGF-2 regulates the synthesis and deposition of various ECM proteins and has been shown to promote the migration of fibroblasts and stimulate them to produce collagenases.

The importance of FGF-2 has also been documented in tendon repair, with studies demonstrating a peak expression in the first week of a midsubstance supraspinatus tendon injury model in the rabbit.[22] A further peak at an eight-week time point was noted in another study, which implies that the FGF may have important roles in a variety of the phases of repair.[23] Several studies have also documented that supplementation with FGF during healing results in superior biomechanical outcomes.[22]

The most abundant FGFs in normal adult tissue are FGF-1 (acidic FGF) and FGF-2 (basic FGF). Although both have been identified during the early stages of bone and tendon repair, FGF-2 is the more potent mitogen.[24] In animal models, local application of FGF-2 facilitated the healing of segmental bone defects and full-thickness defects of the articular cartilage.[25] Due to its release by inflammatory cells early in wound healing, FGF-2 helps to initiate the formation of granulation tissue and plays a role in soft tissue remodeling.[26] FGF-2 supplementation has show significant promise in tendon healing, both in terms of histological characterization[27] and mechanical strength.[28] However, one of the key features preventing natural tendon repair is a significant lack of vascular supply preventing the delivery of essential repair molecules

to the site of damage. During the proliferative phase, there must be significant vascularization of the site of injury in order to achieve a functional repair.

1.5.4 Transforming Growth Factor- β (TGF-β)

The TGF-β family includes TGF-β isoforms 1-3, the bone morphogenic proteins (BMP's) and activins.[29] During embryogenesis, the TGF superfamily has been closely linked to the formation of tendons and their differentiation with other growth factors, but TGF-β has been shown to be a strong stimulator of ECM formation, but a weak stimulator of tenocyte migration and mitogenesis.[30] FGF's are primarily produced by macrophage, fibroblasts, keratinocytes and platelets, and function by binding a heteromeric receptor complex of type I and type II receptors both of which are serine-threonine kinases.[12] A non-signaling type III receptor binds the TGF-β peptide and presents it to the type II receptor, resulting in autophosphorylation and culminating in the activation of the Smad family of transcription factors.[31] The primary gene expressed in the Smad pathway is TGF-β inducible early gene (TIEG).[32] Healing of tendon tissue in TIEG knock out mice suggested that tendon healing can occur in the absence of Smad and that Smad independent pathways of tendon healing also exist.[30] However, TGF-β receptor expression has been shown to be up regulated during injury and repair, concentrated in the epitenon, tendon sheath and repair site, with levels peaking at day 14 and remaining elevated until day 56 in a rabbit flexor tendon model.[33]

Also of interest is that although all three TGF-β isoforms increase collagen type I and III production in cultured tendon fibroblasts, TGF-β1 induces a greater degree of contraction in comparison to the other isoforms.[34] This provides the possibility that the TGF-B isoforms may interact with one another to modulate collagen synthesis during the healing process.

1.5.5 Bone Morphogenic Proteins (BMP's)

Although classically BMP's were associated with bone healing, they also stimulate tendon cell mitogenesis and tendon healing. For example, in BMP-14 knockout mice, a delayed healing response in tendon injury is observed, with smaller, irregular collagen type I fibers observed.[35] The conclusions from several studies in the BMP category have noted that BMP-13 is important in early tendon healing, BMP-14 is important in tendon homeostasis and BMP-12 is required for both.[36] Of note also is that tenoblasts demonstrate elevated levels of BMP-12 and 13 in comparison to tenocytes, which suggest that the immature tenoblast may be more active in tendon remodeling and healing than the mature tenocyte.[37]

A subgroup of the BMP family is the cartilage derived morphogenic proteins (CDMP). CDMP-1 and 2 play crucial roles in embryonic skeletal muscle development, joint morphogenesis and tendon formation.[38] CDMP-2 treated tendon repairs were significantly stronger than untreated repairs at 4 and 6 weeks postoperatively and in rabbits, CDMP injection into transected Achilles tendon resulted in a 35% increase in

mechanical strength 14 days post operatively in comparison to controls, highlighting an important role for this molecule. [39]

1.5.6 Platelet Derived Growth Factor (PDGF)

PDGF, initially isolated from platelets but produced by a variety of tissues including macrophage, vascular endothelium and fibroblasts, is a basic protein of approximately 30 kDa formed by 2 subunits, comprising a family of homo or heterodimeric growth factors including AA, AB, BB, CC and DD isoforms.[40] PDGF binds to two different transmembrane tyrosine kinase receptors comprising alpha and beta units. Binding of PDGF results in receptor dimerization and autophosphorylation, creating an active site for SH2 (Src homology 2) domain containing signaling molecules activating several signaling pathways.[41] Initially during injury, PDGF is released from platelets and stimulates the mitogenicity and chemotaxis of neutrophils, macrophage, fibroblasts and neutrophils to the region of injury.[42] PDGF has also been demonstrated to stimulate macrophage to secret TGF-β and mediates macrophage mediated tissue debridement via phagocytosis and granulation tissue formation.[29] Furthermore, PDGF has been shown to lead to the induction of VEGF and VEGF-2 receptor in cardiac microvascular cells and combined with hypoxic conditions, plays a pivotal role in the stimulation of angiogenesis.[43] Once formed, new blood vessels are fragile and PDGF stimulates the maturation and stability of these newly formed vascular channels by recruiting pericytes to the capillaries.[44] Therefore, although PDGF has an important role in angiogenesis, its angiogenic effect is weaker than FGF-2 or VEGF and is not

essential to blood vessel formation. In terms of tendon repair, most studies have focused on the homodimer PDGF-BB. It was shown that early supplementation (day 3 post injury) in rat patellar tendons, was not beneficial in restoring mechanical properties, but when administered at day 7 post injury, a significant benefit was noted in stimulating matrix production and pyridinoline content.[42]

1.5.7 Vascular Endothelial Growth Factor (VEGF)

The term VEGF includes proteins from 2 families that result from alternative splicing of mRNA from a single, 8 exon, VEGF gene, which include VEGF-A, VEGF-B, VEGF-C, VEGF-D, VEGF-E and placental growth factor. VEGF-A is produced by a variety of cells including endothelial cells, fibroblast smooth muscle cells, platelets, neutrophils and macrophage. The most important member of this group is VEGF-A, a glycosylated protein of 46 to 48 kDa composed of 2 disulfide linked subunits. VEGF-A binds to tyrosine kinase surface receptors Flt-1 (VEGF receptor 1, VEGFR1) and KDR (VEGF receptor 2, VEGFR2), localized to the endothelial surface of capillaries[45] VEGFR1 is required for the organization of blood vessels and in mediating vascular permeability, and the induction of anti-apoptotic genes.[45] VEGFR2 is important for the chemotaxis and proliferation of endothelial cells and in inducing endothelial cell differentiation.[45] In both canine and human tendon transections, VEGF has been associated with the formation of fine new vessels at the tip of the transection in addition to adhesions to the surrounding vascularized connective tissues.[46] Also of note is that in normal human adult Achilles tendon, VEGF mRNA expression is negligible, but is

significantly elevated in ruptured tendon tissue and in embryonic forms. Furthermore, a synergistic role exists between hypoxic conditions and members of the epidermal growth factor family (EGF), which includes TGF-alpha, which increase VEGF expression 30-40 fold, compared to less than a 6-fold increase with either hypoxia or EGF alone.[47]

The expression of VEGF can be induced by hypoxia, and increased levels have been seen after cyclical loading of tendons as well as in tendinitis and ruptured tendons.[47,48,49] Attempts to improve Achilles tendon healing by adding VEGF has shown a possibly improved tensile strength early in the healing period.[50] Increases in VEGF have also been found after flexor tendon injury, with higher levels of mRNA surrounding the repair site in the tendon seven to 10 days after surgery, returning to normal levels within 2 weeks.[51] Previous studies have shown that VEGF is not only re-expressed in tendon overuse injuries but also in a tenotomy model in sheep[52] and during the remodeling of autologous tendon grafts.[53] It may therefore play several roles at multiple stages of tendon healing.

In conclusion, there is a critical role of growth factor signaling in the early stages of tendon healing. Growth factors are critical for coordinating multiple cell types during healing to permit the successful completion of the repair process. During the early phases those growth factors that stimulate the chemotaxis and proliferation of inflammatory cells such as neutrophils and macrophage to the site of injury are important. Later on during the process, growth factors that activate both intrinsic and

extrinsic processes of healing during the proliferative phase are crucial to stimulate not only tenocytes and tenoblast but also fibroblast to produce collagen and ECM, which are required before the remodeling phase can occur. Many of these growth factors work in concert with each other to orchestrate an elegant functional repair of the tendon tissue.

Collectively, the previously mentioned studies in relation to growth factors provide a clear motivation for development of clinically relevant controlled cytokine delivery systems. The characteristics of tendon healing also strongly suggest that multiple cytokines are likely to function synergistically during tendon repair if introduced in a temporally regulated manner. This concept is supported in particular by the aforementioned role of multiple distinct cytokines during the major stages of natural tendon healing. Taken together, previous studies indicate that cytokines can positively influence tendon healing, and suggest that temporally controlled delivery strategies for multiple cytokines are critical to address current clinical limitations associated with tendon healing.

The combination of FGF and VEGF, evaluated by this thesis, may therefore overcome the disadvantages of each cytokine used individually and studies have already demonstrated synergistic effects in other areas of research.[54] We chose to initially focus our research on these two cytokines, as they are known to play a major role in the proliferative phase, during which time the greatest increase in tendon strength occurs.

References

1 **Kujala, U. et al.** ABO blood groups and musculoskeletal injuries. *Injury* **23**, 131-133 (1992).

2 **Mokone, G. G., Schwellnus, M. P., Noakes, T. D. & Collins, M.** The COL5A1 gene and Achilles tendon pathology. *Scand J Med Sci Sport* **16**, 19-26 (2006).

3 **Silver, F. H., Freeman, J. W. & Seehra, G. P.** Collagen self-assembly and the development of tendon mechanical properties. *J Biomech* **36**, 1529-1553 (2003).

4 **Birk, D. E.** Type V collagen: heterotypic type I/V collagen interactions in the regulation of fibril assembly. *Micron* **32**, 223-237 (2001).

5 **Dressler, M. R. et al.** A potential mechanism for age related declines in patellar tendon biomechanics. *J Orthop Res* **20**, 1315-1322 (2002).

6 **Chiquet, M., & Fambrough, D. M.** Chick myotendinous antigen. I. A monoclonal antibody as a marker for tendon and muscle morphogenesis. *J Cell Biol* **98**, 1926-1936 (1984).

7 **Jones, F. S. & Jones, P. L.** The tenascin family of ECM glycoproteins: structure, function, and regulation during embryonic development and tissue remodeling. *Devel Dynam* **218**, 235-259 (2000).

8 **Järvinen, T. A. et al.** Mechanical loading regulates the expression of tenascin-C in the myotendinous junction and tendon but does not induce de novo synthesis in the skeletal muscle. *Cell Sci* **116**, 857-866 (2003).

9 **Ajis, A. & Maffulli, N**. Genes and the Achilles Tendon. *Achilles tendon. Mafulli N and Almekinders LC (Ed). Springer-Verlag London Limited*. (2007).

10 **Frank, C. & Hart, D.** The biology of tendons and ligaments, in *Biomechanics of Diarthrodial Joints*, Vol I, Springer, 39-62 (2003).

11 **Voleti, P.B., Buckley, M.R. & Soslowsky, L.J.** Tendon healing: repair and regeneration. *Ann Rev Biomed Eng* **14**, 47-71 (2012).

12 **Oliva, F., Via, A.G. & Maffulli, N.** Role of growth factors in rotator cuff healing. *Sport Med Arthrosc Rev* **19**, 218-226 (2011).

13 **Barrientos, S. et al:** Growth factors and cytokines in wound healing. *Wound Repair Regen* **16**, 585-601 (2008).

14 **Rozman, P. & Bolta, Z.** Use of platelet growth factors in treating wounds and soft-tissue injuries. *Acta Dermat Alpina Panonica Adriat* **16**,156-158 (2007).

15 **Marsolais, D., Cŏté, C.H. & Frenette J.** Neutrophils and macrophages accumulate sequentially following Achilles tendon injury. *J Orthop Res* **19**, 1203-1209 (2001).

16 **Williams, I., McCullagh, K. & Silver, I.** The distribution of types I and III collagen and fibronectin in the healing equine tendon. *Conn Tissue Res* **2**, 211-227 (1984).

17 **Molloy, T., Wang, Y. & Murrell, G.A.** The roles of growth factors in tendon and ligament healing. *Sport Med* **33**, 381-394 (2003).

18 **Tozer, S. & Duprez, D.** Tendon and ligament: development, repair and disease. *Birth Def Res Part C: Embryo Today: Rev* **75**, 226-236 (2005).

19 **Gabra, N., Khiat, A. & Calabresi, P.** Detection of Elevated Basic Fibroblast Growth Factor During Early Hours of in Vitro Angiogenesis Using a Fast ELISA Immunoassay. *Biochem Biophys Res Comm* **205**, 1423-1430 (1994).

20 **Lee, J., Green, M.H. & Amiel, D.** Synergistic effect of growth factors on cell outgrowth from explants of rabbit anterior cruciate and medial collateral ligaments. *J Orthop Res* **13**, 435-441 (1995).

21 **Besser, D., Presta, M. & Nagamine, Y.** Elucidation of a signaling pathway induced by FGF-2 leading to uPA gene expression in NIH 3T3 fibroblasts. *Cell Growth Differ* **6**, 1009-17 (1995).

22 **Kobayashi, M. et al:** Expression of growth factors in the early phase of supraspinatus tendon healing in rabbits. *J Should Elbow Surg* **15**, 371-377 (2006).

23 **Würgler-Hauri, CC. et al:** Temporal expression of 8 growth factors in tendon-to-bone healing in a rat supraspinatus model. *J Should Elbow Surg* **16**, S198-S203 (2007).

24 **Canalis, E., Centrella, M. & McCarthy, T.** Effects of basic fibroblast growth factor on bone formation in vitro. *J Clin Invest* **81**, 1572-7 (1988).

25 **Provenzano, P.P. et al.** Intrinsic fibroblast-mediated remodeling of damaged collagenous matrices in vivo. *Matrix Biol* **23**, 543-55 (2005).

26 **Gospodarowicz, D., Neufeld, G. & Schweigerer, L.** Molecular and bio- logical characterization of fibroblast growth factor, an angiogenic factor which also

controls the proliferation and differentiation of mesoderm and neuroectoderm derived cells. *Cell Differ* **19**, 1-17 (1986).

27 **Kohno, T. et al.** Immunohistochemical demonstration of growth factors at the tendon-bone interface in anterior cruciate ligament reconstruction using a rabbit model. *J Orthop Sci* **12**, 67-73 (2007).

28 **Bachl, N. et al.** Therapeutic use of growth factors in the musculoskeletal system in sports-related injuries. *J Sports Med Phys Fitness*. **49**, 346-57 (2009).

29 **Chan, K.M. et al**: Expression of transforming growth factor β isoforms and their roles in tendon healing. *Wound Repair Regen* **16**, 399-407 (2008).

30 **Banes, A.J. et al.** PDGF-BB, IGF-I and mechanical load stimulate DNA synthesis in avian tendon fibroblasts in vitro. *J Biomech* **28**, 1505-1513 (1995).

31 **Heldin, C-H., Miyazono, K. & Dijke, P.** TGF-β signalling from cell membrane to nucleus through SMAD proteins. *Nature* **390**, 465-471 (1997).

32 **Tsubone, T. et al:** Effect of TGF□β inducible early gene deficiency on flexor tendon healing. *J Orthop Res* **24**, 569-575 (2006).

33 **Ngo, M. et al:** Differential expression of transforming growth factor-beta receptors in a rabbit zone II flexor tendon wound healing model. *Plast Reconst Surg* **108**, 1260-1267 (2001).

34 **Campbell, B., Agarwal, C. & Wang, J-C.** TGF-β1, TGF-β3, and PGE2 regulate contraction of human patellar tendon fibroblasts. *Biomech Mod Mechanobiol* **2**, 239-245 (2004).

35 **Chhabra, A. et al.** GDF□5 deficiency in mice delays Achilles tendon healing. *J Orthop Res* **21**, 826-835 (2003).

36 **Eliasson, P., Fahlgren, A. & Aspenberg, P.** Mechanical load and BMP signaling during tendon repair: a role for follistatin? *Clin Orthop Rel Res* **466**, 1592-1597 (2008).

37 **Fu, S.C. et al.** The roles of bone morphogenetic protein (BMP) 12 in stimulating the proliferation and matrix production of human patellar tendon fibroblasts. *Life Sci* **72**, 2965-2974 (2003).

38 **Erlacher, L. et al:** Cartilage□derived morphogenetic proteins and osteogenic protein□1 differentially regulate osteogenesis. *J Bone Mineral Res* **13**, 383-392 (1998).

39 **Forslund, C. & Aspenberg, P.** Improved healing of transected rabbit Achilles tendon after a single injection of cartilage-derived morphogenetic protein-2. *Am J Sport Med* **31**, 555-559 (2003).

40 **Dahlgren, L.A., Mohammed, H.O. & Nixon, A.J.** Temporal expression of growth factors and matrix molecules in healing tendon lesions. *J Orthop Res* **23**, 84-92 (2005).

41 **Escobedo, J.A. et al.** cDNA cloning of a novel 85 kd protein that has SH2 domains and regulates binding of PI3-kinase to the PDGF β-receptor. *Cell* **65**, 75-82 (1991).

42 **Chan, B. et al:** Supplementation-time dependence of growth factors in promoting tendon healing. *Clin Orthop Rel Res* **448**, 240-247 (2006).

43 **Hao, X. et al:** Angiogenic effects of sequential release of VEGF-A165 and PDGF-BB with alginate hydrogels after myocardial infarction. *Cardiovasc Res* **75**, 178-185 (2007).

44 **Lindahl, P. et al:** Pericyte loss and microaneurysm formation in PDGF-B-deficient mice. *Science* **277**, 242-245 (1997).

45 **Ferrara, N., Gerber, H-P. & LeCouter, J.** The biology of VEGF and its receptors. *Nature Med* **9**, 669-676 (2003).

46 **Matthews, J.P.** Vascular changes in flexor tendons after injury and repair: an experimental study. *Injury* **8**, 227-233 (1977).

47 **Pufe, T. et al**. The angiogenic peptide vascular endothelial growth factor is expressed in foetal and ruptured tendons. *Virchows Arch* **439**, 579–585 (2001).

48 **Pufe, T. et al.** The influence of biomechanical parameters on the expression of VEGF and endostatin in the bone and joint systems. *Ann Anat* **187,** 461–472 (2005).

49 **Scott, A. et al.** VEGF expression in patellar tendinopathy: A preliminary study. *Clin Orthop Relat Res* **466**, 1598–1604 (2008).

50 **Zhang, F. et al.** Effect of vascular endothelial growth factor on rat Achilles tendon healing. *Plast Reconstr Surg* **112**, 1613–1619 (2003).

51 **Boyer, M.I. et al:** Quantitative variation in vascular endothelial growth factor mRNA expression during early flexor tendon healing: An investigation in a canine model. *J Orthop Res* **19**, 869–872 (2001).

52 **Petersen, W. et al.** The splice variants 120 and 164 of the angiogenic peptide vascular endothelial cell growth factor (VEGF) are expressed during Achilles tendon healing. *Arch Orthop Trauma Surg* **123**, 475-480 (2003).

53 **Petersen, W. et al.** The angiogenic peptide vascular endothelial growth factor (VEGF) is expressed during the remodeling of free tendon grafts in sheep. *Arch Orthop Trauma Surg* **123**, 168-174 (2003).

54 **Holmes, D.I, & Zachary, I.C**. Vascular endothelial growth factor regulates stanniocalcin-1 expression via neuropilin-1-dependent regulation of KDR and synergism with fibroblast growth factor-2. *Cell Sig* **20**, 569-79 (2008).

1.6 Drug Delivery Platforms

Control over cytokine release, and compatibility with standard surgical settings are essential for emerging cytokine delivery systems. Traditional “continuous” delivery approaches have focused on embedding cytokines in bioresorbable polymer microspheres[1,2] or suspending them in collagen sponges.[3] However, although these seminal approaches have been useful in a wide variety of biomedical applications, their application to functional musculoskeletal healing may be practically limited. Polymeric microspheres do not represent a stand-alone device for tissue ingrowth and are difficult to process into structural orthopedic devices while retaining cytokine biological activity. Collagen hydrogels and sponges are also non-ideal carriers, as cytokines rapidly diffuse out of these materials, resulting in short-term delivery and thus limited effect. Indeed, although absorbable collagen sponges are the carrier of choice in current clinical cytokine delivery strategies, it is clear from recent studies that the rapid release of large cytokine doses has serious side effects (e.g., edema, cancer).[4]

A next step toward clinical implementation of controlled cytokine delivery approaches would involve achieving long-term, temporally controlled cytokine release from devices that are already commonly used in standard surgical procedures. We propose that the current limitations in tendon healing can be addressed by modifying standard surgical sutures with coatings, which we have designed to deliver multiple cytokines in a temporally modulated manner.

1.6.1 Surgical Sutures

Surgical sutures are ubiquitous medical devices, which are used routinely in a majority of orthopedic surgeries and the market capitalization of the industry is expected to reach $1.2 billion by 2015 in the USA alone.[5] Sutures have been extensively investigated in terms of their mechanical properties, biocompatibility and biodegradability to meet the requirements specified for clinical uses. In addition to their physical function, surgical sutures also hold promise as a delivery platform for therapeutic molecules, in light of their proximity to damaged tissue and their widespread use in the majority of surgical procedures. These favorable aspects have recently led investigators to develop sutures that can release synthetic drugs, cytokines, or stem cells to enhance tissue healing.[6] Cytokine delivery is particularly promising, as these molecules play a critical role in healing of virtually all tissue types.

Sutures have been utilized in the assisted healing of tissue throughout history. However, suture material represents a foreign body and as such are not protected from the reactions of the immune system. The presence of a foreign body, when it cannot be avoided, must be comprised of a minimally reactive material that results in a non-significant inflammatory response from the host.

Although there are a variety of different types of suture material which have been evaluated in various models[7,8,9,10,11] they all result in various degrees of immune response and thus, have been implicated in adhesion formation in both abdominal

incisions and tendon repair.[7,8]

In the rabbit model, braided nylon has been shown to result in minimal reaction[7] although it did not decrease the rate of adhesion formation. Moreover, the use of polyglactin 910 was associated with the least amount of chronic inflammation microscopically and least amount of fibrosis.[7]

The laboratory group that functioned in the production of the experimental work for this thesis has reported a readily applicable approach to release of cytokines from suture material in a temporally controlled manner over a 6-week period.[6] Further investigation of cytokines and cytokine combinations are required for this cutting edge technology and are partially provided by this thesis. Such cytokine applications have the potential to possess significant advantages over previous applications.

1.6.3 Previous Experimental Work with Biominerals

A series of preliminary experiments conducted by our research group demonstrated the utility of biomineral-coated sutures for the delivery of growth factors in tendon and ligament healing.[6] First, our group demonstrated the versatility of the fabrication technique via the formation of calcium phosphate (CaP) coatings on a variety of suture materials larger than 0 USP (**Figure 1.6.2A**). Furthermore, those preliminary results demonstrate that multiple cytokines can be incorporated onto a single strand of suture material, either in the same region or in distinct locations. In addition, the stability

of protein-loaded biomineral coatings on a suture after 6 passes through the sheep infraspinatus tendon was demonstrated (**Figure 1.6.2B**).

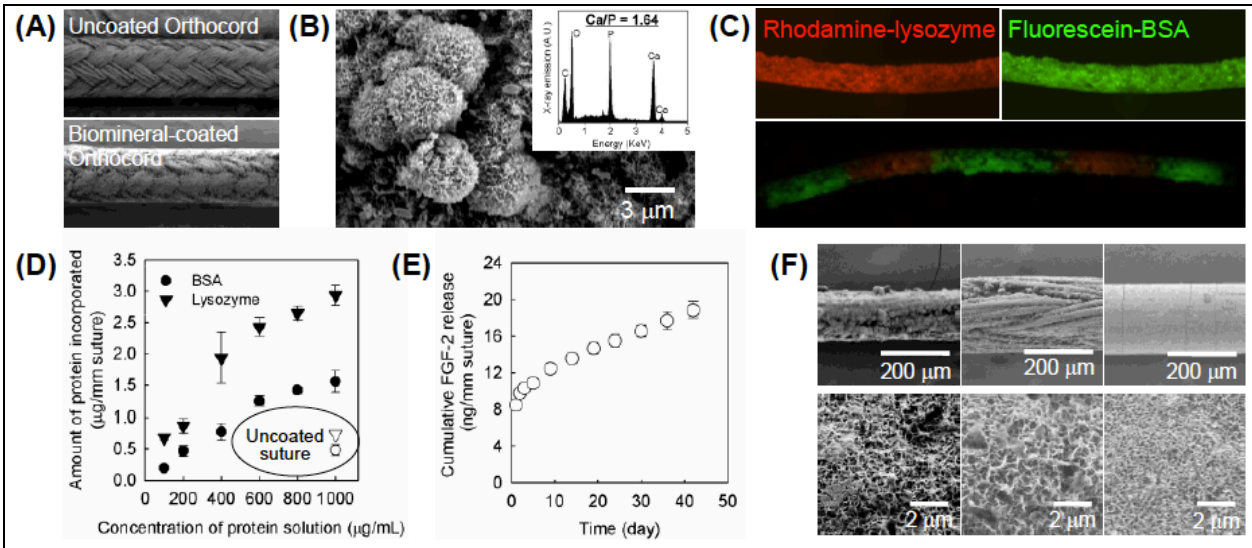

Figure 1.6.2A Surgical sutures as a device platform for therapeutic protein delivery. **(A)** SEM micrographs of uncoated and biomineral coated Orthocord suture (Dupuy Mitek), **(B)** SEM micrograph of porous nanostructure of biomineral coating and energy dispersive x-ray spectrum (EDS) (inset). **(C)** Multiple proteins can be incorporated into a biomineral coating on one suture either in the same location (top) or in distinct locations (bottom). **(D)** Binding isotherm shows efficient incorporation of both an acidic protein (BSA) and a basic protein (lysozyme) and there is no appreciable binding on uncoated suture. **(E)** FGF-2 is released from biomineral-coated suture with sustained release kinetics. **(F)** Biomineral coatings are also successfully formed on Vicryl (Ethicon; polyglactin 910, left) Ethibond Excel (Ethicon; polyethylene terephthalate, center) and Prolene (Ethicon; polypropylene, right). From Lee JS et al.[6]

Preliminary *in vivo* experiments also have demonstrated biocompatibility of biomineral coatings on sutures. In one set of experiments, a ruptured rat Achilles tendon was repaired with either a non-coated or biomineral-coated suture, and we measured macrophage numbers in regions adjacent to each suture. Results demonstrated no

significant difference, in macrophage numbers, which provides preliminary evidence that biomineral coatings do not negatively impact suture biocompatibility. In an additional study, biomineral-coated Orthocord sutures were designed to release FGF-2 over 6 weeks in a sheep rotator cuff repair model[12] (**Figure 1.6.2C)**. FGF-2-releasing sutures significantly increased the thickness of the repaired infraspinatus tendon (3-fold increase), and improved cartilage formation, vascularity, and failure load in the infraspinatus tendon.

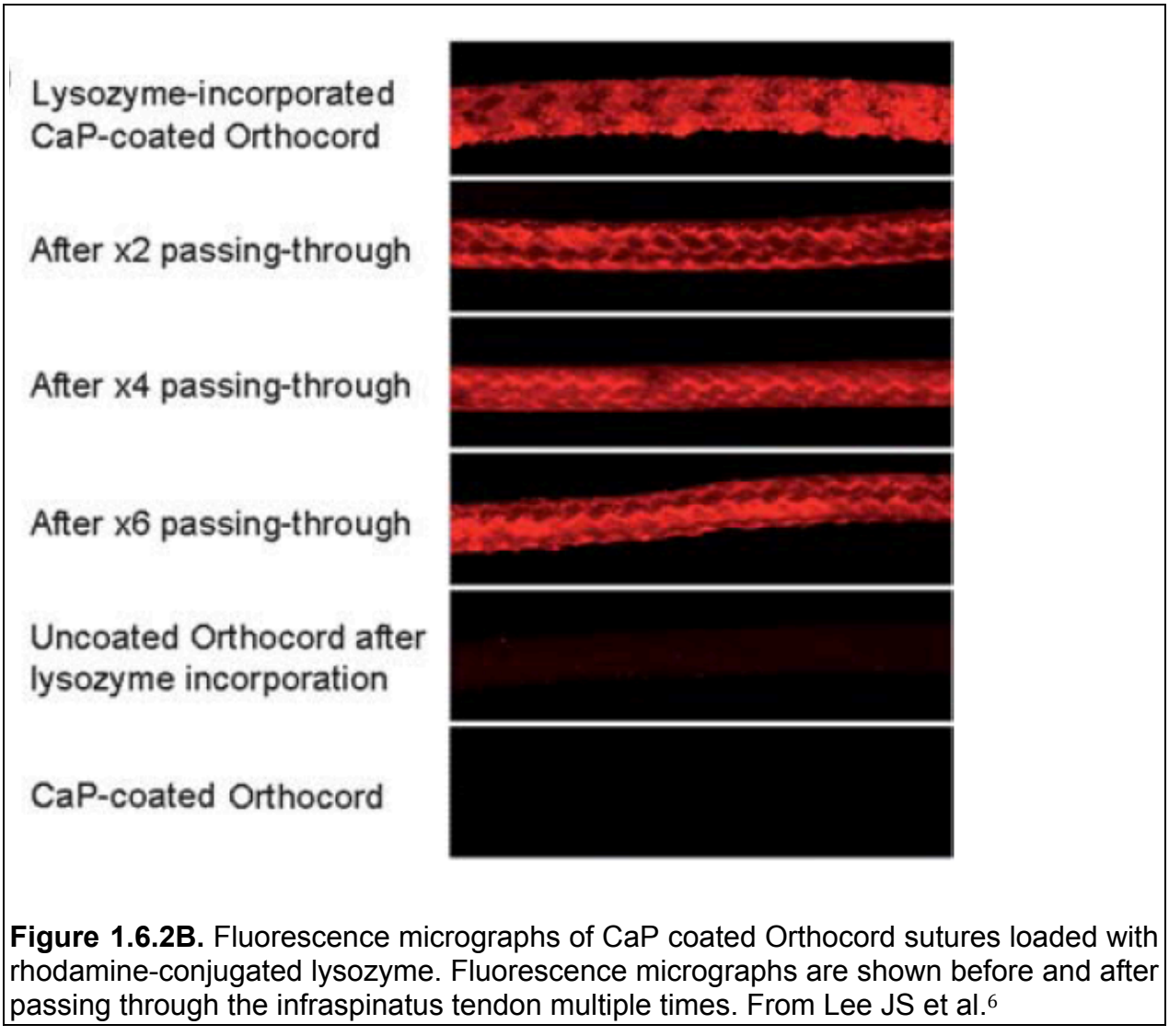

Figure 1.6.2B. Fluorescence micrographs of CaP coated Orthocord sutures loaded with rhodamine-conjugated lysozyme. Fluorescence micrographs are shown before and after passing through the infraspinatus tendon multiple times. From Lee JS et al.[6]

These data provide a first demonstration that cytokine-releasing sutures can promote tissue healing during bone-tendon repair, and this concept will be explored in greater depth in the proposed studies using cytokines known to influence specific processes in tendon healing. Importantly, these experiments also demonstrated no differences in coated suture handling, knotting, and mechanical properties when compared to uncoated sutures.

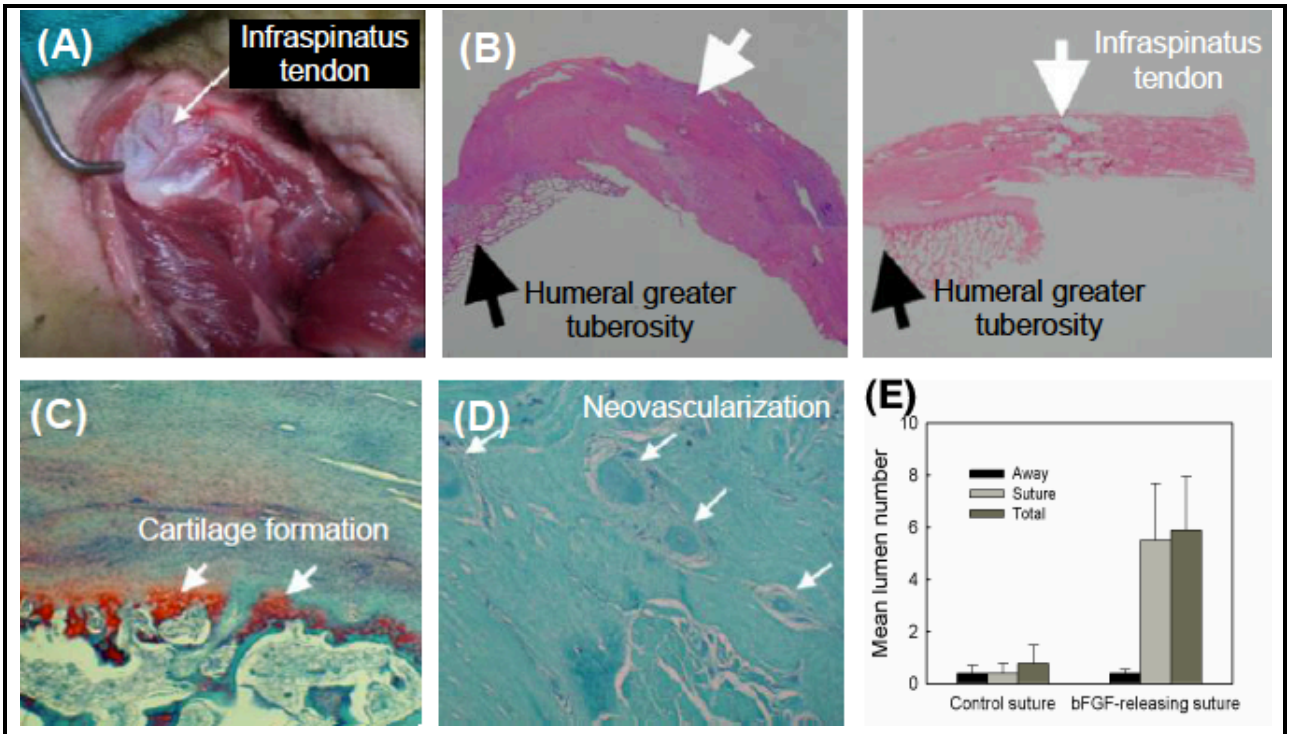

Figure 1.6.2C. Preliminary evience that cytokine releasing sutures promote rotator cuff repair *in vivo*. **(A)** Biomineral coated Orthocord sutures were incorporated with FGF-2 and then used for sheep rotator cuff repair. **(B)** Histology study of acute sheep rotator cuff repair model shows significantly thickened infraspinatus tendon repaired with FGF-2 suture (left) compared to the case when non-cytokine suture was used (right). **(C)** Cartilage formation at the insetion of the infraspinatus and greater tuberosity and **(D)** considerable neovascularity in infraspinatus fibers. **(E)** Bar chart demonstrating a significant increase in angiogenesis (mean lumen number, y axis) near the FGF-2 releasing suture. Note that angiogenesis at a non-releasing suture and away from the FGF-2 suture are not significantly different. From Lu Y et al.[12]

The aforementioned characteristics of natural tendon healing suggest strongly that cytokines can enhance and organize the amount of new tissue formation. However, the newly formed tendon tissue observed in existing cytokine delivery studies did not regenerate the structure and function of healthy tissue. Instead, the observed newly formed tissue at tendon-tendon interfaces typically constituted a reactive scar.

Therefore, although our preliminary results provide an important demonstration that cytokines released from sutures can have effects that are equivalent to cytokine concoctions released from more complex scaffolding materials by other groups, it remains clear that new cytokine delivery regimens or cytokine combinations must be developed to form more natural tissue structure and function.

References

1 **Nguyen, E.H., Schwartz, M.P. & Murphy, W.L**. Biomimetic approaches to control soluble concentration gradients in biomaterials. *Macromol Biosci* **11**, 483-9 (2011).

2 **King, W.J., Pytel, N.J., Ng, K. & Murphy, W.L**. Triggered drug release from dynamic microspheres via a protein conformational change. *Macromol Biosci.* **10**, 580-4 (2010).

3 **Murphy, W.L., Peters, M.C., Kohn, D.H. & Mooney, D.J**. Sustained release of vascular endothelial growth factor from mineralized poly(lactide-co-glycolide) scaffolds for tissue engineering. *Biomat* **24**, 2521-2527 (2010).

4 **Shah, M.M., Smyth, M.D. & Woo, A.S.** Adverse facial edema associated with off-label use of recombinant human bone morphogenetic protein-2 in cranial reconstruction for craniosynostosis. Case report. *J Neurosurg Pediatr* **3**, 255-7 (2008).

5 **US Surgical Sutures Market:** Surgical Procedures Growth to Drive Demand. *GlobalData* (2009).

6 **Lee, J. S. et al.** Controllable protein delivery from coated surgical sutures. *Journal of Materials Chemistry* **20**, 8894-8903 (, 2010).

7 **Whitfield, R. R. et al.** Effects of peritoneal closure and suture material on adhesion formation in a rabbit model. *Am J Obst Gyn* **197**, 644-651 (2007).

8 **Güdemez, E. et al.** Chondroitin sulfate-coated polyhydroxyethyl methacrylate membrane prevents adhesion in full-thickness tendon tears of rabbits. *J Hand Surg* **27**, 293-306 (2002).

9 **Matsusue, Y. et al.** Tissue reaction of bioabsorbable ultra high strength poly (L-lactide) rod: A long-term study in rabbits. *Clin Othop Rel Res* **317**, 246-253 (1995).

10 **Setzen, G. & Williams III, E. F.L.** Tissue response to suture materials implanted subcutaneously in a rabbit model. *Plast Reconst Surg* **100**, 1788-1795 (1997).

11 **Harrison, J. H., Swanson, D. S. & Lincoln, A. F.** A comparison of the tissue reactions to plastic materials: Dacron, ivalon sponge, nylon, orlon, and teflon. *AMA Arch Surg* **74**, 139-144 (1957).

12 **Y. Lu et al.** Histologic evaluation of suture material loaded with basic fibroblast growth factor on acute rotator cuff repair in an ovine model. *Curr Orthop Pract* **22**, 425-431 (2011).

1.7 Imaging Concepts in Tendon Healing

The clinical management of tendon tears remains challenging, with many individuals sustaining re-injury upon return to activity. Clinical return-to-activity criteria include assessments of pain, function and appearance on ultrasound or MRI images, which may differentiate symptomatic vs. asymptomatic tendons, but are not necessarily indicative of the strength of the tissue.[1,2,3] Thus, there is a strong need for *in vivo* quantitative indicators of tendon strength, which would provide more objective assessment of the recovery of mechanical integrity of the tissue. A recent meta-study demonstrated a strong correlation between tendon elastic modulus and ultimate stress[4], such that noninvasive measures of tissue elasticity may serve as an appropriate proxy for tendon strength. Currently, there are no ultrasonography tools that permit the evaluation of a B-mode image and form a correlation between the echogenicity pattern of a tendon tissue and the Young's modulus. However, the still B-mode image remains the current standard for assessment of tendon injuries, particularly in horses.[5] From this image, one is limited to subjective evaluations of cross sectional area, fiber pattern, shape and pixel intensity of the injured and healing tendon. [3,6,7] However, the link between static B-mode images and objective biomechanical evaluations of tendon strength is lacking.

Elastography has emerged as a tool that may assist in providing a link between biomechanical properties and imaging. The principle is that applied strain induced by the transducer results in tendon motion and the B-mode images before and after the

compression can be evaluated. When the compression is uniform, the strain of the tissue can be estimated.[8] However, this assumes strains of less than 1%, whereas strains in horses for example, reach 2.2% to 4.5% when walking and have been recorded as high as 16.6% during galloping in the superficial digital flexor tendons.[9] Thus, there is the limitation of the strain assumptions in this technique, in addition to the fact that the images examine compression in the transverse plane, whereas a longitudinal evaluation may be far more representative in the tendons, along their natural lines of loading.[5]

1.7.1 Shear Wave Elastography

Shear wave elastography imaging (SWI) is a promising approach for assessing tissue elasticity by measuring the propagation speed of shear waves.[10] The clinical viability of SWI has more recently been advanced by Bercoff et al.[11], who introduced an ultrasound-based method in which acoustic force is used to induce shear waves and high frame rate imaging is used to track the propagation speed.[12] Ultrasound SWI has seen use in multiple clinical domains, including imaging for possible tumors[13] and lesions in breast tissue[14], in addition to the evaluation of liver fibrosis.[15]

To overcome some of the problems associated with elastography, supersonic shear imaging was created. In this process, instead of an external operator inducing tendon compression or elongation, the system itself induces mechanical vibration via the used of an acoustic radiation force, created via a focused ultrasonic beam.[14] As this

process is exceedingly rapid, an image acquisition rate of 5000 frames per second is required in order to capture the propagation of the shear waves. To overcome this limitation on equipment, an approach was formulated whereby ultrafast echographic imaging was coupled with the remote generation of a supersonic shear wave in tissue using a modified sequence of ultrasonic beams generating by the transmitting probe.[11,12] This process of wave transmission may be carried out using the same probe for as for image acquisition. The displacement induced in the tendon generates a shear wave, which conveys information regarding the local viscoelastic properties.[14] This process allows a quantitative approach to determine tendon viscoelastic properties using non-invasive modalities. The shear wave speed v_s is linked with shear modulus, μ by a function incorporating the local density ρ (which in soft tissue is 1000 kg m^{-3}) via the equation:

$$\mu = \rho v_s^2$$

In soft tissue applications such as the breast, local stiffness described by Young's modulus *E,* is often approximated by:

$$E = 3\mu$$ [16]

The benefit of this system is that in real time imaging, it enables the computation of shear wave speeds and thus stiffness mapping of the local soft tissue.[14]

However, SWI analysis of tendon presents some unique challenges due to its inherent anisotropy. Recent studies have shown that shear wave speeds are dependent on both fiber-direction and load, due to the strain stiffening behavior of tendinous tissues.[17,18] In addition, it has been reported that ruptured tendons exhibit a reduction in shear wave speed at and adjacent to the site of tissue damage.[19,20] DeWall et al.[20] also found local disruptions of SWI speed in partially torn tendons. Thus, it is possible that SWI speed measurements may serve as a proxy for localized tissue elasticity, and indirectly of strength of a healing tendon.[4]

1.7.2 Acoustoelastography (AE)

Acoustoelastography is a mathematical theory, which attempts to overcome some of the issues with classical elastography, such as transducer induced tendon strain, in a different manner from that employed with SWI. AE relates changes in echo pixel intensity (numerical grey-scale brightness) observed during the loading and unloading of a tendon in the longitudinal plane to the tissues mechanical properties.[5,21]. The AE technique and has been shown to accurately model strain and stiffness in porcine flexor tendons.[22] The principle is that stiffer tissue results in less strain, which results in less detectable changes in the echo intensity of the grey-scale pixels which can then be quantified using imaging software.

It should be noted however that AE and SWI are not the only methodologies for the assessment of mechanical tissue strength, and it is important to take note of some

other techniques. Magnetic resonance elastography[23], both one dimensional[24] and two-dimensional static ultrasound elastography [25] shear wave dispersion ultrasound vibrometry (SDUV)[26] and spatially modulated ultrasound radiation force (SMURF)[27] and acoustic radiation force impulse (ARFI)[28] are all commercially implemented options by the Siemens corporation. However, all of these methods work on principles that occur in three stages:

i) A force, be it operator or imaging induced, stresses the tissue of interest

ii) Tissue displacement occurs which can be measured using either ultrasound or MR imaging techniques

iii) An estimation either quantitative or qualitative of the elastic properties of the tissue can be determined[29]

1.7.3 Microbubble Contrast Angiography (MCA)

Although there are a variety of studies regarding the importance of blood flow and tendon healing, none have been conclusive in obtaining accurate data about vascularity. However, the development of investigations which combine contrast medium injection with ultrasound (contrast enhanced ultrasonography, CEU) have resulted in promising data which are much more sensitive than Doppler imaging.[30] Specifically, such detection of microvascular structures using contrast material, which

relies on the principles of liposomal encapsulated micro bubbles[31], has been thus termed micro bubble angiography (MCA). Studies have been performed which have evaluated the micro-vascular volume in the human Achilles tendon post exercise.[30] In some cases, CEU was able to detect changes in vascularity whereas Doppler analysis was not.[30]

Many studies have concluded that CEU using MCA's is a very sensitive means of detecting even small micro-vascular changes and support its use in the investigation of blood flow in tendon healing studies.[30] It was therefore one of the objectives of this research to evaluate microvascular changes in the context of a surgical repair of an Achilles tendon injury in a rabbit model supplemented with angiogenic growth factors.

References

1 **Devitt, D. et al.** The ability of ultrasonography, magnetic resonance imaging and bone mineral densitometry to predict the strength of human Achilles' tendons. *Arch Phys Med Rehab* **90**, 756-760 (2009).

2 **Masci, L., Spang, C., van Schie, H. T. & Alfredson, H.** 63 Ultrasound And Utc For The Evaluation Of Plantaris Tendon Involvement In Midportion Achilles Tendinopathy. *Br J Sport Med* **48**, A40-A41 (2014).

3 **van Schie, H.T.M. et al:** Monitoring of the repair process of surgically created lesions in equine superficial digital flexor tendons by use of computerized ultrasonography*. Am J Vet Res* **70**, 37–48 (2009).

4 **LaCroix, A. S., Duenwald-Kuehl, S. E., Lakes, R. S. & Vanderby Jr, R.** Relationship between tendon stiffness and failure: a metaanalysis. *J Appl Physiol* **115**, 43-51 (2013).

5 **Ellison, M. E. et al.** Reproducibility and feasibility of acoustoelastography in the superficial digital flexor tendons of clinically normal horses. *Am J Vet Res* **75**, 581-587 (2014)

6 **Gillis, C.** Ultrasonography for monitoring healing and rehabilitation. *Clin Tech Equine Pract* **6**,174–178 (2007).

7 **Micklethwaite, L. et al:** Use of quantitative analysis of sonographic brightness for detection of early healing of tendon injury in horses. *Am J Vet Res* **62** 1320–1327 (2001).

8 **Lustgarten, M. et al.** Elastographic characteristics of the metacarpal tendons in horses without clinical evidence of tendon injury. *Vet Radiol Ultrasound* **55**, 92-101 (2014).

9 **Dowling, B.A. et al.** Superficial digital flexor tendonitis in the horse. *Equine Vet J* **32**, 369–378 (2000)

10 **Sarvazyan, A. P., Urban, M. W. & Greenleaf, J. F.** Acoustic waves in medical imaging and diagnostics. *Ultrasound Med Biol **39***, 1133-1146 (2013).

11 **Bercoff, J., Tanter, M. & Fink, M**. Supersonic shear imaging: A new technique for soft tissues elasticity mapping. *IEEE Trans Ultrason Ferroelectr Freq Control* **51**, 396–409 (2004).

12 **Bercoff, J. & Imagine, S:** Shearwave elastography. *Supersonic Imagine White Paper*. (2008).

13 **Wang, H. K. et al.** Hepatic venous congestion after living donor liver transplantation: quantitative assessment of liver stiffness using shear wave elastography—a case report. In *Transplant Proc* **44,** 814-816 (2012).

14 **Athanasiou, A. et al.** Breast lesions: quantitative elastography with supersonic shear imaging—preliminary results 1. *Radiol*, **256**, 297-303 (2010).

15 **Bavu, É. et al.** Noninvasive In Vivo Liver Fibrosis Evaluation Using Supersonic Shear Imaging: A Clinical Study on 113 Hepatitis C Virus Patients. *Ultrasound Med Biol* **37**, 1361-1373 (2011).

16 **Sarvazyan, A. P. et al.** Biophysical bases of elasticity imaging. In *Acoustical imaging* Springer US 223-240 (1995).

17 **Aubry, S. et al.** Biomechanical properties of the calcaneal tendon in vivo assessed by transient shear wave elastography. *Skelet Radiol* **42**, 1143-1150 (2013).

18 **DeWall, R. J., Slane, L. C., Lee, K. S. & Thelen, D. G.** Spatial variations in Achilles tendon shear wave speed. *J Biomech* 2014 (Epub)

19 **Chen XM et al.** Shear wave elastographic characterization of normal and torn Achilles tendons: a pilot study. *J Ultrasound Med* **32**, 449–455 (2013).

20 **DeWall, R. J., Jiang, J., Wilson, J. J. & Lee, K. S.** Visualizing Tendon Elasticity in an ex Vivo Partial Tear Model. *Ultrasound Med Biol* **40**, 158-167 (2014).

21 **Duenwald-Kuehl, S., Kobayashi, H., Lakes, R. & Vanderby, R.** Time-Dependent Ultrasound Echo Changes Occur in Tendon During Viscoelastic Testing. *J Biomech Eng* **134**, 111006-111009 (2012).

22 **Duenwald, S. E., Vanderby, R. & Lakes, R. S:** Stress relaxation and recovery in tendon and ligament: experiment and modeling. *Biorheol*, **47**, 1-14 (2010).

23 **Klatt, D. et al.** In vivo determination of hepatic stiffness using steady-state free precession magnetic resonance elastography. *Invest Radiol* **41** 841-848 (2006).

24 **Sandrin, L. et al.** Transient elastography: a new noninvasive method for assessment of hepatic fibrosis. *Ultrasound Med Biol* **29**, 1705-1713 (2003).

25 **Friedrich-Rust, M. et al.** Liver Fibrosis in Viral Hepatitis: Noninvasive Assessment with Acoustic Radiation Force Impulse Imaging versus Transient Elastography 1. *Radiol* **252**, 595-604 (2009).

26 **Chen, S. et al.** Shearwave dispersion ultrasound vibrometry (SDUV) for measuring tissue elasticity and viscosity. *Ultrason Ferroelect Freq Cont, IEEE* **56**, 55-62 (2009).

27 **McAleavey, S. et al.** Validation of SMURF estimation of shear modulus in hydrogels. *Ultrasonic Imag* **31**, 131-150 (2009).

28 **Yoneda, M. et al.** Nonalcoholic Fatty Liver Disease: US-based Acoustic Radiation Force Impulse Elastography 1. *Radiol* **256**, 640-647 (2010).

29 **E. Bavu, J.L. et al.** Noninvasive in vivo liver fibrosis evaluation using supersonic shear imaging: A clinical study on 113 hepatitis C virus patients *Ultrasound Med Biol* **37**,1361–1373 (2011).

30 **Pingel, J. et al.** The acute effects of exercise on the microvascular volume of Achilles tendons in healthy young subjects. *Clin Physiol Funct Imag* **33**, 252-257 (2013).

31 **Perflutren Lipid Microspheres**, Definity Imaging, Lantheus Medical Imaging, Inc. Billerica MA

Chapter 2

Research Objectives

2. Research Objectives

A. Laboratory Based Procedures

1. Evaluate the effects of coating small diameter (4-0 and 6-0 USP) suture material with hydroxyapatite (HAP) crystals via nucleation and to determine their suitability for growth factor delivery and use in surgical patients.

The idea behind this portion of the thesis was that due to the small size of suture materials that were utilized in this study, they may exhibit different behaviors than our previous evaluations with larger suture when coated with HAP and therefore evaluation prior to use was required. Furthermore, previous coatings have only evaluated HAP growth up to day 7 incubation, at which time one growth factor was adsorbed to the crystal. We aimed to adsorb 2 growth factors at different time points; thus, we evaluated the effects of crystal growth beyond 7 days on a variety of suture sizes and material types. The hypothesis for section A1 was that HAP can be successfully incorporated onto both 4-0 and 6-0 USP suture sizes and various suture materials beyond the 7-day incubation time point previously used.

2. Determine growth factor release curves for suture material in order to calculate growth factor doses rabbits receive.

The working hypothesis for section A2 was that via incorporation of a radioactive isotope, we could determine how much growth factor was released each day, for a variety of HAP coating thicknesses (incubation days). Thus, the aim of section A2 was to determine the how different growth factor concentrations incorporated onto the HAP layer determine the rate of release of growth factors from the HAP layers. The evaluation of the rate of release of growth factors will permit us to determine the dose of growth factor actually received by the rabbits. The hypothesis was that the rate of release of FGF and VEGF will depend on the concentration of solution of incubation and dependent on the thickness of HAP crystal layer grown on the suture.

B. Surgery Based Procedures

1. Evaluate and compare the effects of growth factor supplementation on ultimate tensile strength and stiffness for the lateral gastrocnemius tendon in a bilateral transection model in the rabbit.

Rabbit lateral gastrocnemius tendons were transected in a bilateral model and repaired with HAP coated suture material. HAP coated suture materials were

incubated with three combinations of two growth factors, absent FGF or VEGF (ZF and ZV, respectively), low dose FGF or VEGF (LF and LV, respectively) and high dose FGF or VEGF (HF and HV, respectively). The hypothesis for section B1 was that the combination of FGF and VEGF will result in a synergistic effect in terms of ultimate tensile strength and stiffness evaluation in a materials testing machine. All combinations of growth factor doses were evaluated in a short-term study of 4-weeks

2. Evaluate and compare the effects of growth factor supplementation on histological organization of healing tendon and the relationship between organization scoring and ultimate tensile strength.

Rabbit lateral gastrocnemius tendons were transected in a bilateral model and repaired with HAP coated suture material. HAP coated suture materials were incubated with combinations of doses of growth factor. The hypothesis in section B2 was that the combination of FGF and VEGF will result in synergistic effect in terms of histological organization that will be superior to the use of non-growth factor coated suture material (zero FGF and VEGF suture ZF/ZV). Thus the improved histological organization should correlate with the ultimate tensile strength. All combinations of growth factor doses were evaluated in a short-term study of 4 weeks

3. Evaluate and compare the effects of our optimal growth factor suture combination, selected from parts B1 and B2, on biomechanical and histological properties in a long term 9-week study.

Upon completion of parts B1 and B2, the optimal growth factor group combination was selected and tested against a control non-growth factor coated suture (ZF/ZV) for the evaluation of long-term (9-week) effects of growth factor supplementation. Biomechanical and histological evaluations were performed, similar to those in parts B1 ands B2.

C. Imaging Based Procedures

1. Evaluate and compare the results for imaging the healing tendons in rabbits using both supersonic shear wave imaging (SWI) and Acoustoelastography (AE) and their individual relationship to parameters of tendon histological organization and mechanical testing.

During the course of healing, bilateral SWI and AE scans on each tendon (medial and lateral gastrocnemius) were performed. The aim of section C1 was to monitor the healing of the tendon using these imaging modalities (SWI and AE) and compare the values with tendon biomechanical data, be it ultimate tensile strength, stiffness or Young's Modulus. The hypothesis was that these

modalities were able to provide non-invasive determinations of biomechanical properties of healing tendons.

2. Evaluate and compare the results for imaging the healing tendons in rabbits using both SWI and AE.

The aim in this portion of the study was to determine if either SWI or AE were superior in determining *in vivo* biomechanical data and to compare the data provided by the two techniques. The hypothesis in section C2 was that no difference in correlation coefficients exists between the two imaging methods.

3. Establish if micro bubble contrast angiography (MCA) was useful in determining blood flow in the healing tendon and how this information related to mechanical testing, histological organization and blood vessel density determination.

The aim for this portion of the study was to evaluate if enhanced angiogenesis as determined via the MCA method, was correlated with increased tensile strength. We aimed to evaluate if superior blood flow at a 2-weeks time point post surgery resulted in higher tensile strengths at the 4-week sacrificial time point. Furthermore, we aimed to correlate blood flow information determine via MCA with histological blood vessel analysis. The hypothesis for section C3

was that enhanced blood flow resulted in higher levels of tendon biomechanical properties.

Chapter 3

Materials and Methods

3. Material and Methods

3.1.1 Suture Material Coating

In the initial portion of the experiment, several small diameter (ranging from 4-0 USP to 6-0 USP) sutures were coated with HAP in order to assess suitability for the surgical portion of the study **(Table 3.1.1A).** Both absorbable and non-absorbable, monofilament and multifilament sutures were evaluated. Previous studies were conducted using large suture of size 0 USP, demonstrated in section 1.6.4. Large diameter sutures are unsuitable for use in our surgical model thus the need to evaluate smaller diameter material. Time points for analysis included 7, 10 and 14 days of incubation in modified simulated body fluid (mSBF). mSBF is a solution with a similar composition to human plasma but with double the concentration of calcium (2.5 mM in plasma, 5.0 mM in mSBF) and phosphate (1.0 mM in plasma, 2.0 mM in mSBF). The mSBF solution is buffered using sodium hydroxide or hydrochloric acid to achieve a final pH of 6.8. Solution was made fresh daily. The generation of the mSBF was conducted as previously described.[1]

Sutures materials listed in **Table 3.1.1A** of 50 mm in length were cut and placed in 15 ml incubation tubes (BD Falcon Tubes, Bedford, MA). Tubes were filled with a minimum of 10 ml of mSBF to ensure sufficient concentration of HAP solution for nucleation. Tubes were placed in a rotary spinner at approximately 30 rpm and incubated for 24 hours at 37^{o}C. After incubation, sutures were washed twice in

phosphate buffered saline (PBS) to remove any loose sedimentation of crystals and to ensure a healthy bed of nucleated crystals remained on the suture material. Samples were then re-incubated in mSBF until the pre-determined time point was reached (7, 10 or 14 days). Samples were analyzed using both scanning electron microscopy (SEM) and confocal microscopy.

Suture	Absorbable/Non-Absorbable	Size	Mono/Multifilament	Source
Polyglactin 910	Absorbable	4-0	Multifilament	Covidien
Polyglactin 910	Absorbable	6-0	Multifilament	Covidien
Nylon	Non-absorbable	4-0	Multifilament	Ethicon
Nylon	Non-absorbable	6-0	Multifilament	Ethicon
Nylon	Non-absorbable	4-0	Monofilament	Ethicon

Table 3.1.1A Suture materials evaluated for suitability for this study.

3.1.2 SEM Analysis

Portions of each suture material listed in **Table 3.1.1A** were fixed onto a SEM mounting platform (pin disc) and subjected to a gold sputter coating. Images were viewed using a scanning electron microscope under varying degrees of magnification (Zeiss LEO 1530-2 FESEM/EDS, Thornwood, NY). Based on this visual analysis, an optimal suture material and time frame for incubation for the surgical portion of the study were selected based on the SEM image analysis.

3.1.3 Confocal Analysis

In order to investigate the feasibility of multiple growth factor incorporation, sutures were incubated in mSBF as previously described to generate the HAP coating. At the first time point, (6 days after the initiation of mSBF incubation) sutures were incubated using a primary label of tetramethylrhodamine (excitation 557 nm, emission 576 nm, Life Technologies, Grand Island, NY)/ 1.5% bovine serum albumin (BSA) (Thermo Fischer Scientific, Waltham, MA) mixture for 6 hours. Sutures were then incubated in mSBF for a further time period of 4 and 8 days, providing total mSBF incubation times of 10 and 14 days. Sutures were then incubated in a secondary label fluorescein isothiocyanate (FITC, 490 nm excitation, 525 nm emission, Life Technologies, Grand Island, NY)/1.5% bovine serum albumin (BSA) for a 6-hour period. After each incubation period, sutures were washed in PBS. After incubation in the fluorochromes, sutures were maintained in darkness until time of study. Following fluorochrome incorporation, sutures were evaluated using confocal microscopy (Nikon A1R confocal system, Melville NY).

3.1.4 FGF/VEGF Implantation and Release

Once the most appropriate nylon and polyglactin 910 suture material, size and incubation time points were identified based on the subjective assessments performed in section 3.1.1 a second experiment to calculate the rate of release of growth factors (FGF and VEGF) from the HAP layers was performed. Four solution concentration

levels were chosen for each growth factor: 0.5 µg/ml, 1 µg/ml, 2.5 µg/ml and 5 µg/ml. The solution concentrations chosen were based on previous studies evaluating the supplementation of VEGF in rat Achilles tendon[2] and FGF in a rotator cuff model in a sheep.[3] Nylon and polyglactin 910 braided sutures of size 4-0 and 6-0 USP were generated using the mSBF and incubated at two time points, previously determined in section 3.1.1 with two different growth factors (VEGF and FGF). The first growth factor (FGF basic (146aa), R and D systems, Minneapolis, MN) was mixed with a known radioactive quantity of ^{125}I- FGF (NEX268,Perkin Elmer, Waltham, MA), using 0.1% BSA in PBS as a carrier. The radioactive isotope for the FGF used in suture incubation was at a concentration of 0.015%. The FGF isotope possessed an activity of 214.1 µCi/µg, equivalent to 85.4 µCi/ml. Standard radioactivity curves were generated for the FGF using serial dilutions of the incubation solution to provide reference levels.

The second growth factor (recombinant human VEGF, (165aa), R and D systems, Minneapolis, MN) was mixed with a known quantity of ^{125}I-VEGF (NEX328, Perkin Elmer, Waltham, MA), using 0.1% BSA in PBS as a carrier at a concentration of 0.0111%. The VEGF isotope possessed an activity of 137 µCi/µg, equivalent to 36.5 ng/100µl. Standard curves were generated for the VEGF using serial dilutions of the incubation solution to provide reference levels. Four suture types were evaluated for the release experiments; 6-0 braided nylon, 6-0 braided polyglactin 910, 4-0 braided nylon and 4-0 braided polyglactin 910. Each suture type and concentration level was subjected to incorporation onto the suture material at a deep layer (HAP crystals grown for 6 days, growth factors (either FGF or VEGF) were then applied and then sutures

were reincubated in mSBF for 4 further day) and a superficial layer (HAP crystals grown for 10 days and then the growth factors were applied, no further reincubation was performed). Growth factor application at each HAP crystal level (superficial and deep) was performed by placing the suture in a 15 ml Falcon tube, adding 10 ml of desired protein solution with radioactive component and then placed in a rotator drum at 37^{o}C for 6 hours at approximately 30 rpm. For each HAP crystal layer level, 3 experimental procedures were performed for each type of suture:

1) A 2 cm section of suture material was placed in simulated body fluid (SBF), which is similar to the composition of plasma and buffered to pH 7.4.

2) A 5 cm section of suture material was passed through samples of rabbit lateral gastrocnemius tendon six times via a tunneling technique. The suture was then knotted with a single throw. The suture (passage and knotted) was then incubated in SBF. 2 cm was an insufficient amount of material to perform a single throw of knot, hence 5 cm had to be used for the knotting procedure.

3) The tendon tissue, through which the 5 cm section of suture was passed through, was also placed in SBF.

The three experimental procedures mentioned above provide an evaluation of suture material with HAP crystals and their behavior in regard to growth factor release. However, a simulation of the surgical technique was also performed using the passage and knotted suture material and the tendon tissue. To evaluate the total dose the rabbit would receive, the passage and knotted suture and the tendon release data were combined for analysis. Corrections were made to express release of growth factor per cm of suture. Radioactive release from the sutures (both unaltered and the passage/knotted suture) and from the tissue was monitored using a scintillation counter (Packard Gamma Counter, Cobra II, GMI-Inc, Ramsey, MN). SBF was changed with each radioactivity reading. Fresh SBF was generated on a per use basis. Readings were made for each level (application of FGF and VEGF at both the superficial 10 day layer of HAP crystals and the deep layer of 6 day crystals) at 2,4,6,8,10,14,18,21,28,34, 42 and 48 days.

3.1.5 Generation of Experimental Suture

Once the most appropriate concentration and release profiles for the suture materials and growth factors were determined based on all the data from sections 3.1.1 to 3.1.4, the experimental suture materials were generated. Sutures were cut to have an optimal working length (100 mm) including the needle and incubated according to methods previously established in section 3.1.1. Sutures chosen for the surgical procedure were 4-0 polyglactin 910 and 4-0 nylon. For the low FGF and VEGF group (LF and LV, respectively), sutures were incubated in 0.5 µg/ml solution of protein. For

the high FGF and VEGF groups (HF and HV, respectively), sutures were incubated in 5 µg/ml solutions. Sutures were placed in 15 ml Falcon tubes and placed in a rotator drum at 37^{o}C for 6 hours for growth factor adsorption at approximately 30 rpm.

For all sutures, FGF was always applied as the deep layer and VEGF applied as the superficial layer. Once coated in HAP and incubated in FGF and/or VEGF using 0.1% BSA in PBS as a carrier, sutures were subjected to lyophilization under vacuum conditions for 12 hours and double sealed in sterile pouches (Paper Self Seal Pouches, Cardinal Health Medical Products, Dublin, OH) prior to surgery. Pouches were sterilized using ethylene oxide, which has previously been shown to be an acceptable method for bioactive materials and products, with only minor reduction in bioactivity.[4,5] Once sterilized, sutures were stored in a freezer at -20^{o}C until required. Once stored, sutures were used in the experimental model within a 30-day period.

Surgical Based Evaluation

3.2.1 Animal Model

The animal study was approved by the UW-Madison Animal Care and Use Committee (Protocol V01554).

Sixty-six, 4 month-old New Zealand White 2-3 kg, male and female rabbits, housed individually were used for this experiment. The animals had free access to feed

and water and were provided with toys and stimuli as required by the Animal Care and Use Committee. Furthermore, 7 animals from an unrelated study of the same breed and age range were utilized for mechanical testing of the lateral gastrocnemius tendon to establish normal biomechanical data for non-operated, normal tendons (NT).

3.2.2 Suture Group and Dose Selection

Using the doses previously identified in the suture release profiles in section 3.1.4, three levels of each growth factor were used (absent, low and high). Three levels of two growth factors provide 9 groups to evaluate all possible outcomes (**Table 3.2.2A**). Control sutures, denoted by the absence of FGF and VEGF (ZF/ZV), were coated using a 0.1% BSA/ PBS solution only.

Utilizing the system described in **Table 3.2.2A**, ZF/ZV represents the control group (surgical transection of the tendon repaired with suture coated in HAP and incubated in 0.1% BSA only – no addition of growth factors). Group allocation to each growth factor was randomized. At the time of surgery, group allocation to each rabbit was randomized. As this was a bilateral study, to minimize the effect of intra-rabbit variation, once assigned to a group, both legs received the same treatment.

Initially, the short term (4-week) portion of the study was performed, including all imaging, biomechanical testing and histology. At the conclusion of the 4-week study, the optimal group from our tested selection was compared to the ZF/ZV control group in a

long term 9-week study period, which evaluated biomechanical and histological data only.

	NT	ZF/ZV	LV	HF	HV	LF	LF/LV	LF/HV	HF/HV	HF/LV	ZF/ZV, LT	?F/?V, LT
FGF	**N/A**	**ABSENT**	**ABSENT**	**HIGH**	**ABSENT**	**LOW**	**LOW**	**LOW**	**HIGH**	**HIGH**	**ABSENT**	**OPTIMAL**
VEGF	**N/A**	**ABSENT**	**LOW**	**ABSENT**	**HIGH**	**ABSENT**	**LOW**	**HIGH**	**HIGH**	**LOW**	**ABSENT**	**OPTIMAL**
N	7	6	6	6	6	6	6	6	6	6	6	6

Table 3.2.2A. Representation of the twelve treatment groups and assortment of growth factors into each group. **Absent – 0 µg/ml incubation level**, **low - 0.5 µg/ml incubation level, high – 5 µg/ml incubation level**. For the randomization of groups for surgical procedures, group identifications were randomized. **NT** represents 7 rabbits of the same breed and age, which were utilized in order to obtain normal values for natural biomechanical data of tendons. Tendons in this group had no surgical procedure. **Groups ZF/ZV (control), LV (low VEGF), HF (High FGF), HV (High VEGF), LF (Low FGF), LF/LV (Low FGF/Low VEGF), LF/HV(Low FGF/High VEGF), HF/HV (High FGF/High VEGF) and HF/LV (High FGF/Low VEGF)** were randomized for the short-term study (4-weeks). **Groups ZF/ZV, LT and ?F/?V, LT** represents the long term (9-week) portion of the study. ZF/ZV, LT represents a repetition of the control ZF/ZV group and the dosages for ?F/?V were determined from the short-term (4-week) portion of the study, representing a group that expressed the highest biomechanical and histological properties.

3.2.3 Surgical Procedure

Rabbits in the surgery group were subjected to bilateral surgical transection and repair of the lateral gastrocnemius tendon. Rabbits were given buprenorphine (0.01-0.05 mg/kg IM), carprofen (4 mg/kg SQ) and midazolam (1 mg/kg IM) prior to surgery. Rabbits were then placed in a sealed gas chamber and anesthetized using isoflurane gas flow, varying between 3-5% of inspired gas at an oxygen flow rate of 3 L/min. Once anesthetized, rabbits were intubated using a 8 Fr endotracheal tube and maintained on an oxygen/isoflurane gas mixture as required in order to keep the rabbits at a surgical plane of anesthesia. A 27g intravenous butterfly catheter was placed in the marginal ear vein to supply a surgical rate (10 ml/kg/hr) fluid therapy (Lactated Ringers Solution, Abbott Laboratories, Abbott Park, IL) . The rabbits were placed on a heat blanket (Hot-Dog system, Augustine Biomedical and Supply, Eden Prairie, MN) in a ventral recumbency position, designed to maintain temperature around 37^{o}C. Legs were clipped (Favorita Clippers, Aesculap, Suhl, Germany) and aseptically prepared using a chlorhexidine scrub of each leg and an alcoholic scrub. The distal foot was wrapped in sterile elastic conforming bandage (Vetwrap, 3M, St. Paul, MN) from the calcaneus distally and encompassed the feet. A paper drape was positioned over the hind legs of the rabbit. Incisions in the paper drape were created in order to pass the hind legs through, so that the mid metatarsus proximally was entirely covered by the drapes. A sterile green towel was then placed over each leg until they were ready for surgery.

A surgical marker pen was used to identify a site 15 mm proximal to the point of the calcaneus. A 15 mm skin incision was made centered 15 mm proximal to the calcaneus on the lateral aspect of the metatarsus, and over the region of the medial and lateral gastrocnemius tendons (**Figure 3.2.3A)**. The skin and subcutaneous tissue were sharply transected using a #15 scalpel blade. The subcutaneous fascia was then separated in proximal and distal directions using Metzenbaum scissors down to the level of the paratenon (**Figures 3.2.3B, 3.2.3C)**. Any hemorrhage was stemmed using hand held monopolar cautery (Cardinal Health Surgical Cautery 65410-183). The paratenon between the medial and lateral gastrocnemius branches was incised and split slightly proximally and distally using Castroviejo Scissors (**Figures 3.2.3C, 3.2.3D)**. Jewelers micro forceps were used to carefully separate the medial and lateral gastrocnemius tendon bundles. Bishop Harman forceps were then used to separate the gastrocnemius tendon bundles along their length, from just proximal to the point of merger near the calcaneus to just distal to the musculotendinous junction.

The leg was then held in slight tarsal flexion, placing the lateral gastrocnemius tendon and Achilles apparatus under tension while Bishop Harman forceps were used to isolate the tendon from the surrounding tissue (**Figure 3.2.3E)**. The lateral tendon was sharply transected 15 mm proximal to the calcaneus with a #15 scalpel blade (**Figures 3.2.3F, 3.2.3G)**. The paratenon was then bluntly dissected off the proximal and distal stumps for approximately 10 mm. The body of the tendon was repaired in apposition using a single locking loop of 4-0 braided nylon (Surgilon, Covidien, Mansfield, MA) coated with an HAP layer containing growth factors assigned to the

correct group identification (**Figure 3.2.3H, 3.2.3I)**. Once the body of the tendon was repaired, a circumferential repair of the paratenon using 4-0 braided polyglactin 910 (Vicryl, Ethicon, Cincinnati, OH) (also coated with an HAP layer containing growth factors identical to the central core suture) was applied in a Silfverskiold epitendinous repair.[6] The subcutaneous fascia was sutured using 6-0 polyglactin 910 (Vicryl, Ethicon, Cincinnati, OH) in a simple continuous pattern (**Figure 3.2.3J**) and the skin was sutured using 3-0 polypropylene (Prolene, Ethicon, Cincinnati, OH) in a cruciate pattern (**Figure 3.2.3K**).

Post-surgery, no external coaptation was provided. Rabbits were allowed to recover and extubated once they began to show signs of movement. Rabbits were individually housed in cage confinement for the duration of the study. A dose of carprofen (4 mg/kg SQ) was provided 6-8 hours post-surgery. Rabbits were carefully monitored to assess difficulties in ambulation or evidence of pain post surgery.

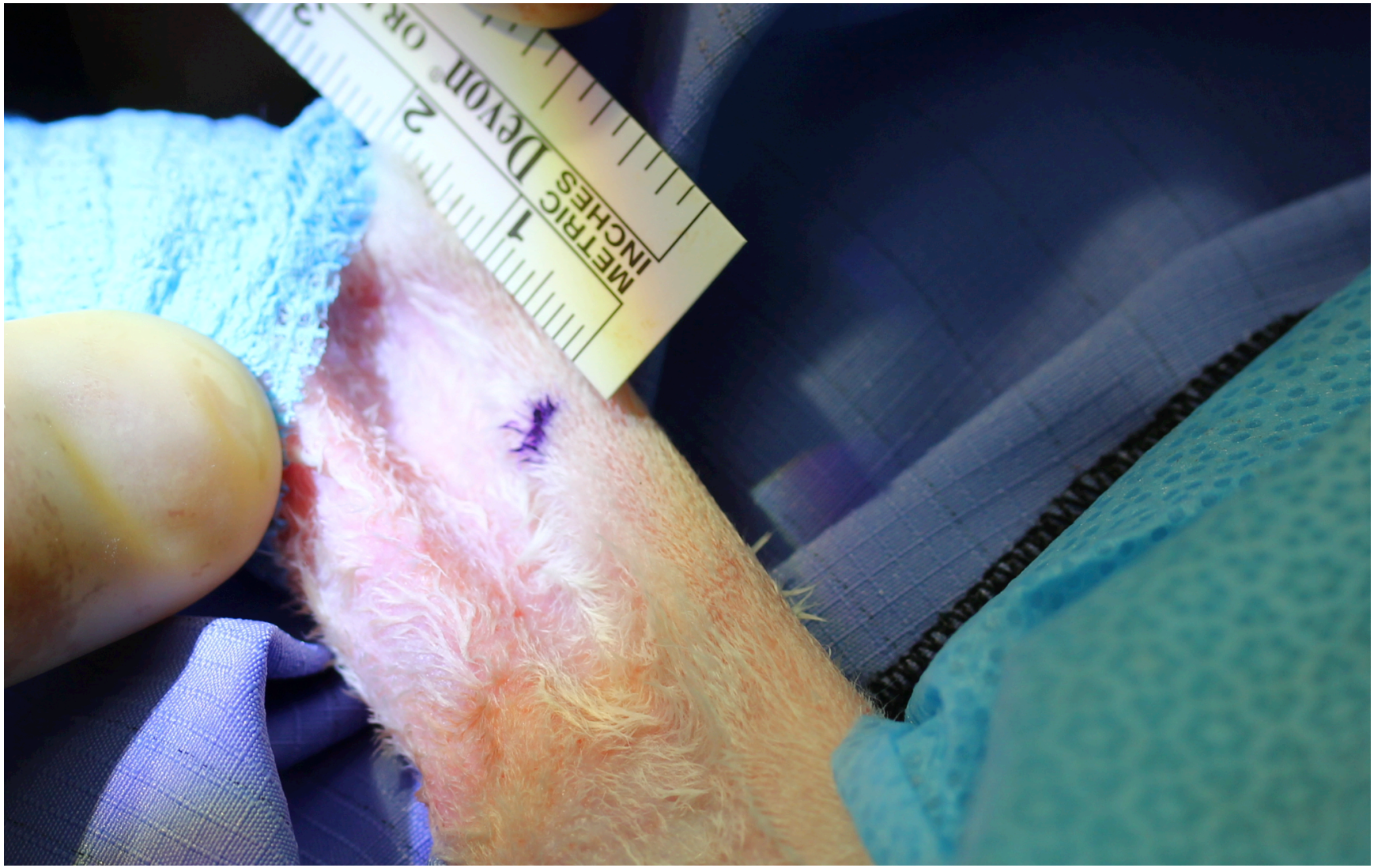

Figure 3.2.3A. Surgical Procedure. A surgical marker was used to make a notation 15 mm proximal to the calcaneus to mark the center of the incision.

Figure 3.2.3B. Anatomical considerations in the approach to the gastrocnemius. The calcaneus can be visualized in the top right corner of the image. In the center of the image are two structures; the combined medial and lateral gastrocnemius bundle at the top and the superficial digital flexor tendon on the bottom. Note how as the superficial digital flexor approaches the calcaneus, it becomes wider and flatter.

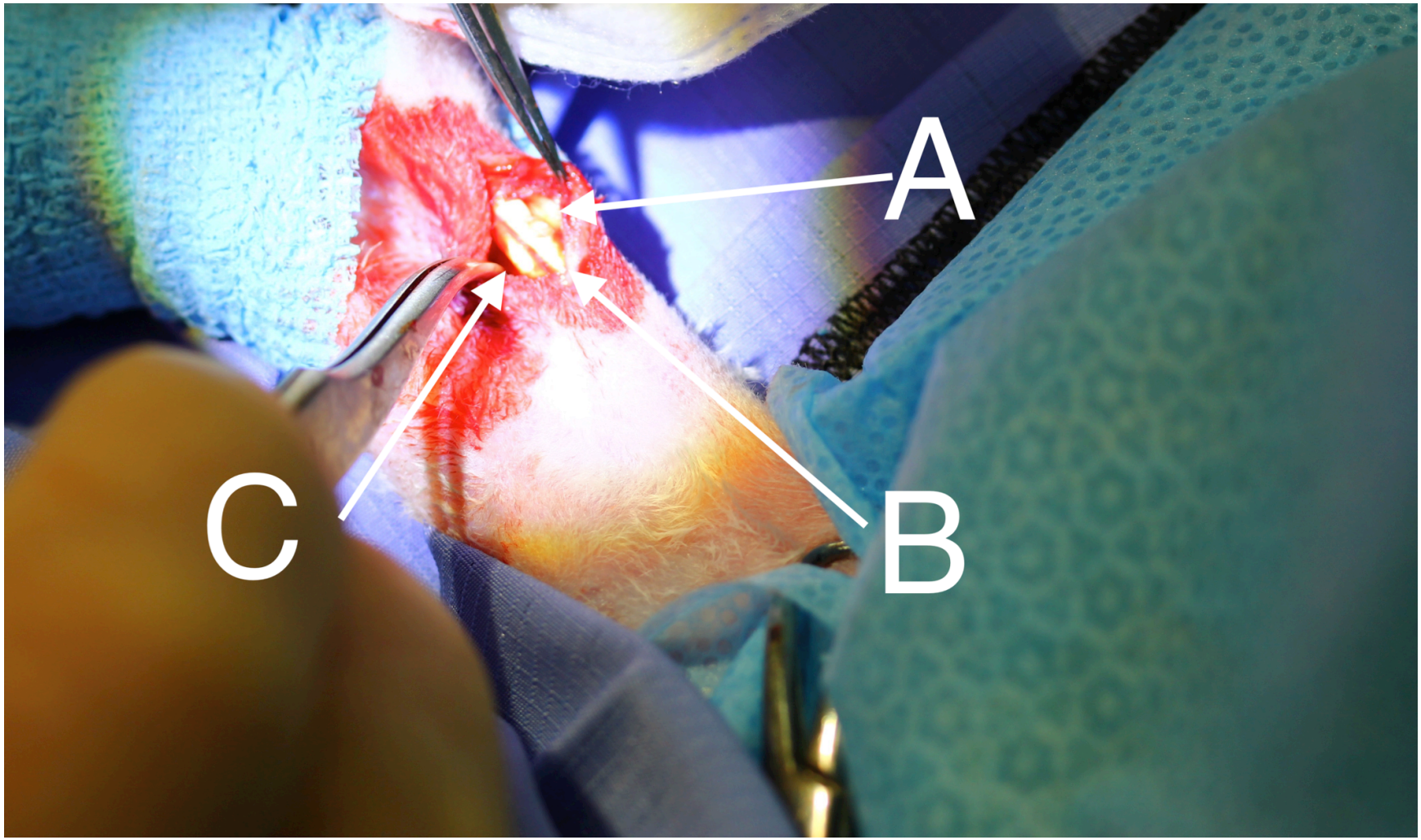

Figure 3.2.3C. Surgical Procedure. After careful dissection, three important structures can be identified**. A.** Superficial digital flexor tendon. **B** Lateral gastrocnemius tendon**. C.** Medial gastrocnemius tendon.

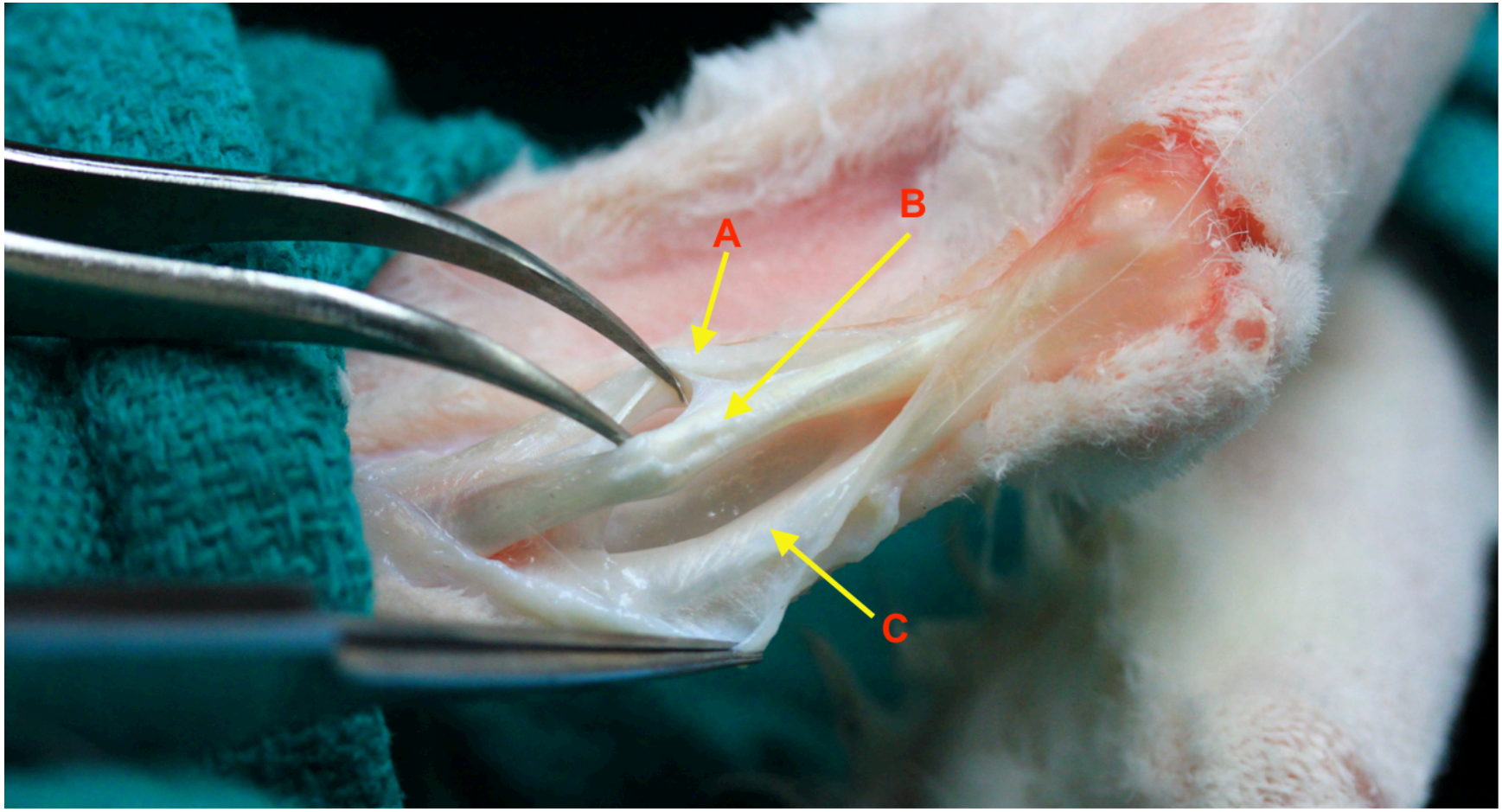

Figure 3.2.3D. Anatomical considerations in the approach to the gastrocnemius. The three structures representing the medial **(A)**, lateral **(B)** gastrocnemius bundles and the superficial digital flexor tendon (SDFT) **(C)** can be visualized. The forceps here are located in the natural sulcus that forms between the medial and lateral gastrocnemius bundles. At the top of the forceps is the medial gastrocnemius bundle. The bottom of the forceps represents the lateral gastrocnemius bundle. At the very bottom of the image is the superficial deep digital flexor tendon (SDFT). Note how the SDFT continues distally around the calcaneus it becomes elongated and flattened.

Figure 3.2.3E. Surgical Procedure. Forceps can be passed underneath the lateral gastrocnemius tendon, isolating it from the surrounding structures. Once isolated, a transection was performed with a #15 blade.

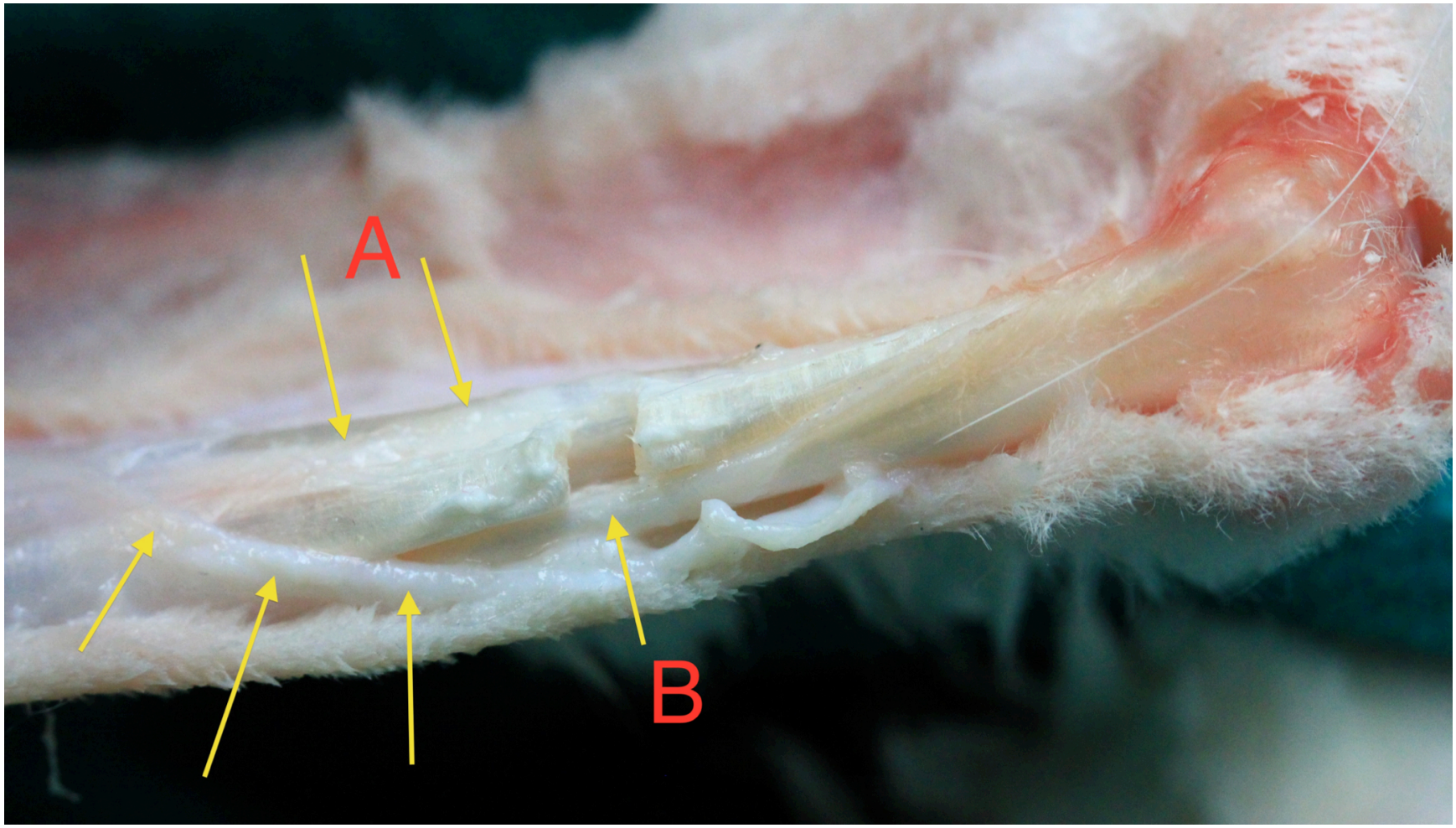

Figure 3.2.3F. Anatomical considerations in the approach to the gastrocnemius. (**A)** Medial gastrocnemius tendon. (**B)** Superficial digital flexor tendon. Between these two structures a transection has been created in the lateral gastrocnemius tendon. Note how there is a 3-4 mm formation of a gap junction between the two transected ends. The unlabeled yellow arrows denote loose fascia encountered on the approach to this region.

Figure 3.2.3G. Surgical procedure. After transection of the lateral gastrocnemius tendon, there was an immediate recoil and retraction of either tendon end.

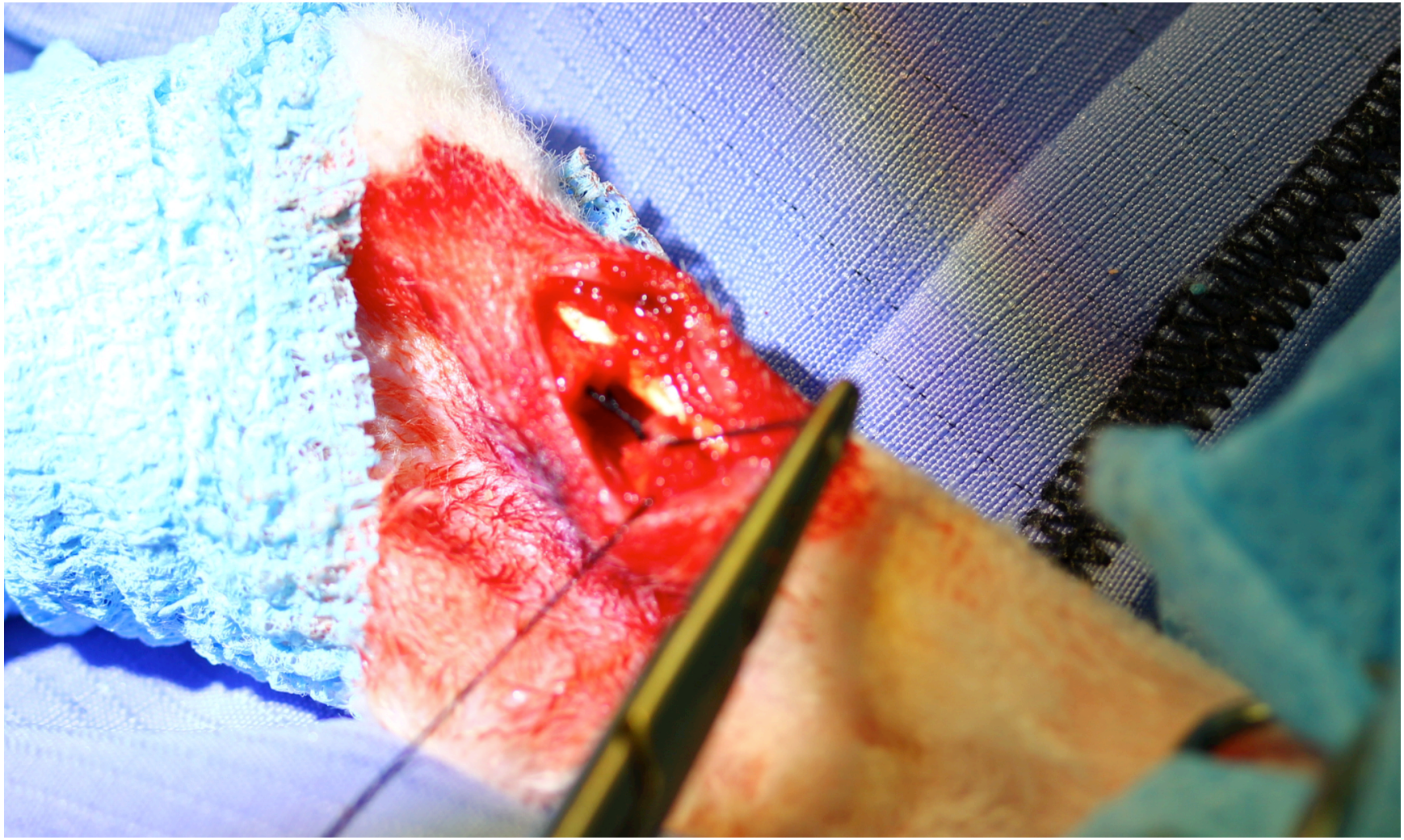

Figure 3.2.3H. Surgical Procedure. A single core suture using 4-0 USP braided nylon was used to create a single locking loop through the core. As the suture was tightened, the ends of the tendon were re-apposed. The calcaneus is in the top left of the image.

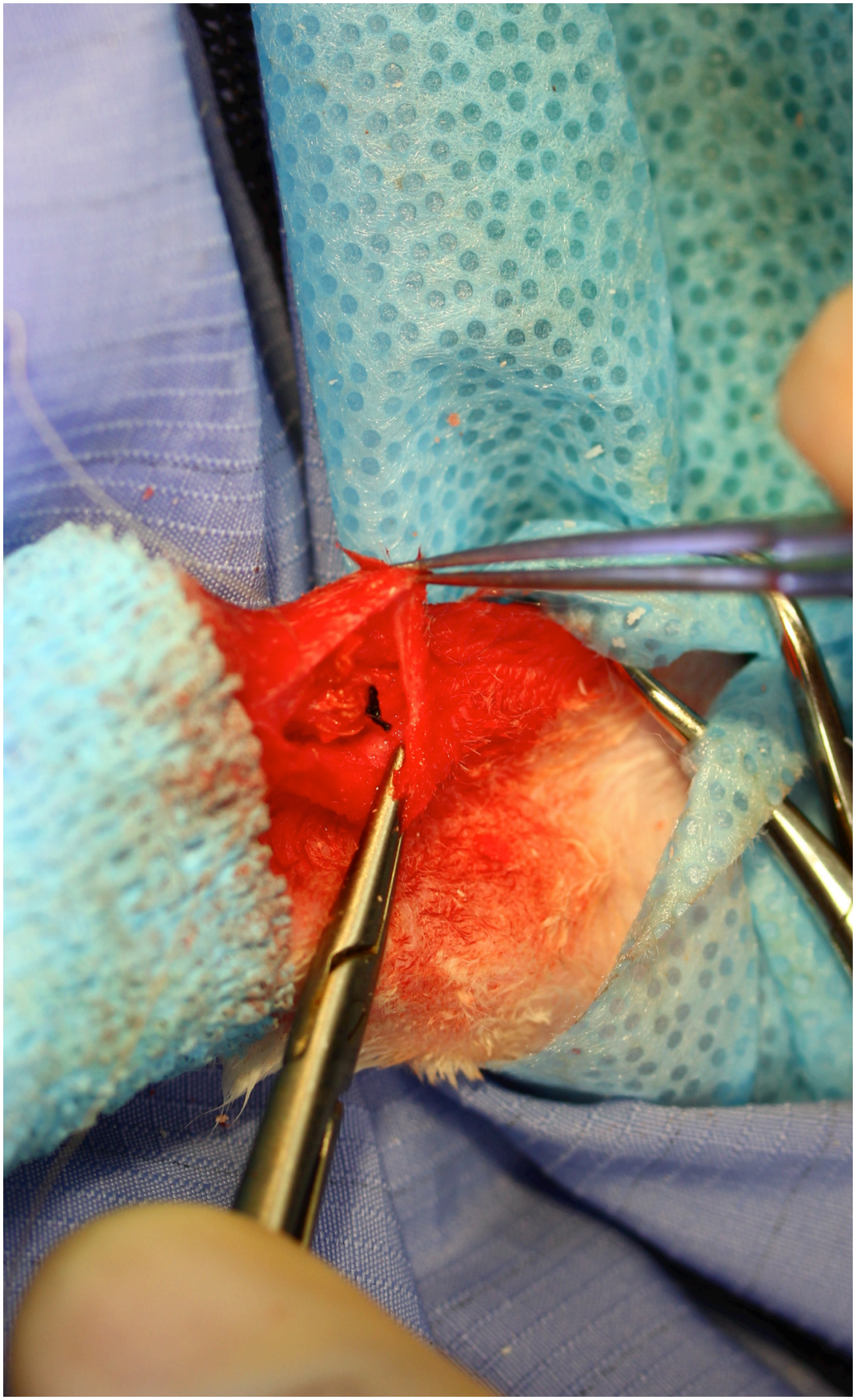

Figure 3.2.3l. Surgical Procedure. The two ends of the tendon were reapposed using 4-0 nylon. Care was taken to avoid overriding the tends during tightening so they were maintained in physiological length and in apposition only.

Figure 3.2.3J. Surgical Procedure. After completion of the paratenon suture with HAP coated 4-0 braided polyglactin 910, the loose connective fascia was sutured over the tendons using non-HAP coated 6-0 polyglactin 910.

Figure 3.2.3K. Surgical Procedure. At the conclusion of the surgery, several cruciate pattern sutures of 3-0 polypropylene were placed in the skin, which were removed 10 days post surgery. Limbs were not bandaged post-operatively.

Imaging Based Evaluation

3.3.1 Anesthesia Technique

For all imaging protocols, rabbits were given buprenorphine (0.01-0.05 mg/kg IM) and midazolam (1 mg/kg IM) prior to induction for imaging. Rabbits were then placed in a gas chamber and anesthetized using isoflurane gas flow at 5% and 3 L/min oxygen flow rate. Once anesthetized, a facial mask was placed and the rabbits were maintained on an oxygen/isoflurane gas mixture according to plane of anesthesia in order to maintain the rabbits in a light plane, which eliminated any movement (**Figure 3.3.1A**)

Figure 3.3.1A. Rabbits were maintained under anesthesia for the imaging portion of the study using a facial mask that delivered the flow of oxygen and anesthetic.

3.3.2 Shear Wave Elastography

For the all surgical short term (4-week) groups, quantitative SWI was performed bilaterally on the medial and lateral gastrocnemius tendons at 0-weeks (pre-surgery), 2 and 4-weeks post-surgery. For the non-operated group (NT), SWI was performed bilaterally on the lateral tendons at one time point prior to euthanasia. All rabbits were placed under general anesthesia to prevent any movement during scanning as described above. Legs were clipped from the calcaneus to the stifle joint using surgical clippers in order to provide a clean imaging surface. Legs were placed in a custom designed mold to maintain the tarsus at 90 degrees flexion for every scan (**Figure 3.3.2A)**.

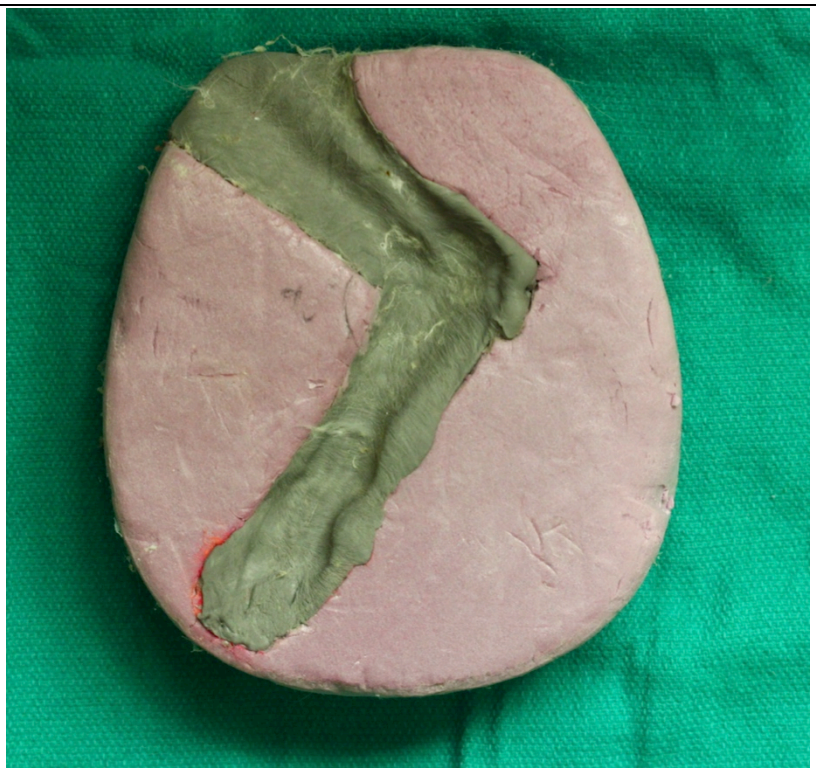

Figure 3.3.2A. Custom designed leg mold which were used to secure the rabbits legs in a fixed 90 degree tarsal angle for every imaging scan with SWI and for all MCA scans.

Shear wave images were collected with the Supersonic Imagine Aixplorer system (Aix-en-Provence, France; software version: 5; preset: superficial MSK; opt: penetrate; persist: high; smoothing: 7). A 50 mm linear transducer (Supersonic Imagine L15-4) was manually positioned over a 2 cm ultrasound standoff pad (Aquaflex, Parker Laboratories, Fairfield, NJ) placed over the lateral side of the leg, with ultrasound gel added to enhance contact with the pad and leg. A single operator performed all ultrasound scans to eliminate inter-observer variability.[7] The transducer was positioned to visualize the entire length of the Achilles tendon unit along the longitudinal axis, extending from the gastrocnemius muscle-tendon junction to the calcaneal insertion, and was shifted appropriately to obtain views of the lateral or medial tendon **(Fig 3.3.2B).** Minimal transducer pressure was applied to avoid strain-stiffening effects.[8] SWI speeds were measured within a 15 mm square region of interest (ROI) at 3 locations along the tendon: centered over the tendon repair (distal), 15 mm proximal to the repair (mid) and 20 mm proximal to the repair (proximal). Three repeated images were obtained at each location without repositioning the transducer, but after sufficient image refresh time **(Figure 3.3.2C).**

SWI speed measures were obtained post hoc from exported DICOM images. A custom MATLAB (Mathworks, Inc., Natick, MA) graphical user interface (GUI) was used to manually select sub-regions within the region of interest (ROI), which only included the tendon tissue of interest. The mean SWI speeds across repeated images were then computed. Distal, mid and proximal regions of SWI analysis were evaluated to determine significant differences among the SWI speeds. The region demonstrating the

greatest change between time points 0,2 and 4 weeks post surgery, was then chosen for evaluation in further comparisons with biomechanical data.

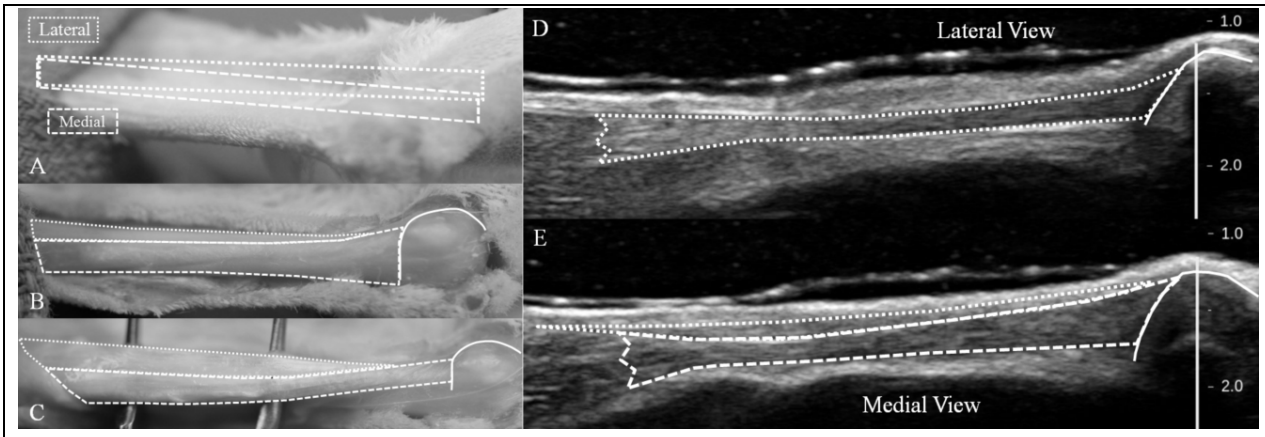

Figure 3.3.2B Representative anatomical and ultrasound images showing relative location of the calcaneus, and lateral and medial gastrocnemius tendons. **A:** Transducer position for imaging lateral and medial tendons. **B:** View of Achilles tendon unit (fascia intact). **C:** View of Achilles tendon unit (exterior fascia removed). Tendon unit rotated to obtain better view of lateral tendon. **D:** Ultrasound image of lateral tendon. Lateral tendon is highlighted in the outline, with the calcaneus to the left of the image **E:** Ultrasound image of medial tendon, with the medial tendon highlighted in the outline, with the calcaneus to the left of the image. From Martin J, Biedrzycki AH et al.[9]

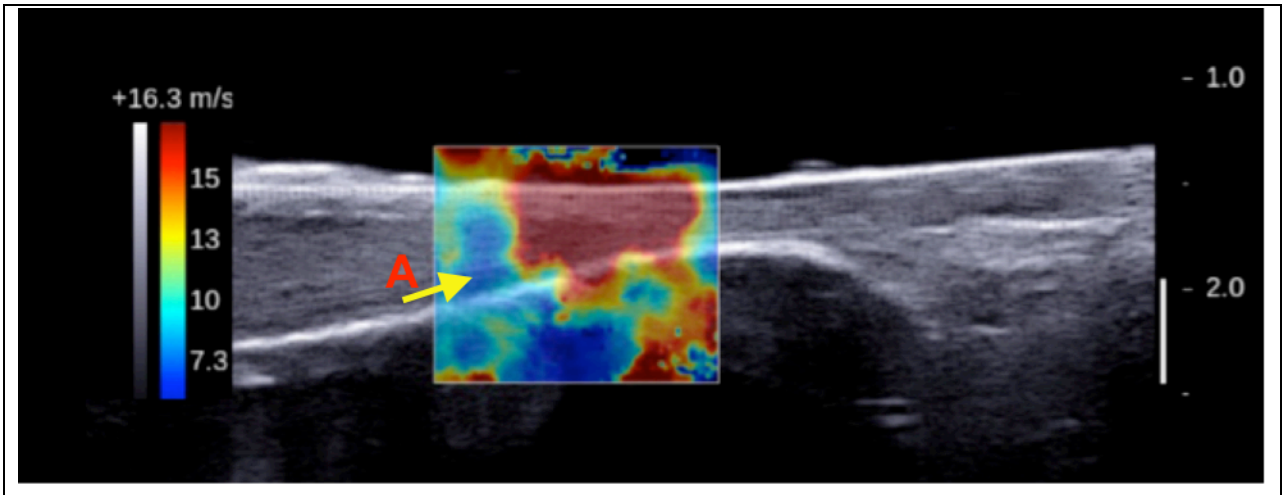

Figure 3.3.2C. Shear wave speed in intact, normal tendon. Shear wave velocity exceeds 16.3 m/s in the majority of the tendon body. Note that at the level of the musculotendinous junction **(A)** there is a reduction in shear wave speed, indicating a softening of the tissue in the muscle. Proximal to the left, distal (calcaneus) to the right.

3.3.3 Acoustoelastography

AE cineloops were collected with the Supersonic Imagine Aixplorer system (Aix-en-Provence, France). A 50 mm linear transducer (Supersonic Imagine L15-4) was manually positioned over a 2 cm ultrasound standoff pad (Aquaflex, Parker Laboratories, Fairfield, NJ), and placed over the lateral side of the leg, with ultrasound gel added to enhance contact with the pad and leg. A single operator performed all ultrasound scans. The transducer was positioned to visualize the entire length of the Achilles tendon unit along the longitudinal axis, extending from the gastrocnemius muscle-tendon junction to the calcaneal insertion, and was shifted appropriately to obtain views of the lateral or medial tendon, just as was carried out for the SWI analysis (**Figure 3.3.2B**). Once positioned over the correct anatomical structure, a 5 second cineloop was recorded comprising elongation and relaxation of the tendon. Three appropriate cineloops were created for each anatomical structure. Cineloops were exported as DICOM files and viewed using Echo Soft Imaging Software (radius 15, spacing along rows 5, spacing between rows 5) (Echo Soft RV, Echo Metrix, Fitchburg, WI). Using this software, files were cropped to comprise the stretch phase of tendon elongation. A ROI was placed over the central portion of the repair on a lateral tendon, or a similar location on the medial tendon, with the knowledge that the surgical procedure was performed 15 mm proximal to the calcaneus. Maximum Pathology Index (PI), a metric generated using the Echo Soft software, images and values were generated from the analysis and recorded for each cineloop (**Figure 3.3.3A).** Mean values of all three cineloop recordings were then computed for each rabbit tendon.

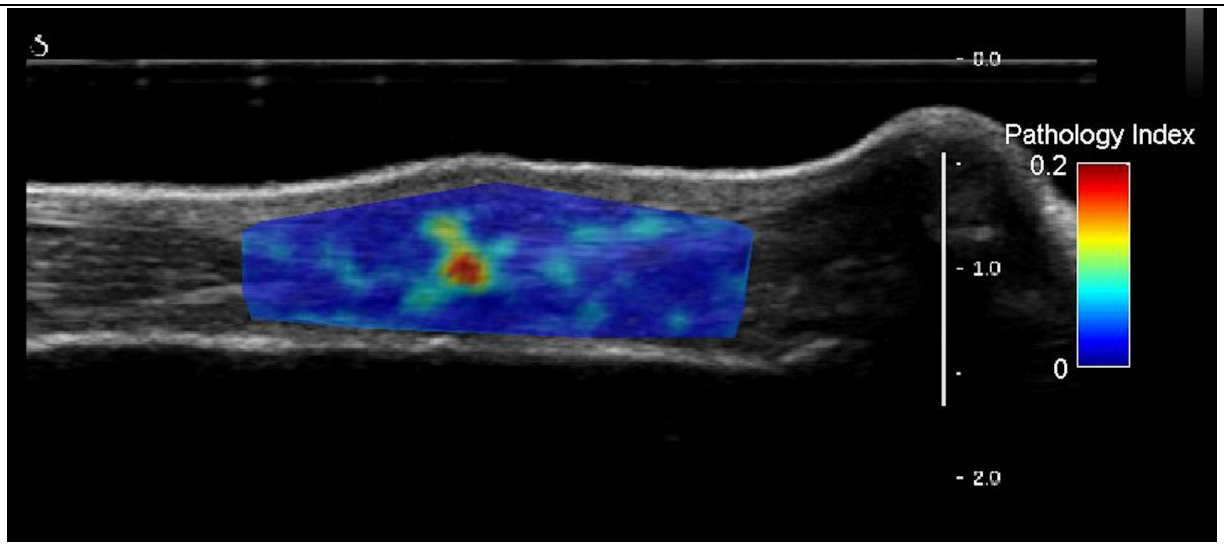

Figure 3.3.3A. Representation of visual Pathology Index evaluation. Note how in the center of the healing region is an area of high (>0.2) pathology index (PI), which is located in the region of the surgical site. The remainder of the tendon maintains low PI values.

3.3.4. Microbubble Contrast Angiography

MCA cineloops were collected with the Siemens Acuson S2000 ultrasound scanner (Siemens, Mountain View CA). A linear probe (14L5), using a frequency of 10.0 MHZ was manually positioned over a 2 cm ultrasound standoff pad (Aquaflex, Parker Laboratories, Fairfield, NJ) placed over the lateral side of the leg, with ultrasound gel added to enhance contact with the pad and leg. A single operator performed all ultrasound scans. The transducer was positioned to visualize a region 15 mm proximal to the calcaneus on the lateral gastrocnemius tendon only, having confirmed the anatomical region using B mode imaging. Once in position, the contrast agent detection, or cadence mode was activated with a frequency of 5.0 MHz. We utilized the

microbubble-based contrast agent Definity (Lantheus Medical Imaging, Inc. Billerica MA), administered intravenously in the marginal ear vein of the rabbit. The Definity consists of perflutren lipid microspheres (mean diameter, 1.1 μm – 3.3 μm) that are composed of octafluoropropane gas encapsulated in an outer lipid shell consisting of (R) – hexadecanoic acid, 1-[(phosphonoxy)methyl]-1,2ethanediyl ester. Definity is a blood-pool contrast agent, which remains in the vessels until it dissolves. Definity must first be activated via the rapid and violent agitation in the Vialmix activation unit. After activation, each mL of the milky white suspension contains a maximum of 1.2×10^{10} perflutren lipid microspheres, and approximately 150 μL/mL (1.1 mg/mL) octafluoropropane. Each rabbit received 0.15 ml, or 1.8×10^{9} microspheres. Upon injection, a 30 second cineloop was recorded using the cadence mode. The exact same procedure was repeated on the contralateral leg.

DICOM images were processed using Osirix (Osirix DICOM Viewer, Pixmeo SARL, Bernex, Switzerland). A region of interest centered over the central portion of the tendon was isolated and exported as a MOV file. MOV files were then imported and analysed using an analysis program (Image J, Image processing and analysis in Java, NIH), where they were transformed into 8-bit greyscale images using a virtual stack. Stack frames were then analysed as the program calculated mean pixel values for each ROI, with mean pixel values plotted against time (**Figure 3.3.4A**). Mean upslope and downslope and standard deviations were calculated using a commercial spread sheet (Excel 2012, Microsoft, Richmond, VA). Parameters recorded were mean baseline, mean baseline + 10%, mean Baseline + 85%, mean peak values, and time to peak.[10]

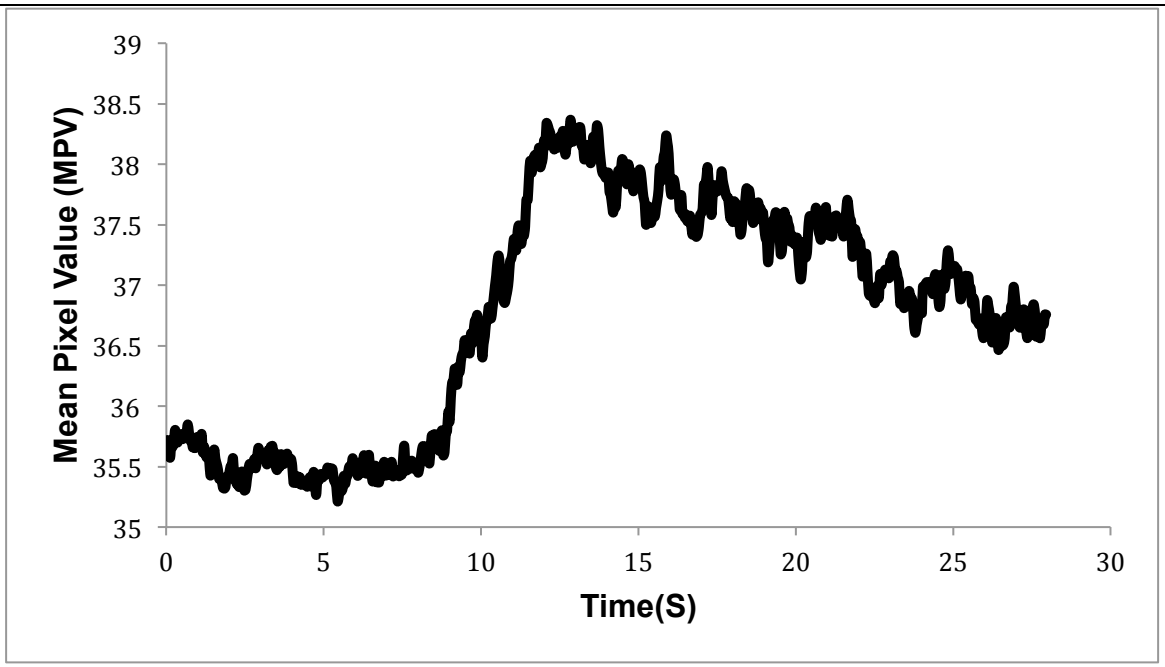

Figure 3.3.4A. Graph example of mean pixel volume plotted against time. Note how there is a noisy baseline, a sudden elevation to a peak followed by a gradual decline. In this example, 10% above baseline to 80% of peak represents an increase in mean pixel value of 2.3.

Biomechanical and Histological Evaluation

3.4.1 Euthanasia

At the given time point as denoted for either the short-term study (4-weeks post surgery) or the long-term study (9-weeks post surgery), rabbits were euthanatized for mechanical and histological evaluation. Rabbits were placed inside a gas chamber and anesthetized using isoflurane gas flow using 5% at 3 L/min. Once anesthetized, an overdose with 450 mg pentobarbital into the marginal ear vein was administered.

3.4.2 Anatomical Dissection

After euthanasia, an incision was made on the lateral aspect of the limb, centered over the mid metatarsal region, approximately 15 mm cranial to the original surgical incision, so as to not disturb any macroscopic evidence of healing or infection. The skin was dissected back over the calcaneus and Achilles tendon and the incision was extended to expose the musculotendinous junction. After removal of any surrounding fascia, the repair of the lateral gastrocnemius tendon was inspected, photographed and the tendon thickness at the incision site and repair location were measured in 4 regions, just proximal to the repair, at 2 sites proximal and distal centered around the repair and at one location just distal to the repair using a hand-held digital micrometer (General Tools, NY). The center of the repair was determined macroscopically and known to be located 15 mm proximal to the calcaneus.

In addition, at the time of harvest, tendon structures were macroscopically evaluated and subjectively scored according to several parameters, including presence of inflammation, obvious vascularity and presence of adhesions. Each category was on a 4-point numerical scale from 0 (absent), 1 (mild), 2(moderate) and 3 (severe).

Following this procedure, limbs were randomly assigned to mechanical testing or to histological evaluation. If a limb was assigned to mechanical testing, the gastrocnemius muscle was transected approximately 50 mm above the musculotendinous junction. The medial gastrocnemius tendon bundle was isolated and

an approximately 20 mm portion of this tendon was removed. The calcaneus was disarticulated from the calcaneo-talar junction using bolt cutters. The entire calcaneus-lateral gastrocnemius tendon- lateral gastrocnemius muscle unit was then placed in a 50 ml sealed tube (Falcon Tubes) and filled with saline solution until mechanical testing. Samples were placed in a refrigerator at 4^{o}C for a maximum of 4 hours, at which time they were placed in a water bath at 37^{o}C and subjected to mechanical testing at body temperature.

If a leg was assigned to histological evaluation, after thickness measurements and photographs of the tendon were performed, the lateral gastrocnemius tendon and medial gastrocnemius tendons were isolated and bluntly dissected distally to the point of merger of the two tendons into the common Achilles tendon, which is approximately 7-9 mm proximal to the point of the calcaneus. At this point, the lateral tendon was transected. The proximal transection of the lateral gastrocnemius occurred approximately 25-30 mm proximal to the point of the calcaneus to ensure the entire block of tissue comprising the repair was excised.

The excised portion of the tendon was then placed in OCT solution (Tissue-Tek, VWR, Radnor, PA), in a cryoblock (Tissue Path™ Disposable Base Molds, 34 mm x 24 mm x 5 mm, Fisher Scientific, Pittsburgh, PA) and markers were placed so as to be able to identify the proximal-distal and cranial-caudal orientation of the tissue. The tendon tissue-OCT unit were then carefully immerse in liquid nitrogen to ensure appropriate

freezing of the tissue mass. The frozen section was then labeled and placed in deep freeze at -80^{o}C until histological evaluation.

The remaining section of medial gastrocnemius tendon was then excised from the rabbit to form a calcaneal-medial gastrocnemius tendon- medial gastrocnemius muscle block that would be subjected to mechanical testing. Measurements of thickness for the medial gastrocnemius tendon were also recorded. Thus, each rabbit contributed a medial and lateral gastrocnemius tendon for mechanical testing and a lateral gastrocnemius portion for histological evaluation.

3.4.3 Biomechanical Testing

Tendons were tested in uniaxial tension using a MTS 858 Bionix Test System (MTS Systems Corp., Eden Prairie, MN) with a 2225 N load cell. The proximal portion of the tendon was placed in a custom designed cryoclamp, and the calcaneus was rigidly clamped at the distal end. Solid carbon dioxide was used in the cryoclamp to freeze the muscle onto the testing platform of the clamp. Tendons were kept moistened with saline solution at 37^{o}C. Preconditioning began when the proximal muscle portion reached 0^{o}C in the clamped section, indicating freeze binding to the clamp. Tendons were preconditioned with 10 cycles to 3% strain at a rate of 2.5 mm/s There was no break between pre-conditioning and testing. Initial grip-to-grip tendon length was then recorded when the load cell registered 0 N for either tension or compression of the tendon, representing the original tendon length. Thickness measurements calculated in

situ previously were used to estimate the tendon cross-sectional area, which was assumed to be elliptical.

Tendons were stretched at a rate of 2.5 mm/s to failure. Force and elongation data were continuously sampled at a rate of 50 Hz. Elongation was used to compute the average strain along the tendon. Mean tendon stress was determined by dividing axial force by the average cross-sectional areas of the 4 locations determined along the length of the tendon. Ultimate stress was taken as the peak stress reached during loading. Young's modulus was calculated from the linear portion of the stress-strain curve.

Thus, biomechanical testing provided 5 parameters for evaluation: structural data (ultimate tensile strength (UTS) and stiffness) and material data (strain, Young's modulus and ultimate stress).

3.4.4 Histology

Eight sequential longitudinal samples from the central portion of the tendon were sectioned at 7 μm thicknesses on a Leica CM1950 (Wetzlar, Germany) cryostat. Following the sectioning, sections were randomized and subjected to four different histological imaging protocols. Two sections were stained with haematoxylin and eosin (H&E) and two further samples were stained with alcian blue and analyzed using a previously described tendon scoring system (**Table 3.2.7A and B**). Tendon scoring

was determined using the overall score, which includes parameters such as inflammation and vascularity. In addition, a tendon maturation score, which utilized the scores for parallel spindle cells, parallel collagen fibers, mature tendon tissue and gap filled parameters only, was implemented. The tendon maturation score permitted the evaluation of histology parameters strictly limited to tendon maturity and removes any potential bias from an excessive inflammatory response.

For H&E staining, the frozen sections were fixed in 10% buffered formalin (Fischer Scientific, Waltham, MA) for 20 mins followed by washing the tissue in distilled water. Nuclei were then stained by immersion in Gill II haematoxylin (Leica Biosystems, Nussloch, Germany) for 3 minutes. Slides were then washed in distilled water and immerse in a bluing agent (Fisher Scientific, Waltham, MA) for 30 seconds followed by washing in distilled water. Slides were then briefly immersed in 95% ethanol, followed by staining of the cytoplasm in eosin (Leica Biosystems, Nussloch, Germany) for 3 minutes, and dipped once in distilled water. Slides were then dehydrated by immersion in 1 change of 95% ethanol for 1 min followed by 3 changes of 100% ethanol (Fisher Scientific, Waltham, MA) for 10 dips each. Slides were then immersed in 2 changes of xylene (Fisher Scientific, Waltham, MA) for 2 minutes each, before mounting on slides with cytoseal 60 (VWR, Radnor, PA) using glass coverslips (Fischer Scientific, Waltham, MA).

The staining procedure for alcian blue followed a similar protocol to the H&E staining. After fixation of the tissue in 10% formaldehyde, slides were washed in

distilled water and then stained in alcian blue solution (Sigma-Aldrich Corp. St. Louis, MO) for 30 minutes. Slides were then placed under running tap water for 2 minutes, followed by a rinse in distilled water. A nuclear counterstain in fast red solution (Sigma-Aldrich Corp. St. Louis, MO) was then performed for 5 minutes, followed by a rinse in tap water for 1 minute. The dehydration procedure through 95% ethanol, 3 changes of 100% ethanol for 1 minute and 10 dips each occurred, as previously specified. Slides were then cleared with xylene and mounted on glass slides with cytoseal 60 and cover slipped.

Slides from each rabbit were then blinded to the reviewer, randomized and viewed using standard bright field microscopy (Leica Microsystems, Buffalo Grove, IL). Images were recorded using imaging software (Scion Imaging version 4.0.2, Scion Corp, Frederick, MA). Each rabbit was assigned a histology score and a tendon maturation score based on previously established criteria (**Table 3.4.4A and 3.4.4B**).

Categories	Scores
Cellularity/ Round Cells	
Marked	1
Moderate	2
Mild	3
Minimal	4
Proportion of spindle cells oriented parallel	
<25%	1
25-50%	2
50-75%	3
>75%	4
Proportion of collagen/fibers oriented parallel	
<25%	1
25-50%	2
50-75%	3
>75%	4
Proportion of mature tendon fibers	
<25%	1
25-50%	2
50-75%	3
>75%	4
Proportion of tendon gap filled	
<25%	1
50-75%	2
25-50%	3
>75%	4
Total score	**20**

Table 3.4.4A Tendon Scoring System Part 1

Categories	Scores
Suture Inflammation (around suture holes)	
Marked	1
Moderate	2
Mild	3
Minimal	4
Inflammation tissue percent of total tendon	
>75%	1
50-75%	2
25-50%	3
<25%	4
Total scores	**8**

Table 3.4.4B. Tendon Scoring System, Part 2

3.4.5 Immunofluorescent Procedure

Two samples from each section were subjected to CD31 (platelet endothelial cellular adhesion molecule (PECAM-1) or MAC387 (calprotectin) antibodies for evaluation of neovascularization and macrophage infiltration, respectively. Experimental and control slides were selected and removed from the -80^{o}C freezer and allowed to thaw for 15 minutes at room temperature. Sections on the slide were circled using a Hydrophobic Barrier Pen (Vector Lab, Burlington, CA). Slides were then fixed in cold (refrigerated at 4^{o}C) acetone for 10 minutes. Slides were then allowed to air dry after this procedure for 15 minutes. Slides were then washed in 1X TBS-Tween-20 (990 mls. TBS, 10 mls Tween-20) once for 5 minutes. Following this, slides were washed twice in 1X TBS for 5 minutes each time. Slides were then blocked by using 1% normal donkey serum (Abcam, Cambridge, MA) for 30 minutes at room temperature.

Following the blocking procedure, primary antibodies were applied. For CD31, primary antibodies were incubated overnight at 4^{o}C, using mouse anti-rabbit IgG1 at a 1:10 dilution, with PBS and 1.5% normal donkey serum. Slides were placed in a humidification chamber to prevent slides from drying out. For MAC387, a mouse anti-rabbit monoclonal IgG1 antibody at 1:100 dilutions in PBS and 1.5% normal donkey serum was utilized and incubated overnight at 4^{o}C in a humidification chamber. The next step involved washing the slides in 1X TBS solution for 15 minutes each time. The secondary antibody was Alexa Fluor488 (excitation 488 nm, emission 522 nm) applied and incubated for 60 minutes at room temperature in darkness. For the CD31, the secondary antibody was a polyclonal IgG donkey anti-mouse heavy and light chain with at 1:200 dilution in PBS and 1.5% normal donkey serum. For the MAC387, the secondary antibody was a polyclonal donkey anti-mouse IgG heavy and light chain Alexa Fluor 594 (excitation 590 nm, emission 617 nm) at 1:200 dilution with PBS and 1.5% normal donkey serum.

Slides were then again washed in 1X TBS for 15 minutes each time. Fluoroshield mounting media with 4',6-diamidino-2-phenylindole (DAPI, excitation 358 nm, emission 461 nm) was then applied (Abcam, Cambridge, MA) and the slides were coverslipped and placed in a dark container until visualization under a florescence microscope.

3.5 Statistical Analysis

Analysis of variance were performed followed by a post-hoc Tukey's test to separate differences among groups using an alpha value of 0.05, if the data are normally distributed as determined by the Kolmogorov–Smirnov test. If data were normally distributed, the Kruskal–Wallis test will be used to separate differences among groups. For the paired study design, the Student's paired t test was used for statistical analysis for mechanical testing data and histological analysis between the treatment groups if the data were normally distributed as determined by the Kolmogorov–Smirnov test. If not normally distributed, the Mann-Whitney U test was performed to separate differences between control and cytokine treatment groups. Differences were considered significant at a probability level of 95% ($p<0.05$). Probabilities between 0.05 and 0.15 were classified as trends. If the t-test evaluations failed to reject the null hypothesis, a post-hoc power evaluation was performed to identify achieved power.

A two-way factorial analysis of variance was performed to determine the significance of each level of growth factor on the ultimate tensile strength.

For analysis of correlation values, Pearson's correlation coefficients with significance levels were calculated. Correlation R-values between 0.2 and 0.4 were considered weak, 0.4 to 0.7 moderate and any correlation above 0.7 were considered strong. For analysis of method of failure data, a chi-squared evaluation of mechanisms of failure was performed.

For SWI evaluations on lateral tendons, we performed a two-way repeated measure ANOVA to assess the effects of scanning location (proximal/mid/distal) and time point (0, 2, 4 weeks) on SWS. For medial tendon SWI and all AE data, we performed a one-way repeated measures ANOVA to assess the effects of time point on SWI or AE and to evaluate if any differences exist among the groups for either lateral or medial branches. All main effects were followed up with post-hoc pairwise comparisons using Tukey's method of multiple comparison evaluation.

We performed linear regression to assess the relationship between SWI and AE parameters, including ultimate tensile strength, stiffness, maximum stress and strain and elastic modulus (Young's Modulus). We also assessed the sensitivity and specificity of SWS, elastic modulus and ultimate strength only, due to having obtained SWI values for intact normal tendons. SWI was the only modality that was performed on this normal group. Thus, we were able to distinguish the surgically repaired tendons from the intact tendons (medial and non-surgical lateral). This was done by comparing individual SWI measures to mean values from each group (control or treated) and assigning them to the group for which they have a lower z score.

All statistical analyses were performed with SAS V.8e software (SAS Inc., Cary NC) and Prism 6 (Graph Pad Software Inc., La Jolla CA)

References

1 **Murphy, W.L.** Bioinspired growth of crystalline carbonate apatite on biodegradable polymer substrata. *J Am Chem Soc* **124**, 1910-1917 (2002).

2 **Zhang, F. et al.** Effect of vascular endothelial growth factor on rat Achilles tendon healing. *Plast Reconstr Surg* **112**, 1613-1619 (2003).

3 **Lu, Y. et al.** Histologic evaluation of suture material loaded with basic fibroblast growth factor (bFGF) on acute rotator cuff repair in an ovine model. *Curr Orthop Pract* **22**, 425-431 (2011).

4 **Hodde, J. et al.** Effects of sterilization on an extracellular matrix scaffold: part I. Composition and matrix architecture. *J Mater Sci Mater Med* **18***,* 537-543 (2007).

5 **Hodde, J. et al.** Effects of sterilization on an extracellular matrix scaffold: part II. Bioactivity and matrix interaction. *J Mater Sci Mater Med* **18,** 545-550 (2007).

6 **Henderson, J., Sutcliffe, M., & Gillespie, P.** Epitendinous suture techniques in extensor tendon repairs—an experimental evaluation. *J Hand Surg* **36**, 1968-1973 (2011).

7 **Peltz, C.D. Haladik, J.A. Divine, G. & Siegal, D.** ShearWave elastography: repeatability for measurement of tendon stiffness. *Skeletal Radiol* **42,** 1151-1156 (2013).

8 **Kot, B.C.W. et al.** Elastic Modulus of Muscle and Tendon with Shear Wave Ultrasound Elastography: Variations with Different Technical Settings. *PLoS ONE* **7**, e44348 (2012).

9 **Martin, J. et al.** In Vivo Measures Of Shear Wave Speed As A Predictor Of Tendon Elasticity And Strength. *Submitted to Ultrasound Med Biol* (2014).

10 **Ziegler, L. E., O'Brien, R. T., Waller, K. R. & Zagzebski, J. A**. Quantitative contrast harmonic ultrasound imaging of normal canine liver. *Vet Radiol Ultrasound* **44**, 451-454 (2003).

Chapter 4

Results

4. Results

Laboratory Based Evaluation

4.1.1. SEM Suture Material Analysis

HAP crystals were able to be generated on all materials and followed a similar pattern (**Figure 4.1.1A**). For any given time point however, the appearance of the crystals on the absorbable polyglactin 910 appeared more organized and complete than the non absorbable nylon. (**Figure 4.1.1B**). The crystal formation on the suture material appeared complete in most samples. Crystals tended to form plate like structures (**Figure 4.1.1C**), which increased the surface area for growth factor adsorption. While most suture samples and sizes appeared like suitable candidates for incorporation into the surgical evaluation, several potential limitations were identified with the non-absorbable small diameter monofilament nylon (**Figure 4.1.1D and 4.1.1E**). In areas, the suture was devoid of an HAP layer, which appeared to have cracked off the structure. There were in addition several areas of deep fissuring present in areas of the suture where the HAP was identified. For all samples, coatings up to day 14 appeared too brittle and cracking was observed in some cases at this time period (**Figure 4.4.1F**). For braided material, no significant defects in the HAP layer were observed up to approximately day 12. In all cases, polyglactin 910 appeared superior to nylon, and larger diameter sutures in general, appeared to have a better HAP crystalline layer. Braided materials throughout the incubation period also were superior in their acquisition of crystals than monofilament suture material.

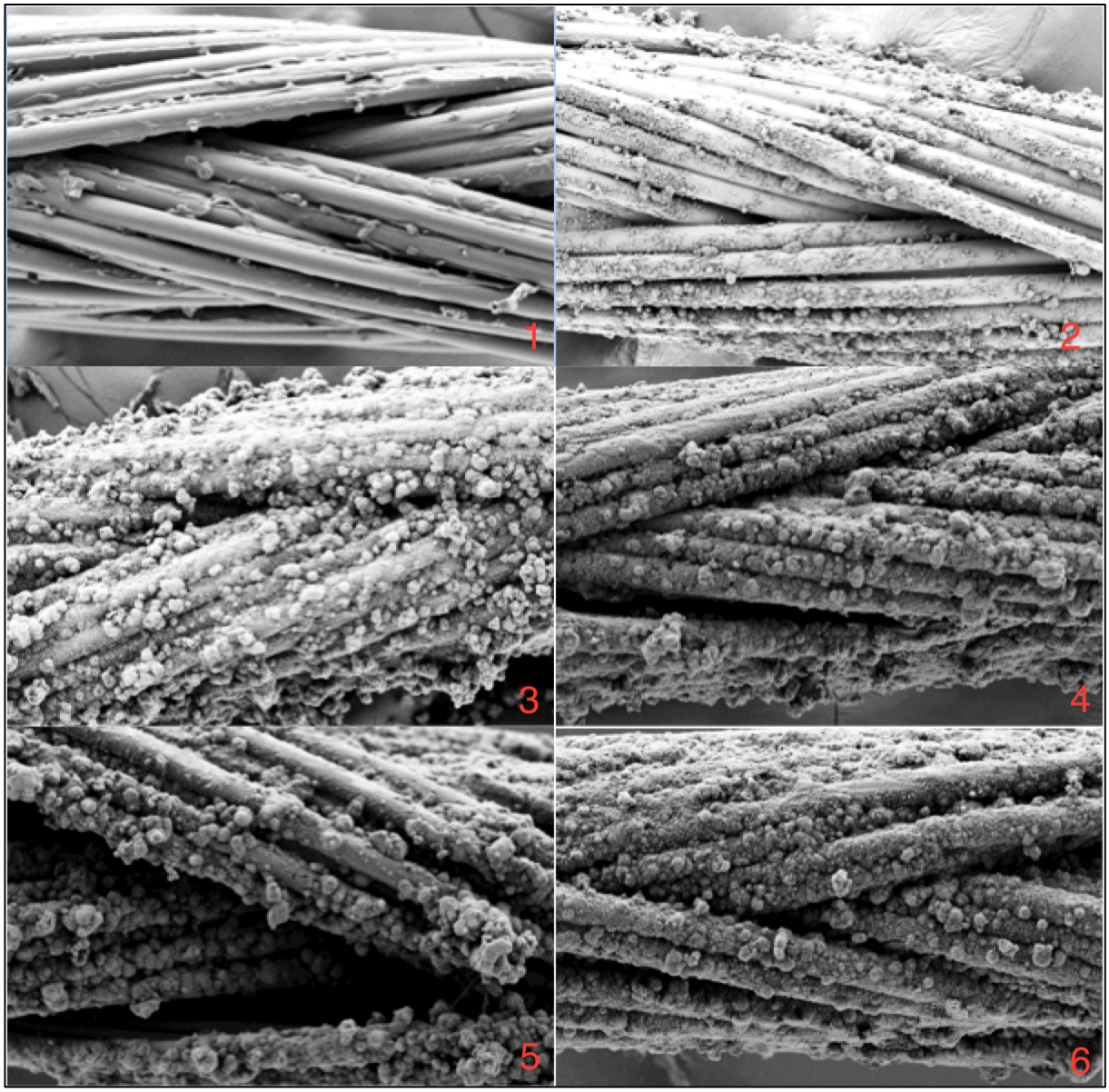

Figure 4.1.1A Scanning Electron Micrograph (SEM) of HAP crystal growth. Growth of HAP on 4-0 braided Nylon Suture material. **1**) Day 0 uncoated suture. **2**) Day 2. **3**) Day 4. **4**) Day 6. **5**) Day 8. **6**) Day 10. 300X magnification.

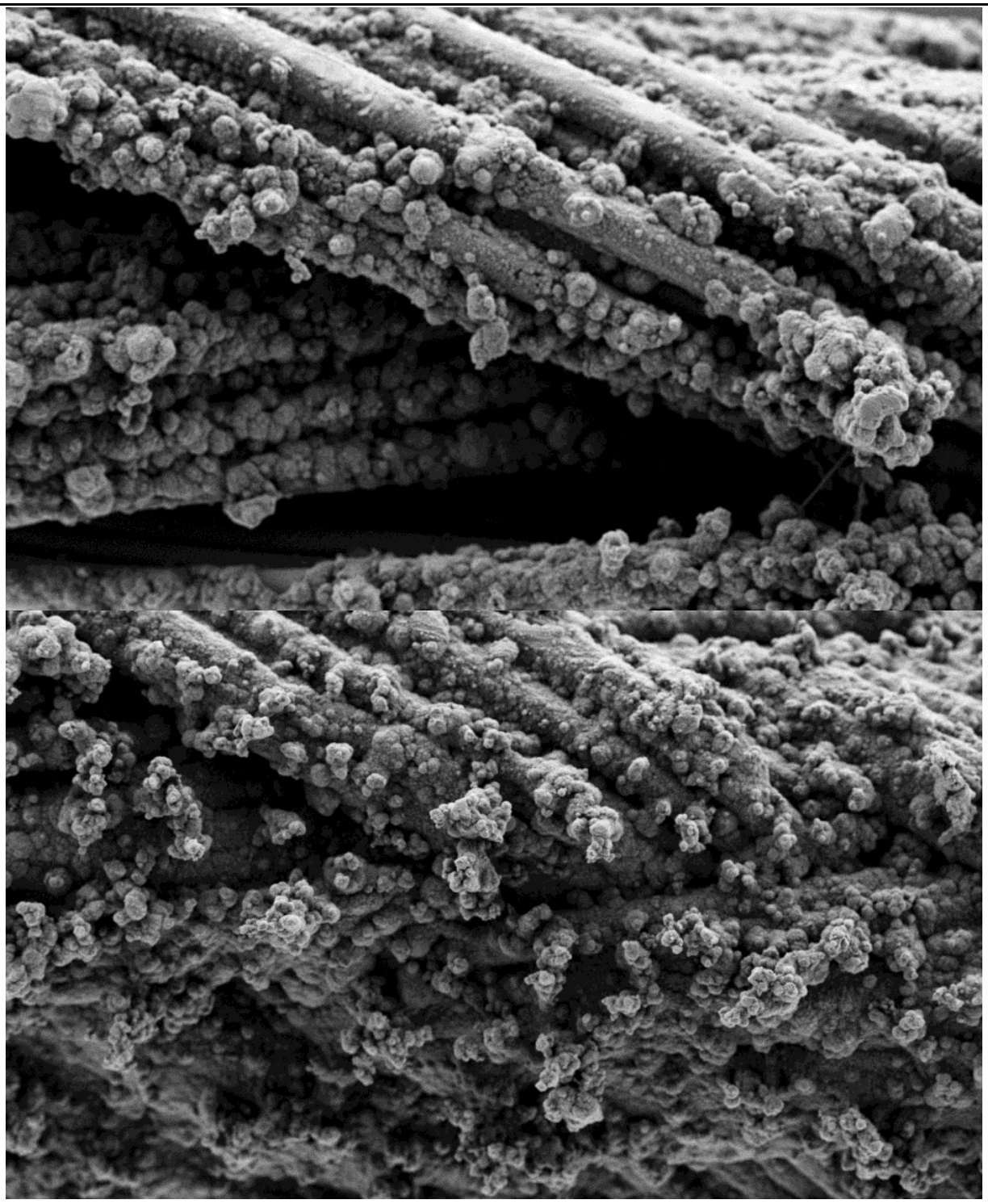

Figure 4.1.1B SEM of 4-0 nylon **(Top)** and 4-0 polyglactin 910 **(Bottom)** at the same time point (Day 8). Note that fibers of the nylon can still be readily seen whereas there appears to be more complete HAP crystal uptake in the polyglactin 910 sample. 300X magnification.

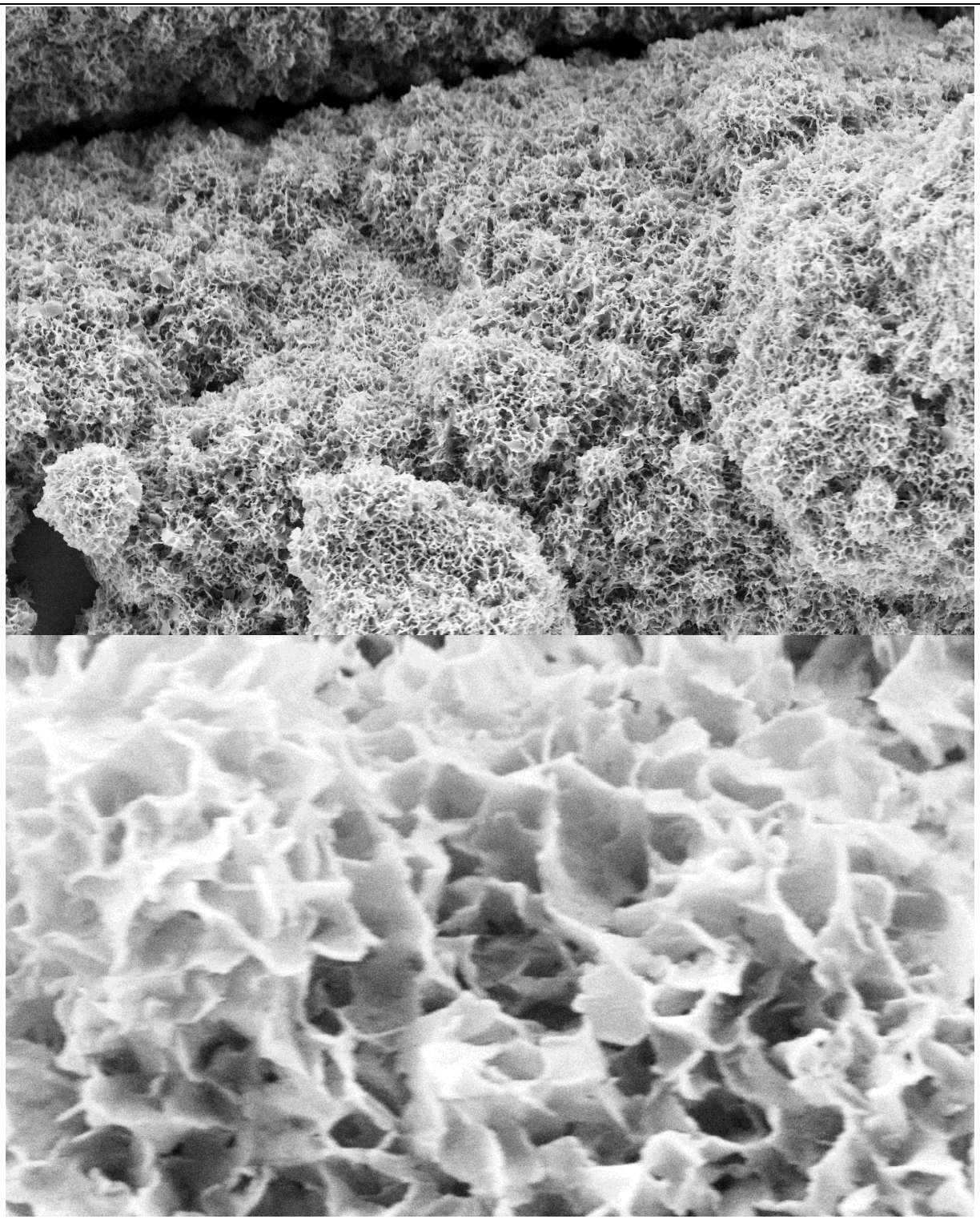

Figure 4.1.1C (Top) SEM of Day 14 4-0 Nylon. 10,000X magnification **(Bottom)** SEM of Day 14 4-0 Nylon. Note the plate like appearance to the HAP crystals, which increases the surface area of the suture for adhesion of growth factors. 100,000X magnification

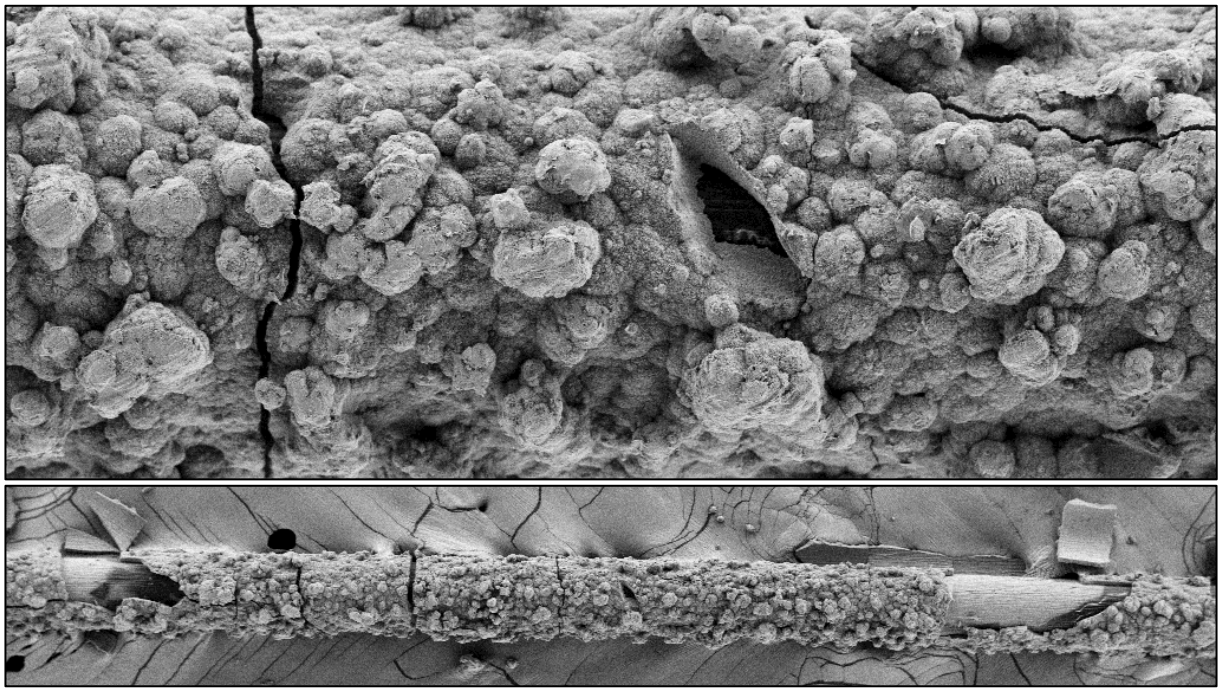

Figure 4.1.1D (Top) SEM of Day 10 6-0 monofilament nylon**.** 1,000X magnification **(Bottom)** SEM of Day 10 6-0 monofilament nylon. Note the deep fissures in the top picture and the high degree of cracking of the HAP layer off the suture material in the bottom image. 150X magnification

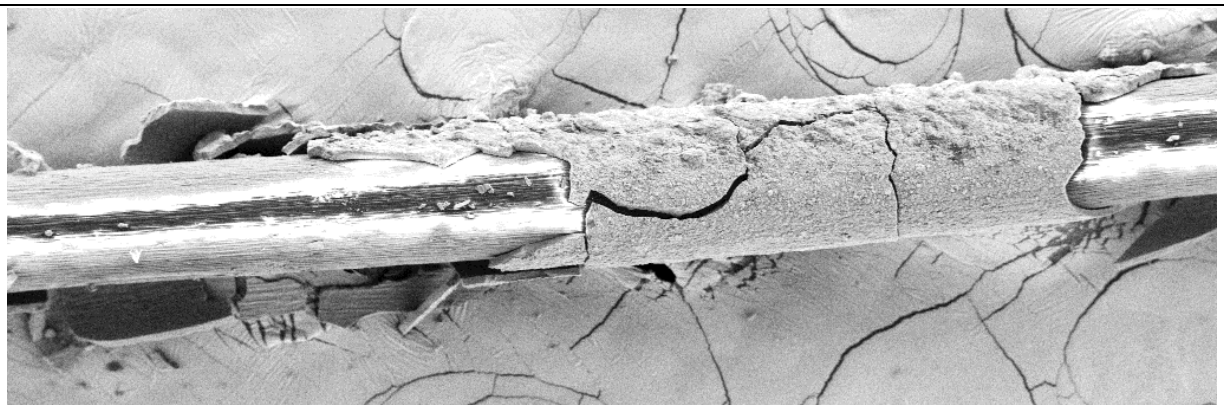

Figure 4.1.1E SEM of 6-0 monofilament nylon. Note the high degree of cracking of the HAP layer. In some areas there is a complete absence of HAP. 300X magnification

Figure 4.1.1F SEM of 6-0 monofilament nylon. Magnified image demonstrating the interface between the HAP and the suture layer. 2,200X magnification

4.1.2 Confocal Microscopy Analysis

Rhodamine (fluoresces red, applied day 7) and fluorescein isocyanate (fluoresces green, applied day 14) were successfully incorporated onto all sutures. However, it was noted that the 14-day time point for HAP growth resulted in unexpected cracking of the HAP layer, even on braided suture material. (**Figure 4.1.2A**). When the time points of suture HAP crystal growth and fluorescent marker application were modified to day 6 and day 10 from day 7 and day 14 respectively, no adverse effects were noted. Day 6 application with rhodamine followed by day 10 application of fluorescein resulted in no co-localization of growth factors and no cracking or adverse effects of the HAP crystal layers (**Figure 4.1.2B, 4.2.1C**). However, it was also possible

to apply the growth factors simultaneously at day 6, resulting in perfect co-localization (**Figure 4.1.2D, 4.1.2E**)

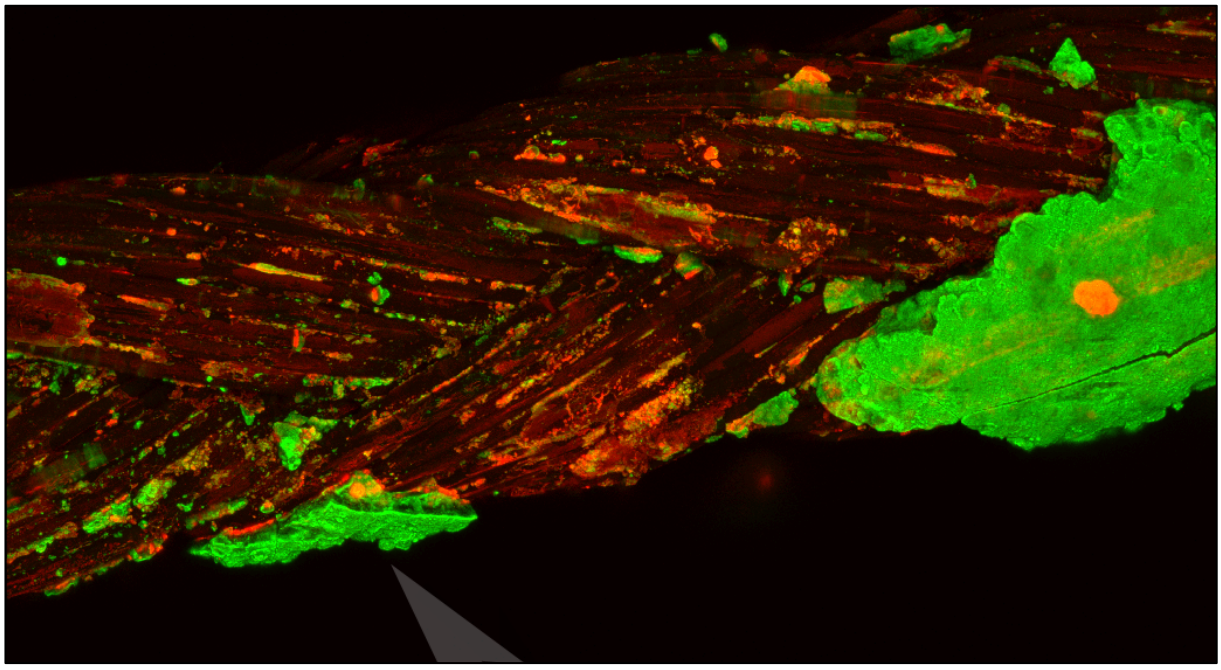

Figure 4.1.2A. Confocal microscopy image of 4-0 polyglactin 910 suture at day 14. There is a significant reduction in the fluorescence of the day 7 applied rhodamine and the day 14 applied fluorescein. To the right of the image, a large green plate of HAP crystal remains; however, the majority of the suture is devoid of significant fluorescence. 100X magnification.

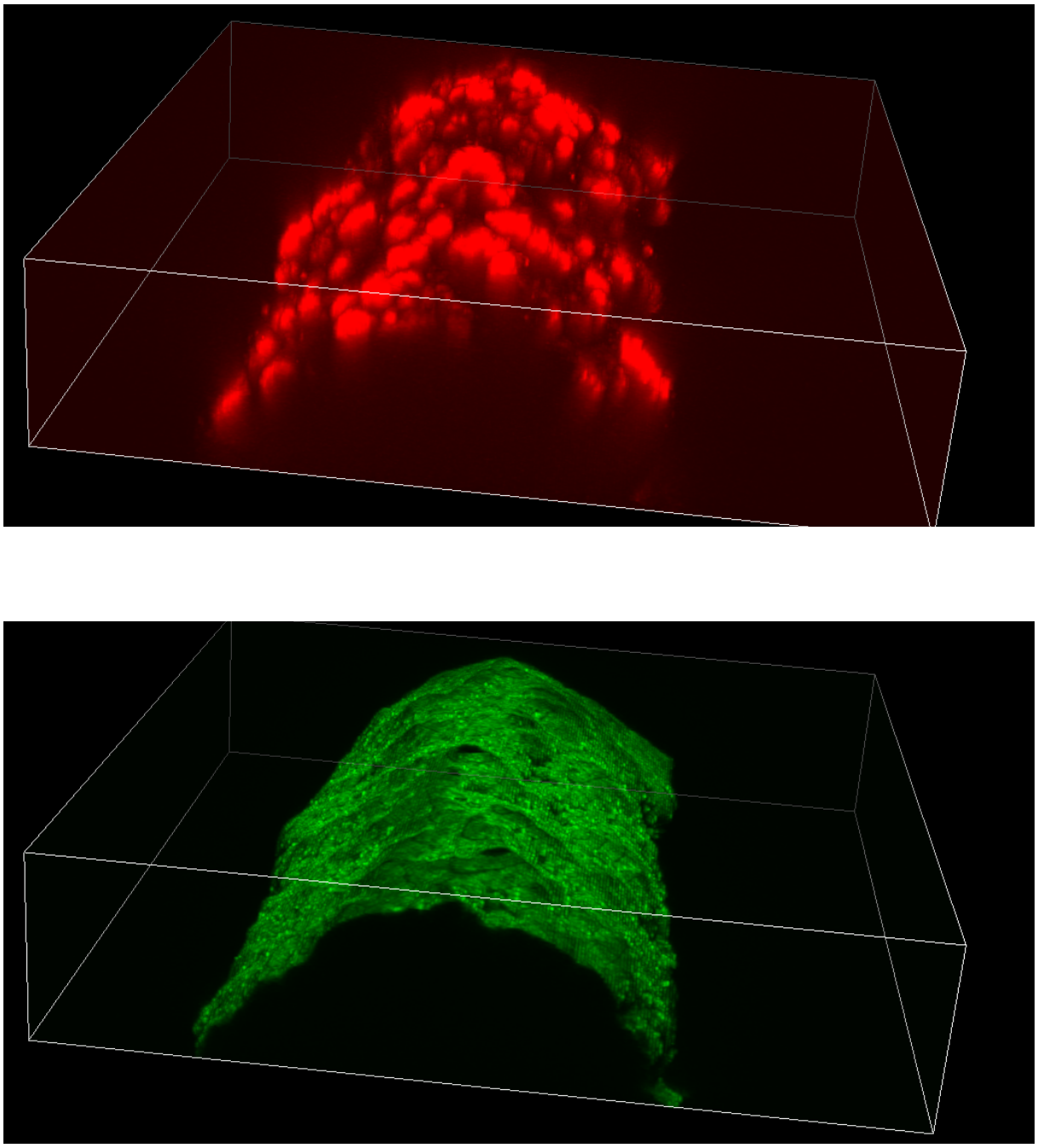

Figure 4.1.2B. Confocal microscope 3-D Z-stacked series of polyglactin 910 suture material. Rhodamine was applied at day 6 (**Top**) followed by re-incubation in mSBF. Fluorescein was then applied at day 10 (**Bottom**). Note it appears that the red layer is more globular in nature and appears to be overlain by a flat sheet of the green layer. 100X magnification

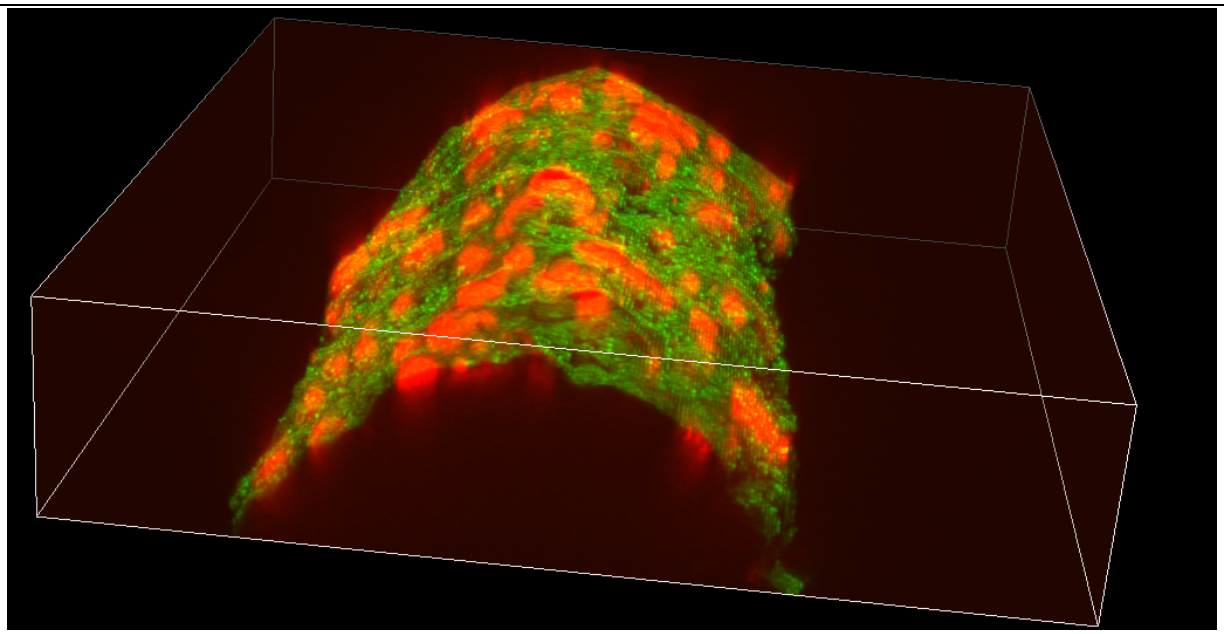

Figure 4.1.2C. Confocal microscope 3-D Z-stacked series of polyglactin 910 suture material. Rhodamine was applied at day 6 followed by re-incubation in mSBF. Fluorescein was then applied at day 10. The overlay of these two in this image demonstrates the success in spatial separation of the two fluorochromes. There was no co-localization. 100X magnification

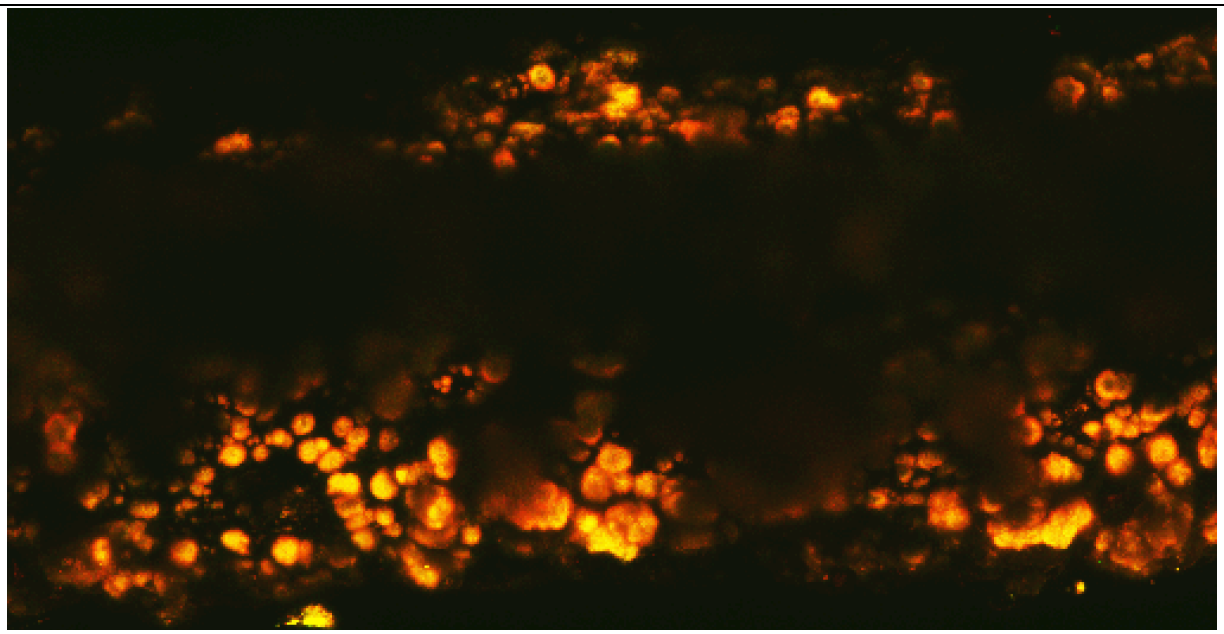

Figure 4.1.2D. Confocal microscope image of Day 10 application of rhodamine and fluorescein on the same section of suture and crystals. Note that both fluorochromes adsorb to the same portions of the HAP plate, resulting in near total co-localization. 100X magnification.

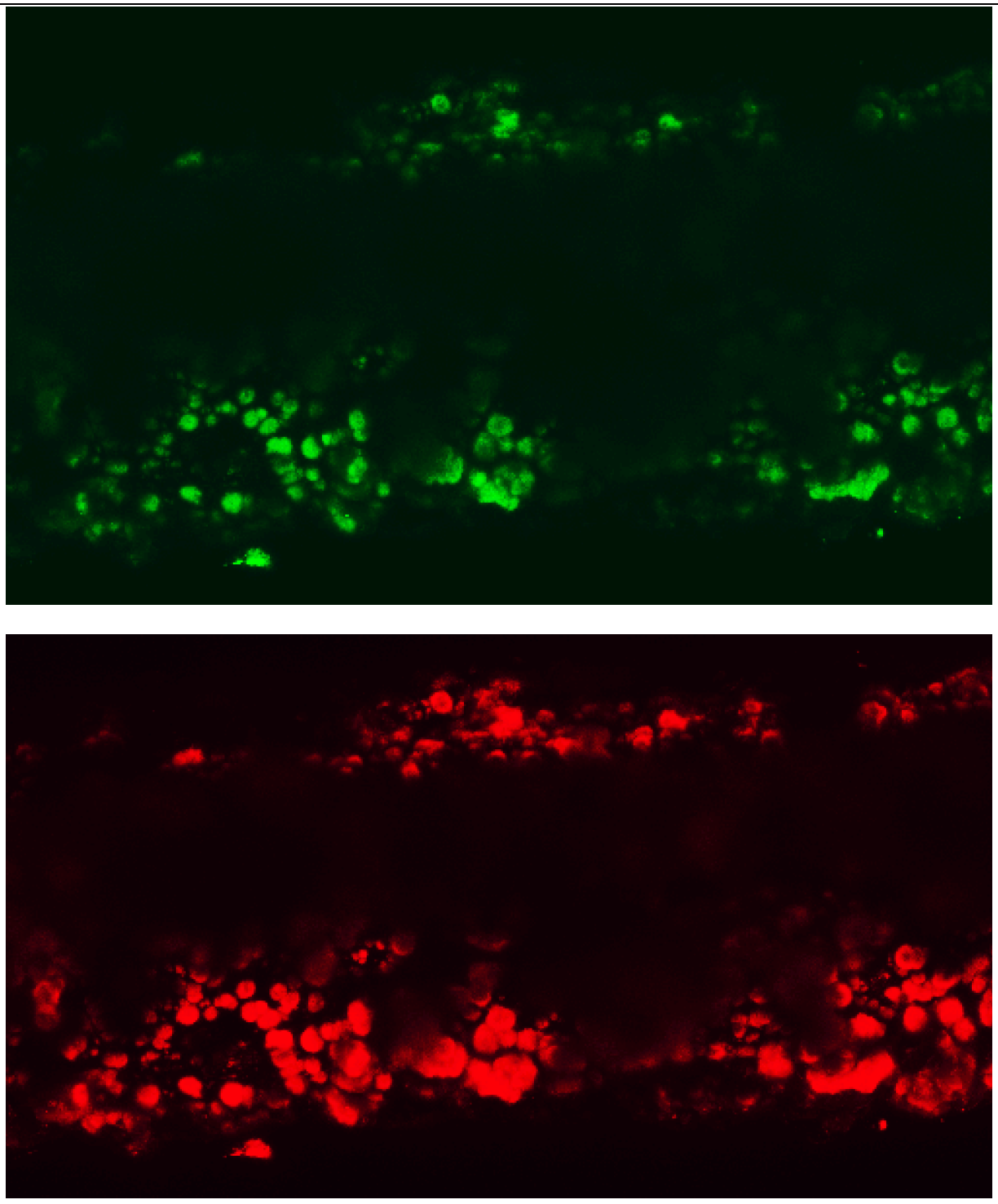

Figure 4.1.2E. Confocal microscope image of day 10 application of rhodamine and fluorescein on the same section of suture and crystals. (**Top)** highlighting the green fluorescein binding the HAP layer. (**Bottom**) highlighting the red rhodamine binding to the HAP layer. 100X magnification.

4.2 FGF/VEGF Implantation and Release

The release of FGF over a 6-week time period from the HAP layer on suture materials are demonstrated in **Figures 4.2.1 (A-D)** representing release from the superficial HAP layer and **Figures 4.2.2 (A-D**), representing release from the deep HAP layer. The release of VEGF over a 6-week time period from the HAP layer on suture materials are demonstrated in **Figures 4.2.3 (A-D)** representing release from the superficial HAP layer and **Figures 4.2.4 (A-D),** representing release from the deep HAP layer. In all figures in section 4.2, the top graph demonstrates the release from suture materials, which were not handled in a surgical manner (i.e., suture and HAP crystals only). In all figures in section 4.2, the bottom graph demonstrates the summation of release from both the suture material that was pulled through the samples of tendon tissue and knotted (pulled and knotted suture) and release from the crystals which were deposited in the tendon tissue itself after the suture was pulled through. Throughout all the results of the release data, several key points can be identified. The binding and release of proteins to 4-0 suture materials is always superior to 6-0 suture materials. The binding and release of protein to polyglactin 910 is always superior to nylon. FGF appears to have a greater affinity for the HAP crystals than VEGF and thus the cumulative release values (pulled and knotted suture and tendon tissue combined) for FGF are higher than VEGF, despite identical incubation concentrations. When growth factors are applied to the superficial layers (day 10 HAP crystals), there is a larger initial (days 1-4) burst release, followed by a prolonged plateau. The deeper layers (day 6 HAP crystal) observe a smaller initial burst and plateau at a later date than the

superficial layers. The cumulative total over the 6 week time period of binding and release of proteins are superior when applied to the superficial group than the deep group, implying some protein is lost during the HAP re-incubation period for the deep group. In addition, when polyglactin 910 was used, it tends to dissolve between days 21-day 28. This represented a total of 5-6 weeks that the suture had been exposed to solution, including the 10 days of incubation in mSBF. Associated with the dissolving of the polyglactin 910 suture is a secondary burst, which is smaller than the initial day 1-4 burst. The action of pulling the suture material through tendon tissue in the pulled, knotted and tissue groups resulted in a disturbance of the HAP crystals and a higher initial burst than just the undisturbed suture and HAP crystals alone. Although we did not record the precise time points, we encountered autolysis of tendon tissue between days 28-40. The complete dissolution of tissue in the SBF fluid occasionally resulted in small bursts of FGF/VEGF release. In general, the cumulative release form the passage, knotted and tendon tissue is superior to the suture material alone. Based on our calculation regarding the amount of suture material implanted in the rabbit, we were able to calculate approximate doses received by the rabbit at the 4-week period, and to suggest a minimum value for the 9-week period (**Figure 4.2.5A).**

4.2.1 FGF Superficial Layer Release

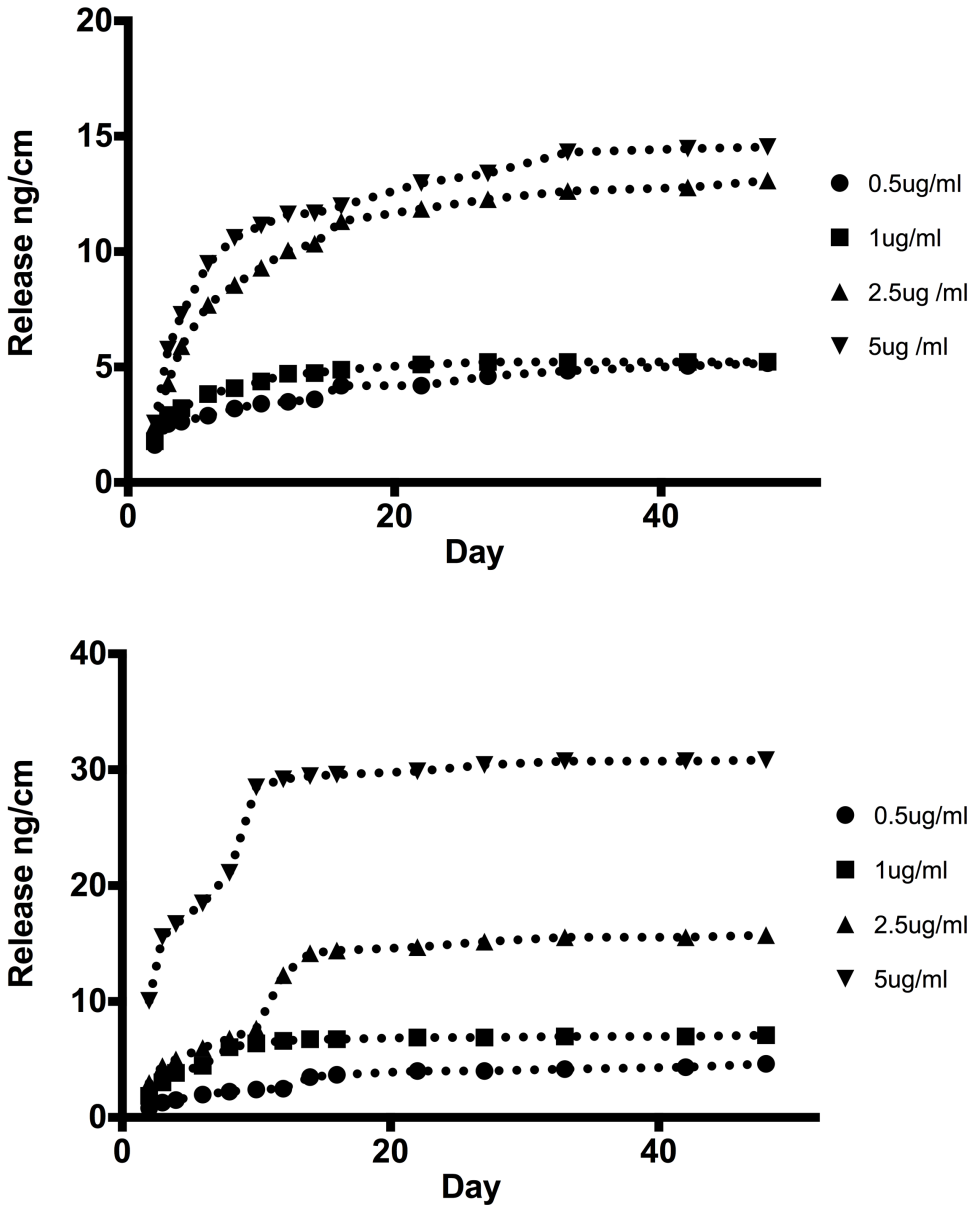

Figure 4.2.1A. Superficial Layer, FGF release, 6-0 nylon. (Top) Suture only. (Bottom) Suture pulled through, knotted and tendon tissue combination release. Release of FGF from 6-0 nylon suture after adsorption onto the HAP crystal layer at day 10 of incubation (superficial layer). In both cases, there is a rapid increase in the cumulative release until approximately day 16. Following this, there is a gradual plateau in the FGF levels attained. Note that the suture on its own (**top**) at the highest concentration releases approximately 15 ng/cm of suture by 6 weeks, whereas the passage, knotted and tissue combination (**bottom)** has achieved a release equivalent to 32 ng/cm by 6 weeks.

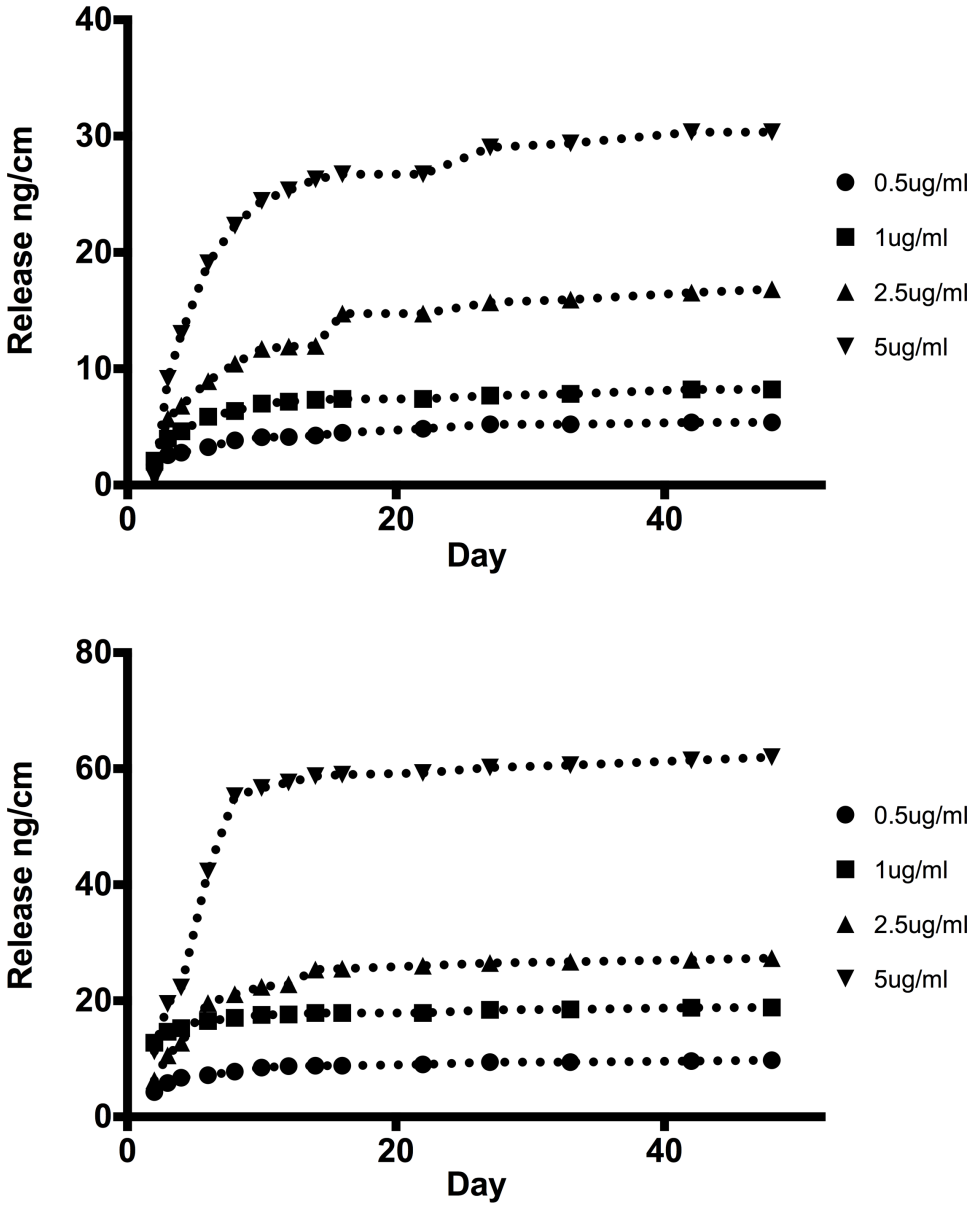

Figure 4.2.1B. Superficial Layer, FGF release, 6-0 polyglactin 910. (Top) Suture only. (Bottom) Suture pulled through, knotted and tendon tissue combination release. Release of FGF from 6-0 polyglactin 910 suture after adsorption onto the HAP crystal layer at day 10 of incubation (superficial layer). In both cases, there is a rapid increase in the cumulative release until approximately day 16. Following this, there is a gradual plateau in the FGF levels attained. Note that the suture on its own (**top**) at the highest concentration releases approximately 30 ng/cm of suture by 6 weeks, whereas the passage, knotted and tissue combination (**bottom**) has achieved a release equivalent to 60 ng/cm by 6 weeks. Note also how there is a slight secondary burst in the top suture image at approximately 21 days as the polyglactin 910 suture dissolves.

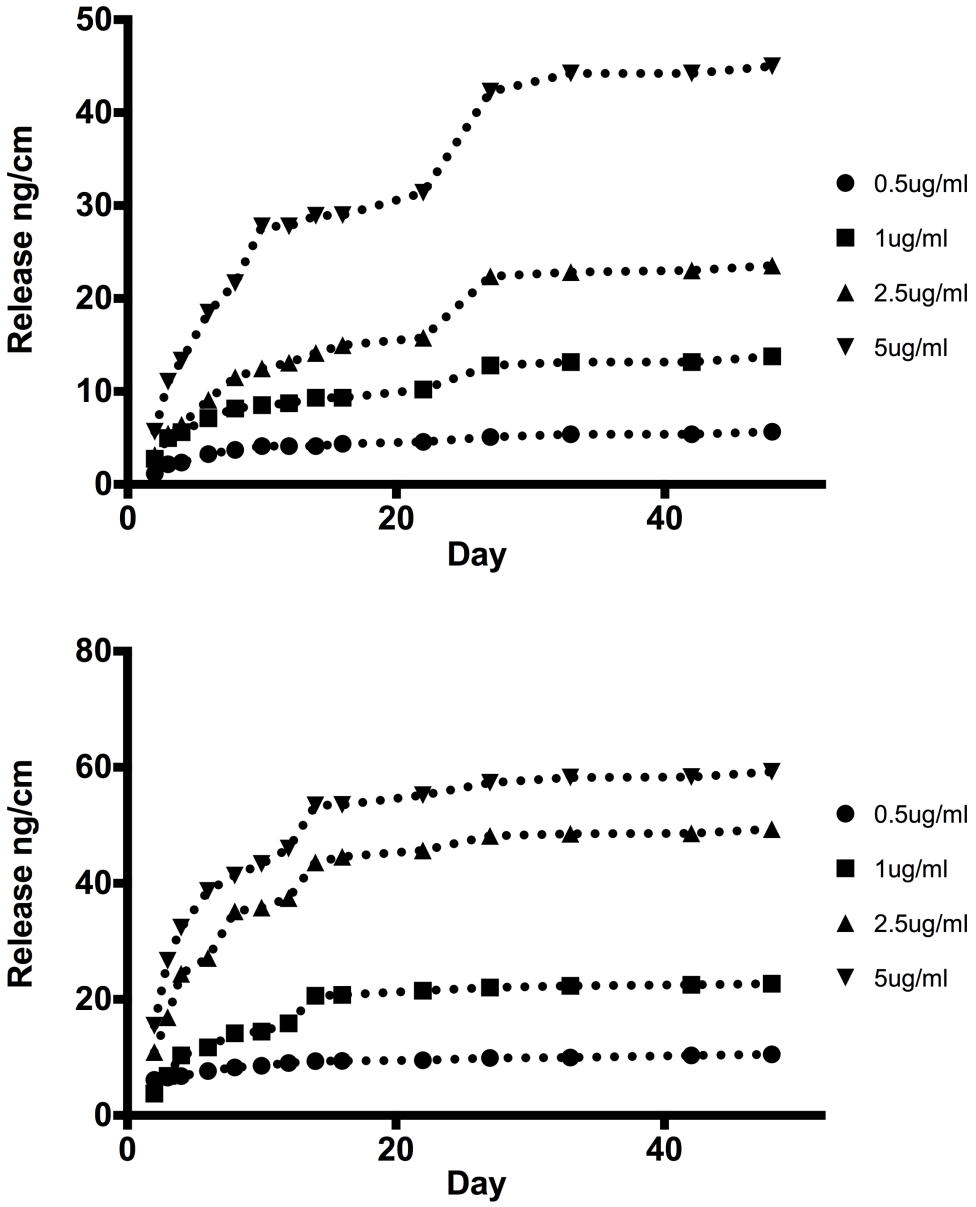

Figure 4.2.1C. Superficial Layer, FGF release, 4-0 nylon. (Top) Suture only. (Bottom) Suture pulled through, knotted and tendon tissue combination release. Release of FGF from 4-0 nylon suture after adsorption onto the HAP crystal layer at day 10 of incubation (superficial layer). In both cases, there is a rapid increase in the cumulative release level on the y-axis until approximately day 16. Following this, there is a gradual plateau in the FGF levels attained. Note that the suture on its own (**top**) at the highest concentration releases approximately 50 ng/cm of suture by 6 weeks, whereas the passage, knotted and tissue combination (**bottom)** has achieved a release equivalent to 60 ng/cm by 6 weeks.

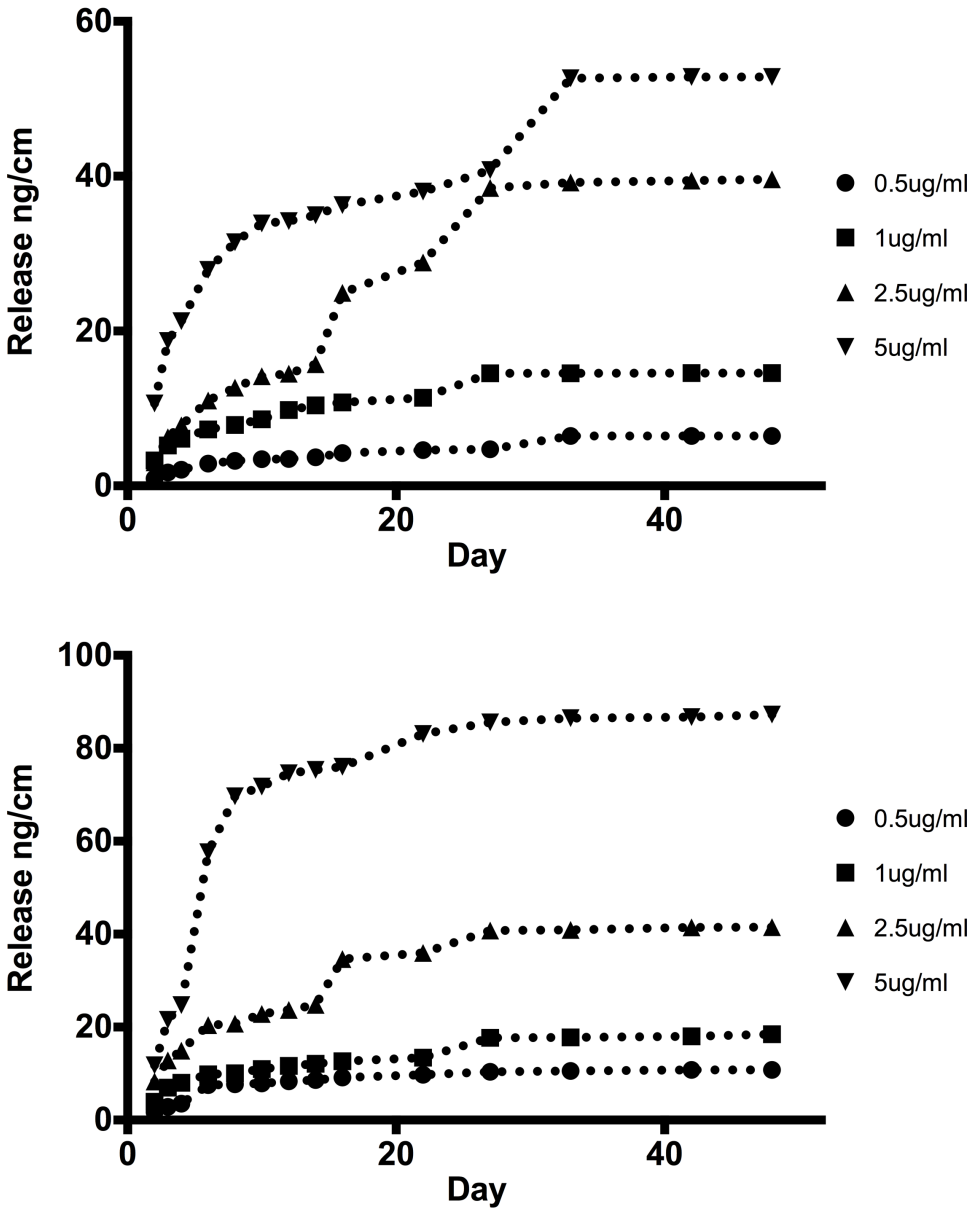

Figure 4.2.1D. Superficial Layer, FGF release, 4-0 polyglactin 910. (Top) Suture only. (Bottom) Suture pulled through, knotted and tendon tissue combination release. Release of FGF from 4-0 polyglactin 910 suture after adsorption onto the HAP crystal layer at day 10 of incubation (superficial layer). In both cases, there is a rapid increase in the cumulative release level on the y-axis until approximately day 16. Following this, there is a gradual plateau in the FGF levels attained, although the **top** demonstrates a secondary burst around day 21. Note that the suture on its own (**top**) at the highest concentration releases approximately 55 ng/cm of suture by 6 weeks, whereas the passage, knotted and tissue combination (**bottom**) has achieved a release equivalent to 85 ng/cm by 6 weeks.

4.2.2 FGF Deep Layer Release

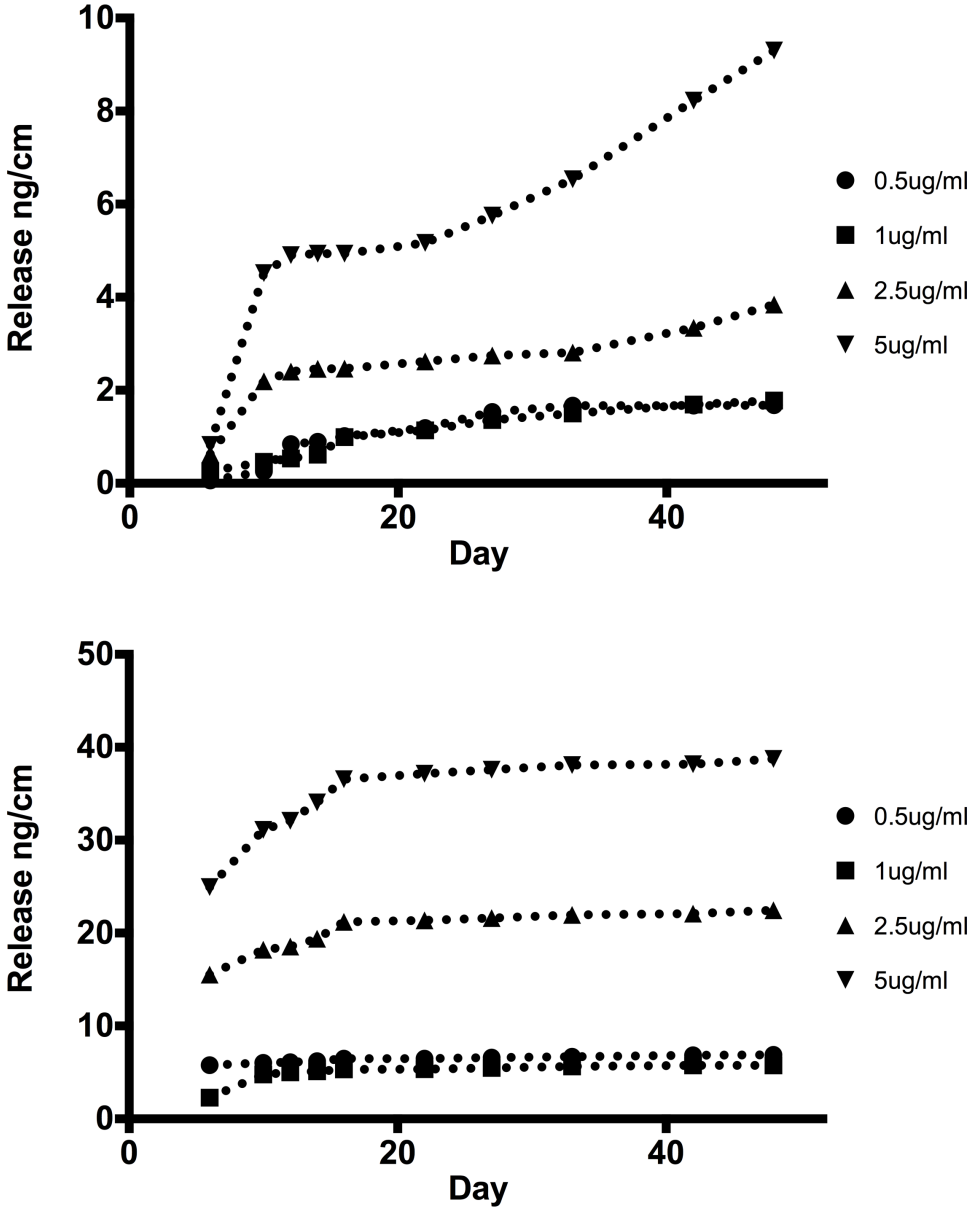

Figure 4.2.2A. Deep Layer, FGF release, 6-0 nylon. (Top) Suture only. (Bottom) Suture pulled through, knotted and tendon tissue combination release. Release of FGF from 6-0 nylon suture after adsorption at day 6 of incubation (deep layer). For the suture only (**top**) there is a more gradual rise to day 48 achieving a peak of 9 ng/cm. The kinetics of the (**bottom**) resemble more the superficial release data, peaking at 35 ng/cm at day 48.

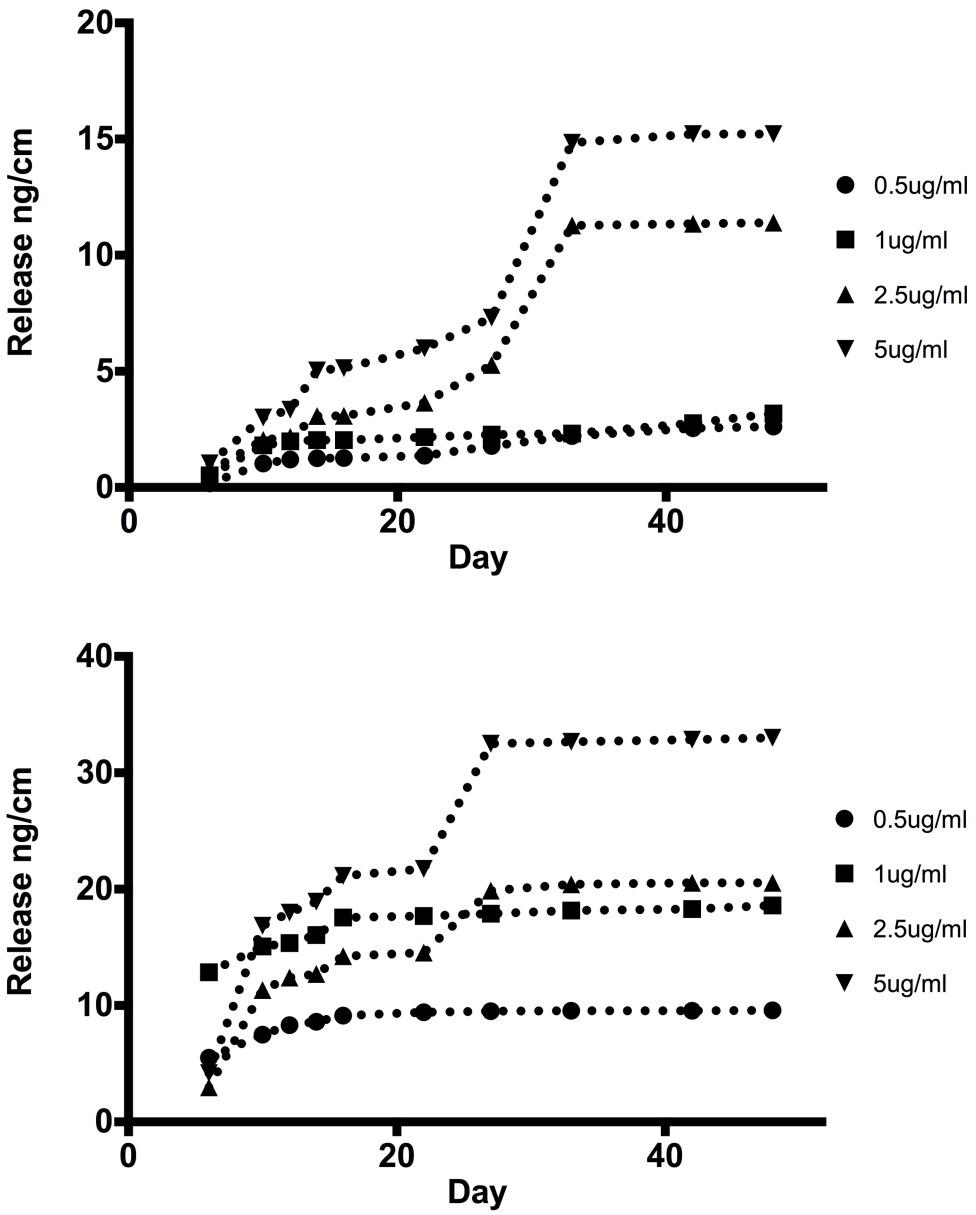

Figure 4.2.2B. Deep Layer, FGF release, 6-0 polyglactin 910. (Top) Suture only. (Bottom) Suture pulled through, knotted and tendon tissue combination release. Release of FGF from 6-0 polyglactin 910 suture after adsorption at day 6 of incubation (deep layer). For the suture only (**top**) there is a more gradual rise to day 48 achieving a peak of 16 ng/cm. The kinetics of the (**bottom**) resemble more the superficial release data, peaking at 35 ng/cm at day 48. Both groups here however demonstrate the secondary burst as the polyglactin 910 dissolves at day 21.

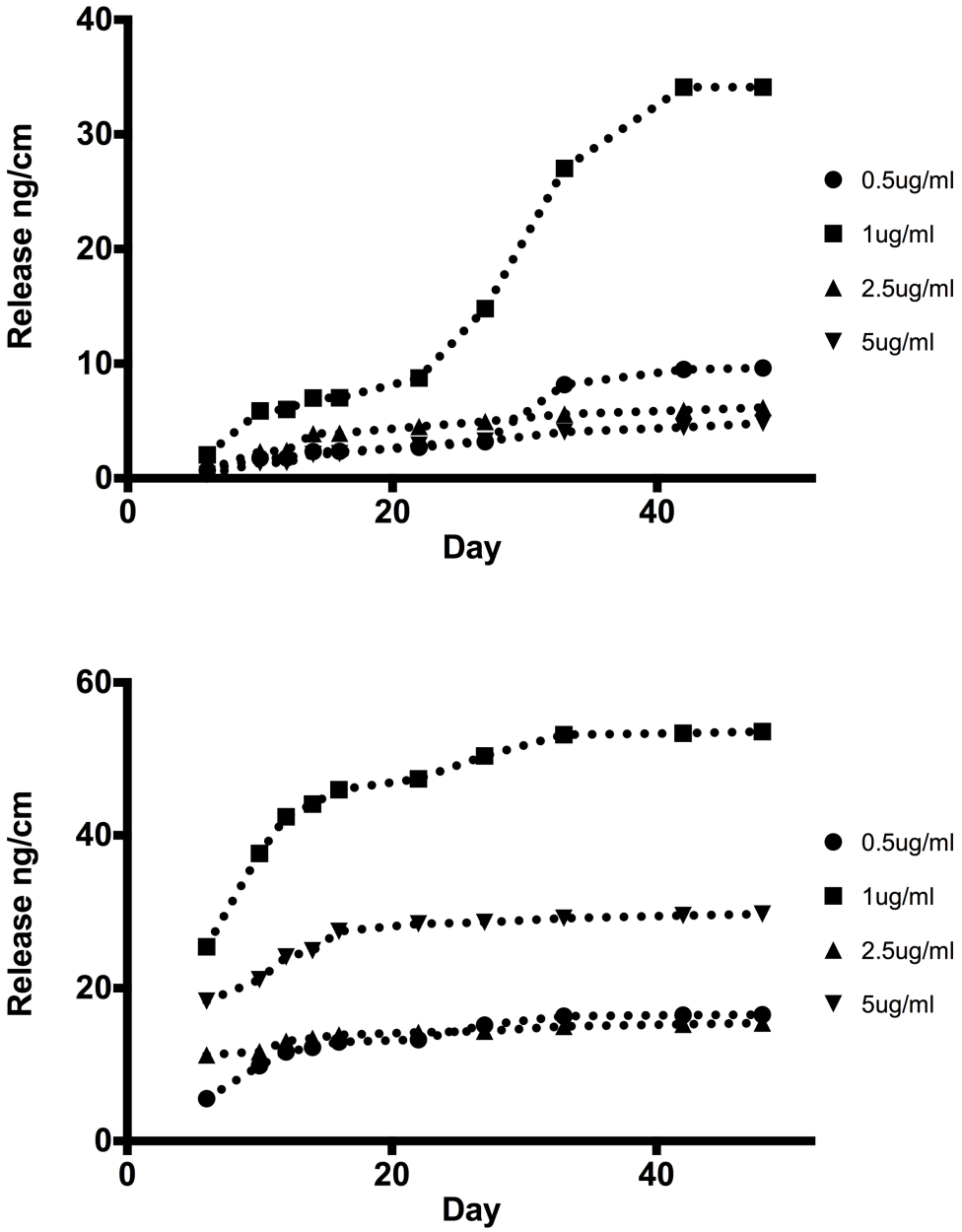

Figure 4.2.2C. Deep Layer, FGF release, 4-0 nylon. (Top) Suture only. (Bottom) Suture pulled through, knotted and tendon tissue combination release. Release of FGF from 4-0 nylon suture after adsorption at day 6 of incubation (deep layer). For the suture only (**top**) there is a more gradual rise to day 48 achieving a peak of 33 ng/cm, associated with a secondary burst. The kinetics of the (**bottom**) resemble more the superficial release data, peaking at 65 ng/cm at day 48.

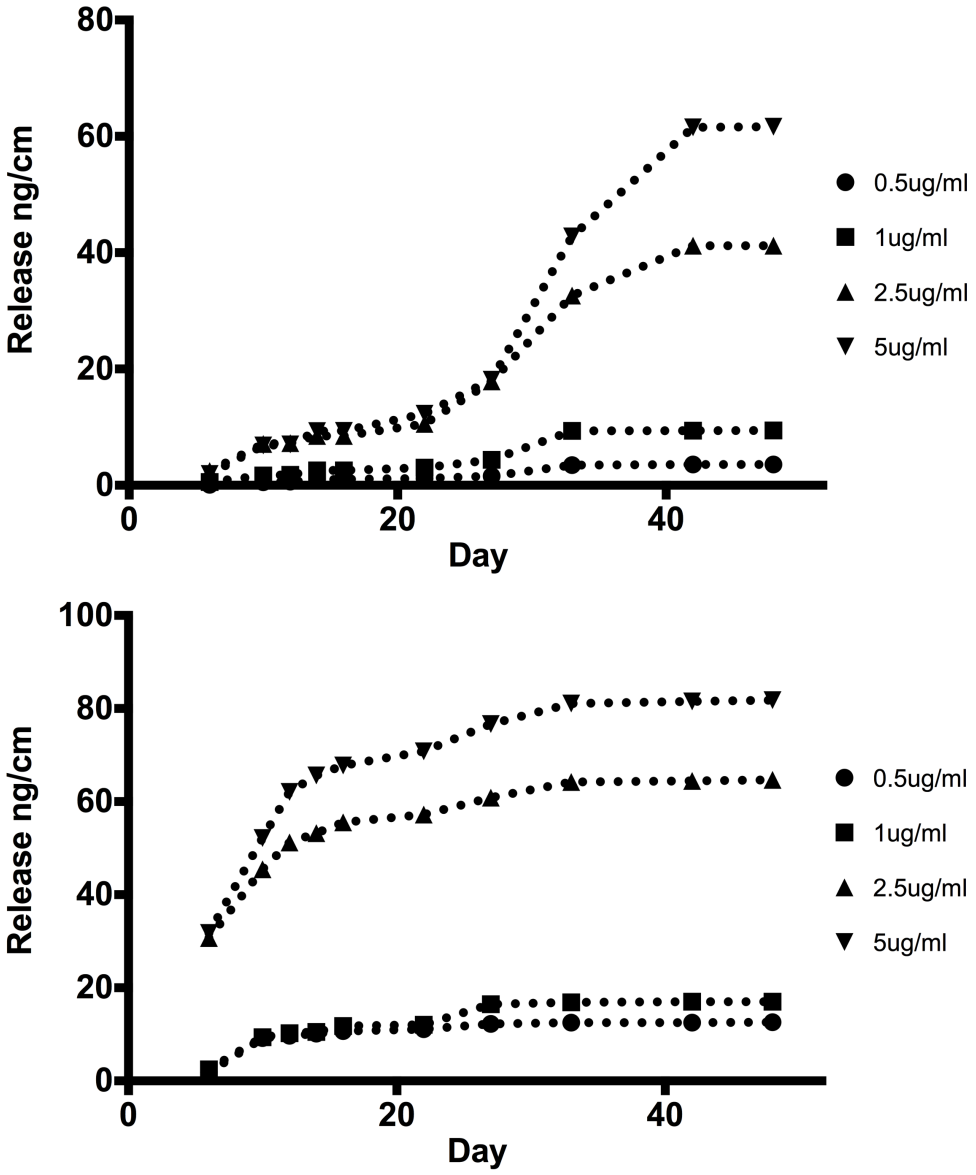

Figure 4.2.2D Deep Layer, FGF release, 4-0 polyglactin 910. (Top) Suture only. (Bottom) Suture pulled through, knotted and tendon tissue combination release. Release of FGF from 4-0 polyglactin 910 suture after adsorption at day 6 of incubation (deep layer). For the suture only (**top**) there is a more gradual rise to day 48 achieving a peak of 60 ng/cm following a secondary burst. The kinetics of the (**bottom**) resemble more the superficial release data, peaking at 80 ng/cm at day 48. Both groups here however demonstrate the secondary burst as the polyglactin 910 dissolves at day 21.

4.2.3 VEGF Superficial Layer Release

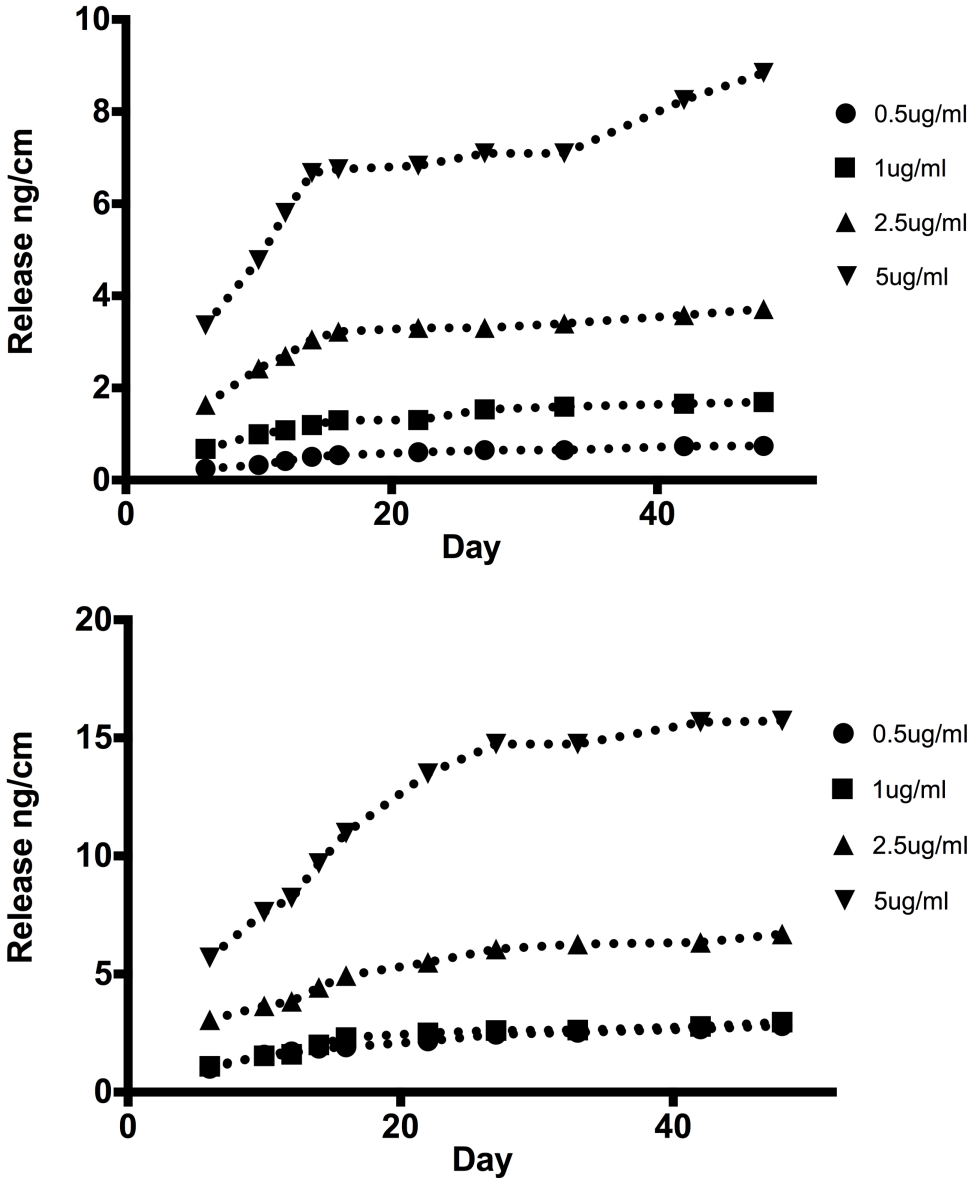

Figure 4.2.3A Superficial Layer, VEGF release, 6-0 nylon. (Top) Suture only. (Bottom) Suture pulled through, knotted and tendon tissue combination release. Release of VEGF from 6-0 nylon suture after adsorption at day 10 of incubation (superficial layer). For the suture only (**top**) there is a gradual rise to day 48 achieving a peak of 9 ng/cm. There is a more gradual rise (**bottom**) peaking around day 21 after which a plateau occurs, maximum release occurring at 17 ng/cm.

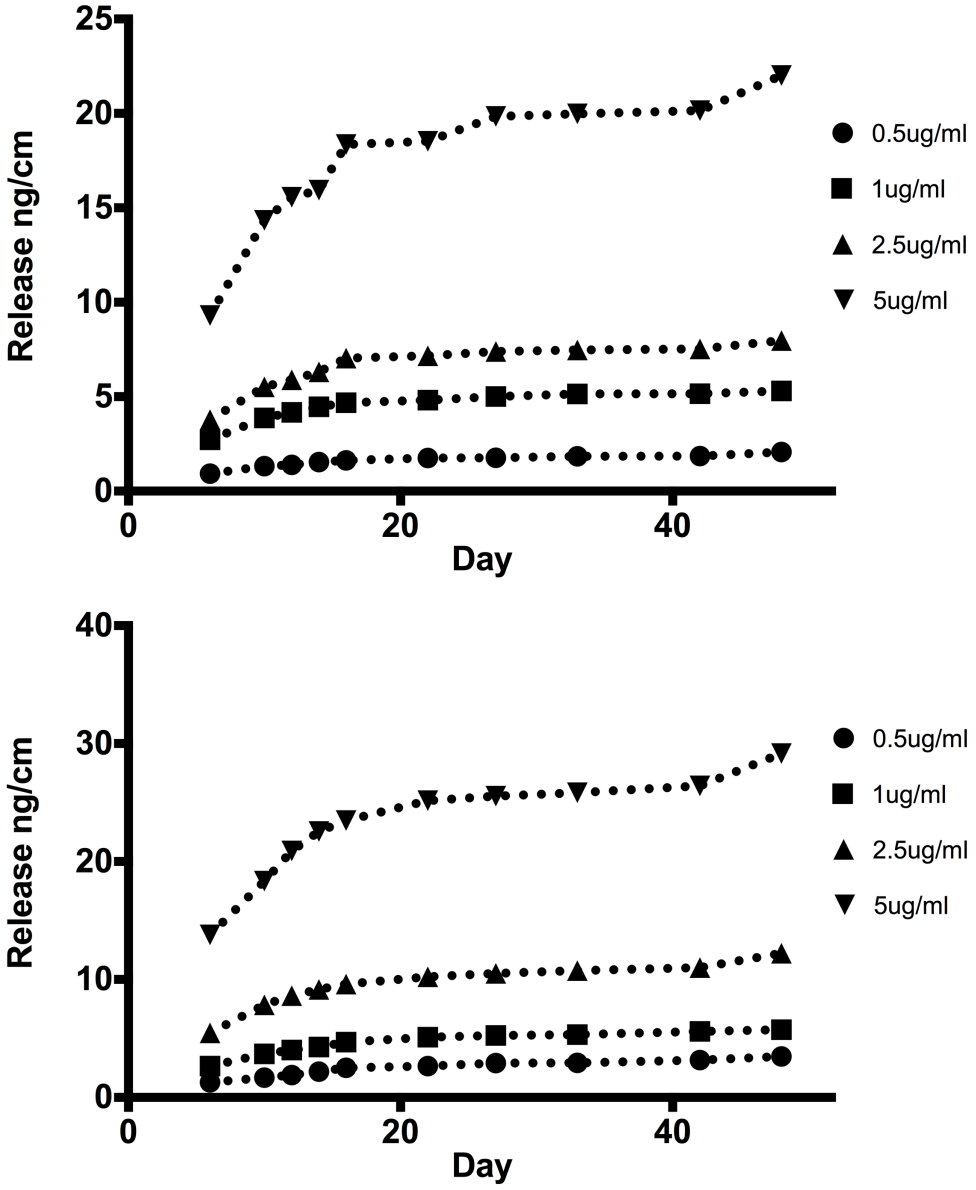

Figure 4.2.3B Superficial Layer, VEGF release, 6-0 polyglactin 910. (Top) Suture only. (Bottom) Suture pulled through, knotted and tendon tissue combination release. Release of VEGF from 6-0 polyglactin 910 suture after adsorption at day 10 of incubation (superficial layer). For the suture only (**top**) there is a gradual rise to day 48 achieving a peak of 23 ng/cm. There is a more gradual rise (**bottom**) peaking around day 21 after which a plateau occurs, maximum release occurring at 30 ng/cm.

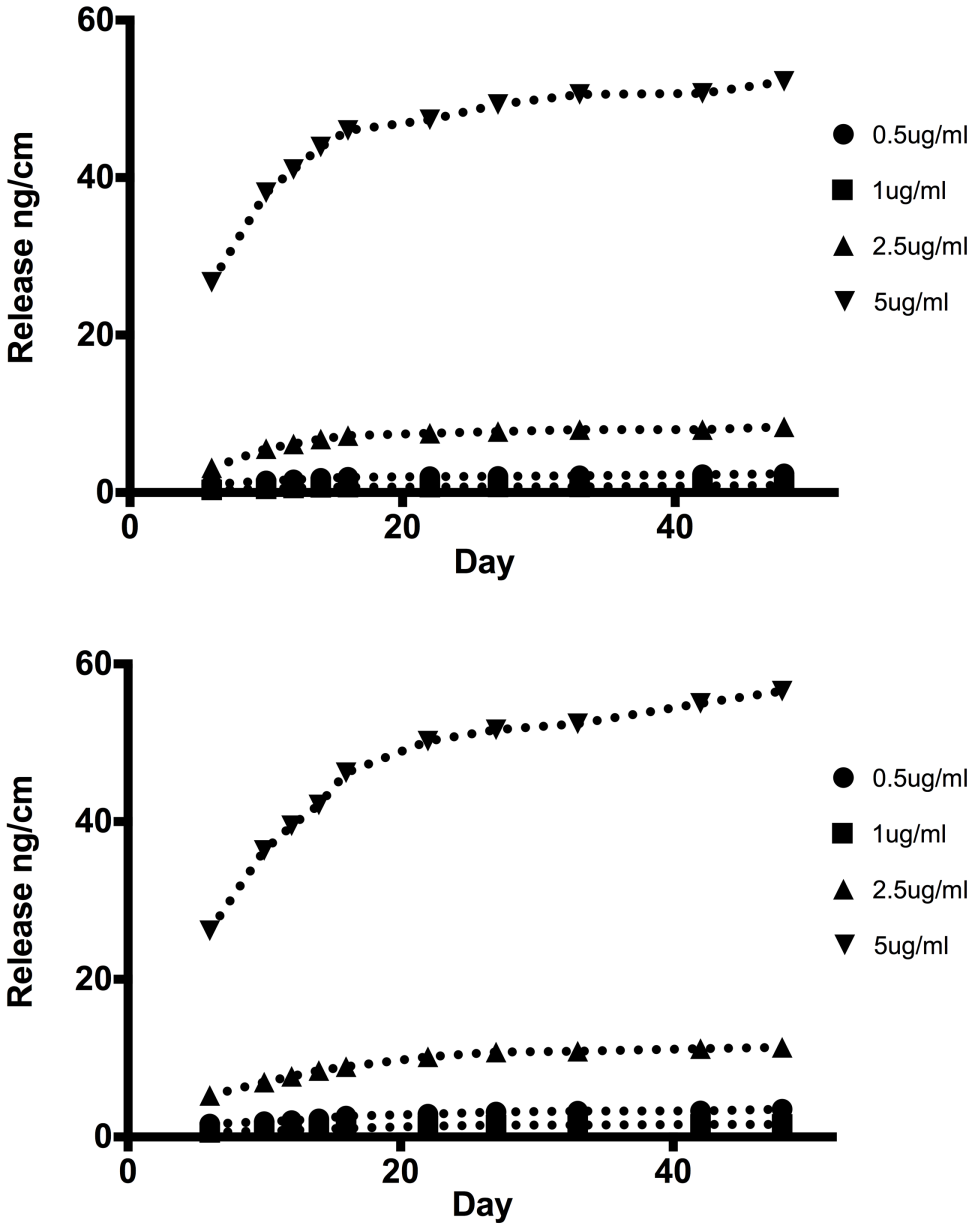

Figure 4.2.3C Superficial Layer, VEGF release, 4-0 nylon. (Top) Suture only. (Bottom) Suture pulled through, knotted and tendon tissue combination release. Release of VEGF from 4-0 nylon suture after adsorption at day 10 of incubation (superficial layer). For the suture only (**top**) there is a gradual rise to day 48 achieving a peak of 55 ng/cm. There is a more gradual rise (**bottom**) peaking around day 21 after which a plateau occurs, maximum release occurring at 55 ng/cm also. Note that binding of the 5 µg/ml group appears far superior to the other groups.

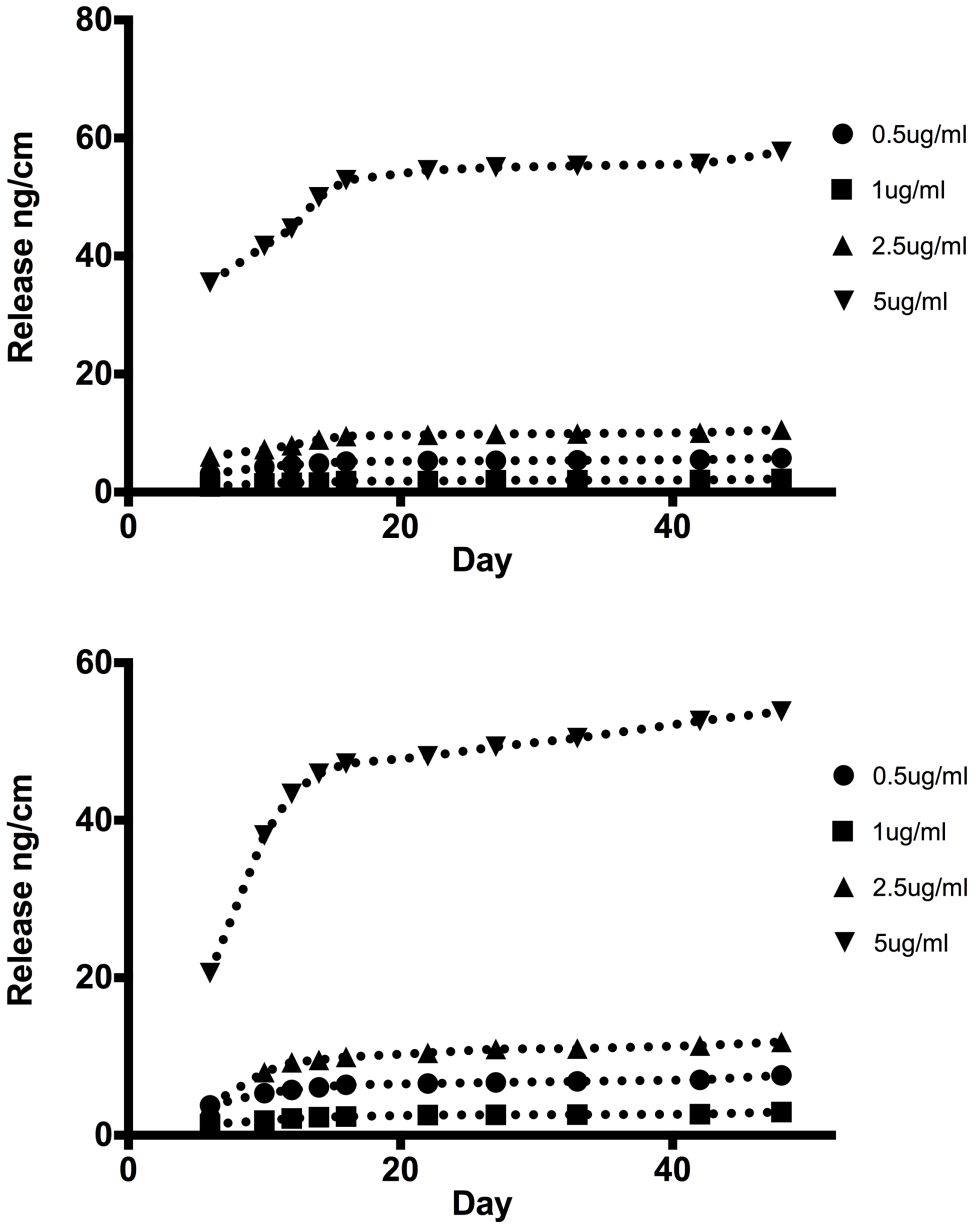

Figure 4.2.3D Superficial Layer, VEGF release, 4-0 polyglactin 910. (Top) Suture only. (Bottom) Suture pulled through, knotted and tendon tissue combination release. Release of VEGF from 4-0 polyglactin 910 suture after adsorption at day 10 of incubation (superficial layer). For the suture only (**top**) there is a gradual rise to day 48 achieving a peak of 55 ng/cm. There is a more gradual rise (**bottom**) peaking around day 21 after which a plateau occurs, maximum release occurring at 55 ng/cm also. Note that binding of the 5 µg/ml group appears far superior to the other groups.

4.2.4 VEGF Deep Layer Release

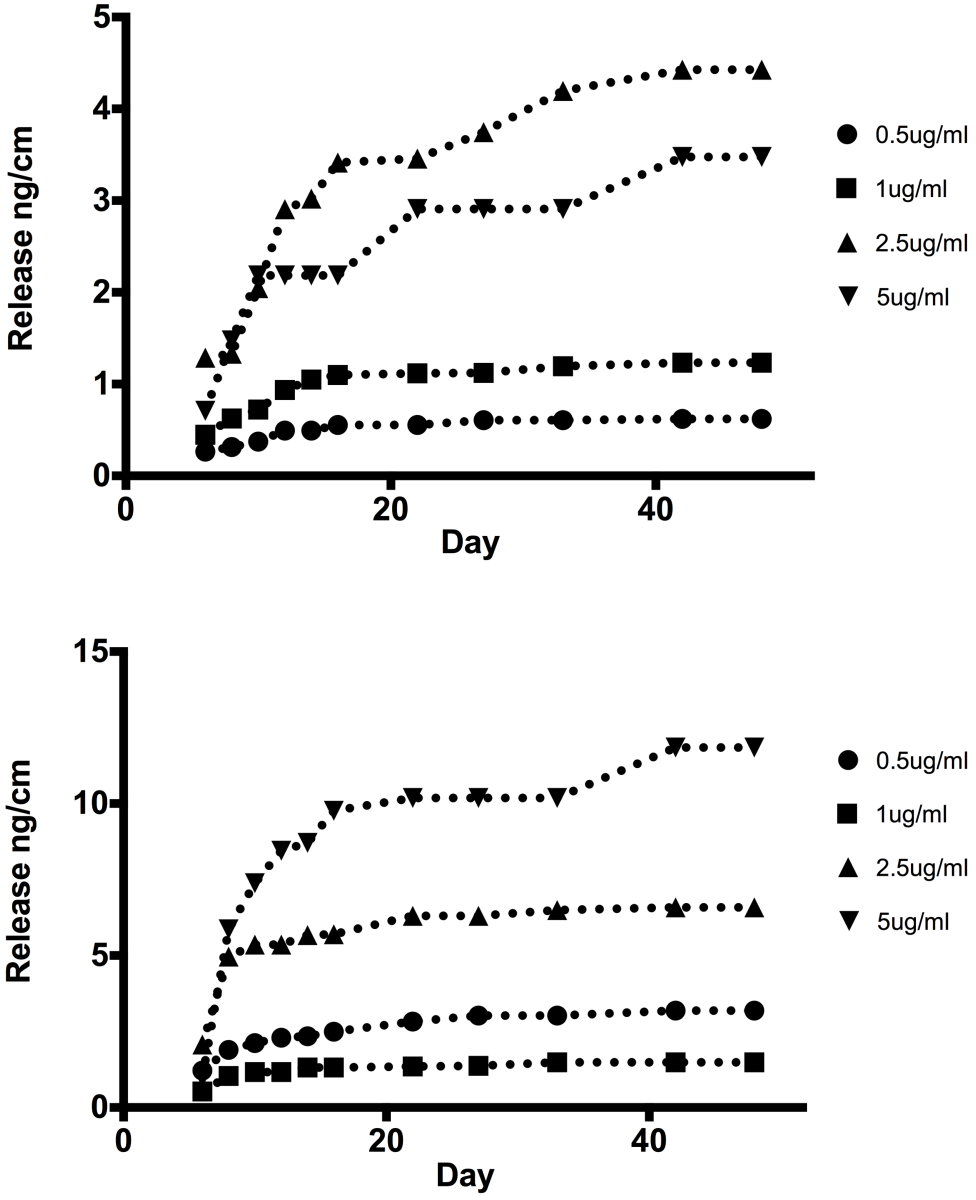

Figure 4.2.4A Deep Layer, VEGF release, 6-0 nylon. (Top) Suture only. (Bottom) Suture pulled through, knotted and tendon tissue combination release. Release of VEGF from 6-0 nylon sutures after adsorption at day 6 of incubation (deep) For the suture only (**top**) there is a more gradual rise to day 48 achieving a peak of 6 ng/cm. There is a more gradual rise (**bottom**) peaking around day 18 after which a plateau occurs, maximum release occurring at 13 ng/cm also. Note that binding for this deeper layer is inferior to the superficial layer.

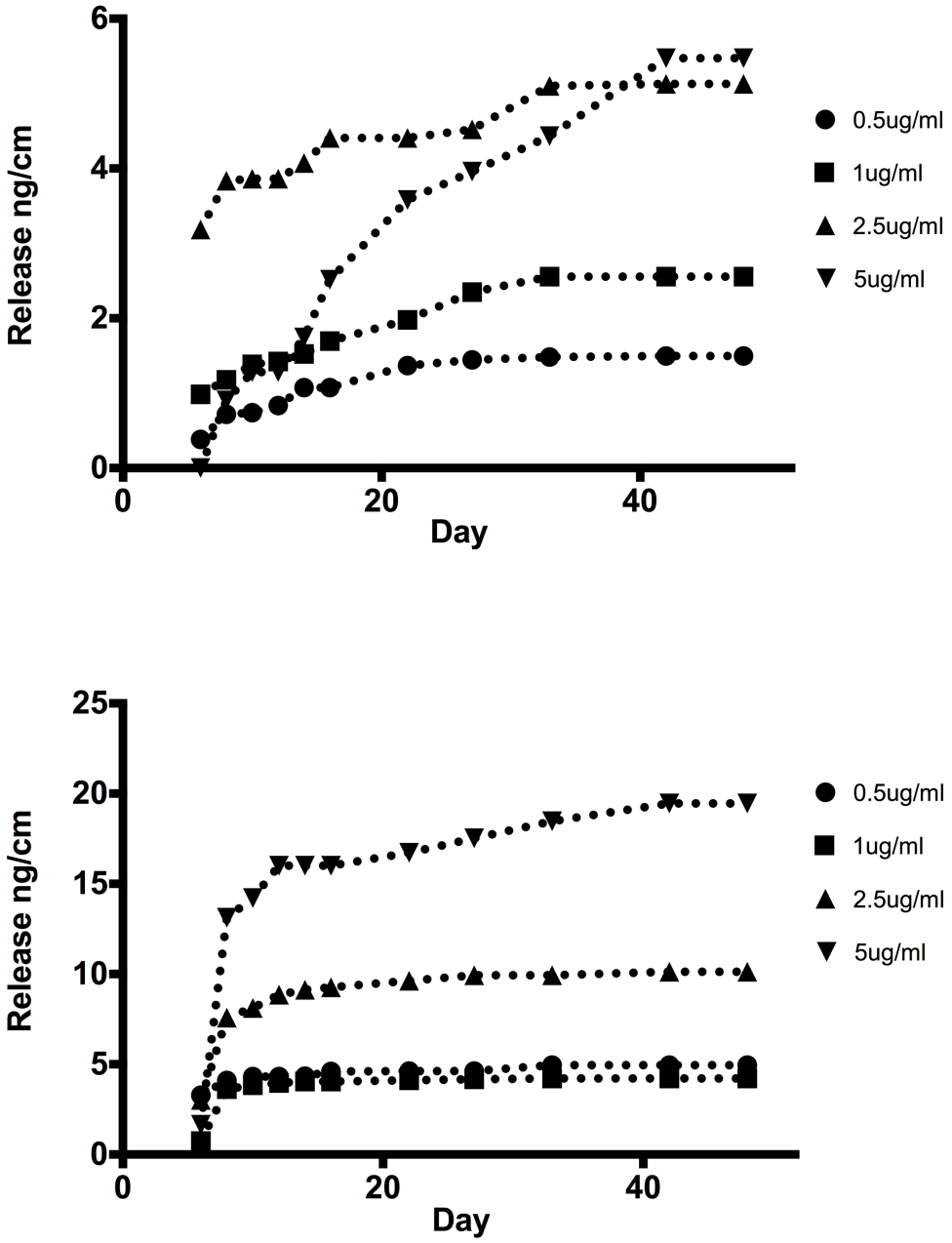

Figure 4.2.4B Deep Layer, VEGF release, 6-0 polyglactin 910. (Top) Suture only. (Bottom) Suture pulled through, knotted and tendon tissue combination release. Release of VEGF from 6-0 polyglactin 910 suture after adsorption at day 6 of incubation (deep) For the suture only (**top**) there is a more gradual rise to day 48 achieving a peak of 5 ng/cm, particularly for the 2.5 µg/ml group There is a more gradual rise (**bottom**) peaking around day 14 after which a plateau occurs, maximum release occurring at 20 ng/cm also. Note that binding for this deeper layer is inferior to the superficial layer.

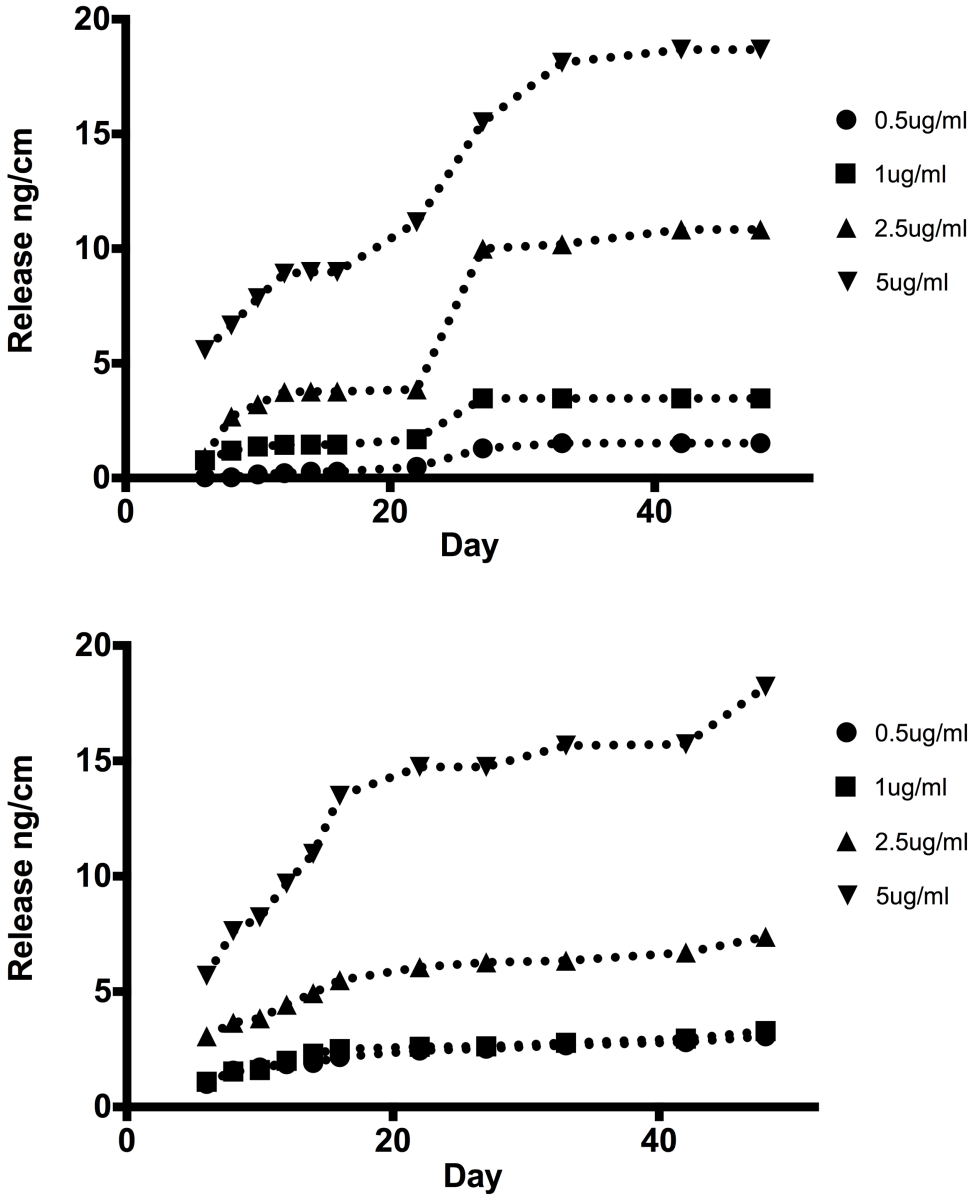

Figure 4.2.4C Deep Layer, VEGF release, 4-0 nylon. (Top) Suture only. (Bottom) Suture pulled through, knotted and tendon tissue combination release. Release of VEGF from 4-0 nylon sutures after adsorption at day 6 of incubation (deep) For the suture only (**top**) there is a more gradual rise to day 48 achieving a peak of 20 ng/cm. There is a more gradual rise (**bottom**) peaking around day 18 after which a plateau occurs, maximum release occurring at 45 ng/cm also.

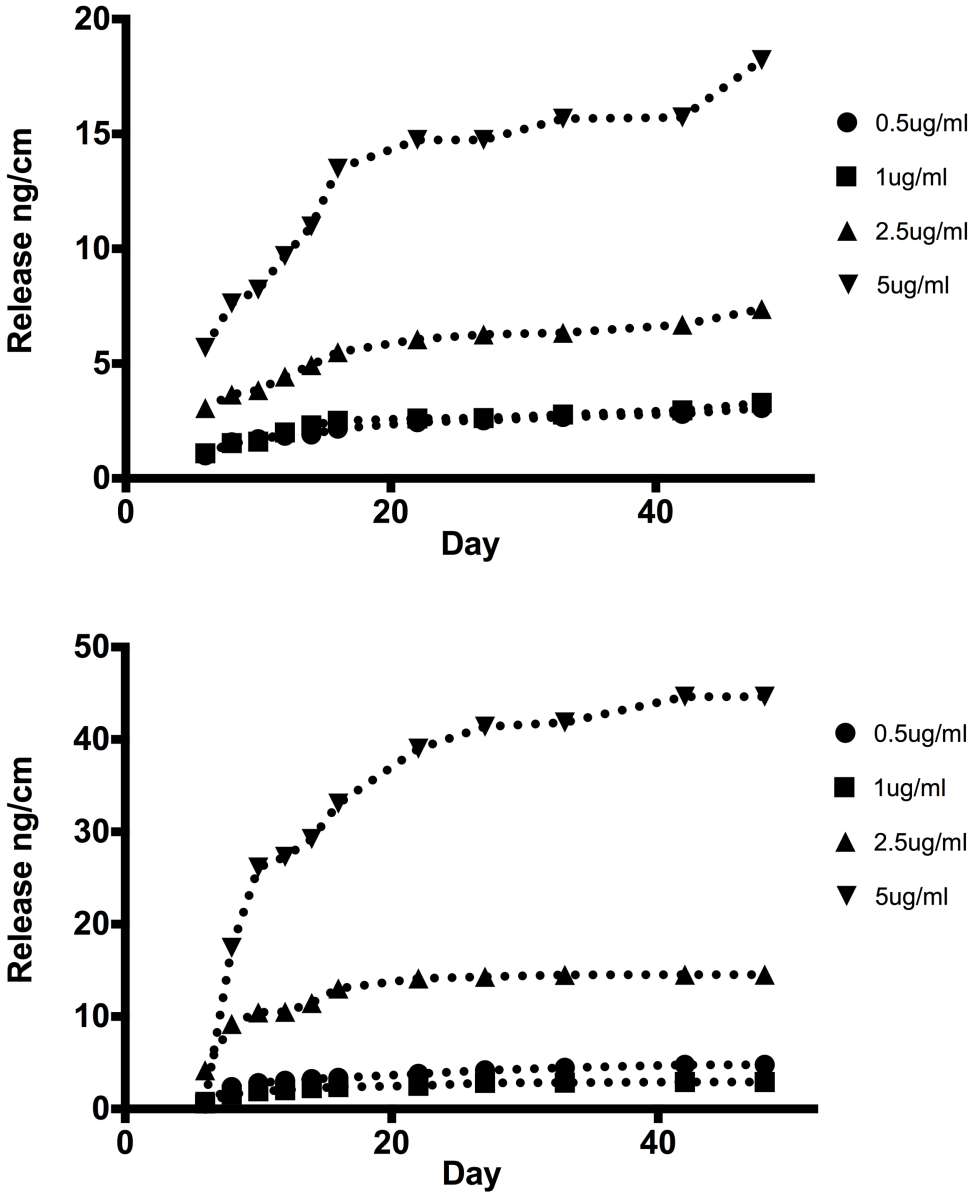

Figure 4.2.4D Deep Layer, VEGF release, 4-0 polyglactin 910. (Top) Suture only. (Bottom) Suture pulled through, knotted and tendon tissue combination release. Release of VEGF from 4-0 polyglactin 910 sutures after adsorption at day 6 of incubation (deep) For the suture only (**top**) there is a more gradual rise to day 48 achieving a peak of 20 ng/cm. There is a more gradual rise (**bottom**) peaking around day 18 after which a plateau occurs, maximum release occurring at 20 ng/cm also.

4.2.5 Determination of Doses for the Surgical Procedure

For both FGF and VEGF, the 5 μg/ml high dose and 0.5 μg/ml low dose group were selected based on the release data obtained is sections 4.2.1-4.2.4 and available published literature. Previous studies have documented the successful improvement in biomechanical strength of tendons with the use of 1000 ng FGF delivered in a canine model to evaluate tendon healing[1]. In addition, 500 ng delivery was also shown in a study by Hamada et al. to have a significant biomechanical improvement on tendon tensile strength. Based on previous published literature and our experimental release data, our aim was to for our high group to deliver approximately 1000 ng over a 4-week time period. As demonstrated in **Figure 4.2.5A**, at the 4 week time point using a solution incubation concentration of 5 μg/ml, we attained 980 ng release. The similarities provided by published literature and our data in **Figure 4.2.5A** provide the evidence for our use of the 5 μg /ml incubation solution to represent our high FGF dose. In selection of a low group, several studies have documented using at least a 4 fold difference in dosages between high and low groups[2] with others demonstrating differences of 100 fold in concentrations between groups.[3] Based on previous published literature and our released data in **Figure 4.2.5A**, our aim was for the low group to be incubated at a concentration approximately 10 fold lower than the high group, which provides the 0.5 μg /ml incubation value. **Figure 4.2.5A** demonstrates that the low dose system delivers approximately an 8-fold decrease in FGF to the target tendon over 4 week, releasing 120 ng in this time period.

In rats, a study by Zhang et al, demonstrated significant improvements in tensile strength of the tendons of Sprague Dawley rats that were subject to injections of 5 μg /ml VEGF into the site of injury.[4] Our aim was to replicate the dose used in the Zhang study which provided our incubation solution of 5 μg/ml, delivering 650 ng over the 4-week time period. Using a similar low dose group as we did for the FGF (incubation at 0.5 μg/ml), our low dose solution group delivers 90 ng of VEGF over the 4-week time period.

Our surgical groups therefore comprised sutures containing zero, low and high levels of FGF (ZF, LF and HF, respectively) and zero, low and high levels of VEGF (ZV,LV and HV, respectively) . Although we did not have a 9-week release time point, we calculated that the total minimum amount (which is attained at 6-weeks) for the HF 9-week group was in excess of 1100 ng and for the LF 9-week group was in excess in 150 ng. For the HV 9-week group, the total minimum amount received was 850 ng and for the LV 9-week group was 100 ng (**Figure 4.2.5A)**.

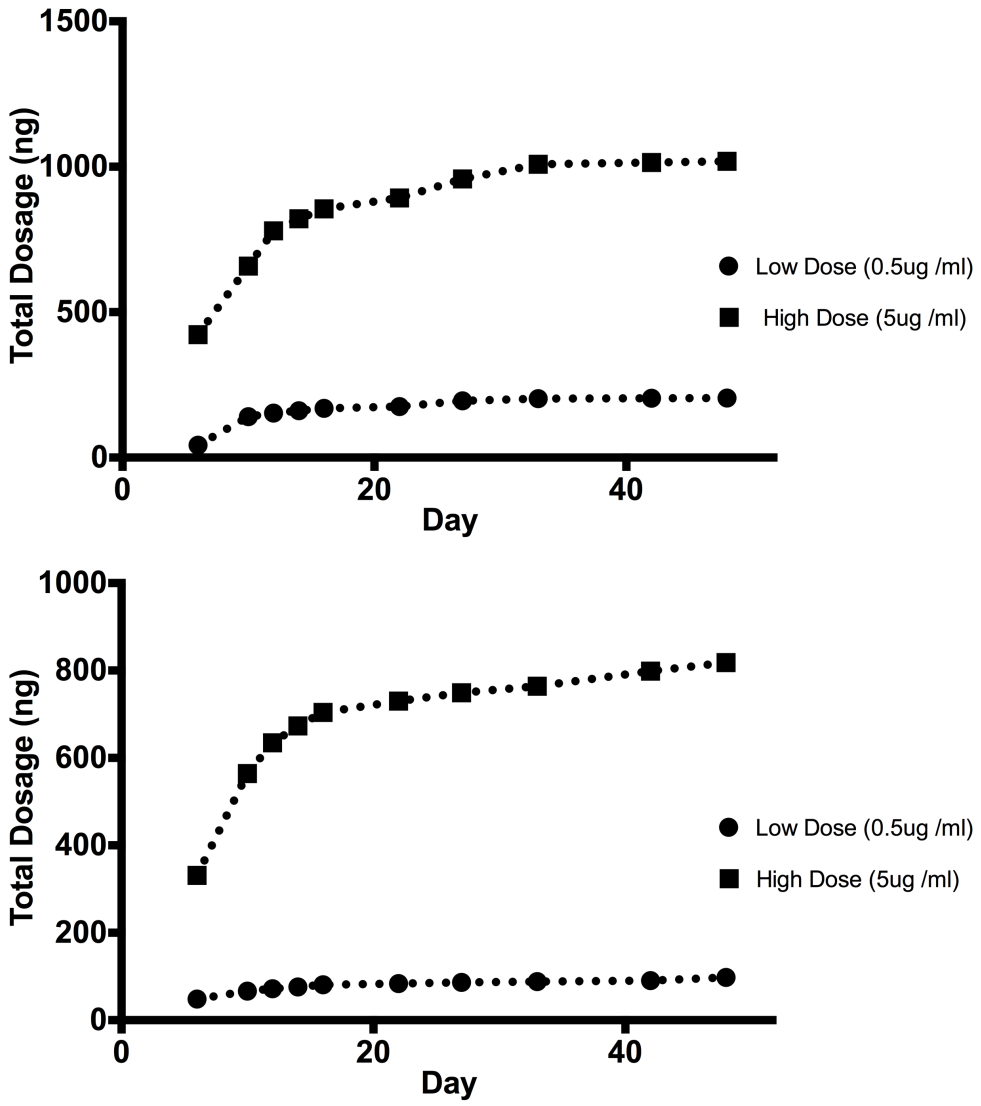

Figure 4.2.5A. Total rabbit cumulative dose delivered, (Top) FGF. (Bottom) VEGF. Based on calculation that approximately 4 cm of 4-0 nylon suture and 11 cm of polyglactin 910 suture are required to repair a rabbit tendon, data extrapolated from the FGF deep and VEGF superficial data were used to calculate doses for the rabbits per tendon. For the FGF release (**top**), by the 4-week time point (28 days), the high dose has received 980 ng of FGF and the low dose group 120 ng. By the 9-week time point, the high dose group has received in excess of 1100 ng and the low dose group in excess of 150 ng. For the VEGF release (bottom), by the 4-week time point, the high dose group has received 650 ng of VEGF and the low dose group 90 ng. By the 9-week time point, the high dose group has received in excess of 850 ng and the low dose group is in excess of 100 ng. Note that the efficiency of the release of VEGF is inferior to FGF, despite incubation at identical concentrations. The FGF release is further impacted by the deep layer position of the protein, which reduces its binding.

Surgical Based Evaluation, 4-Weeks

Values are reported as mean ± SEM. Box and whisker plots of graphs represent 5-95 percentiles, with the mean value identified in the center. If bar charts are utilized data is demonstrated as mean ± SEM. Non-parametric discrete data is presented as median value and range.

4.3.1 Animal Model

In total, 77 animals were utilized for this study. This number comprises 7 rabbits that were utilized for the non-operated normal tendon (NT) evaluation, the 54 rabbits that represent numbers in the 4-week protein groups evaluation and 12 rabbits that represent the 9-week protein group evaluation. In addition, 4 rabbits had to be replaced. One rabbit sustained a fractured tibia 2 weeks into the study and required early euthanasia. Sixty-six New Zealand White rabbits were used for the surgical component of the study (55 were male, 11 female), weighed 3.2 kg ± 0.03 kg, with ages between 4-6 months. Seven rabbits were non-operated controls (NT group; 1 male, 6 females), with a mean weight of 2.9 kg ± 0.07 kg and mean age of 5 months. The NT group represents a non-operated, non-manipulated sample of normal rabbits selected from the rabbit population to make inferences about properties of the gastrocnemius tendons of the general rabbit population. There was no statistically significant difference between the body weight and age of the rabbits in the surgical groups vs. non-surgical group.

It was noted that during the course of the study, the resting angle of the tarsus was altered for the rabbits that underwent surgical repair (**Figure 4.3.1A**). An observation was made that the resting flexion angles were altered from an accute angle prior to surgery to a more obtuse angle at the 2 week time point.

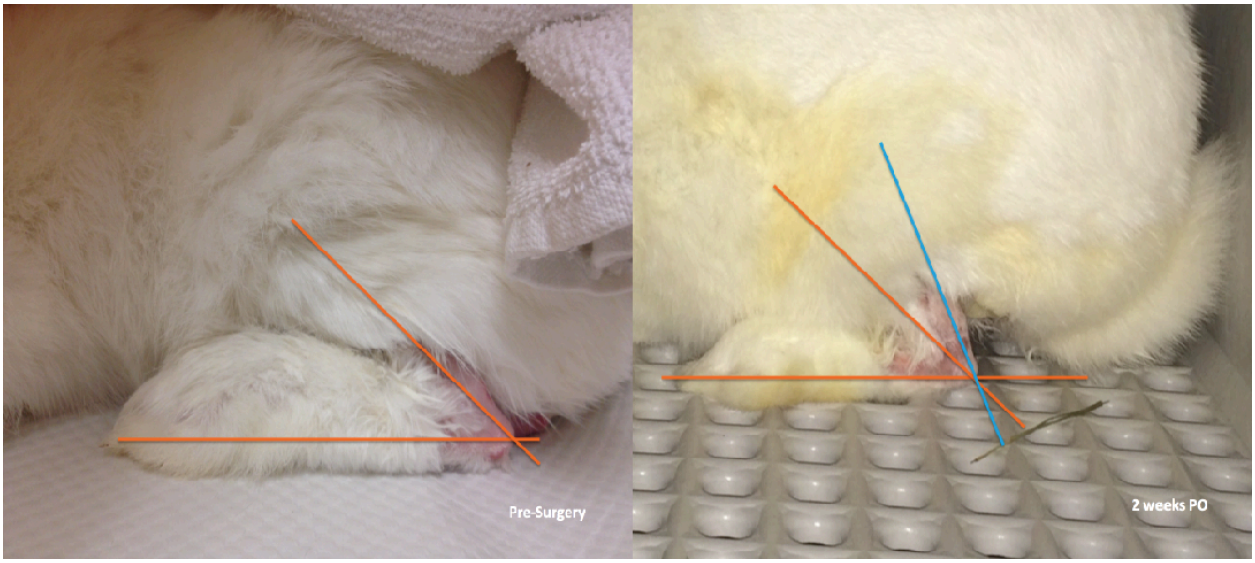

Figure 4.3.1A. Demonstration of the changes in resting angle of the tarsus between the time prior to surgery (**left**) and two weeks post surgery (**right**). Orange angle lines are the same in both images.

4.3.2 Cross Sectional Area Analysis, 4-weeks

There were no outliers detected for any group in terms of cross sectional area. Data for all groups were normally distributed. Non-operated, normal lateral gastrocnemius tendons (NT) had a mean cross sectional area of 6.72 mm^2 ± 0.51 (**Table 4.3.2A**). A significant difference in cross sectional area was identified among all the groups ($p<0.01$) (**Figure 4.3.2A, Figure 4.3.2B, Table 4.3.2B**)

There was no significant difference among the control suture (ZF/ZV) and the low VEGF (LV), low FGF (LF) and the combination of low FGF/low VEGF (LF/LV) groups (8.66 ± 1.57 mm^2, 15.44 ± 2.17 mm^2, 14.13 ± 1.37 mm^2, 14.67± 1.58 mm^2, respectively). There was no significant difference among any protein coated suture group (LV, HF, HV, LF, LF/LV, LF/HV, HF/HV and HF/LV, respectively) (15.44± 2.17 mm^2, 18.54± 1.76 mm^2, 14.35 ± 1.53 mm^2, 14.13± 1.37 mm^2, 14.67 ± 1.58, 15.08 ±1.11 mm^2, 19.97 ± 2.14 mm^2, 18.91 ± 1.49 mm^2, respectively). Only the HF, HV, LF/LV HF/HV and LF/LV groups were significantly different from ZV/ZV group. Data for tendon cross sectional areas from each group are demonstrated in **Figure 4.3.2A.**

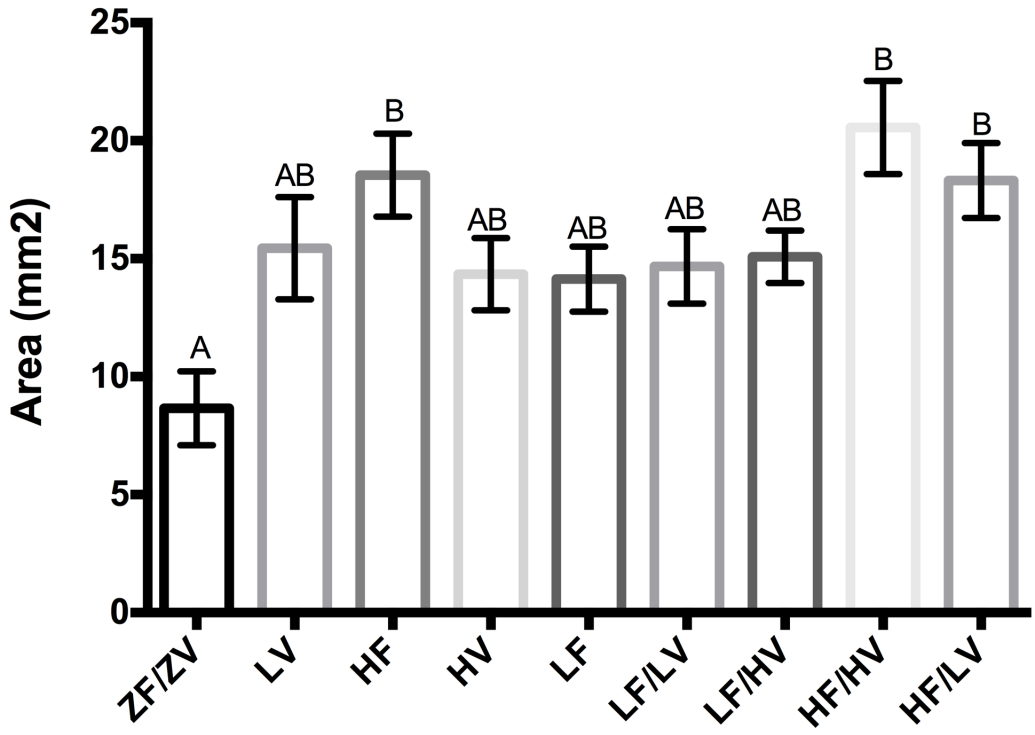

Figure 4.3.2A Bar chart of cross sectional area, 4-week evaluation, lateral gastrocnemius tendon. Different letters denote significant differences among groups ($p<0.01$). Data shown as mean ± SEM.

Rabbit ID	Limb	Cross Sectional Area (mm^2)
1876	Left	6.61
1876	Right	5.90
1880	Left	4.33
1880	Right	4.83
1881	Left	6.88
1881	Right	5.19
4530	Left	4.12
4530	Right	5.27
1872	Left	9.29
1872	Right	7.79
1873	Left	8.55
1873	Right	10.58
1879	Left	7.50
1879	Right	7.26

Table 4.3.2A. Cross sectional area of lateral gastrocnemius tendons in non- surgical control group (NT) (6.72 ± 0.51 mm^2; group mean ± SEM).

Group	Cross Sectional Area (mm^2) ± SEM
NT	6.72 0.51
ZF/ZV	8.66 1.57
LV	15.44 2.17
HF	18.54 1.76
HV	14.35 1.53
LF	14.13 1.37
LF/LV	14.67 1.58
LF/HV	15.08 1.11
HF/HV	19.97 2.14
HF/LV	18.91 1.49
ZF/ZV, LT	10.94 1.51
HF/HV, LT	7.23 0.63

Table 4.3.2B. Cross sectional area measurement data for all test groups of the lateral gastrocnemius tendons. NT – Normal Tendon, ZF – zero FGF dose, LF – low FGF dose, HF, high FGF dose, ZV – zero VEGF dose, LV, low VEGF dose, HV, high VEGF dose, LT – Long term (8 weeks) groups. Data for groups summarized in **Figure 4.3.2A.**

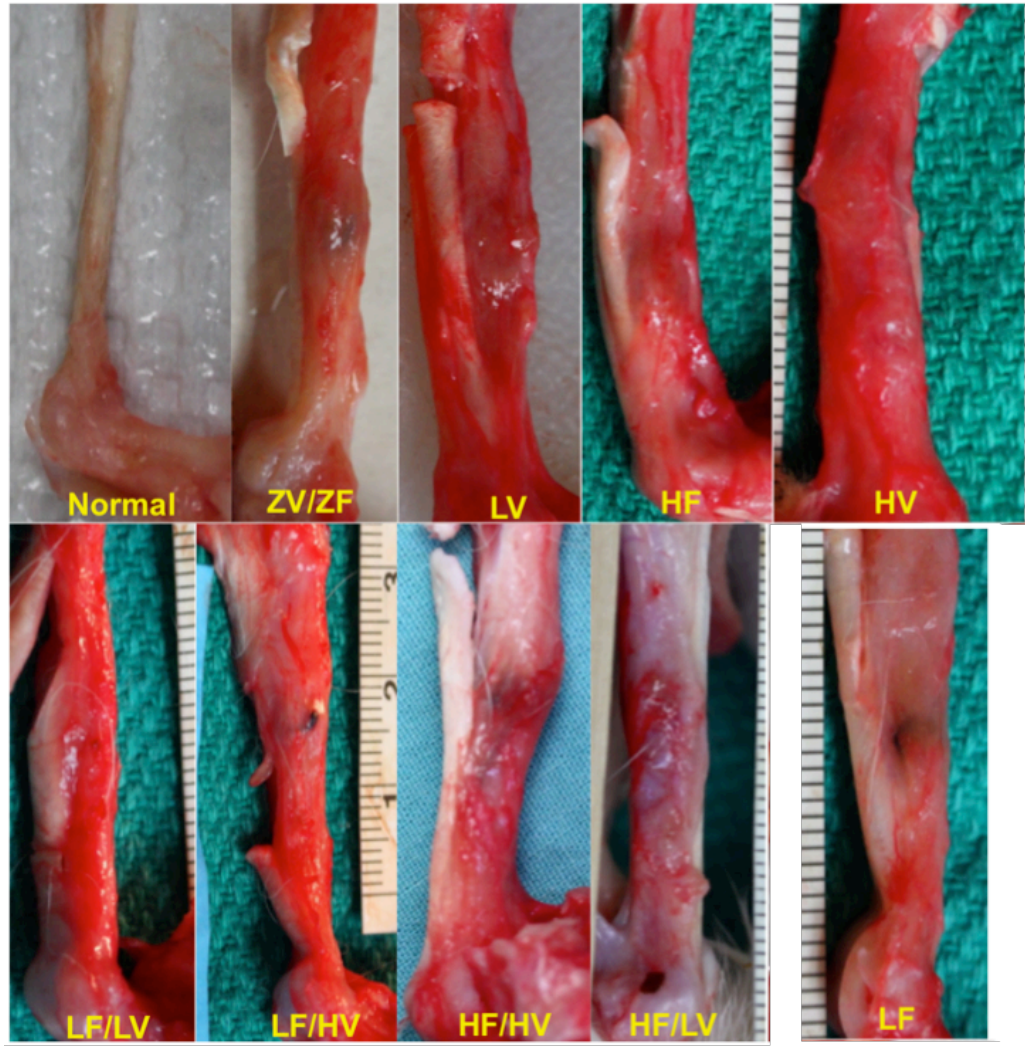

Figure 4.3.2B. Representative samples from all groups. (**Top)** Normal non-operated tendons (NT). Tendon appearance is thin, white and linear. Representations of control suture (ZF/ZV) and groups LV, HF, HV groups. Black nylon suture can be seen in the central region of the tendons. Note how the tendons are not elongated and the suture remains in the region 15mm from the calcaneus. Tendons are globular and red. (**Bottom)** Tendons from LF/LV, LF/HV, HF/HV,HF/LV and LF group.

4.3.3 Biomechanical Testing Analysis

All mechanical testing was performed within 6 hours of sample collection. Tendons were all maintained in water baths at 37^{o}C prior to testing. In addition, they were kept moistened by the application of 0.9% saline solution throughout the testing to prevent drying. (**Figure 4.3.3A**).

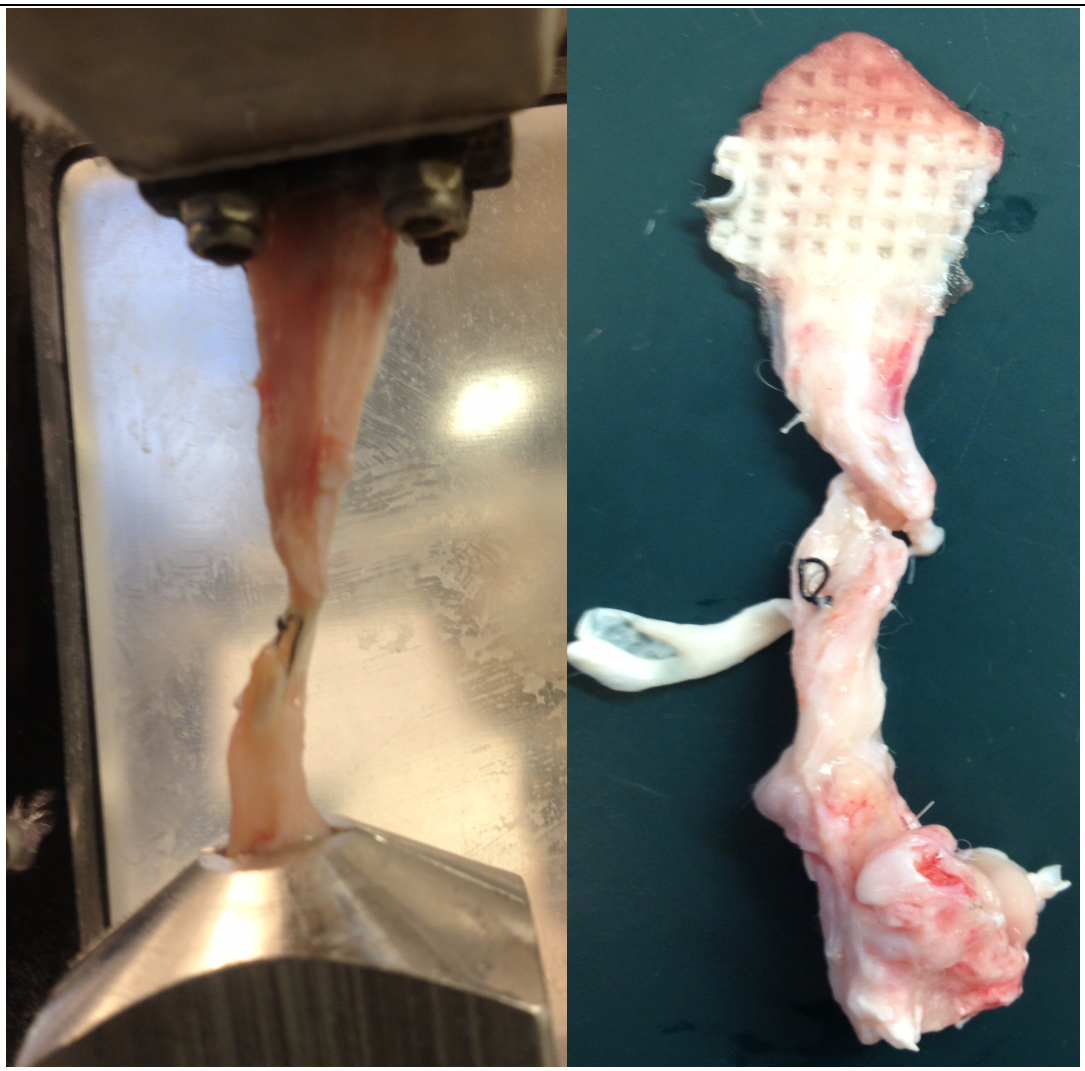

Figure 4.3.3A. Left Tendon in position with cryogrip (top) and calcaneal anchor (bottom). Note the suture is about to fail at the central portion. The nylon suture marker can be seen. **Right** Example of tendon post failure in the central region.

There was a significant difference in the failure pattern of the tendons among all the groups (**Figure 4.3.3B**). For the non-surgical group (NT) 71% of failures occurred via disruption of the Achilles insertion on the calcaneus. Among the remaining groups, there was a significant difference for mode of failure between the groups ($p< 0.001$). For the ZF/ZV and LF, HF, LV, HV, LF/LV groups, all failures (100%) occurred through the site of repair (as depicted in **Figure 4.3.3A**). For the majority of the double coated groups, there was a mixture between failure of the repair site and avulsions from the calcaneus. The HF/HV group had 83% of failures occur through avulsion of the calcaneus.

Several biomechanical parameters were evaluated, including ultimate tensile strength (N), stiffness (N/mm^2), stress (MPa), strain (%) and Young's modulus, or elastic modulus (MPa) for both medial and lateral tendons. Results for each group are tabulated **in Tables 4.3.3A** and **4.3.3B** for the lateral gastrocnemius tendon of all groups and in **Tables 4.3.3C** and **4.3.3D** for medial gastrocnemius tendons. In addition, at the time of harvest, tendon structures were macroscopically evaluated and subjectively scored according to several parameters, including presence of inflammation, obvious vascularity and presence of adhesions. Each category was on a 4-point numerical scale from 0 (absent) to 3 (severe). These parameters were all compared with biomechanical variables in order to ascertain the presence of any correlation.

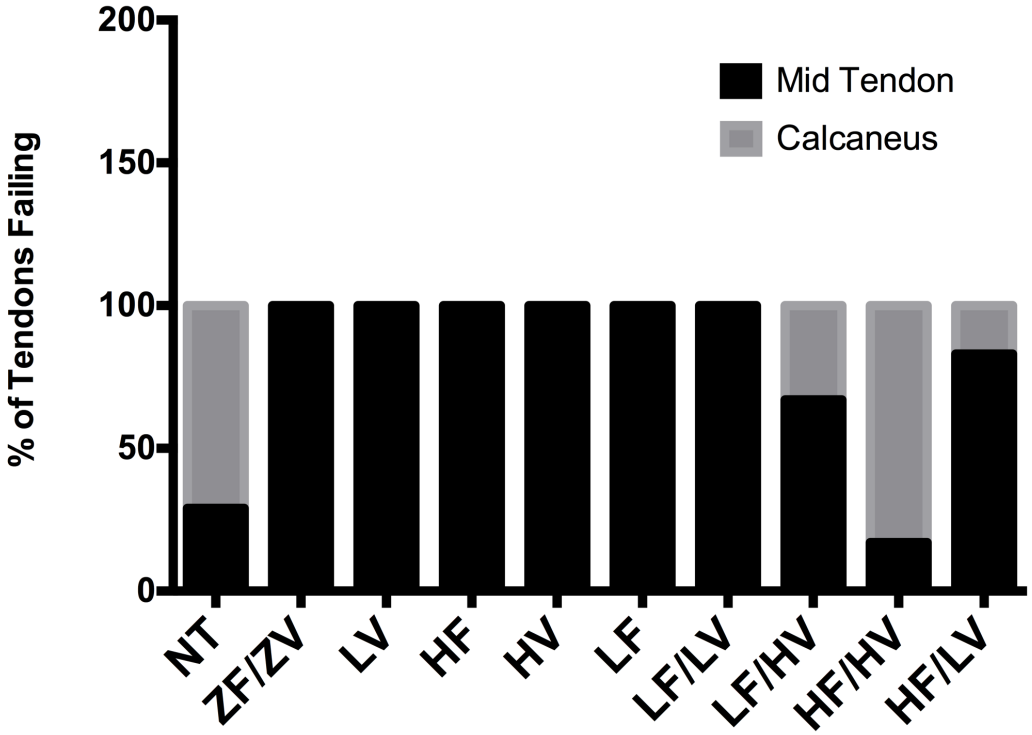

Figure 4.3.3B. Bar chart demonstrating modes of failure for all groups at the 4-week period. The non-operated normal group contained a mixture of failure patterns. The single coated groups all failed mid tendon, double coated groups had a mixture, with group HF/HV significantly having more tendons fail by calcaneal avulsion ($p<0.01$).

Group	UTS ± SEM (N)	Stiffness ± SEM (N/mm)
Normal	184.5 11.35	41.62 2.75
ZF/ZV	150.88 16.27	30.05 3.01
LV	163.92 11.99	22.48 2.44
HF	222.00 15.93	45.53 2.57
HV	216.58 19.22	39.33 3.21
LF	209.08 25.86	37.55 2.53
LF/LV	207.50 18.53	38.68 4.00
LF/HV	197.08 22.15	33.47 1.50
HF/HV	318.67 20.30	57.63 3.06
HF/LV	163.92 16.41	29.80 3.89

Table 4.3.3A Ultimate tensile strength and stiffness data ± SEM for short term (4-week) parameters, lateral gastrocnemius tendon.

Group	Strain ± SEM (%)	Stress ± SEM (MPa)	Young's Modulus ± SEM (MPa)
Normal	26.96 2.04	28.55 2.19	167.1 14.45
ZF/ZV	24.06 3.75	18.04 2.27	141.57 15.21
LV	20.38 3.00	10.63 1.59	81.87 13.01
HF	23.73 3.07	12.48 1.35	112.05 9.47
HV	22.15 1.76	15.94 2.01	132.29 14.65
LF	20.89 2.96	17.13 3.09	102.62 14.17
LF/LV	21.90 2.25	14.56 0.61	109.80 11.36
LF/HV	22.35 3.50	12.98 0.85	106.07 11.39
HF/HV	19.47 2.33	16.27 1.46	142.00 21.05
HF/LV	23.20 3.16	9.15 1.05	73.98 8.90

Table 4.3.3B Strain, stress and Young's modulus data ± SEM for short term (4-week) parameters, lateral gastrocnemius tendon.

Group	UTS ± SEM (N)	Stiffness ± SEM (N/mm)
Normal	N/A N/A	N/A N/A
ZF/ZV	266.92 15.69	58.63 3.24
LV	213.92 13.91	47.88 9.32
HF	270.17 16.69	67.05 3.20
HV	263.75 18.33	68.68 4.78
LF	290.25 19.92	64.37 2.55
LF/LV	246.58 11.76	67.00 4.12
LF/HV	276.75 25.73	66.25 3.78
HF/HV	234.50 10.90	63.10 4.39
HF/LV	269.33 17.84	66.07 1.60

Table 4.3.3C. Ultimate tensile strength and stiffness data ± SEM for short term (4-week) parameters, medial gastrocnemius tendon.

Group	Strain ± SEM (%)		Stress ± SEM (MPa)		Young's Modulus ± SEM (MPa)	
Normal	N/A	N/A	N/A	N/A	N/A	N/A
ZF/ZV	29.75	3.10	23.42	0.61	214.14	27.24
LV	24.72	3.75	30.58	2.30	211.56	37.37
HF	21.35	1.61	37.32	6.55	274.00	37.49
HV	22.32	2.81	47.27	9.96	331.35	24.22
LF	28.32	2.12	41.78	7.93	290.17	46.38
LF/LV	19.77	1.31	34.20	2.93	289.17	27.10
LF/HV	20.52	2.13	36.88	4.21	274.58	26.07
HF/HV	17.55	2.05	37.78	2.49	325.81	21.47
HF/LV	20.63	2.24	40.03	6.16	304.23	34.88

Table 4.3.3D. Strain, stress and Young's modulus data ± SEM for short term (4-week) parameters, medial gastrocnemius tendon.

4.3.4 Inflammation, Vascularity and Adhesion Score Evaluation

UTS was moderately correlated with inflammation score (**Figure 4.3.4A**, r=0.5) and poorly correlated with adhesion score (**Figure 4.3.4B,** r=0.039). However, there was no correlation between UTS and vascularity score (**Figure 4.3.4C,** r=0.05)**.** There was weak correlation between stiffness and inflammation score (**Figure 4.3.4D**, r= 0.39). However, both the vascularity score and the adhesion score were moderately correlated with the stiffness (**Figure 4.3.4E** r=0.45 and **Figure 4.3.4F**, r=0.40, respectively). Cross sectional area of the tendon was moderately correlated with the inflammation score (**Figure 4.3.4G**, r=0.5) and weakly correlated with the adhesion score (**Figure 4.3.4H,** r=0.39**).** However, there was deemed to be no correlation between cross sectional area and vascularity (**Figure 4.3.4I**, r=0.07).

No correlation was present between strain and inflammation, vascularity or adhesion scores (**Figures 4.3.4J** r=0.08, **Figure 4.3.4K** r=0.06, **Figure 4.3.4L** r=0.01, respectively). There was no correlation between stress and inflammation, vascularity or adhesion scores (**Figures 4.3.4M** r=0.05, **Figure 4.3.4N** r=0.05, **Figure 4.3.4O** r=0.04, respectively). There was no correlation between Young's modulus and inflammation, vascularity or adhesion scores (**Figure 4.3.4P** r=0.19, **Figure 4.3.4Q** r=0.19, **Figure 4.3.4R** r=0.16, respectively).

In general, the inflammation scores for ZF/ZV (control suture group) were lower than many of the other test groups (**Table 4.3.4A**). There were no significant differences

among the inflammation scores in the test groups containing any combination of LF/HF or LV/HV. In general, the highest vascularity scores occurred for the HV group, median 2.5, range 1-3), followed by LV (2, 1-3) LF/HV (2, 2-3) and HF/LV (2, 1-3) with median score=2)(**Table 4.3.4A**). There was a tendency for groups with high levels of VEGF to have higher vascularity scores (p=0.08). There were no significant differences among the groups in adhesion scores (**Table 4.3.4A**), indicating that the presence of FGF or VEGF did not contribute to adhesions in comparison to ZF/ZV (control sutures).

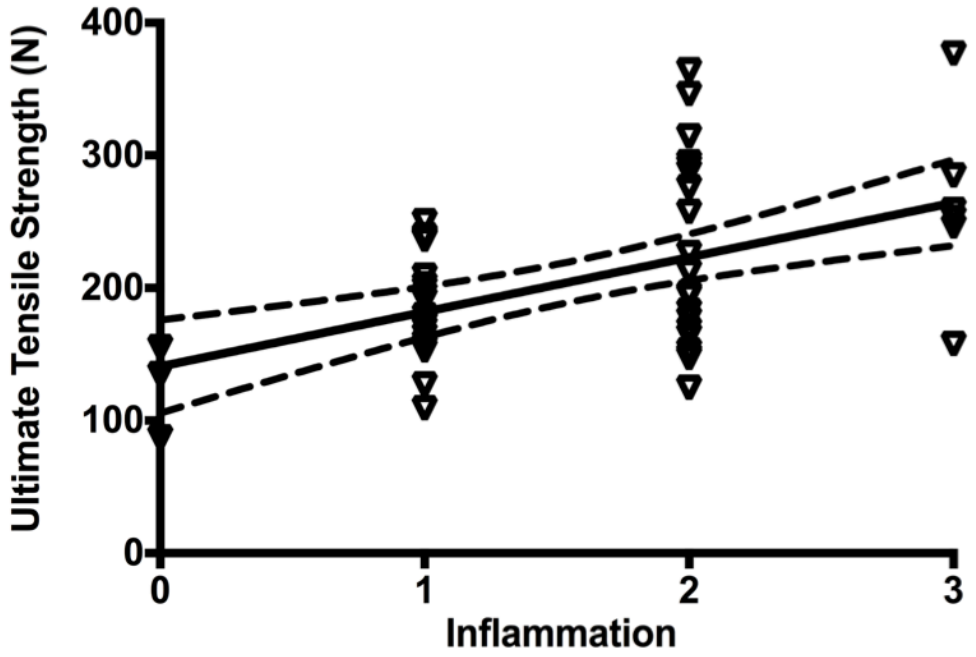

Figure 4.3.4A XY scatter plot of UTS and Inflammation score, lateral tendon, 4-week groups. There was moderate correlation between the inflammation score and ultimate tensile strength (r= 0.50. p<=0.00011). Correlation and 95% confidence intervals provided.

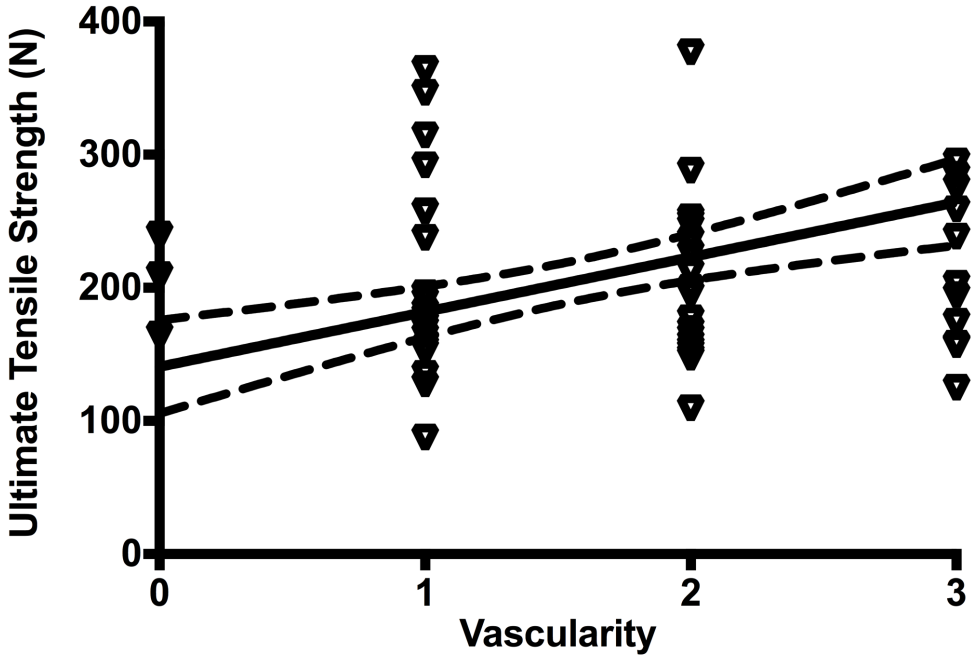

Figure 4.3.4B XY scatter plot of UTS and vascularity score, lateral tendon, 4-week groups. There was no correlation between ultimate tensile strength and vascularity score (r= 0.05, p=0.72) Correlation and 95% confidence intervals provided

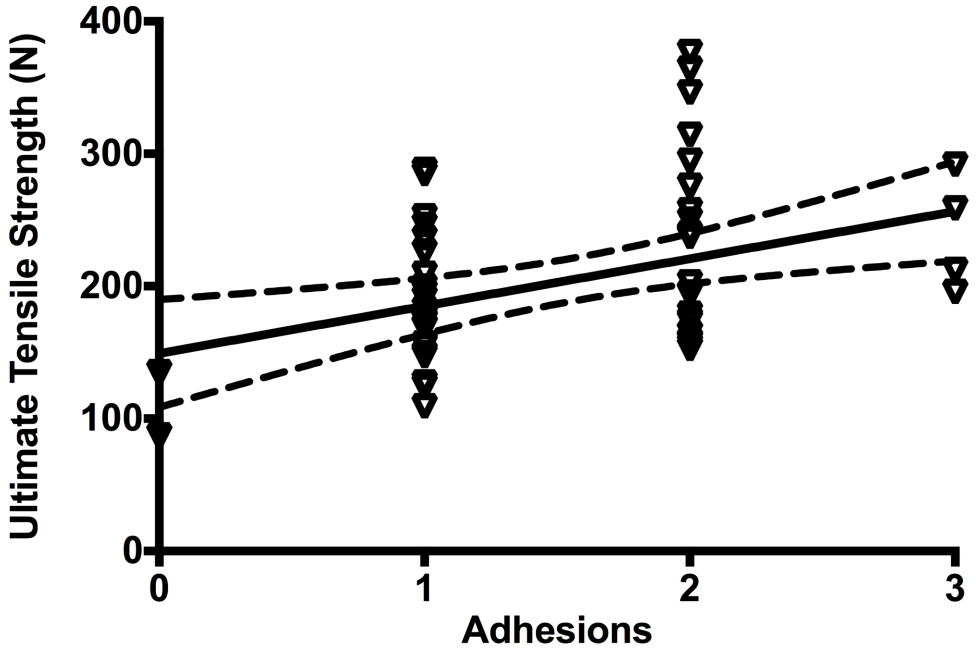

Figure 4.3.4C XY scatter plot of UTS and adhesion score lateral tendon, 4-week groups. There was weak correlation between ultimate tensile strength and adhesion score (r = 0.39, p= 0.003). Correlation and 95% confidence intervals provided.

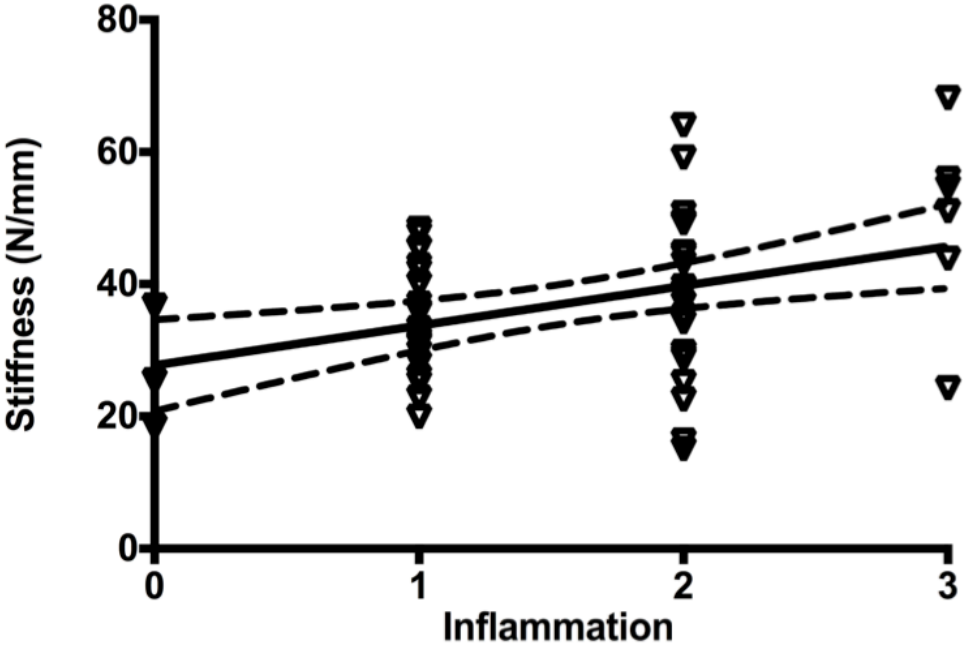

Figure 4.3.4D XY scatter plot of stiffness and inflammation score, lateral tendon, 4-week groups. There was weak correlation between stiffness and the inflammation score (r=0.39, 0.003) Correlation and 95% confidence intervals provided.

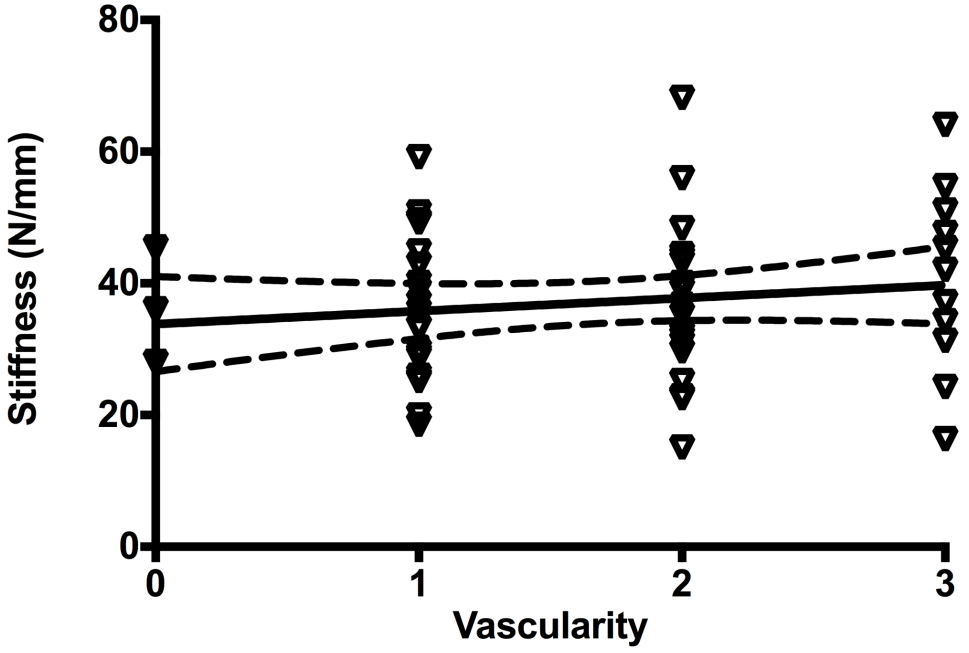

Figure 4.3.4E XY scatter plot of stiffness and vascularity score, lateral tendon, 4-week groups. There was moderate correlation between stiffness and the vascularity score (r=0.45, p=0.006) Correlation and 95% confidence intervals provided.

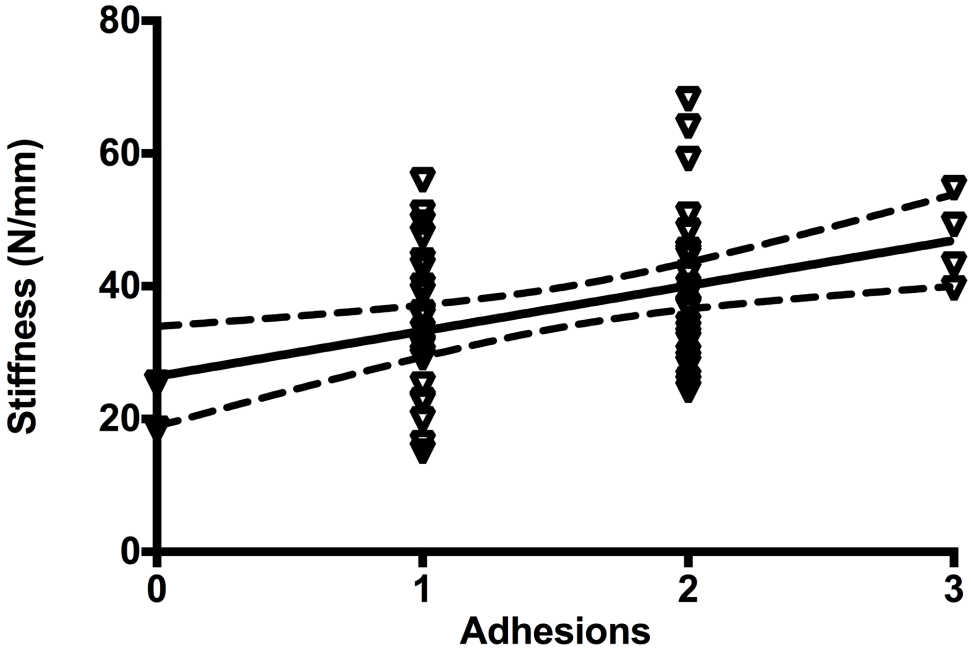

Figure 4.3.4F XY scatter plot of stiffness and adhesion score, lateral tendon, 4-week groups. There was moderate correlation between stiffness and the adhesion score (r=0.40, p=0.0028) Correlation and 95% confidence intervals provided.

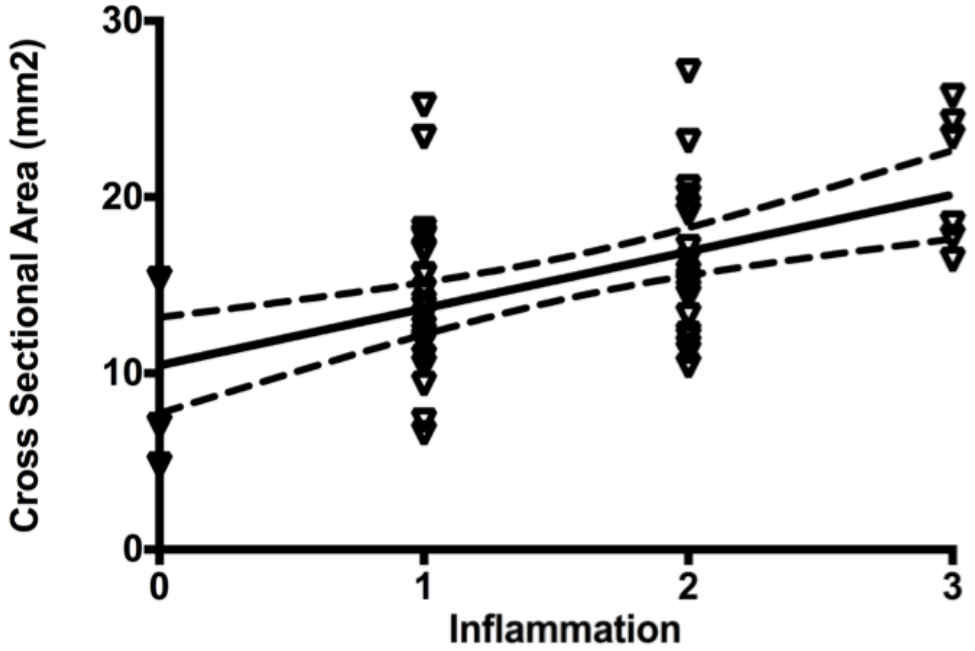

Figure 4.3.4G XY scatter plot of cross sectional area and inflammation score, lateral tendon, 4-week groups. There was moderate correlation between cross sectional area and the inflammation score (r=0.5, p=000118) Correlation and 95% confidence intervals provided.

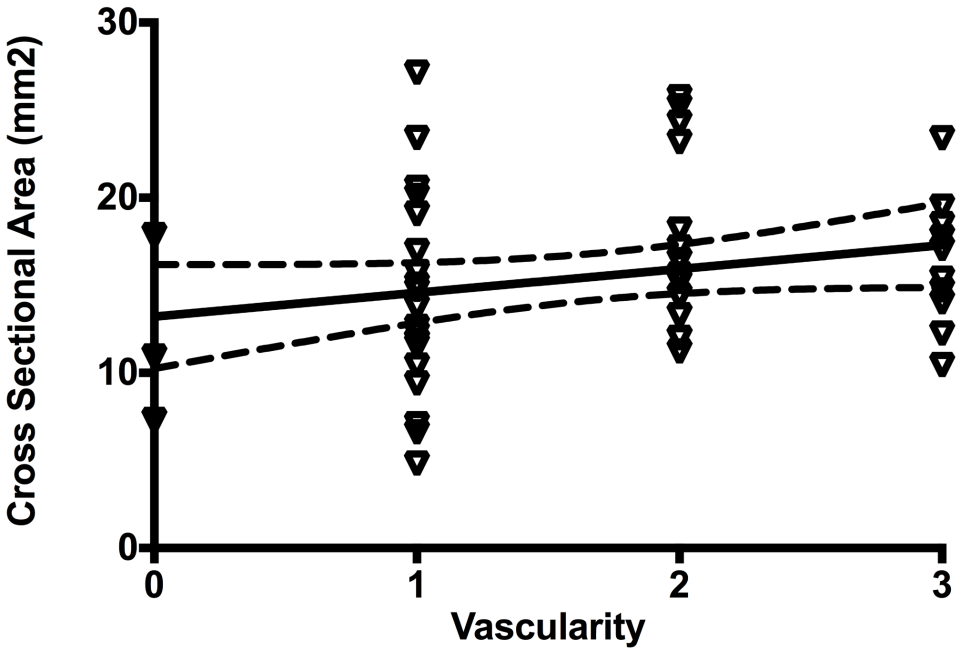

Figure 4.3.4H XY scatter plot of cross sectional area and vascularity score lateral tendon, 4-week groups. There was no correlation between cross sectional area and the vascularity score (r=0.07 p=0.61) Correlation and 95% confidence intervals provided.

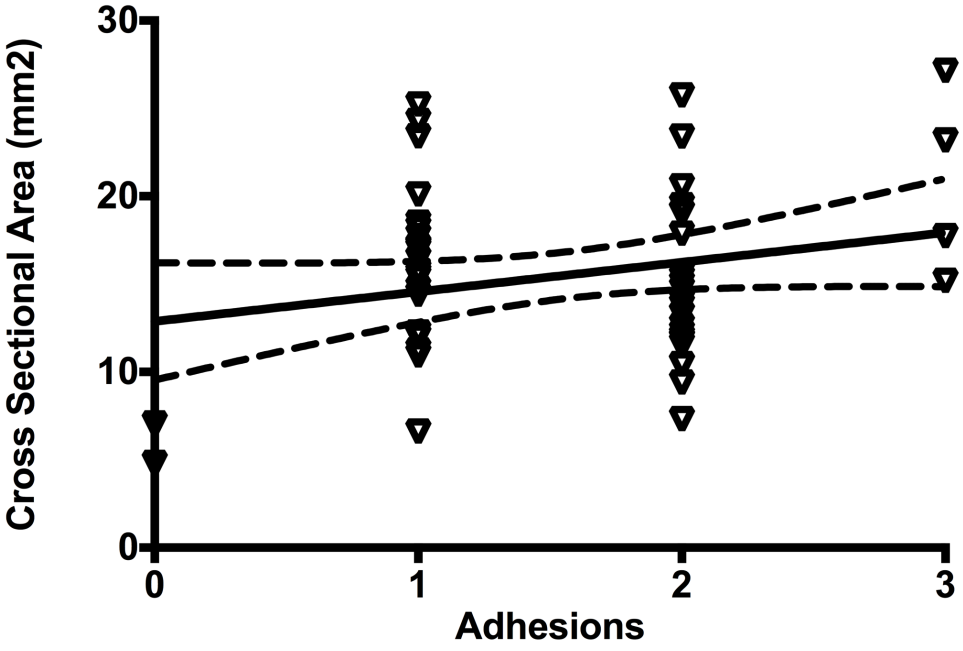

Figure 4.3.4I XY scatter plot of cross sectional area and adhesion score, lateral tendon, 4-week groups. There was weak correlation between cross sectional area and the adhesion score (r=0.39, p=0.0036) Correlation and 95% confidence intervals provided.

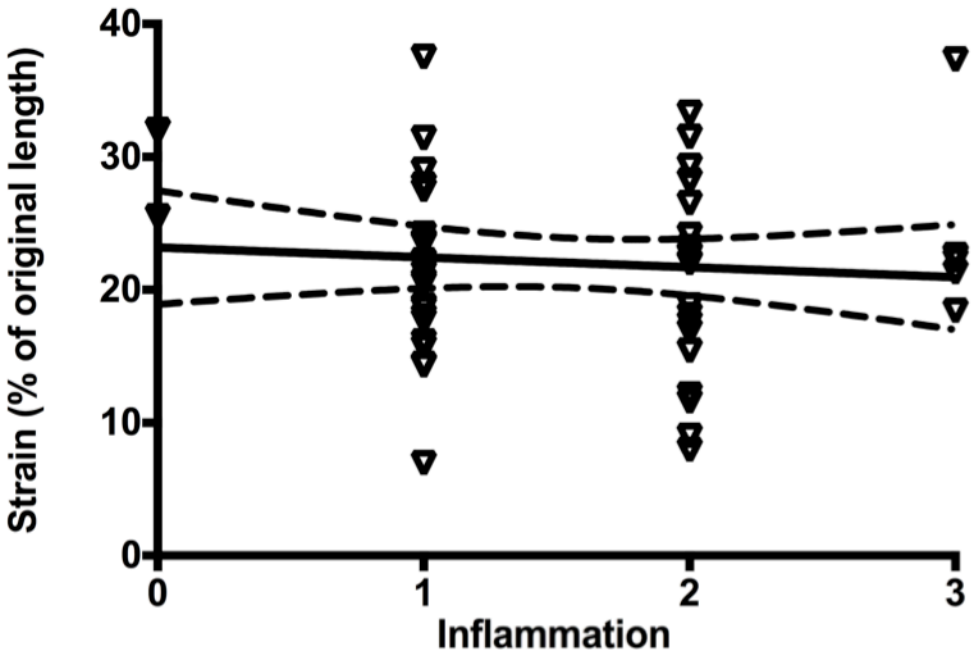

Figure 4.3.4J XY scatter plot of strain and inflammation score, lateral tendon, 4-week groups. There was no correlation between strain and the inflammation score (r=0.08, p=0.57) Correlation and 95% confidence intervals provided.

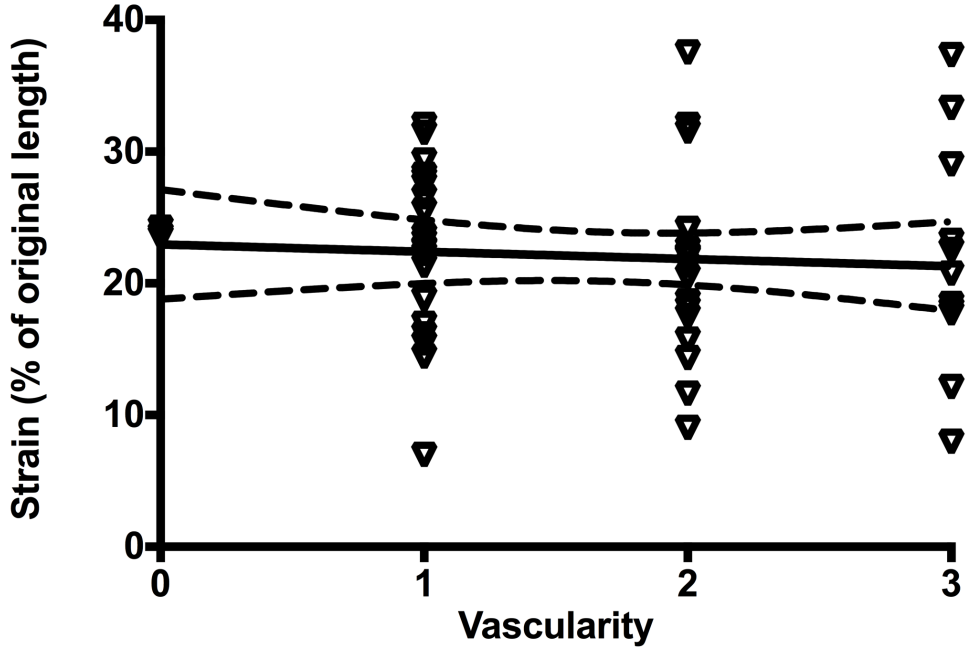

Figure 4.3.4K XY scatter plot of strain and vascularity score, lateral tendon, 4-week groups. There was no correlation between strain and the vascularity score (r=0.06, p=0.67) Correlation and 95% confidence intervals provided.

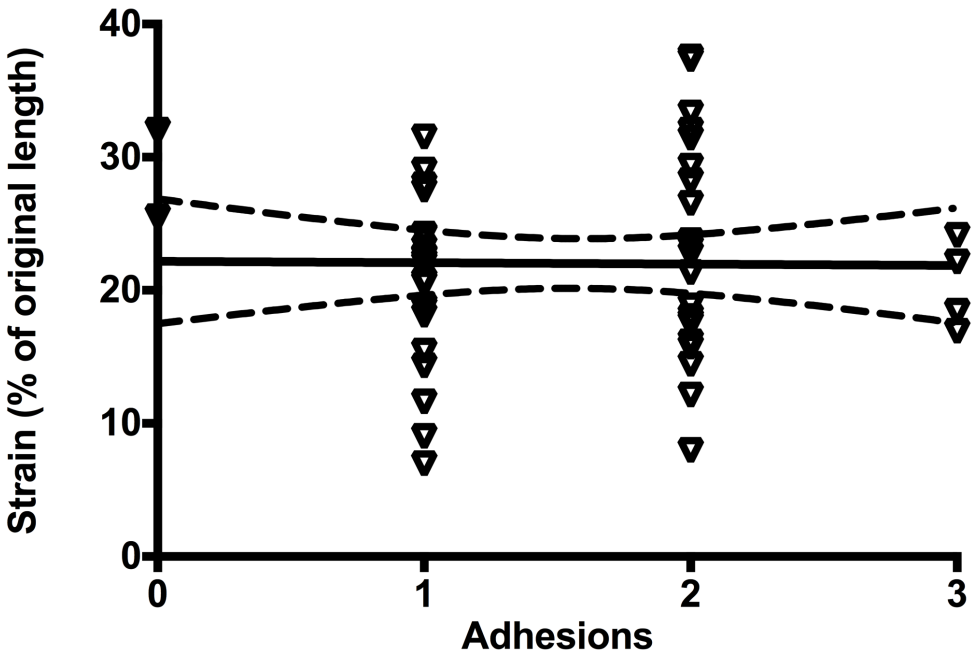

Figure 4.3.4L XY scatter plot of strain and adhesion score, lateral tendon, 4-week groups. There was no correlation between strain and the adhesion score (r=0.01 (p=0.94). Correlation and 95% confidence intervals provided.

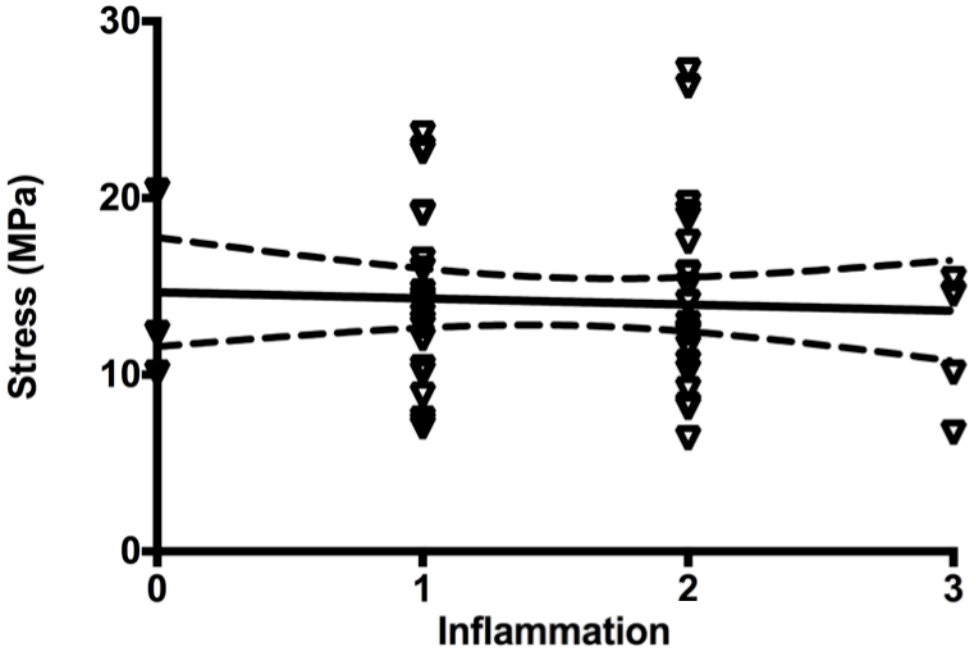

Figure 4.3.4M XY scatter plot of stress and inflammation score, lateral tendon, 4-week groups. There was no correlation between stress and the inflammation score (r=0.05 (p=0.72) Correlation and 95% confidence intervals provided.

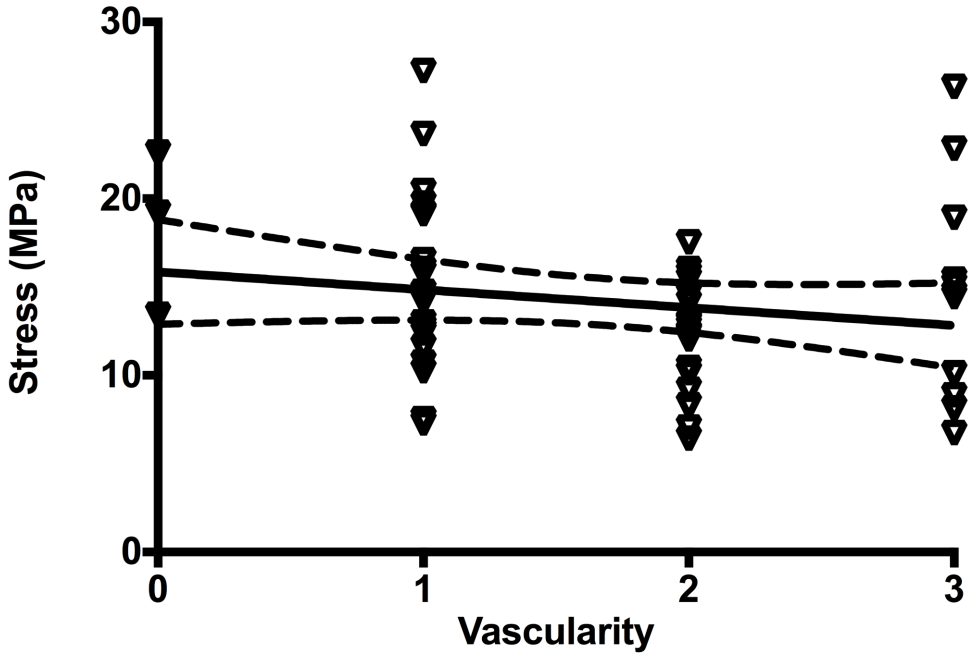

Figure 4.3.4N XY scatter plot of stress and vascularity score, lateral tendon, 4-week groups. There was no correlation between stress and the vascularity score (r=0.05, p=0.72) Correlation and 95% confidence intervals provided.

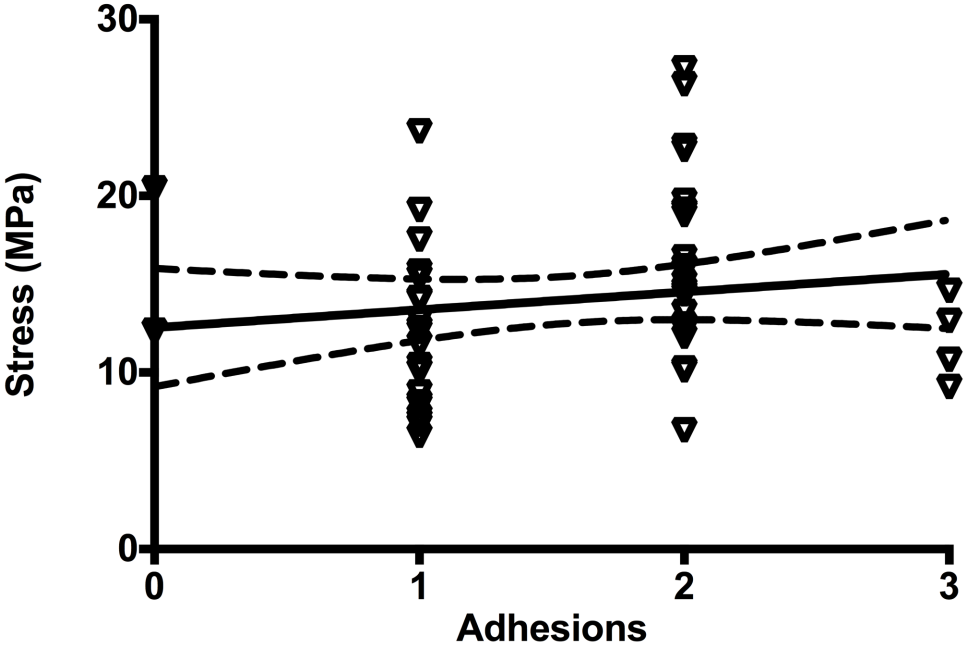

Figure 4.3.4O XY scatter plot of stress and adhesion score, lateral tendon, 4-week groups. There was no correlation between stress and the adhesion score (r=0.04, p=0.77) Correlation and 95% confidence intervals provided.

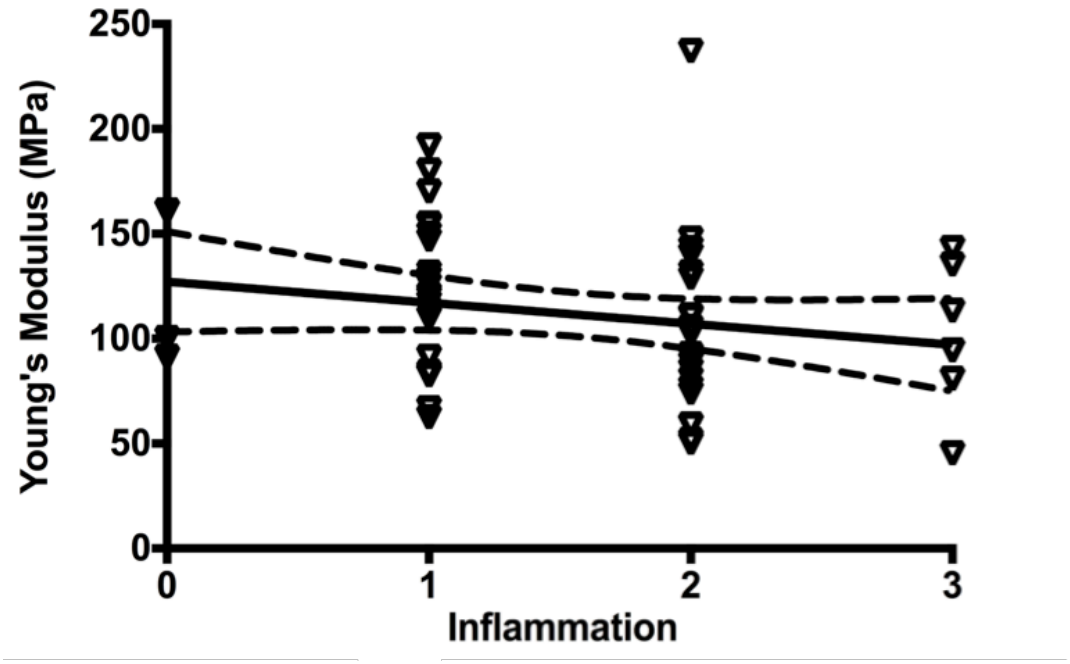

Figure 4.3.4P XY scatter plot of Young's Modulus and inflammation score, lateral tendon, 4-week groups. There was no correlation between Young's Modulus and inflammation score, (r=0.19, p=0.168) Correlation and 95% confidence intervals provided.

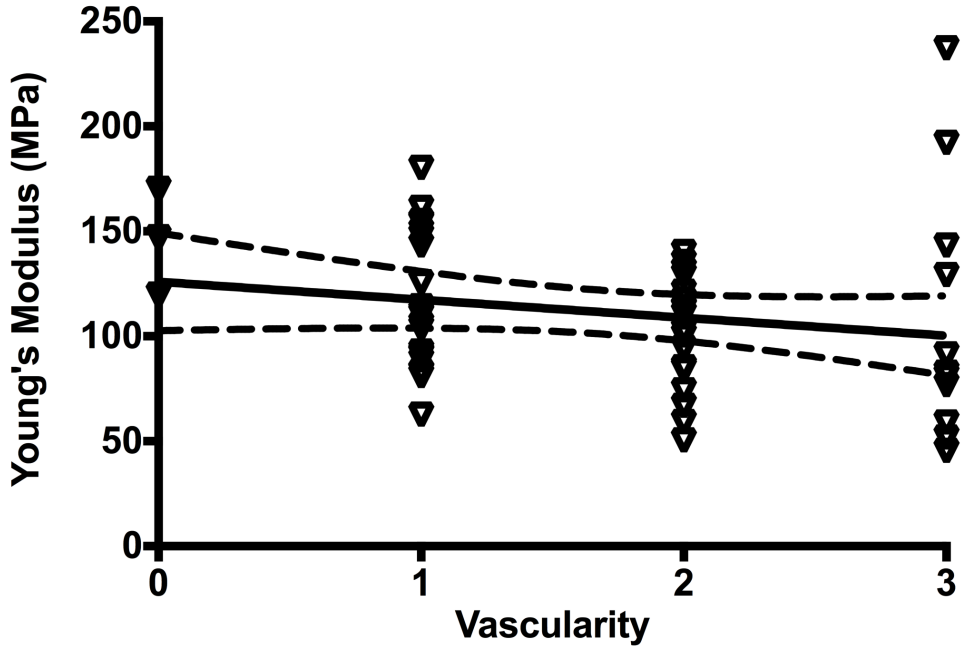

Figure 4.3.4Q XY scatter plot of Young's Modulus and vascularity score, lateral tendon, 4-week groups. There was no correlation between Young's Modulus and vascularity score, score (r=0. 19, p=0.168) Correlation and 95% confidence intervals provided.

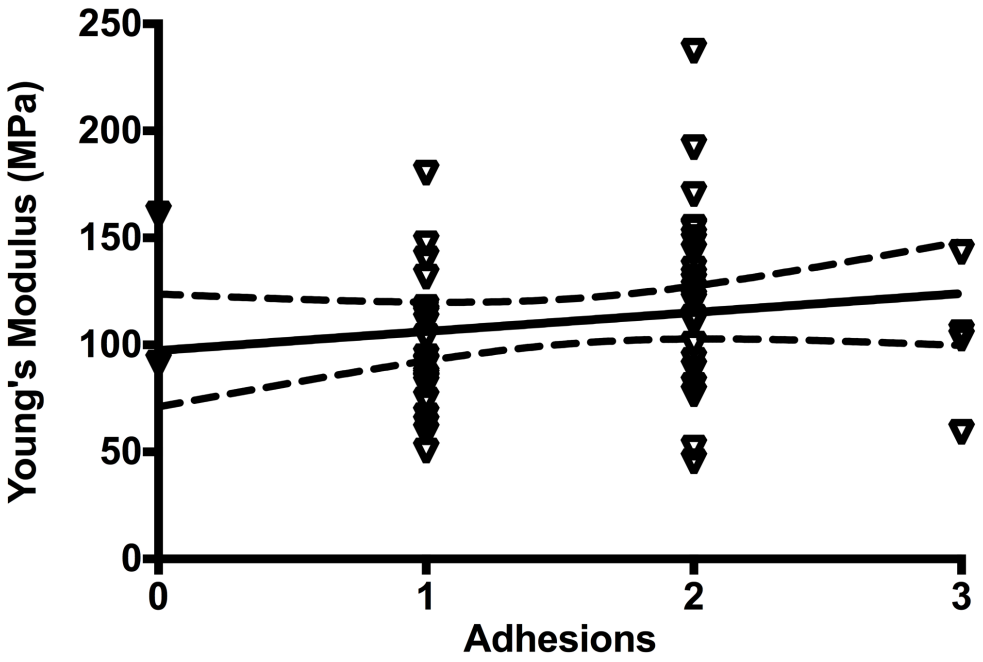

Figure 4.3.4R XY scatter plot of Young's Modulus and adhesion score, lateral tendon, 4-week groups. There was no correlation between Young's Modulus and adhesion score, (r=0.16, p=0.24) Correlation and 95% confidence intervals provided.

Inflammation Score Data

Group	Median	Maximum	Minimum
ZF/ZV	0.5	1	0
LV	2	2	1
HF	1	3	1
HV	1	2	1
LF	2	2	1
LF/LV	1.5	3	1
LF/HV	1.5	2	1
HF/HV	2	3	2
HF/LV	2	3	1

Vascularity Score Data

Group	Median	Maximum	Minimum
ZF/ZV	1	2	0
LV	2	3	1
HF	1.5	2	0
HV	2.5	3	1
LF	1	3	1
LF/LV	1	3	1
LF/HV	2	3	2
HF/HV	1.5	3	1
HF/LV	2	3	1

Adhesion Score Data

Group	Median	Maximum	Minimum
ZF/ZV	0.5	2	0
LV	1	2	1
HF	1.5	2	1
HV	1.5	2	1
LF	2	2	1
LF/LV	1.5	2	1
LF/HV	1.5	2	1
HF/HV	2	3	2
HF/LV	1.5	3	1

Table 4.3.4A Inflammation (**Top**), vascularity (**Middle**) and adhesion scores (**Bottom**) data. ZF/ZV (control suture) tended to have the lowest scores.There were no significant differences among the protein coated suture groups.

4.3.5 Ultimate Tensile Strength, 4-weeks

There were significant difference among all the surgical groups tested in the short term (4-week) ($p<0.001$, **Figure 4.3.5A**). There were no signficant difference detected among the ZF/ZV LV, LF/HV and HF/HV groups. The HF/HV group was significantly different from all other groups. There were no significant differences among any of the growth factor coated sutures, with the excpetion of HF/HV as previously noted.

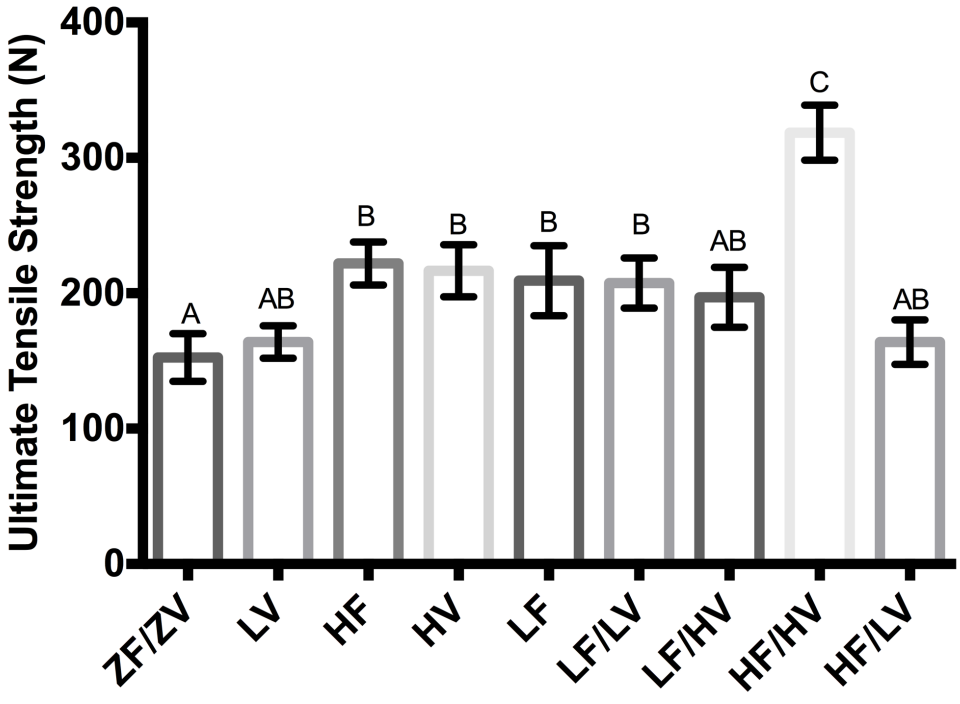

Figure 4.3.5A Bar chart of ultimate tensile strength for the short term (4 week) groups, lateral gastrocnemius tendon. Different letters among groups denote significant

differences ($p<0.05$). The HF/HV group was significantly superior to any other group. Data shown as mean ± SEM.

In the two way anova factorial analysis of data, there was a significant difference identified among the three levels of FGF (Figure **4.3.5B)** and the three levels of VEGF (**Figure 4.3.5C**). There was no signficant difference between the absence of FGF and the 0.5 µg/ml incubation dose. In addition there was no signficant difference between the 0.5 µg/ml incubation dose and the 5 µg/ml incubation dose. However, a significant difference was identified between the absence of FGF (0 µg/ml incubation dose) and the 5 µg/ml incubation dose ($p<0.05$).

There was no signficant difference between the absence of VEGF (0 µg/ml incubation dose) and the 0.5 µg/ml incubation dose (**Figure 4.3.5C**). However, the 5 µg/ml incubation dose of VEGF was significantly different to both 0.5 µg/ml incubation dose and the 0 µg/ml incubation dose ($p<0.05$).

When the factorial analysis data was combined, there was a significant effect for FGF ($p=0.0027$) and a significant effect for VEGF ($p=0.0023$) on the UTS. There was a signficant main interaction effect between FGF and VEGF ($p=0.015$) For the 0 µg/ml incubation dose and the 0.5 µg/ml incubation dose for both FGF and VEGF, there was no signficant interaction effect, increasing each factor resulted in a linear, parrallel and predictable increase in ultimate tensile stregnth (**Figure 4.3.5B and C**). When the level of FGF was increased to 5 µg/ml incubation dose, there was no signifcant difference between the 0 µg/ml incubation dose and the 0.5 µg/ml incubation dose of VEGF.

However, when the 5 µg/ml incubation dose levels of both VEGF and FGF were combined, a signficant interaction occured, which resulted in UTS values of the lateral gastrocnemius tendon greater than those anticipated from linear extrapolation from the 0 µg/ml incubation dose and the 0.5 µg/ml incubation dose (**Figure 4.3.3B and C**).

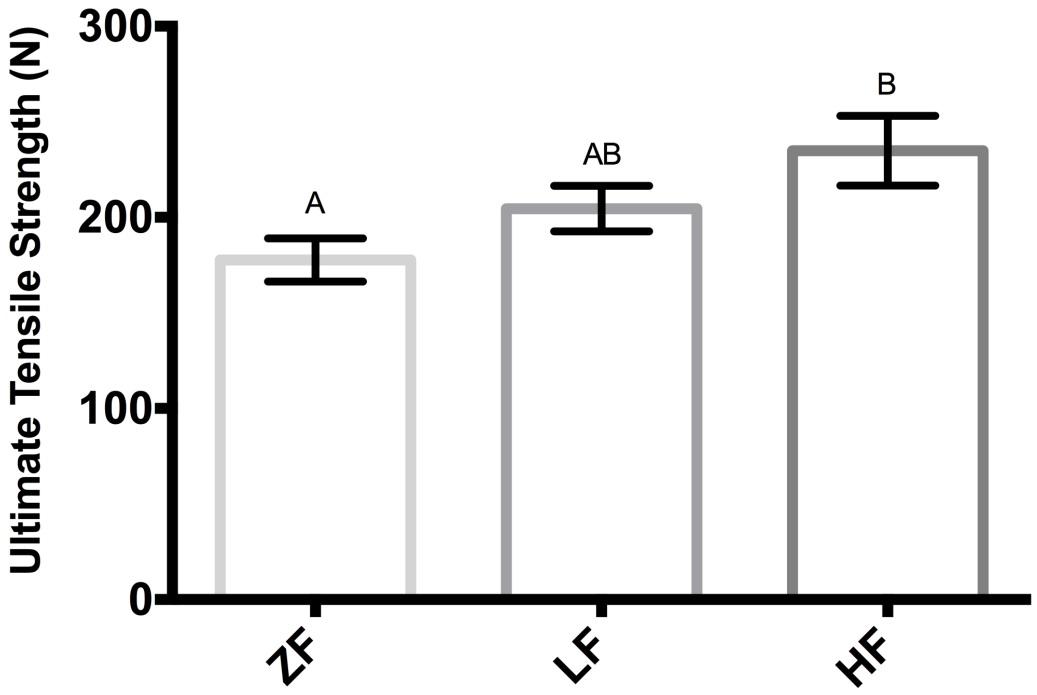

Figure 4.3.5B. Bar chart of ultimate tensile strength, lateral gastrocnemius tendon, of the 3 doses of FGF used in the short term (4-week) study. Different letters among groups denote significant differences ($p<0.05$). Data shown as mean ± SEM.

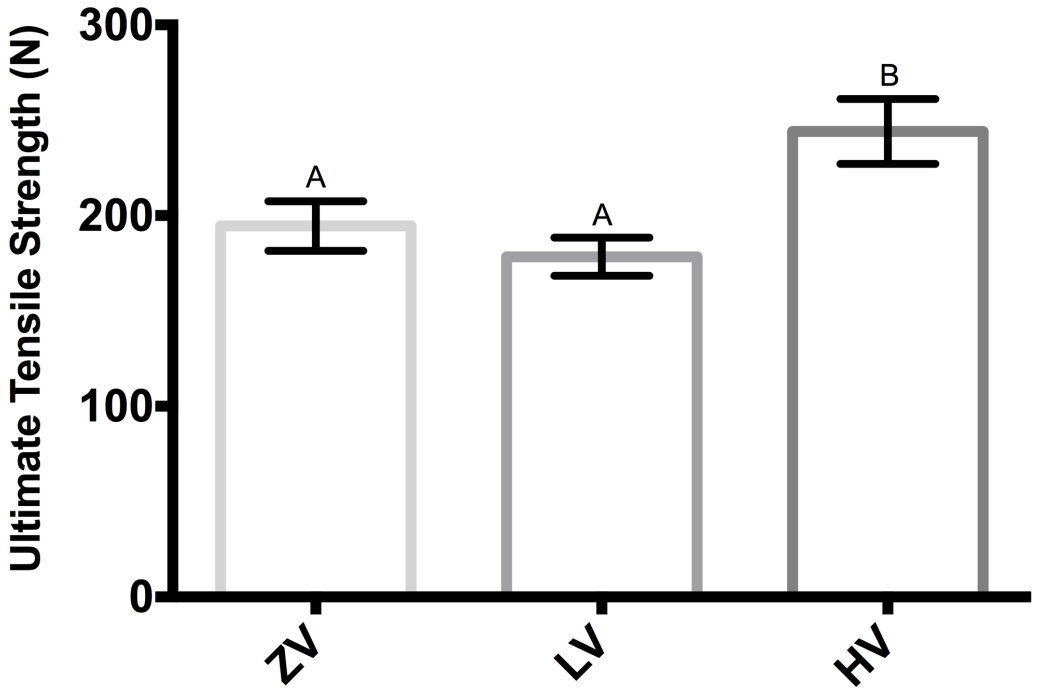

Figure 4.3.5C Bar chart of ultimate tensile strength, lateral gastrocnemius tendon, of the 3 doses of VEGF used in the short term (4-week) study. Different letters among groups denote significant differences ($p<0.05$).Data shown as mean ± SEM

4.3.6 Stiffness, 4-weeks

A significant difference in stiffness was identified among all the surgical group ($p<0.001$, **Figure 4.3.6A**). There was no significant difference among groups ZF/ZV, LV,HV, LF, and HF/LV groups . Significant differences were identified among the ZF/ZV HF, LF/LV and HF/HV groups.

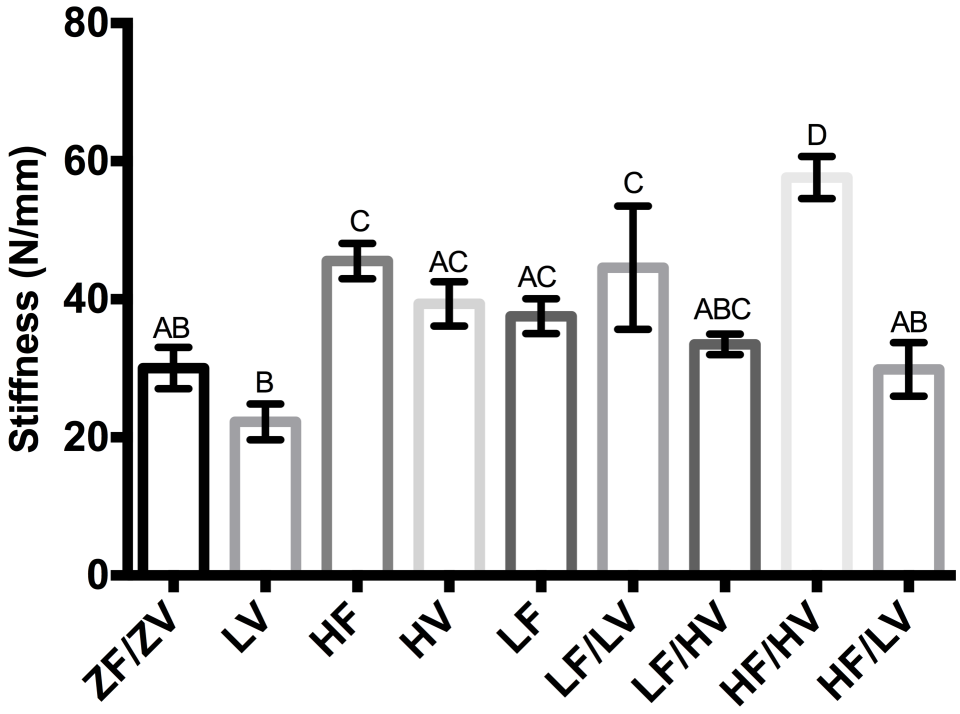

Figure 4.3.6A Bar chart of stiffness for the short term (4-week) groups, lateral gastrocnemius tendon. Different letters among groups denote significant differences ($p<0.05$). The HF/HV group was significantly superior to any other group. Data shown as mean ± SEM.

4.3.7 Stress, 4-weeks

A significant difference in maximum stress was identified among all the surgical groups ($p=0.0017$). The majority of the experimental suture groups (LV, HF,HV, LV, LF/LV, LF/HV, HF/HV and LF/HV) were significantly inferior in terms of maximum stress compared to the ZF/ZV group. There was no significant difference in stress tolerance between the ZF/ZV and LF groups ($p<0.05$).

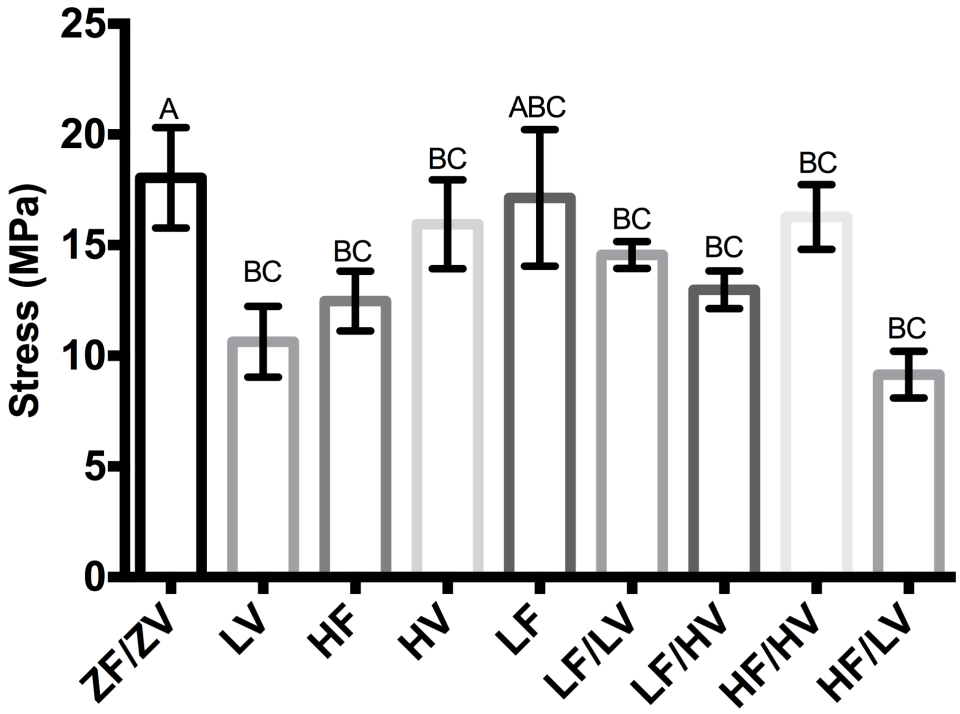

Figure 4.3.7A Bar chart of stress for the short term (4-week) groups, lateral gastrocnemius tendon. Different letters among groups denote significant differences ($p<0.05$). Data shown as mean ± SEM.

4.3.8 Strain, 4-weeks

There was no significant difference among the groups in regard to maximum tendon strain (**Figure 4.3.8A)**

4.3.9 Youngs Modulus, 4-weeks

A significant difference in Young's modulus was identified among all the surgical groups ($p=0.00102$, **Figure 4.3.9A**). The majority of the suture groups (ZF/ZV, HF,HV,LF,LF/LV, LF/HV and HF/HV groups) were not signficantly different among each other. However, both ZF/ZV and HF/HV groups had higher Young's moduli than LV and HF/LV groups.

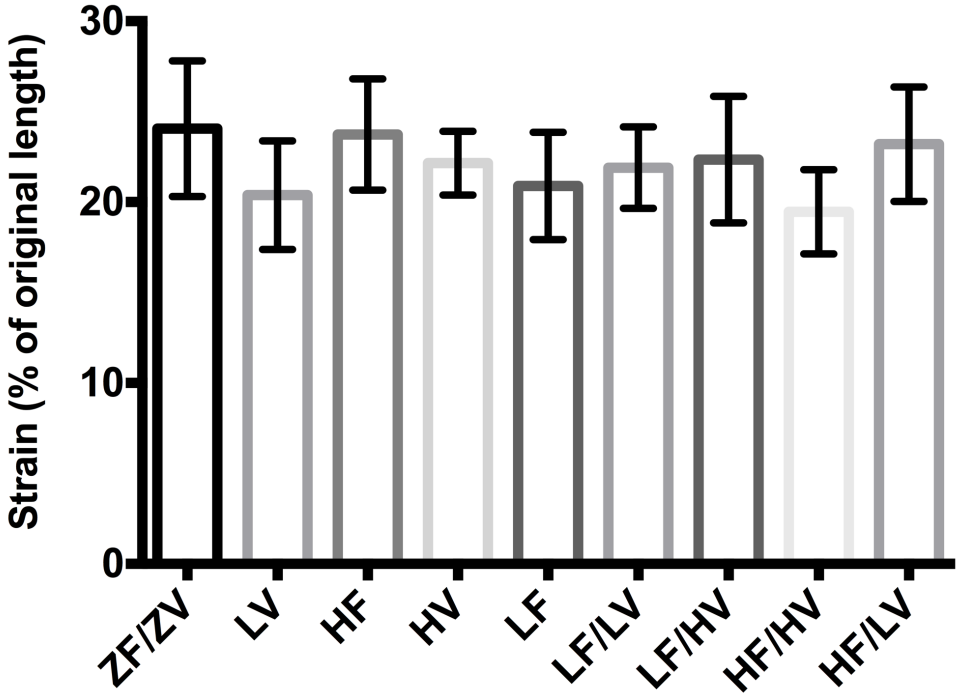

Figure 4.3.8A Bar chart of strain for the short term (4-week) groups, lateral gastrocnemius tendon. In this case, there were no significant differences among the groups (p=0.81). Data shown as mean ± SEM.

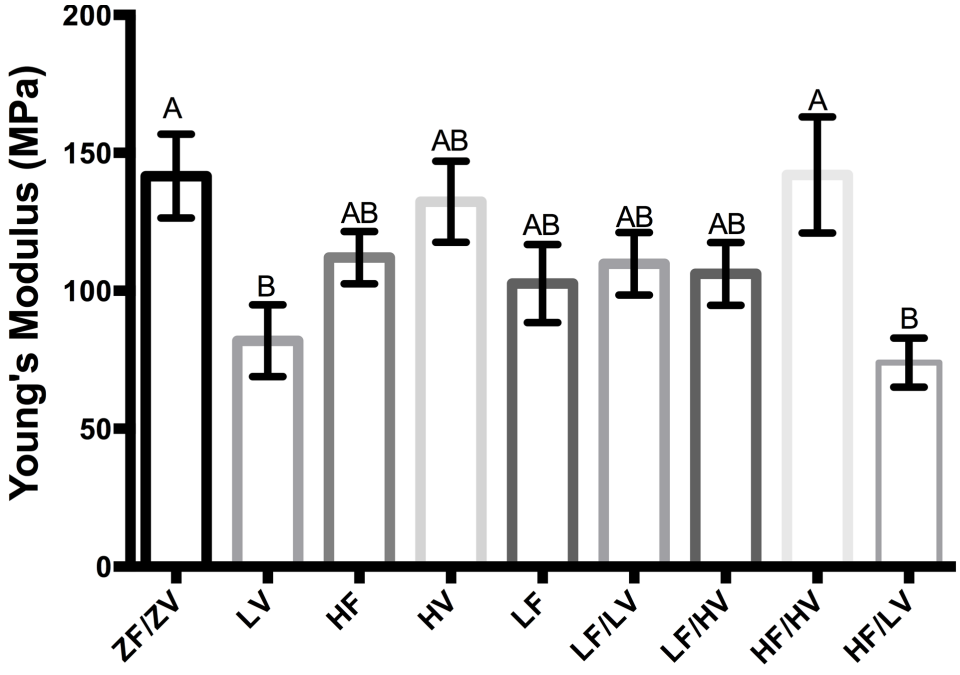

Figure 4.3.9A Bar chart of Young's modulus for the short term (4-week) groups, lateral gastrocnemius tendon. Different letters among groups denote significant differences (p<0.05). Data shown as mean ± SEM.

4.4.1 Medial UTS, 4-weeks

There were no significant differences amoung the groups in terms of the ultimate tensile strength of the medial gastrocnemius tendon as evaluated at 4-weeks (**Figure 4.4.1A,** p=0.1677).

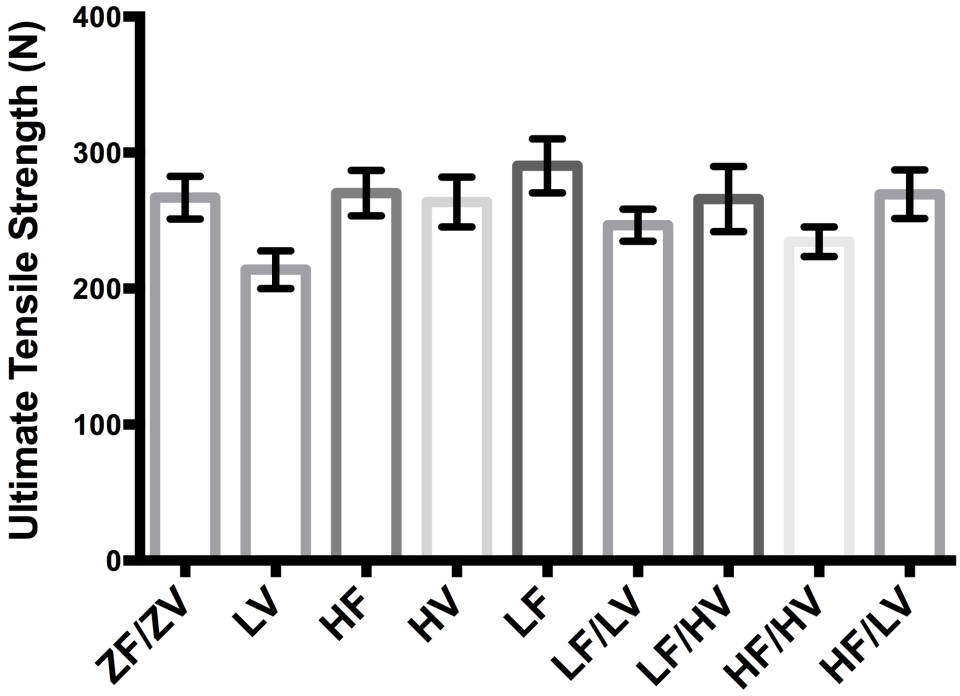

Figure 4.4.1A Bar chart of ultimate tensile strength for the short term (4-week) groups, medial gastrocnemius tendon. No significant differences were identified (p=0.1677) Data shown as mean ± SEM.

4.4.2 Medial Stiffness

There were no significant differences among the stiffness of the medial gastrocnemius tendon among the groups at the 4 week time point (p=0.0093).

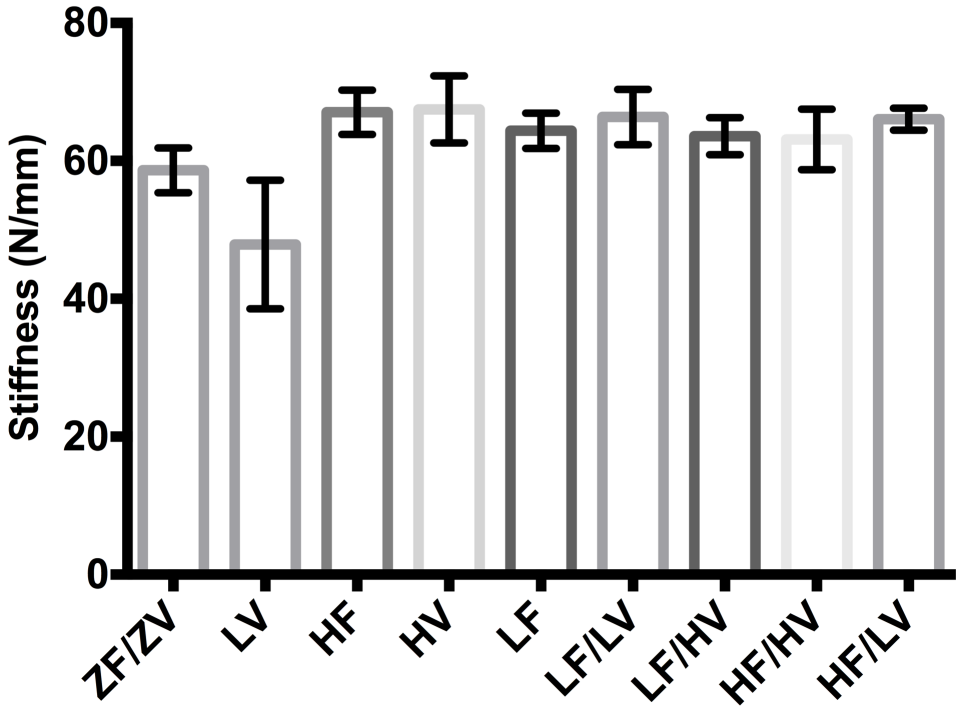

Figure 4.4.2A Bar chart of stiffness for the short term (4-week) groups, medial gastrocnemius tendon. No significant differences were identified (p=0.093). Data shown as mean ± SEM.

4.5.1 Histology, 4-weeks

There was moderate correlation between histology score and ultimate tensile strength (r= 0.46, p=0.0046, **Figure 4.5.1A)**, with the trend that superior correlation scores had higher ultimate tensile strength. There was weak correlation between histology score and stiffness (r= 0.39, p=0.0027, **Figure 4.5.1B**), with the trend that superior correlation scores had higher ultimate tensile strength. There were significant differences in histology score among the groups (p<0.01, **Figure 4.5.1C**). The ZF/ZV group was not significantly different among the LV, HF, HV, LF/LV, LF/HV and the HF/LV groups. The optimal histological group was HF/HV, which was significantly different among all other groups, except the LF group (**Figure 4.5.1C**).

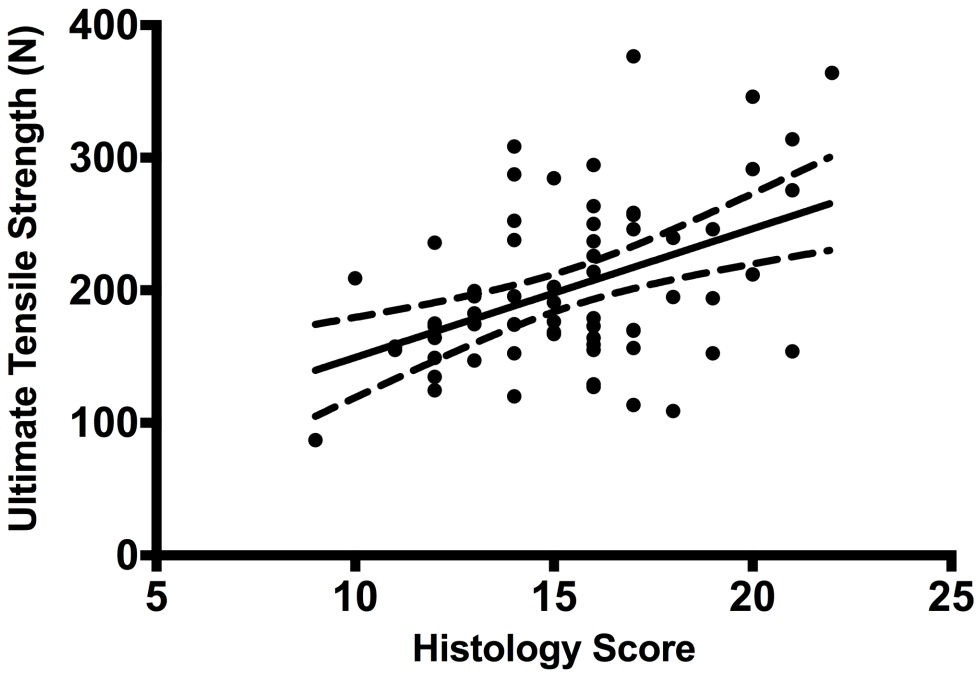

Figure 4.5.1A. XY scatter plot of ultimate tensile strength and histology scores for the short term (4-week) groups, lateral gastrocnemius tendon. There was moderate correlation among the data (r=0.46 p=0.0046). Bands denote 95% confidence intervals.

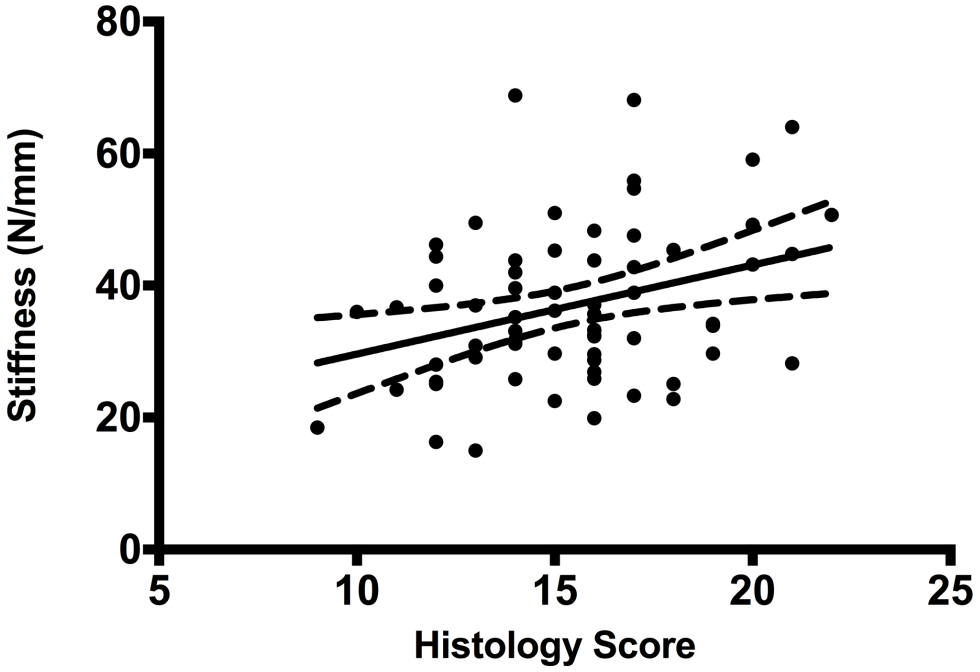

Figure 4.5.1B. XY scatter plot of stress and histology scores for the short term (4-week) groups, lateral gastrocnemius tendon. There was moderate correlation among the data (r=0.40 p=0.0027). Bands denote 95% confidence intervals.

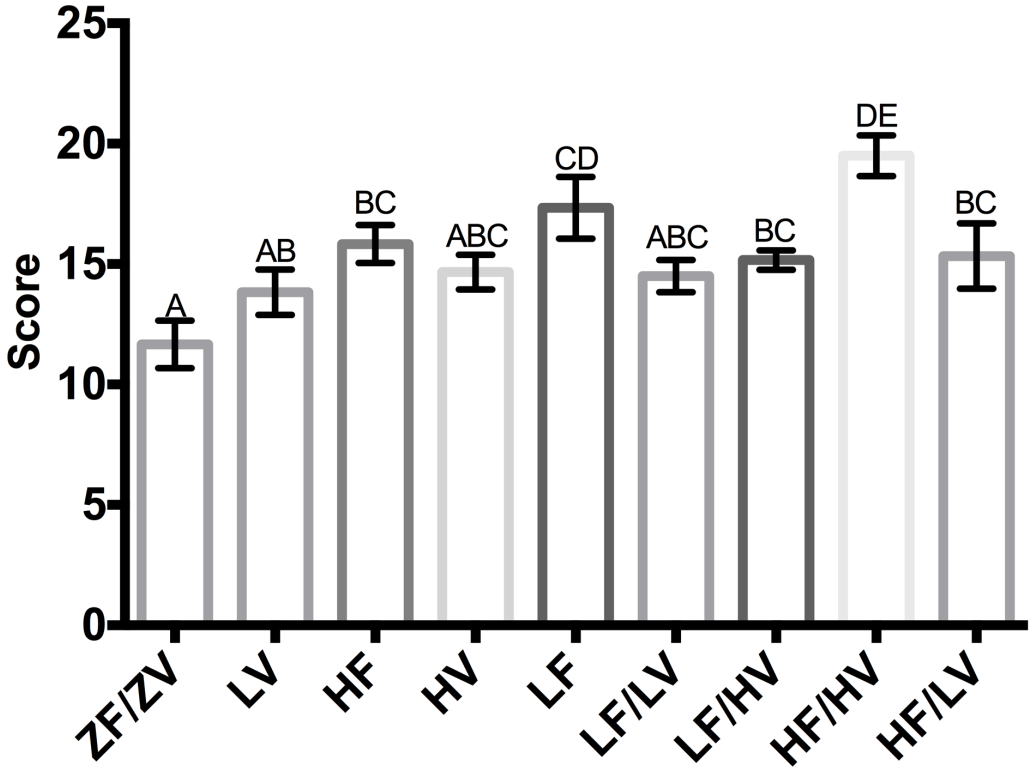

Figure 4.5.1C. Bar chart of histology score for the short term (4 week) groups, lateral gastrocnemius tendon. There were significant differences among the groups in histology score($p<0.001$). The HF/HV group score was superior to ZF/ZV, LV, HF, HV, LF/LV, LF/HV and HF/LV groups. There were no significant differences identified among the ZV/ZF group and the LV, HV and LF/LV groups. Data shown as mean ± SEM.

4.5.2 Tendon Maturation Score

An evaluation was performed to ascertain if differences could be determined via a tendon maturation scoring system based on selected parameters from the overall score. For UTS, there was a moderate correlation between UTS and the maturation score ($r= 0.42$, $p=0.0004$, **Figure 4.5.2A**). In terms of stiffness, a moderate correlation was also identified ($r=0.49$, $p<0.0001$, **Figure 4.5.2B**).

An evaluation of the ANOVA for the maturation score for the tendons (**Figure 4.5.2C**) reveals similar results to the overall histology score (**Figure 4.5.1C**).

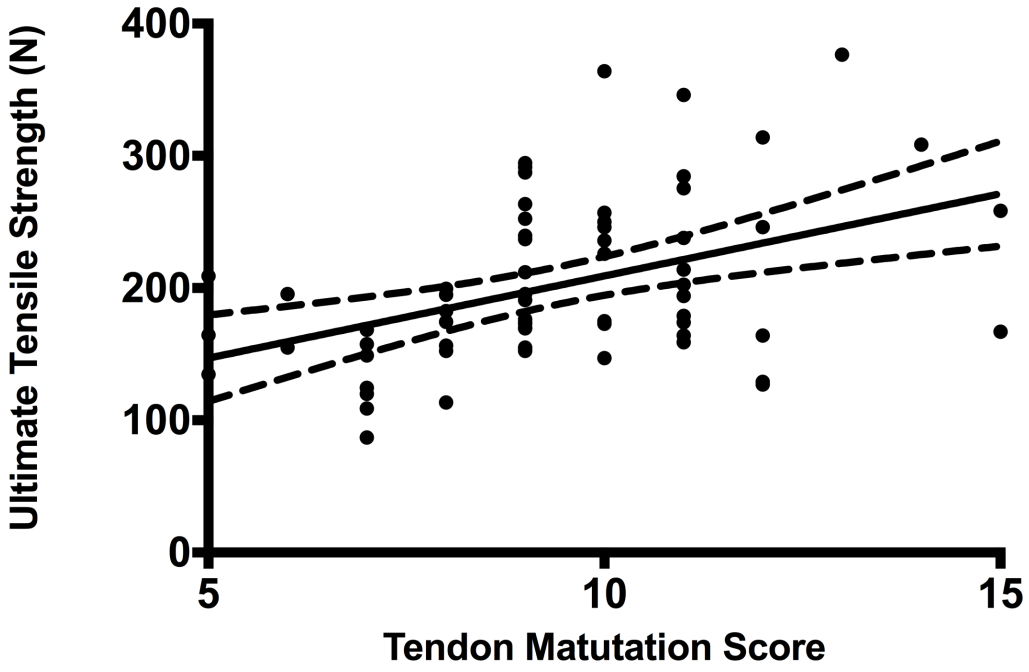

Figure 4.5.2A. XY scatter plot of ultimate tensile strength and tendon maturation scores for the short term (4-week) groups, lateral gastrocnemius tendon. There was moderate correlation among the data (r= 0.42, p=0.0004). Bands denote 95% confidence intervals.

There were significant differences in tendon maturation score among the groups (**Figure 4.5.2C)**. The control ZF/ZV group was significantly less mature histologically than the majority of the protein coated groups, with the exception of LV and HF/LV groups. There were no significant differences in tendon maturation scores among the majority of the protein coated groups, with the exception of LV and HF/LV groups. A plot of both histology and tendon maturation scores (**Figure 4.5.2D, 4.5.2E**) demonstrated the similarities in correlation parameters between the two scoring systems. There were

no significant differences between the slopes of the overall histology scoring system and the tendon maturation parameters as evaluated in relation to the ultimate tensile strength (p=0.3803, **Figure 4.5.2D**). There were no significant differences between the two scoring systems in relation to stiffness (p=0.756, **Figure 4.5.2E**).

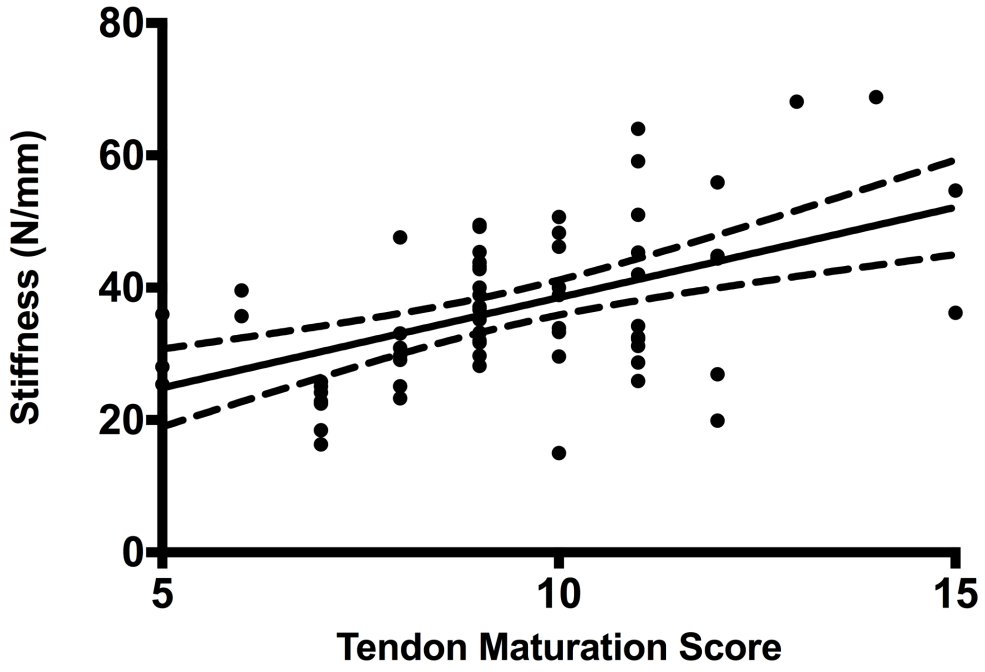

Figure 4.5.2B. XY scatter plot of stiffness and tendon maturation scores for the short term (4-week) groups, lateral gastrocnemius tendon. There was moderate correlation among the data (r=0.49, p<0.0001). Bands denote 95% confidence intervals.

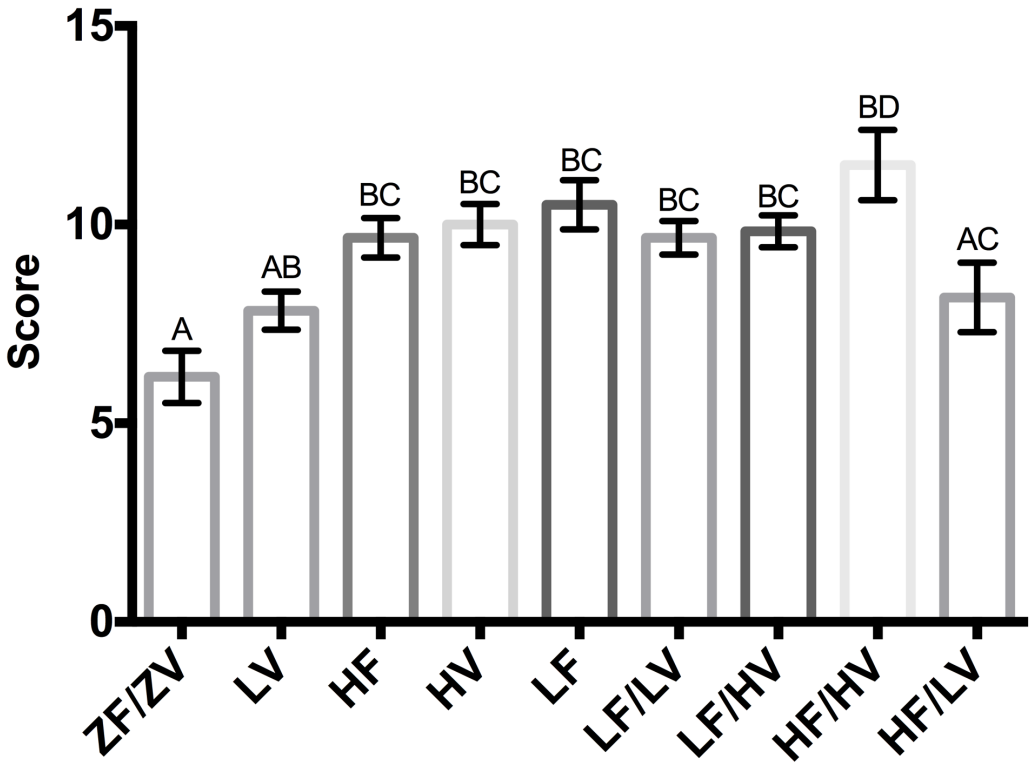

Figure 4.5.2C. Bar chart of tendon maturation score for the short term (4-week) groups, lateral gastrocnemius tendon. There were significant differences among the groups in tendon maturation score ($p<0.001$). The HF/HV group score was superior to ZF/ZV, LV, HF, HV, LF/LV, LF/HV and HF/LV groups. There were no significant differences identified among the ZV/ZF group and LV, HV and LF/LV groups. Data shown as mean ± SEM. The HF,HV,LF,LF/LV, LF/HV and HF/HV group scores were superior to the ZF/ZV group. ($p<0.001$).

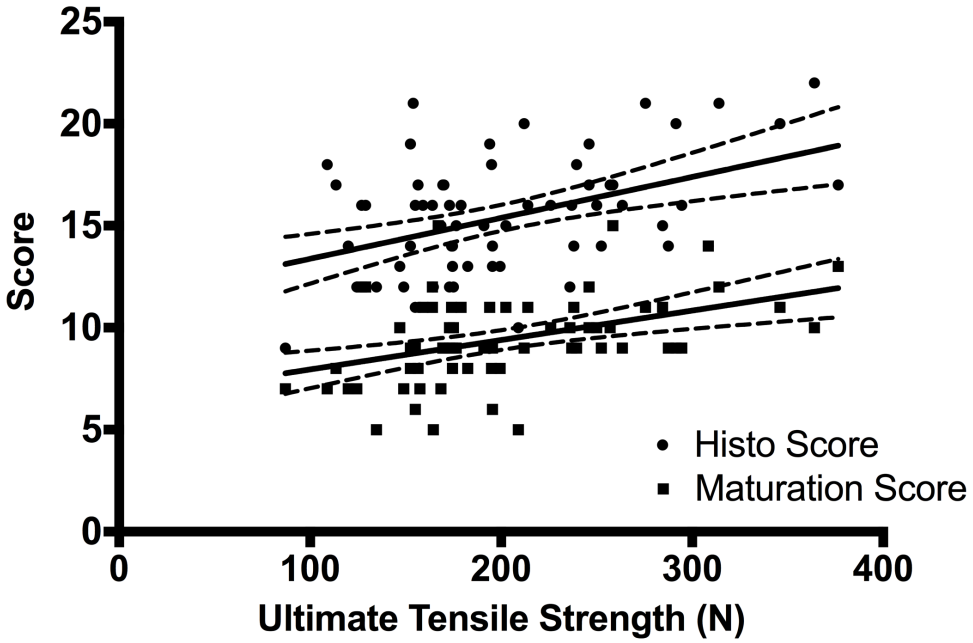

Figure 4.5.2D XY scatterplot comparison of histology score and tendon maturation score for ultimate tensile strength. Linear regression comparison of the two slope gradients determines that they were not significantly different between each other (p= 0.3803). Bands denote 95% confidence intervals.

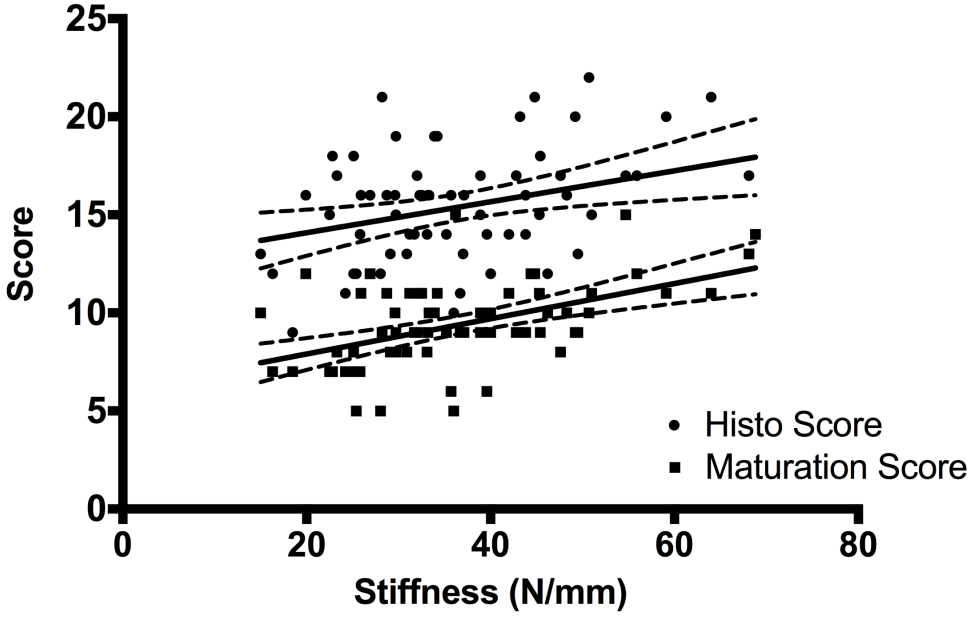

Figure 4.5.2E XY scatterplot comparison of histology score and tendon maturation score for stiffness. Linear regression comparison of the two slope gradients determines that they were not significantly different between each other (p= 0.756). Bands denote 95% confidence intervals.

4.5.3 Histology and Fluorescence, 4-weeks

Histological evaluation for collagen orientation, inflammation, and cellularity was performed. On histological evaluation, it was noted that for the ZF/ZV group, there was significant hyper cellularity and the presence of round cells. Furthermore, the orientation of the collagen bundles appeared random and haphazard (**Figure 4.5.3A**). In general, there was minor inflammation, consisting of neutrophils and lymphocytes, in close proximity around the suture material, highlighted in **Figure 4.5.3B**. In addition, the random nature of collagen was also apparent in the HV group where collagen fibers at 90 degrees to each other were often identified (**Figure 4.5.3B**). The integration of the suture material into the tendon occurred without any evidence of reaction (**Figure 4.5.3B, 4.5.3C**) and although in the FGF/VEGF combination groups fiber orientation improved, there were still areas where round cells would remain trapped within bundles of collagen (**Figure 4.5.3D**).

Negative histology controls were conducted for CD31 and macrophage MAC387 (**Figure 4.5.3E**). Results of histology controls demonstrated that non-specific binding did not occur. However, although binding for CD31 was excellent and specific to the endothelium, there was a significant paucity and lack of binding for the macrophage (**Figure 4.5.3F**). Some take up of the macrophage antibody did occur by cells with a larger appearance, suggested of macrophage in all groups, although cell numbers were few. For CD31 binding, the ZF/ZV groups demonstrated a significant paucity of blood vessels, which were sparsely located inside the tendon proper or in proximity to any

suture material (**Figure 4.5.3G**). In the LV group at 4 weeks, there appeared to be a reduced density of blood vessels in the body of the tendon in comparison to the other growth factor groups, with the exception of the ZF/ZV group (**Figure 4.5.3H**). In the HF group at 4 weeks, there were no blood vessels located with the body of the tendon, as they were confined to the area around the suture or to the periphery (**Figure 4.5.32I**) In the HV group at 4 weeks, there was a greater proportion of blood vessels, which were identified intermingled among the crimp pattern of the tendon (**Figure 4.5.3J, 4.5.3K**).

In groups HF/HV and HF/LV (**Figure 4.5.3K, 4.5.3L**), there were a greater proportion of the blood vessels located in close proximity to the suture material. The body of the tendon remained devoid of blood vessels.

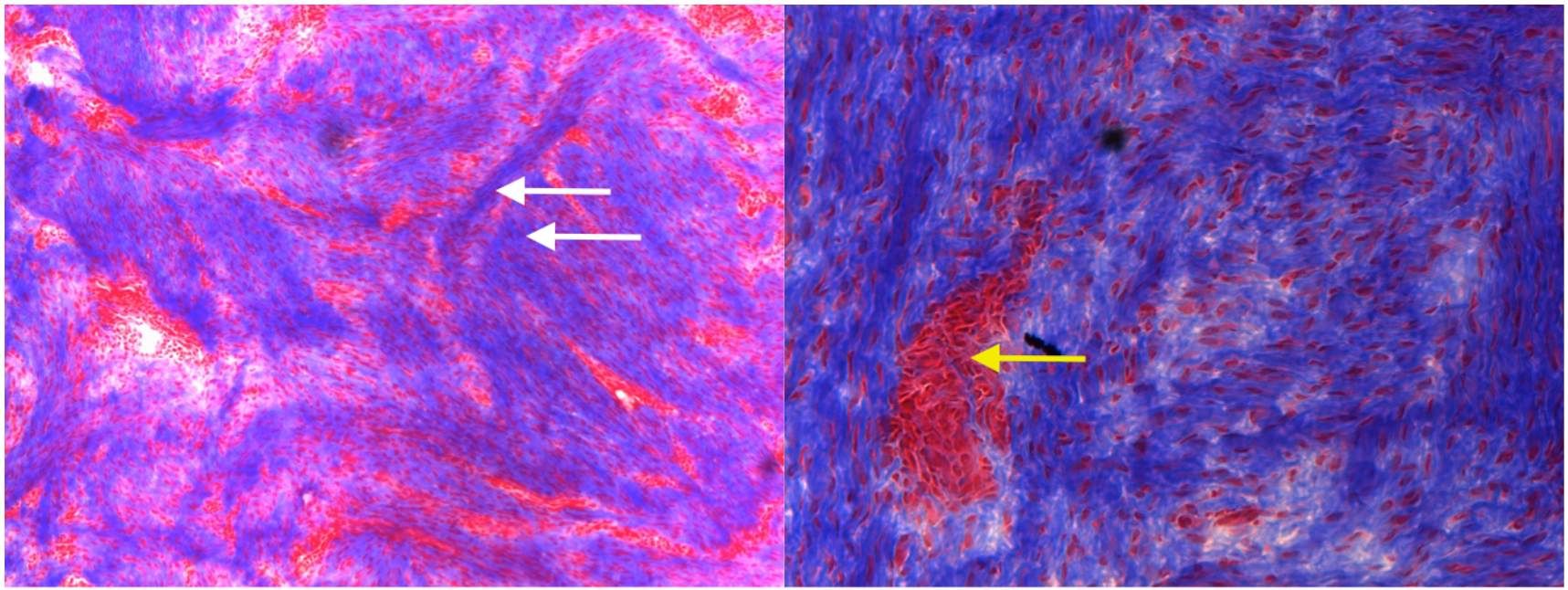

Figure 4.5.3A H&E (20X) (**left**), alcian blue (20X) (**right)** of ZF/ZV tendon at 4 weeks. Note the relative hyper cellularity (yellow arrow) and poor collagen orientation (white arrows) in both images. There are few spindle cells and collagen bundles in the tendon.

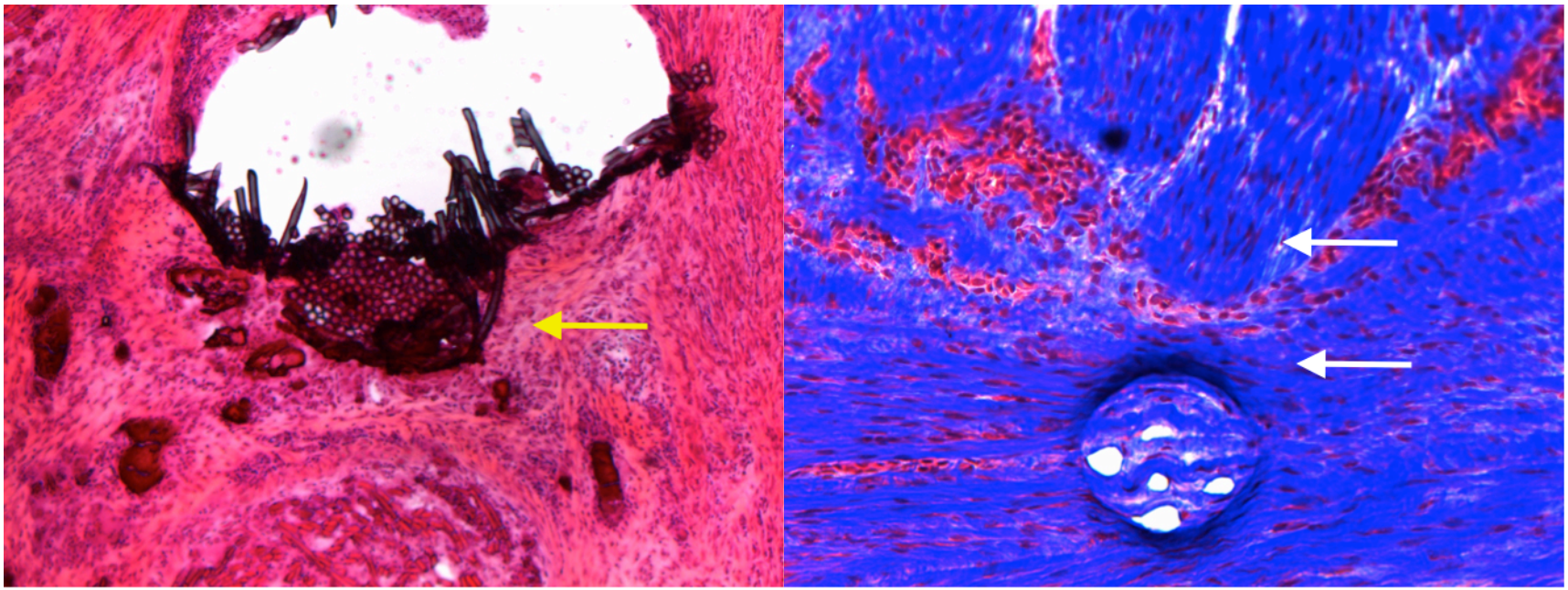

Figure 4.5.3B H&E (10X) (**left**), alcian blue (20X) (**right)** of HV tendon (**left**) and LV tendon (**right**) at 4 weeks. In both images, collagen fibers at 90 degrees to each other can be identified (white arrows). There was good integration of the suture material in the tendon tissue and relatively low inflammation around the suture (yellow arrow).

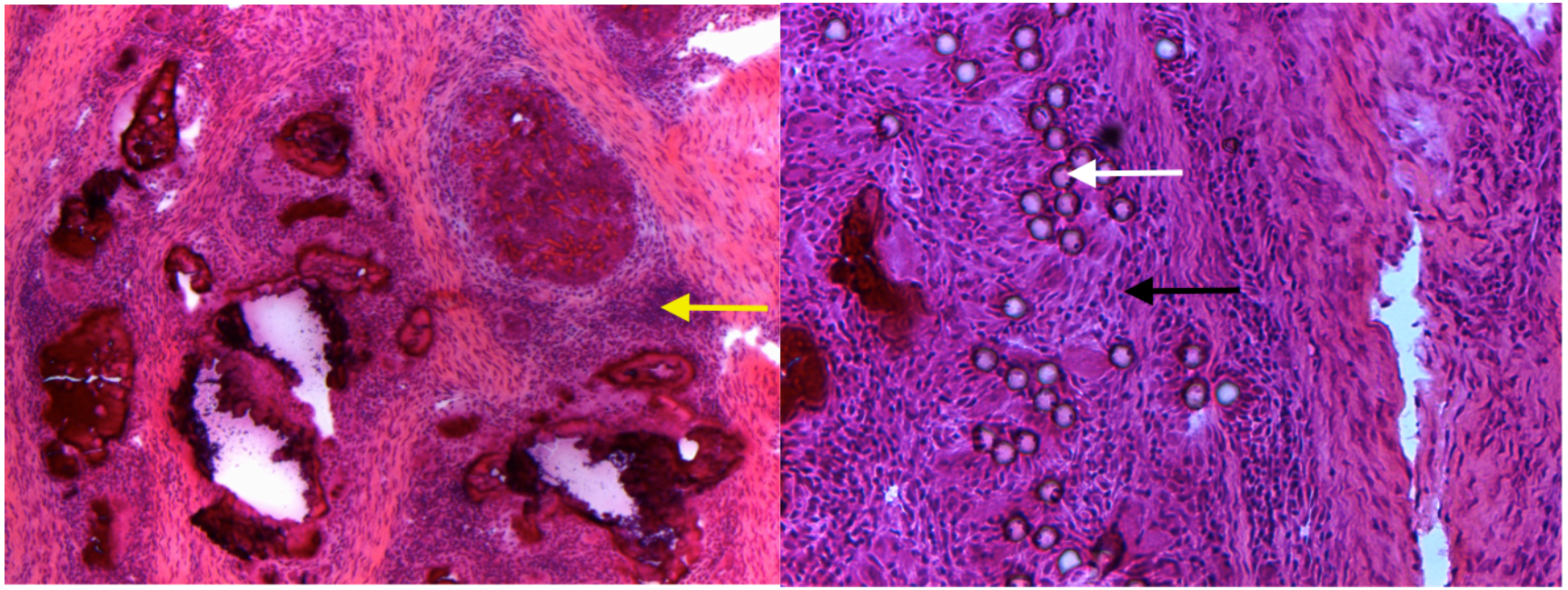

Figure 4.5.3C H& E (10X) (**left**) (20X, **right**) of HV tendon (**left**) and LF/LV tendon (**right**) at 4 weeks. Note the marked round cell numbers and inflammation in the left image (yellow arrow). The association of suture material (white arrow) with inflammatory cells (black arrow) can also be identified

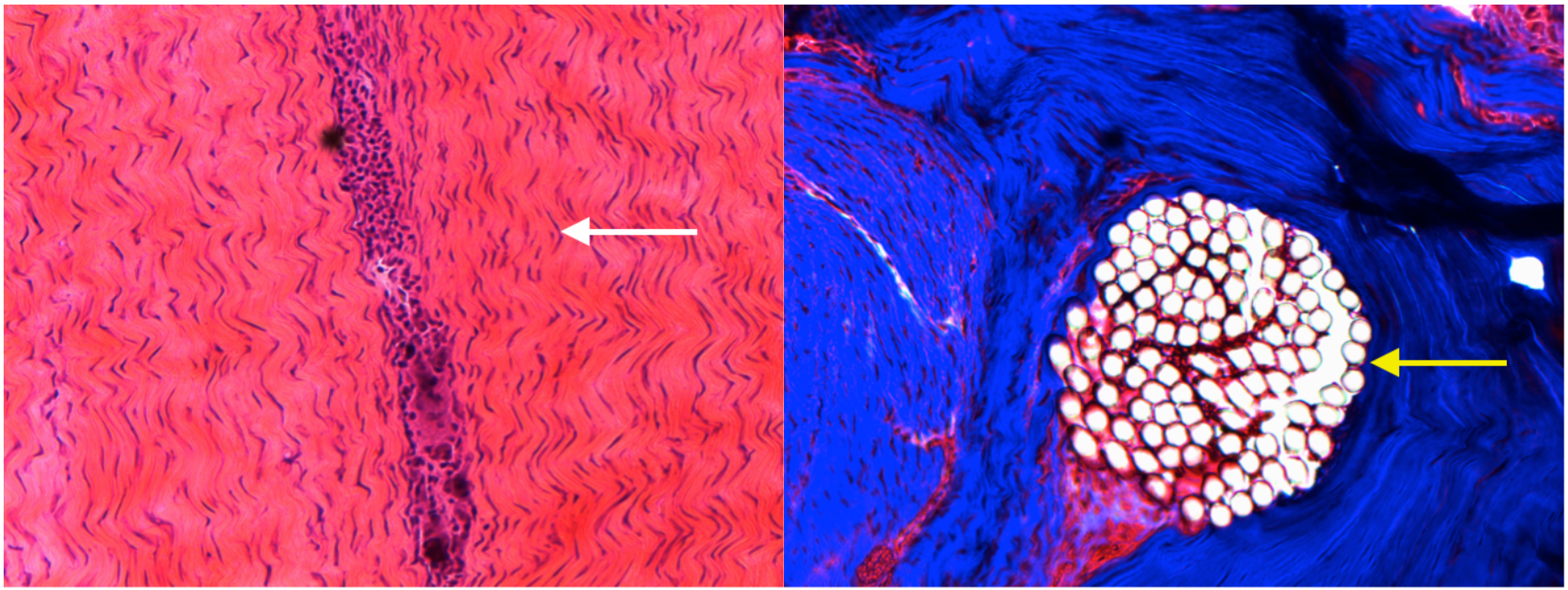

Figure 4.5.3D H&E (20X) stain (**left**), alcian blue (20X) (**right**) of HV tendon at 4 weeks. Note how there was crimp to the collagen waveform with spindle cells (white arrow) There was excellent integration of the suture material (yellow arrow) among the collagen bundles.

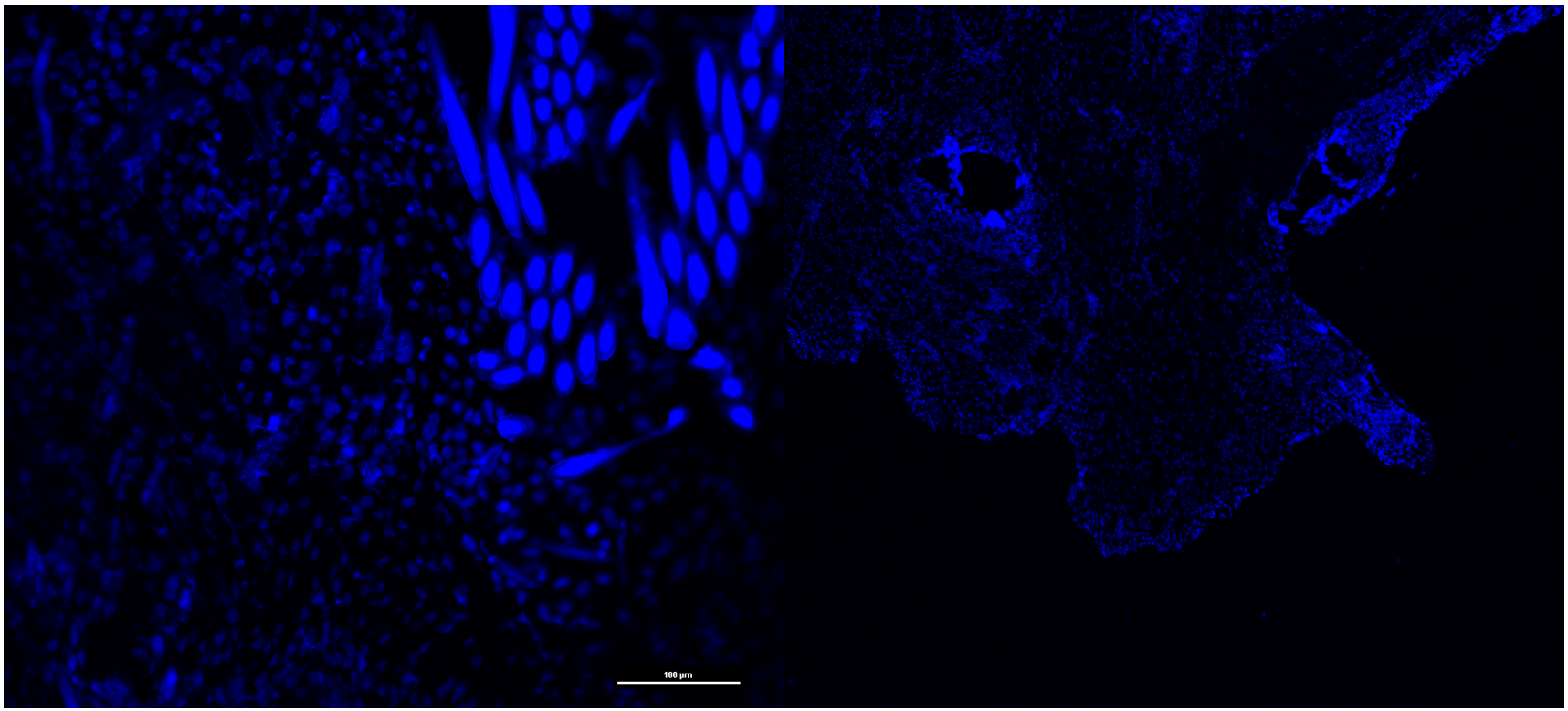

Figure 4.5.3E. CD31 (**left**, 20X) and MAC387 (**right**, 4X) of ZF/ZV tendon at 4 weeks, negative control staining. Neither control demonstrated any non-specific binding.

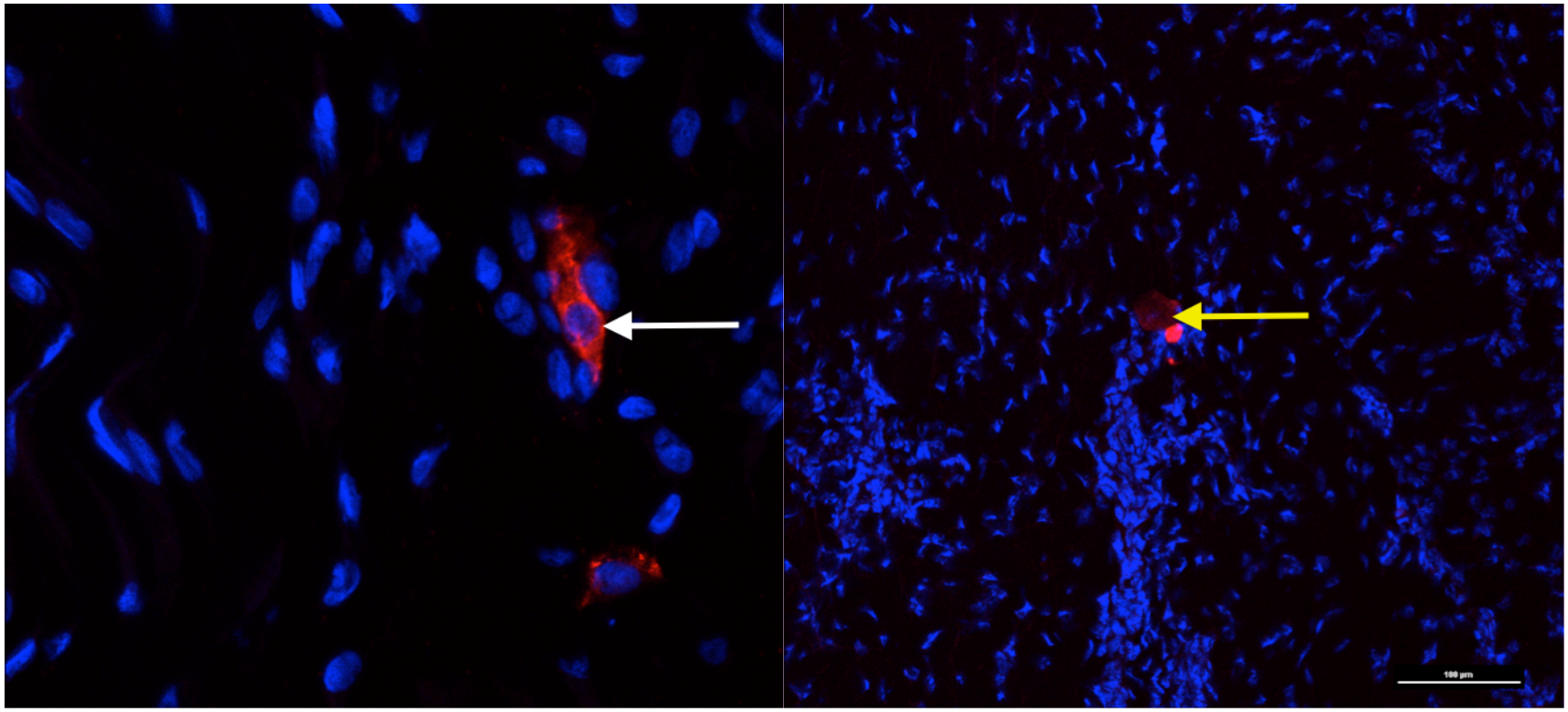

Figure 4.5.3F MAC387 40X (**left**) and 20X (**right**) fluorescence, HF/HV tendon. Staining was weak for MAC387. However, the cell on the left image appears spindle shaped (white arrow) and the image on the right has more diffuse cytoplasmic uptake (yellow arrow) for MAC387.

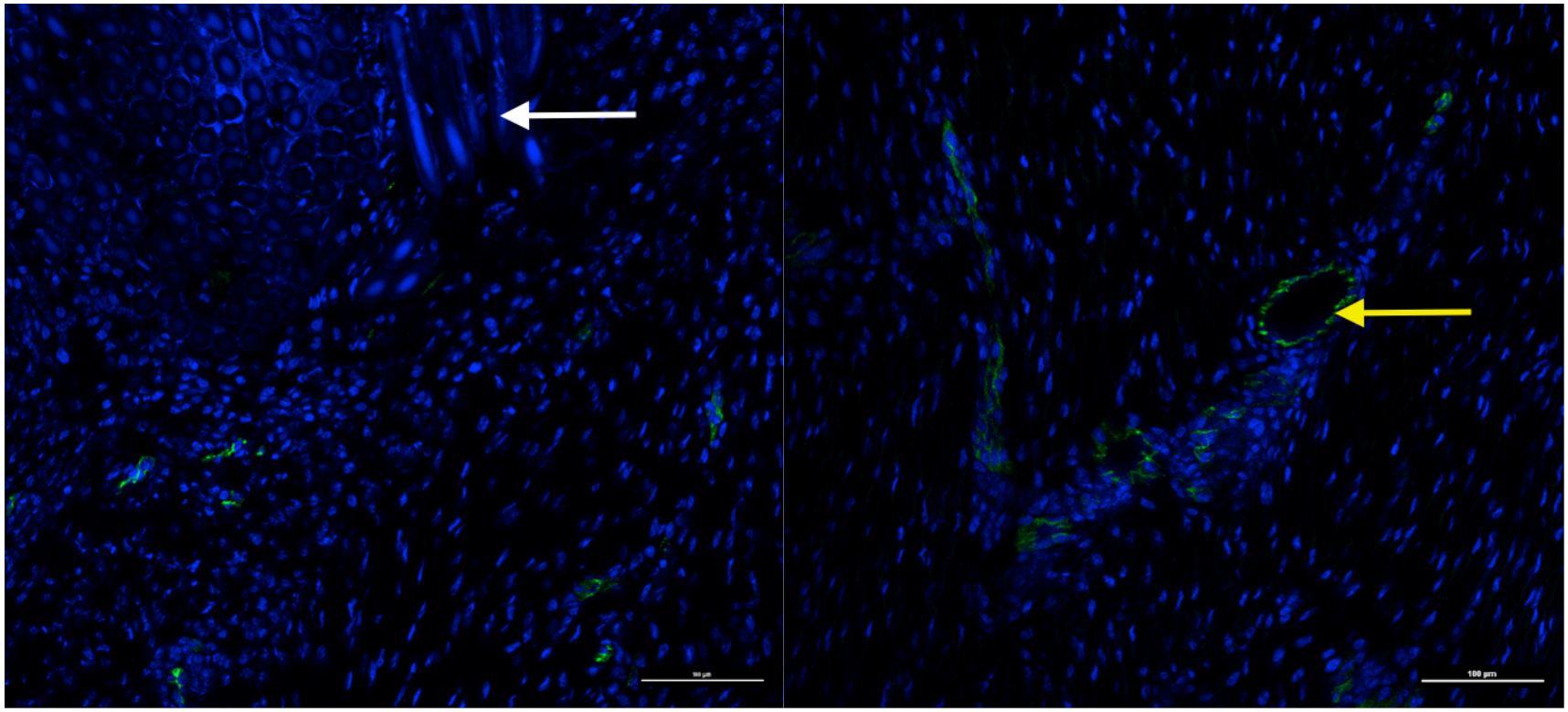

Figure 4.5.3G CD31 20X (**left and right**) of ZF/ZV tendon (**left**) and LV tendon (**right**) at 4 weeks. Note the relative paucity of blood vessels around the suture material on the left (white arrow). There were some mature lumina identifiable on the image on the right (yellow arrow).

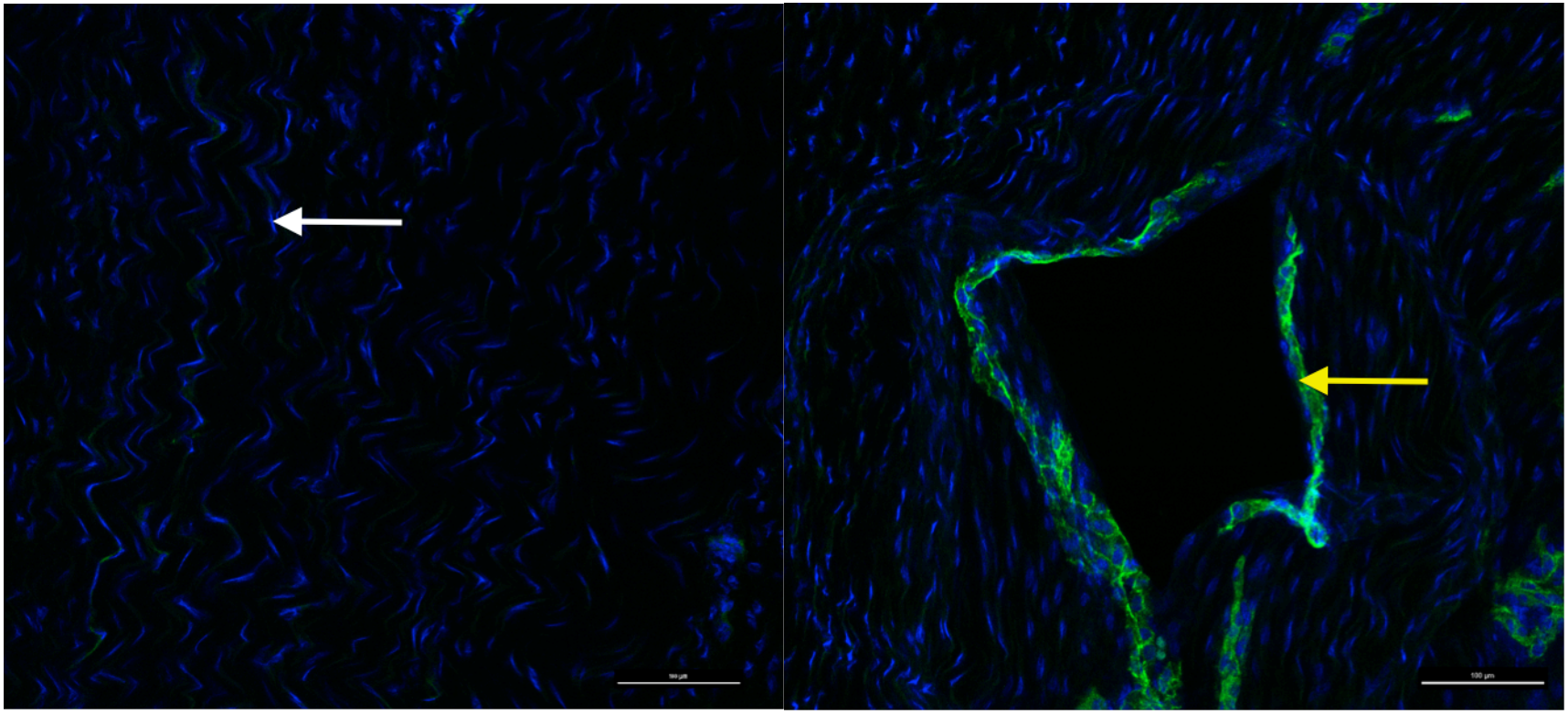

Figure 4.5.3H CD31 20X (**left and right**) of HF tendon (**left**) and HV tendon (**right**) at 4 weeks. Note the absence of any blood vessels in the crimp waveform pattern (white arrow) of the image on the left. However, a large blood vessel can be identified in the waveform pattern of the image on the right (yellow arrow).

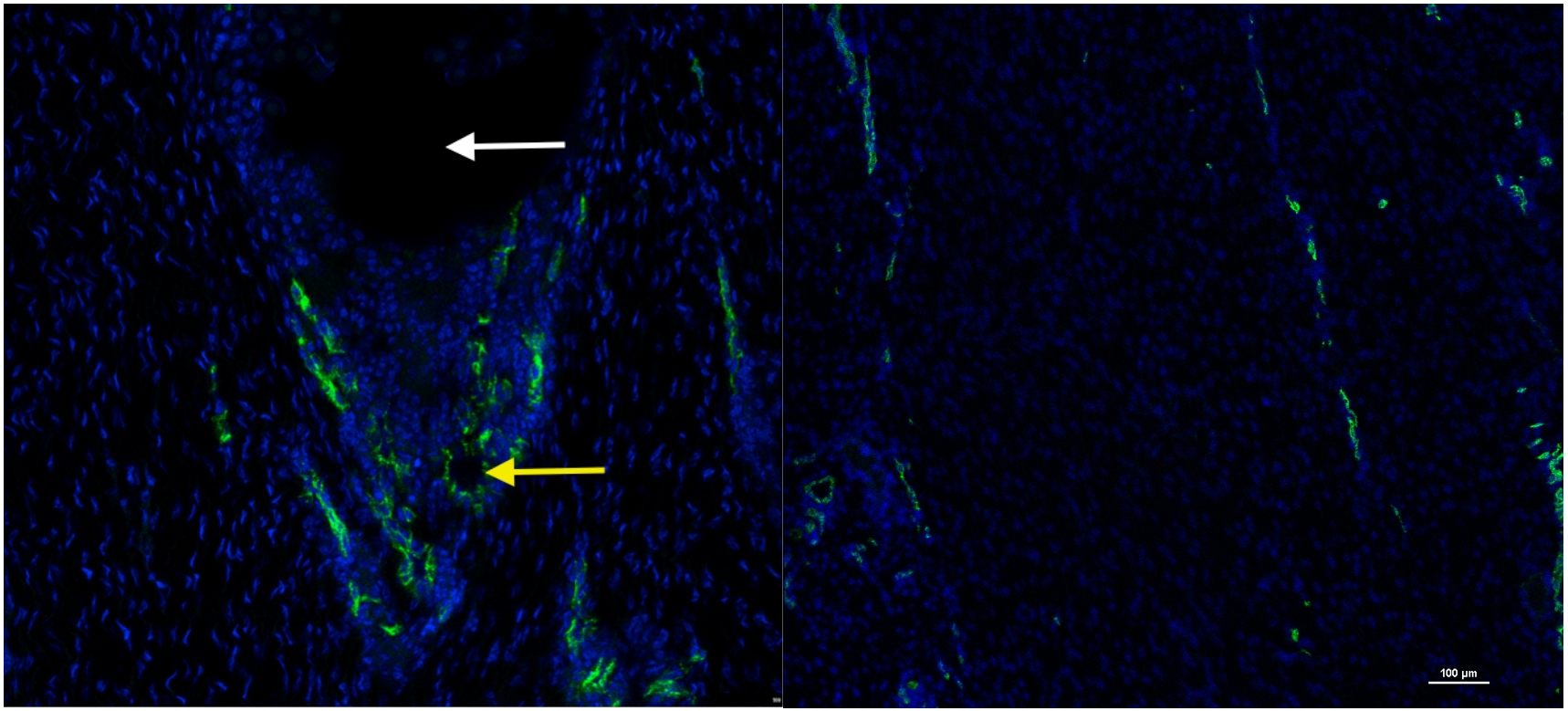

Figure 4.5.3l CD31 20X (**left and right**) of HV tendon (**left**) and LF tendon (**right**) at 4 weeks. The HV tendon possessed several blood vessels (white arrow) located around a section of suture material (yellow arrow). In the central portion of the tendon of the image on the right, there are only a few blood vessels located in the body of the tendon.

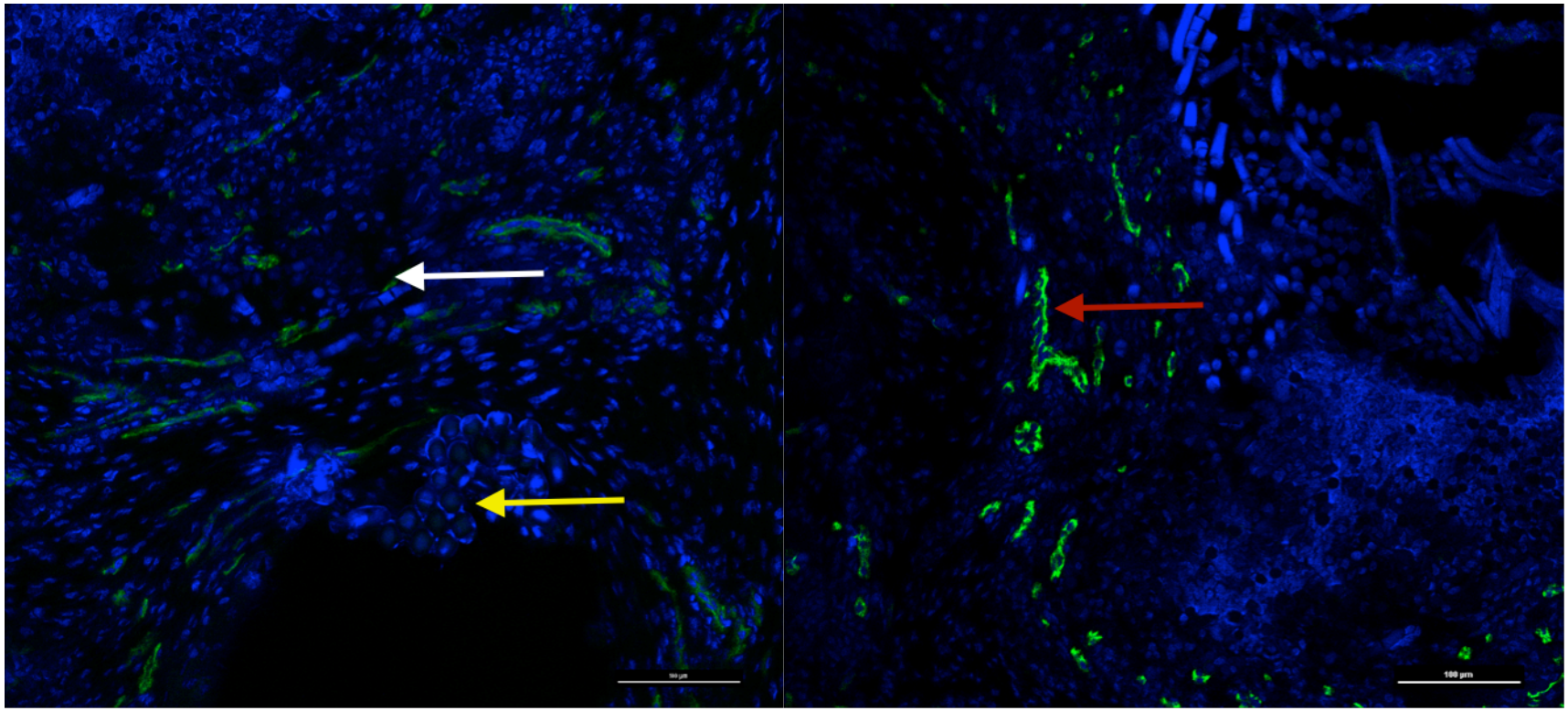

Figure 4.5.3J CD31 20X (**left and right**) of HF/HV tendon (**left**) and HF/LV tendon (**right**) at 4 weeks. There were many blood vessels (white arrow) around the suture (yellow arrow) in the HF/HV group. In addition, some larger vessels can be seen around the suture material section on the right (red arrow).

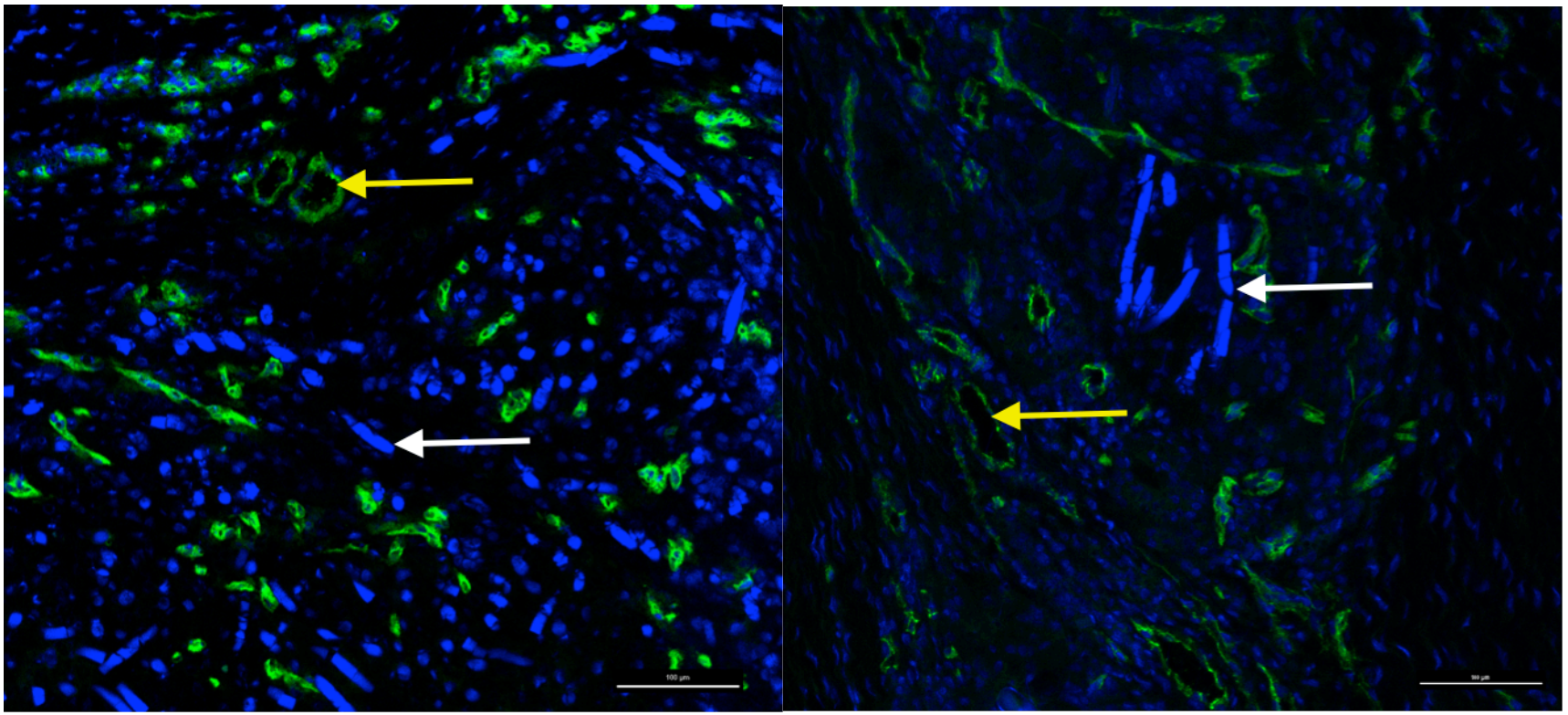

Figure 4.5.3K CD31 (20X) of HF/LV tendon at 4 weeks. There was significant neovascular formation (yellow arrows) centered on the suture material (white arrows) in both of these images.

4.5.4 Selection of Optimal Growth Factor Group

Based on the summary of the evalution of the 4-week data, we identified that the HF/HV group resulted in signficantly higher ultimate tensile strength and stiffness in comparison to any other protein group. The HF/HV group demonstrated a superior histology in comparison to several other protein groups and the ZF/ZV control suture. Based on this data, the HF/HV group was selected for evaluation in a 9-week study in comparison to a ZF/ZV control suture.

4.6. 9-Week (Long Term) Evaluation

4.6.1 Cross Sectional Area, 9-weeks

There was a significant difference between the cross sectional areas of the ZF/ZV LT (10.94 mm^2 ± 1.49) and HF/HV LT groups (7.23 mm^2 ± 0.63), (p=0.045) (**Figure 4.6.1A, 4.6.1B)**. There was a significant difference among the cross sectional area measurements of NT, ZF/ZV LT and HF/HV LT groups (p=0.0044). The NT group was not significant different to the HF/HV LT group. The power of the test given that the true difference in means between the NT and the HF/HV LT group is at least Δ 2 mm^2, is 49%. The ZF/ZV LT group was significantly different to the NT group (p =0.0042).

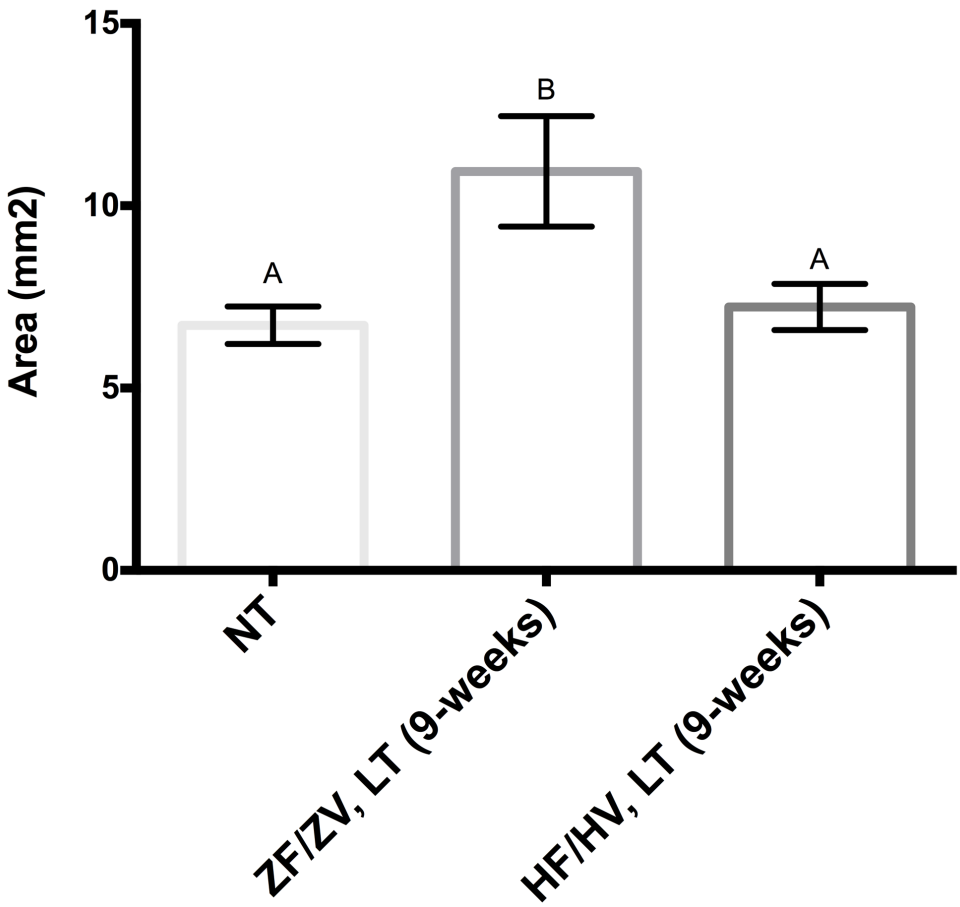

Figure 4.6.1A Bar chart of cross sectional areas. Different letters among groups denote signifcant differences. There were no signficant differences between the NT and HF/HV LT groups. The ZF/ZV group was signifcantly larger than either the NT or HF/HV groups at 9-weeks. Data shown as mean ± SEM.

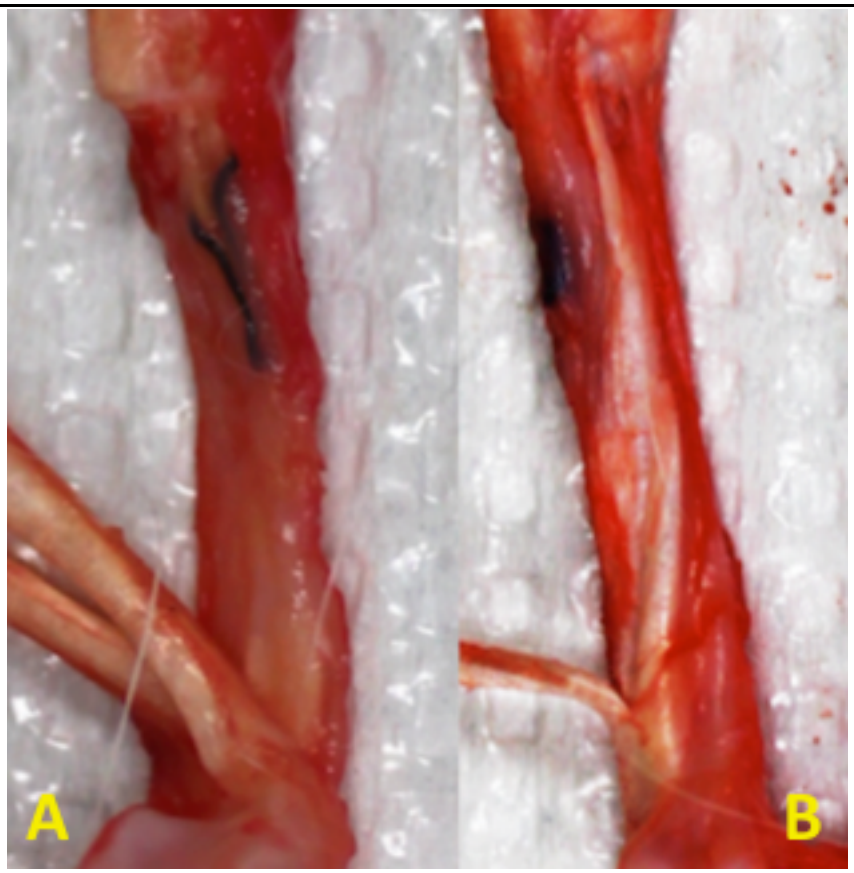

Figure 4.6.1B ZF/ZV LT tendon (A) and HF/HV LT tendon (B) Note these tendons do not have the globular appearance of the 4-week groups centered on the black nylon suture and appear as a more uniform structure

4.6.2 Ultimate Tensile Strength, 9-weeks

There were no signficant differences in UTS between the ZF/ZV LT and HF/HV LT groups at 9-weeks (**Table 4.6.2A, Figure 4.6.2A**). For the 9-week data of ultimate tensile strength, for a minimum difference in group means of Δ 13.6 N, power is 0.15, as determined. Thus, there was a 85% probability of having committed a type II error.

Group	UTS ± SEM (N)	Stiffness ± SEM (N/mm)
ZF/ZV LT	166.75 22.41	33.4 3.71
HF/HV LT	205.75 26.4	36.23 6.13

Table 4.6.2A Ultimate tensile strength and stiffness data for the 9-week groups. Data shown as mean ± SEM.

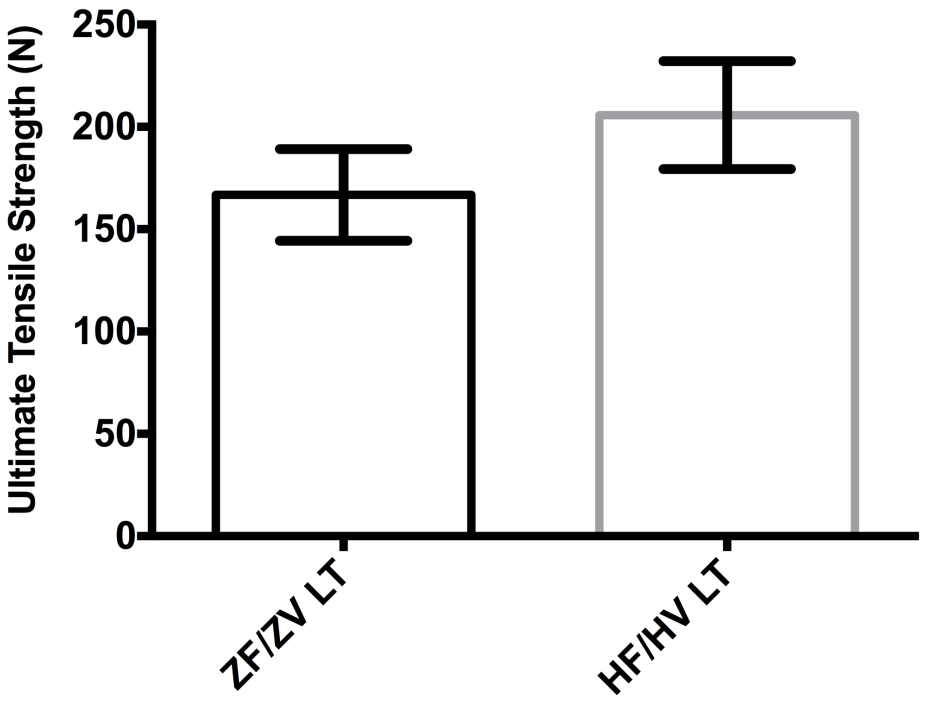

Figure 4.6.2A Bar chart of ultimate tensile strength of two groups, ZF/ZV and HF/HV suture at the 9-week time points. No significant difference were determined at 9-weeks. Data shown as mean ± SEM.

4.6.3 Stiffness, 9-weeks

There were no signficant differences in stiffness between the ZF/ZV LT and HF/HV LT groups at 9-weeks (**Table 4.6.2A, Figure 4.6.3A**). At the 9-week time point, for a minimum difference between the HF/HV LT and NT group means of Δ 13.6, power is 0.65, as acheived Thus, there was a 35% probability of having comitted a type II error.

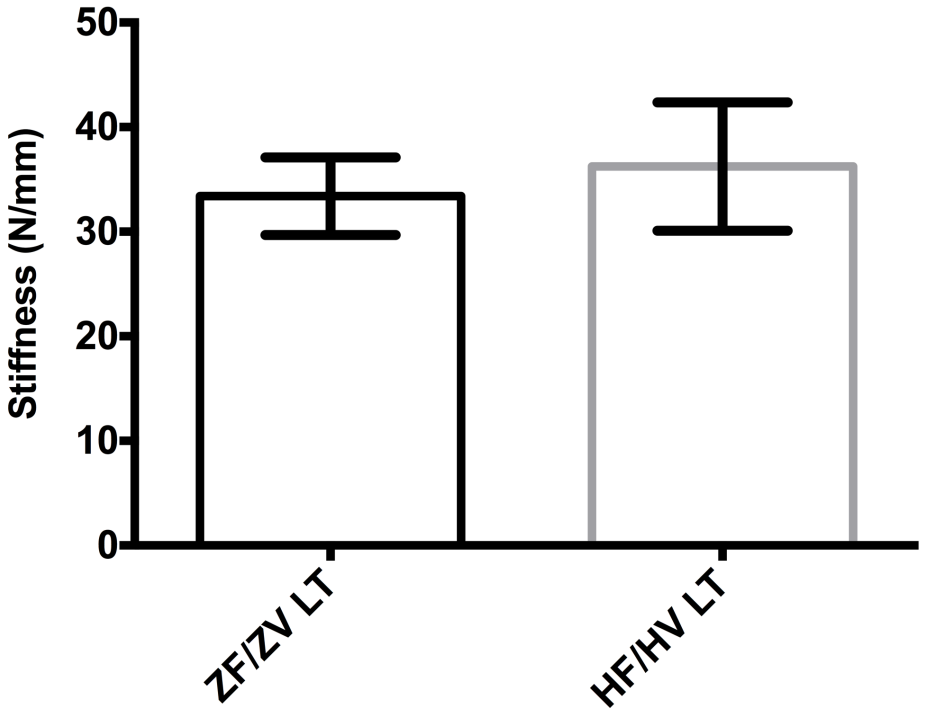

Figure 4.6.3A Bar chart of stiffness of two groups, ZF/ZV and HF/HV suture at the 9-week time points. No significant difference were determined at 9-weeks. Data shown as mean ± SEM.

4.6.4 Stress, Strain and Young's Modulus, 9-weeks

There were no significant differences in strain between the ZF/ZV LT and HF/HV LT groups (**Table 4.6.4A ,Figure 4.6.4A**). There were no significant differences in

Young's modulus between the ZF/ZV LT and HF/HV LT groups (**Figure 4.6.4B**). The stress at 9-weeks was significantly greater for the HF/HV LT group than the ZF/ZV group (p=0.02, **Figure 4.6.4C**).

Group	Strain ± SEM (%)	Stress ± SEM (MPa)	Young's Modulus ± SEM (MPa)
ZF/ZV LT	25.21 2.51	20.56 1.45	145 10.96
HF/HV LT	25.32 2.12	25.21 0.9	158 12.39

Table 4.6.4A Strain, stress and Young's modulus data for the 9-week groups. Data shown as mean ± SEM.

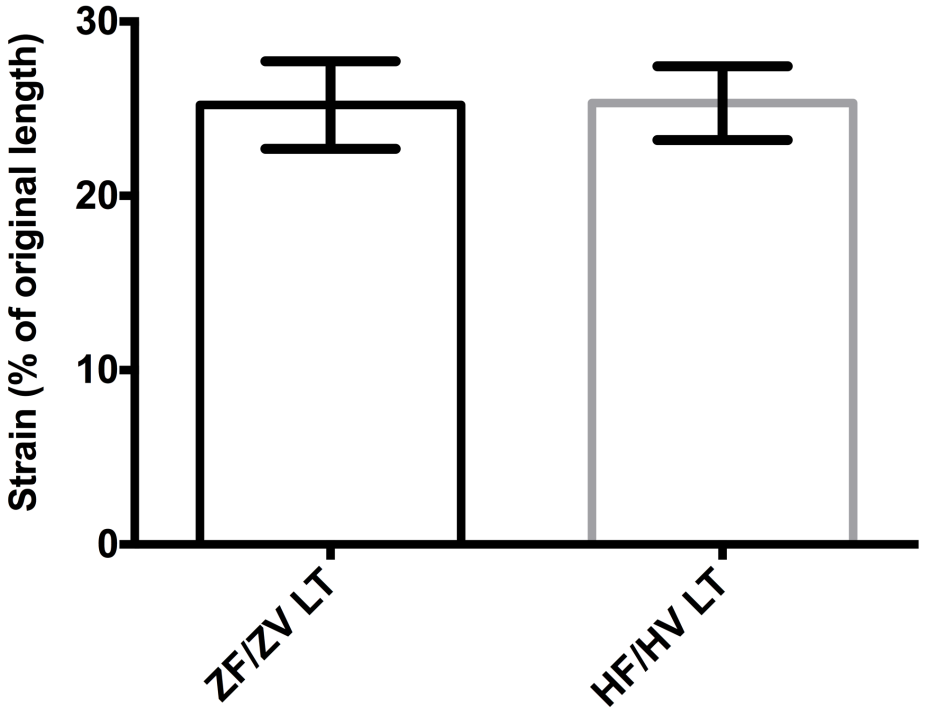

Figure 4.6.4A Bar chart of strain of two groups, ZF/ZV and HF/HV suture at the 9-week time points. No significant difference were determined at 9-weeks. Data shown as mean ± SEM.

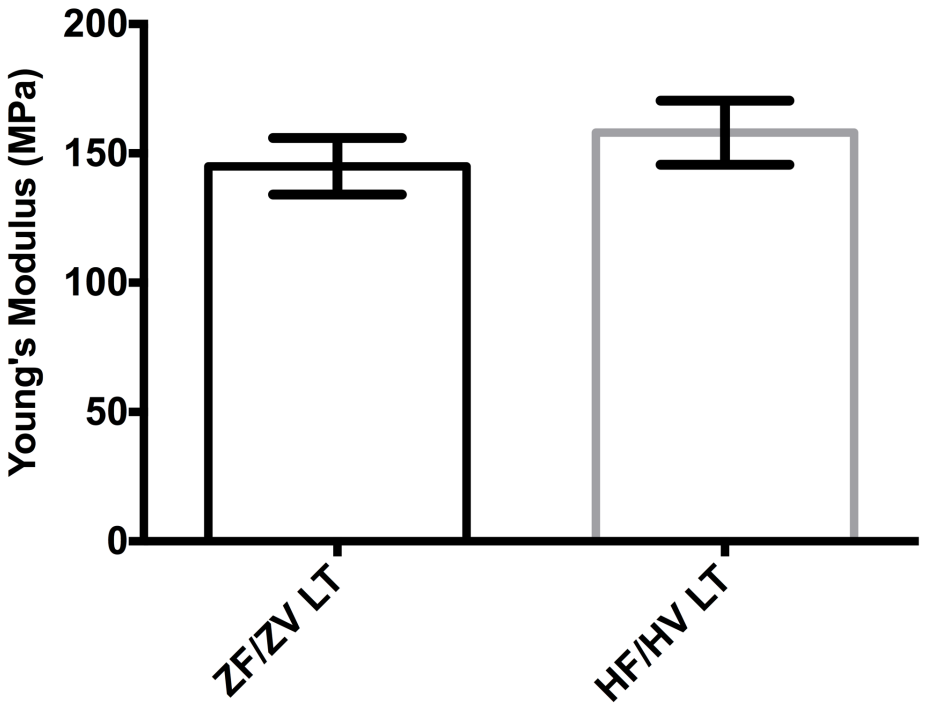

Figure 4.6.4B Bar chart of Young's modulus of two groups, ZF/ZV and HF/HV suture at the 9-week time points. No significant differences were determined at 9-weeks. Data shown as mean ± SEM.

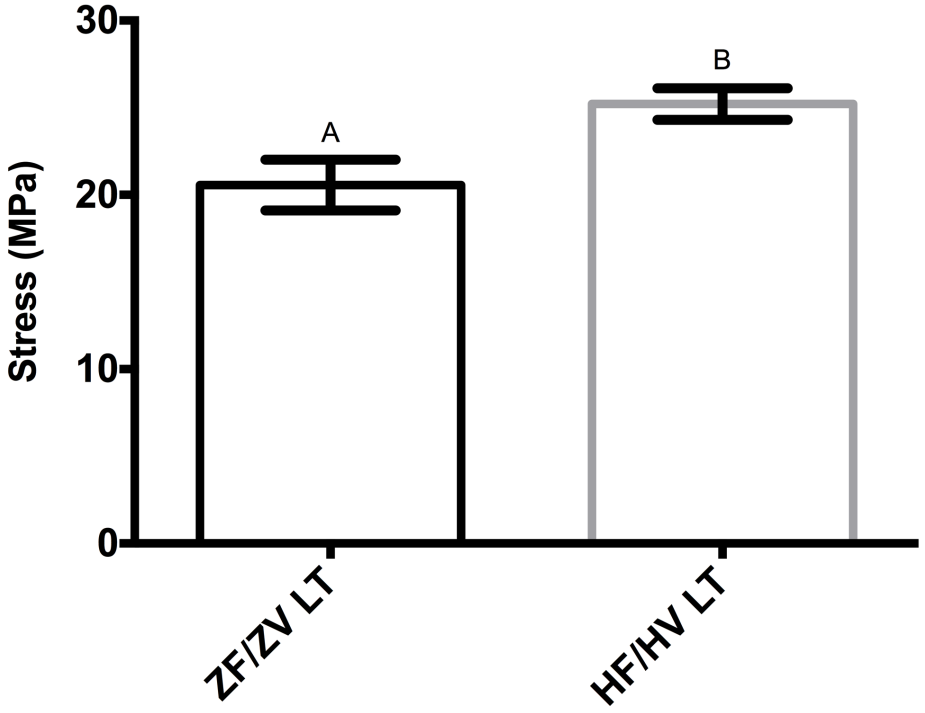

Figure 4.6.4C Bar chart of stress of two groups, ZF/ZV and HF/HV suture at the 9-week time points. The HF/HV group had significantly greater stress at 9-weeks than the ZF/ZV group (p=0.02). Different letters denote significant differences between groups. Data shown as mean ± SEM.

4.7.1 Comparison of 4 and 9-week Ultimate Tensile Strength

There were no significant differences between the ultimate tensile strength of the lateral gastrocnemius tendons for the control long term group (ZF/ZV LT) and the HF/HV LT group at the 9-week time point, although there was a significant difference between the two groups at the 4-week time point (**Figure 4.7.1A**). At the 9-week time point, there were no signficant differences among the non operated normal tendons (NT) and the ZF/ZV LT and HF/HV LT groups, although at the 4-week time point, the HF/HV group was superior to the NT group.

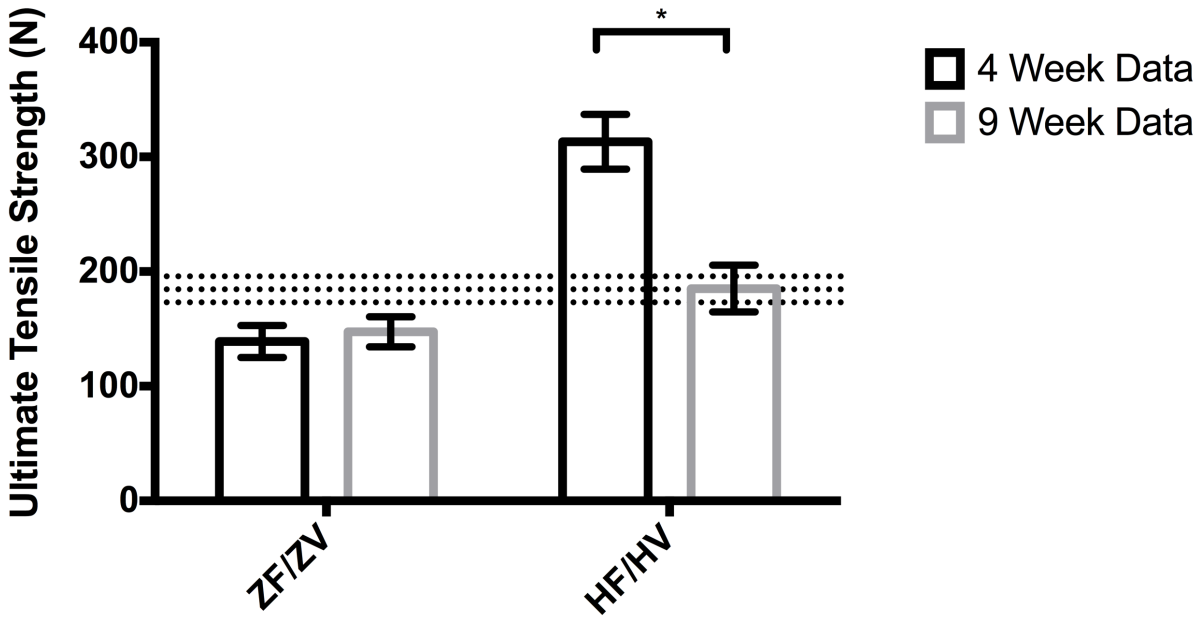

Figure. 4.7.1A Bar chart of ultimate tensile strength of two groups, ZF/ZV and HF/HV groups at the 4 and 9-week time points. Although a significant difference was identified between the ZF/ZV and HF/HV groups at 4-weeks,, there was no significant difference at between then at 9-weeks. Data shown as mean ± SEM. Horizontal dotted lines represent the mean ± SEM for the NT group.

4.7.2 Comparison of 4 and 9-week Stiffness

There was no significant difference between the stiffness of the lateral gastrocnemius tendons for ZF/ZV LT and HF/HV LT groups at 9-weeks. At the 9-week time point, there were no signficant differences among the non operated controls (NT) and ZF/ZV LT or HF/HV LT. There was a signficant difference between the stiffness of the 4 and 9 week HF/HV groups ($p<0.05$, **Figure 4.7.2A**). At 9-weeks, there was no signficant difference between the HF/HV LT and NT groups. At 9-weeks, there was no signficant difference between the ZF/ZV LT and NT groups.

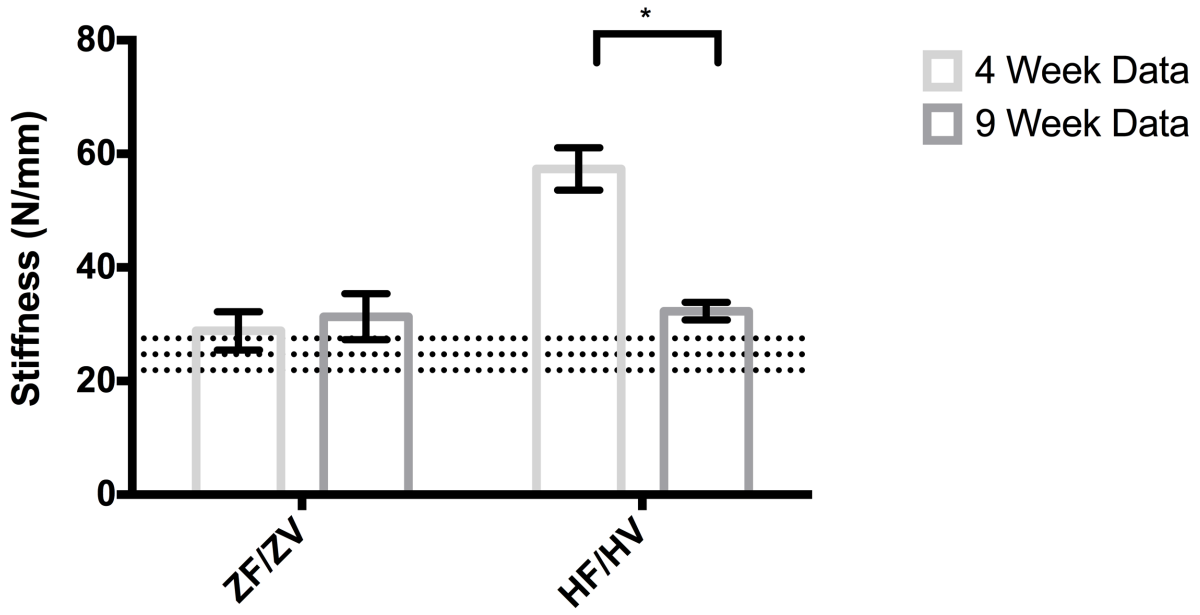

Figure 4.7.2A Bar chart of stiffness of two groups, ZF/ZV and HF/HV suture at the 4 and 9-week time points. Although a significant difference was identified between the ZF/ZV and HF/HV groups at 4-weeks, there was no significant difference between them at 9-weeks. Data shown as mean ± SEM. Horizontal dotted lines represent the mean ± SEM for the NT group.

4.7.3 Comparison of 4 and 9-week Histology

The long-term control suture ZF/ZV LT was significantly superior in histological score than the 4-week control suture (ZF/ZV). There was no significant difference between the ZF/ZV LT and the short-term (HF/HV) group histology score. The 4-week HF/HV group was significantly superior to the ZF/ZV LT group histology score. There was no significant difference in histology score between 4-week HF/HV and 9-week HF/HV LT group histology scores. The HF/HV LT group was significantly superior to the ZF/ZV LT group histology score ($p<0.0001$, **Figure 4.7.3A**).

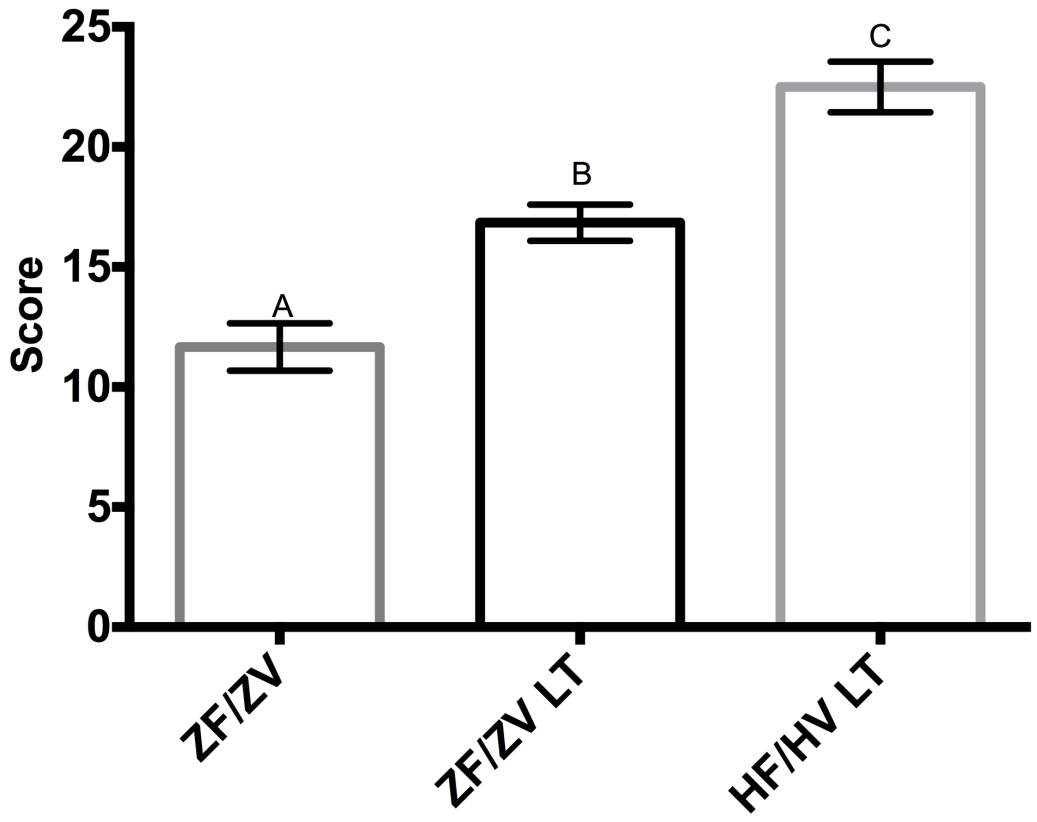

Figure 4.7.3A. Bar chart of histology score for the 4-week control group (ZF/ZV), the 9-week control group (ZF/ZV LT) and the 9-week optimal group (HF/HV LT). Histology scores were significantly different among the groups. Data shown as mean ± SEM.

In the ZF/ZV 9-week group there was a random nature to the deposition of collagen within the surgical site. In the ZF/ZV 9-week group there were several areas devoid of tendon material, which appeared as gaps in the tendon. In the HF/HV 9-week group there was considerable parallel alignment of collagen fibers with infilling of gaps between bundles, in direct contrast to the ZF/ZV 9-week group **(Figure 4.7.3B).** Tenocyte morphology was more spindle cell like in the HF/HV 9-week group.

Immunofluorescent evaluation of the ZF/ZV 9-week group identified a paucity of vascularity or blood vessels around the suture material. The remainder of the tendon, including the core and peripheral locations, were lacking in CD31 binding. In the HF/HV 9 week group, blood vessel locations were confined to two regions, the periphery of the tendon and around the suture material (**Figure 4.7.3C**). In the HF/HV 9 week group There was no binding of CD31 identified anywhere within the core bundle of the well aligned collagen fibers.

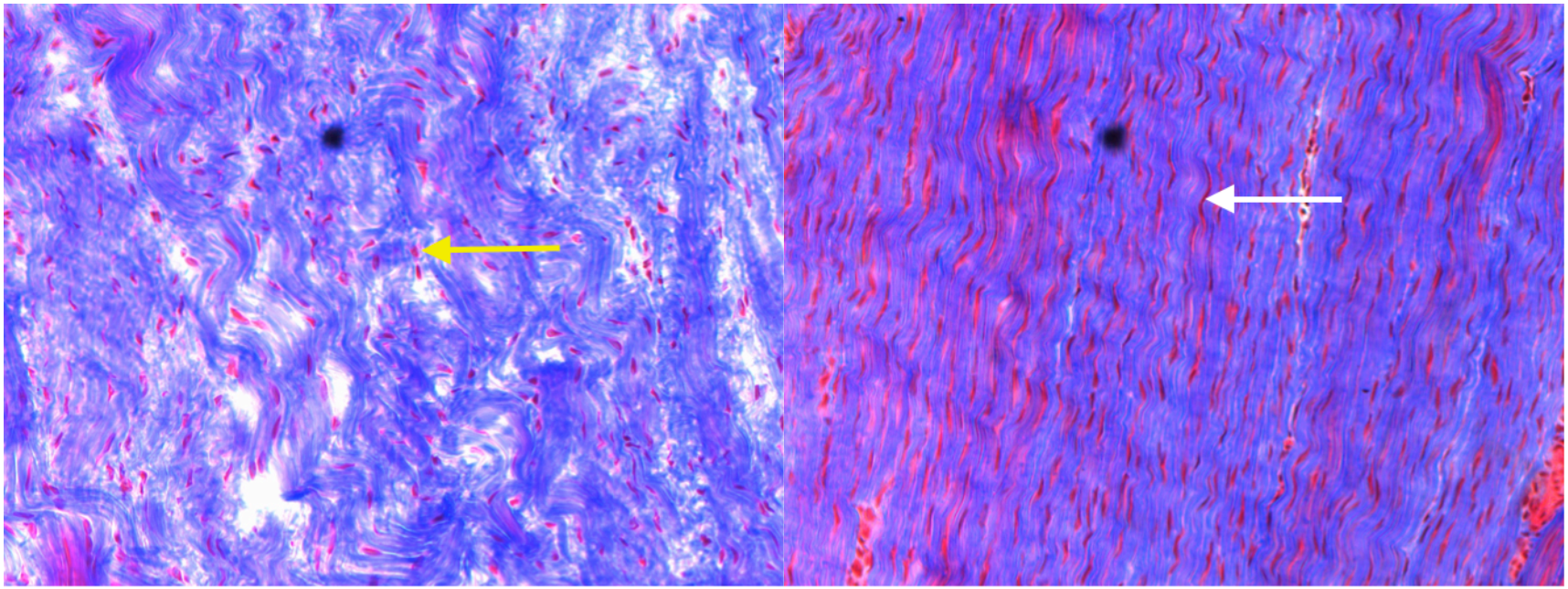

Figure 4.7.3B. Alcian blue (20X) (**left**), (20X) (**right**) of ZF/ZV tendon (**left**) and HF/HV tendon (**right**) at 9-weeks. Note the relatively poor and immature fiber pattern on the ZF/ZV tendon, the presence of round, immature tenocytes (yellow arrow) and the more haphazard orientation of the collagen bundles. The HF/HV 9-week tendon demonstrated uniform waveform, mature spindle shaped tenocytes (white arrow), less gap formation between bundles and a more mature tendon fiber appearance.

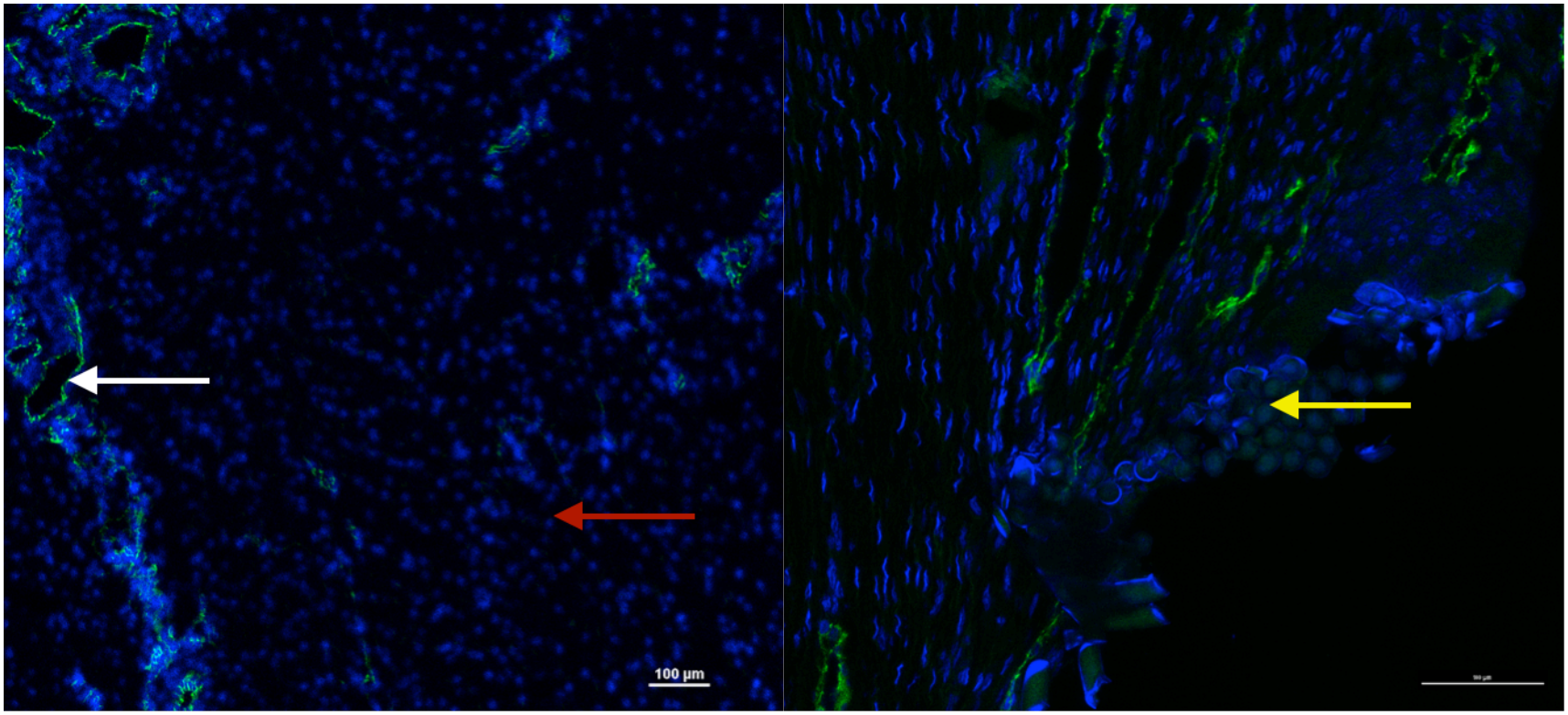

Figure 4.7.3C. CD31 (20X) of HF/HV tendon at 9-weeks . It should be noted that blood vessels in this group existed either at the periphery of the tendon (white arrow) (**left**) or around the suture material (yellow arrow)(**right**). There were no blood vessels in the body of the tendon (red arrow).

4.8 Imaging Analysis

4.8.1 Shear Wave Analysis

The mean tendon shear wave imaging speed (SWI speed) at baseline was 10.5 ± 2.1 m/s over the entire length of the tendon, with significantly higher speeds obtained at the distal (10.9 ±2.1 m/s) and mid (11.0 ±2.1 m/s) locations, relative to the proximal (9.5 ±2.1 m/s) location ($p<0.05$).

SWI speed significantly decreased in the repaired lateral tendons two weeks after surgical repair, with the greatest decrease seen in the distal ROI (21% decrease, $p< 0.001$). SWI speed decreased to a lesser extent at mid and proximal locations (18% and 11% decrease respectively, $p < 0.001$). For all groups, there was a trend for a slight recovery of SWI speed between two and four weeks at the distal location, though this change was not significant ($p = 0.09$, **Figure 4.8.1A**)

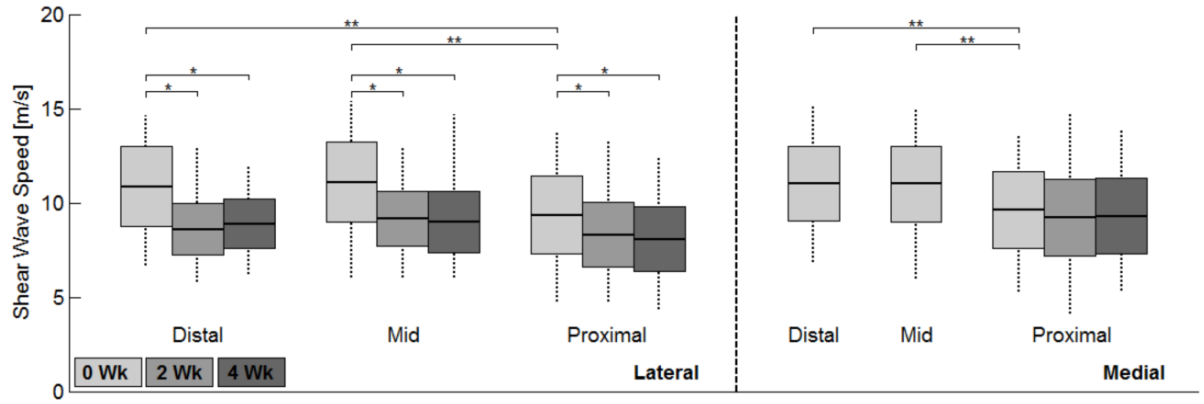

Figure 4.8.1A Box and whisker plots demonstrating spatial and temporal variation in SWI speeds. Significant differences ($p < 0.0167$) shown for time point (*) and scanning location (**).

4.8.2 Relationship between SWI Speed, UTS, Stiffness Stress and Young's Modulus

When both non-operated lateral normal tendons (NT) and surgically transected tendons were considered together in the analysis, both the ultimate tensile strength ($r = 0.52$, $p < 0.001$), stiffness ($r=0.41$, $p<0.001$), stress ($r=0.5$, $p=0.001$) and Young's modulus ($r=0.52$, $p<0.001$) were significantly and moderately correlated with post-surgical SWI speeds (**Figures 4.8.2A,B,C,D**). When surgically repaired tendons were considered separately from the NT group, ultimate strength remained significantly and positively correlated with SWI speeds (**Table 4.8.2A**). However, Young's Modulus was not significantly correlated with shear wave speeds in these surgical cases.

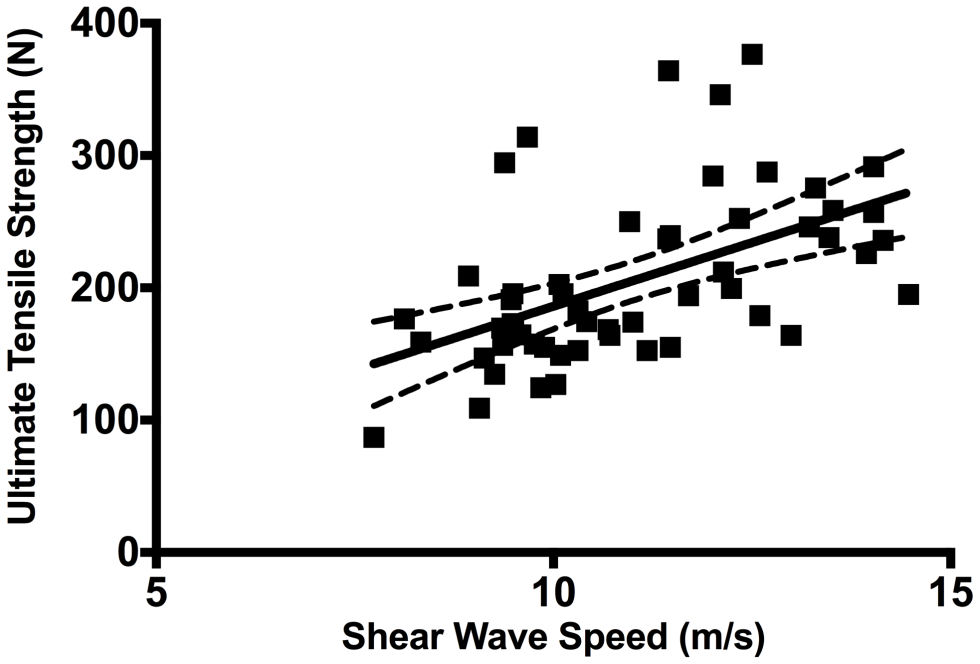

Figure 4.8.2A XY scatter plot of ultimate tensile strength and shear wave speed for the short term (4-week) groups. There was moderate correlation among the data ($r= 0.52$, $p<0.0011$). Bands denote 95% confidence intervals.

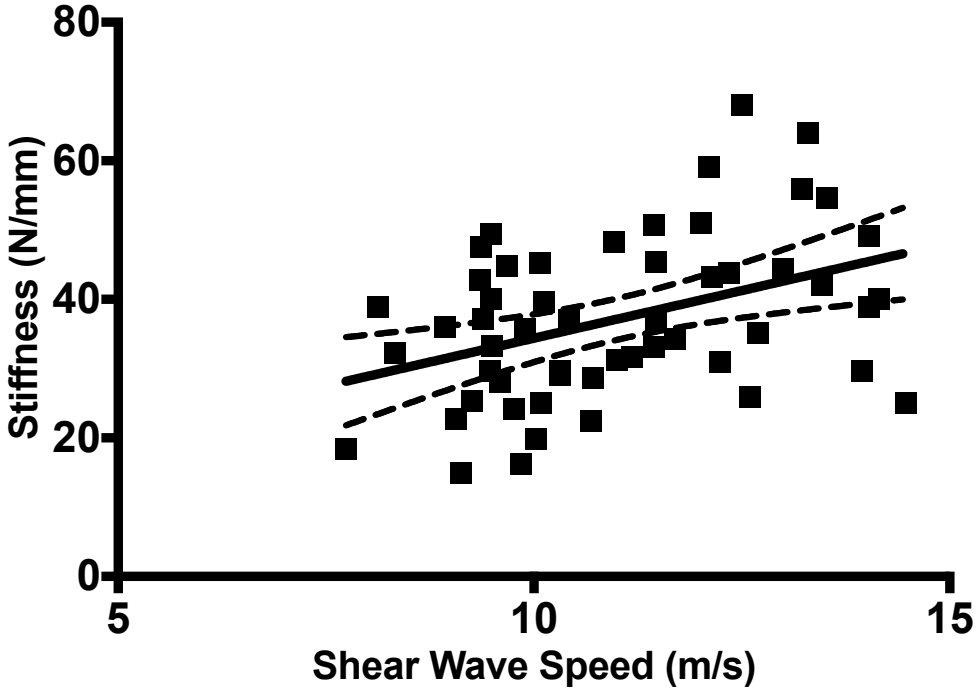

Figure 4.8.1B. XY scatter plot of stiffness and shear wave speed for the short term (4-week) groups. There was moderate correlation among the data (r= 0.41, p=0.002). Bands denote 95% confidence intervals.

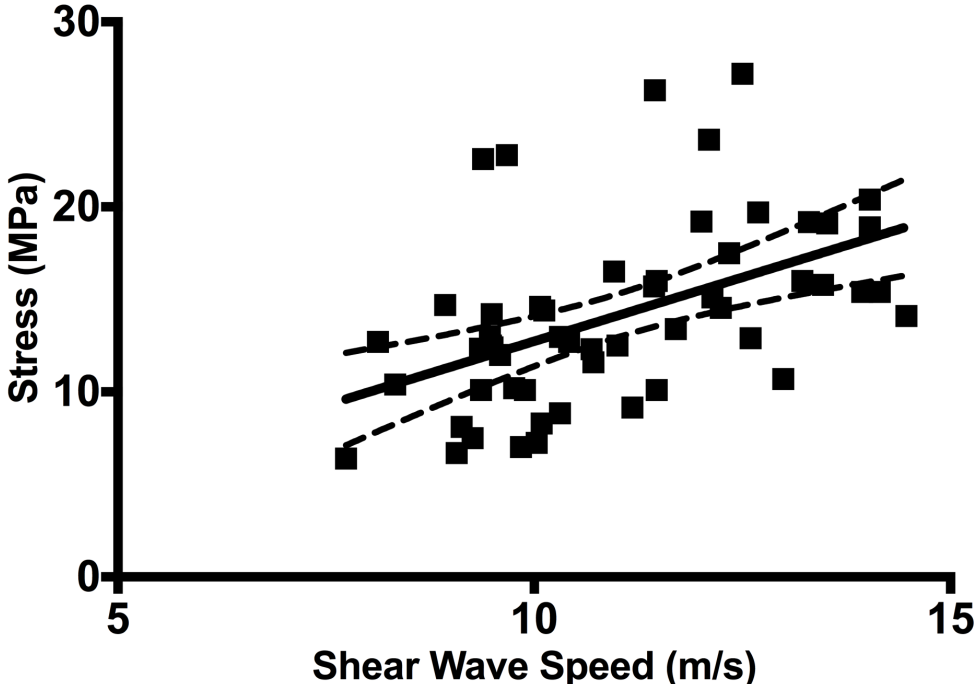

Figure 4.8.2C XY scatter plot of stress and shear wave speed for the short term (4-week) groups. There was moderate correlation among the data (r=0.5, p=0.001). Bands denote 95% confidence intervals.

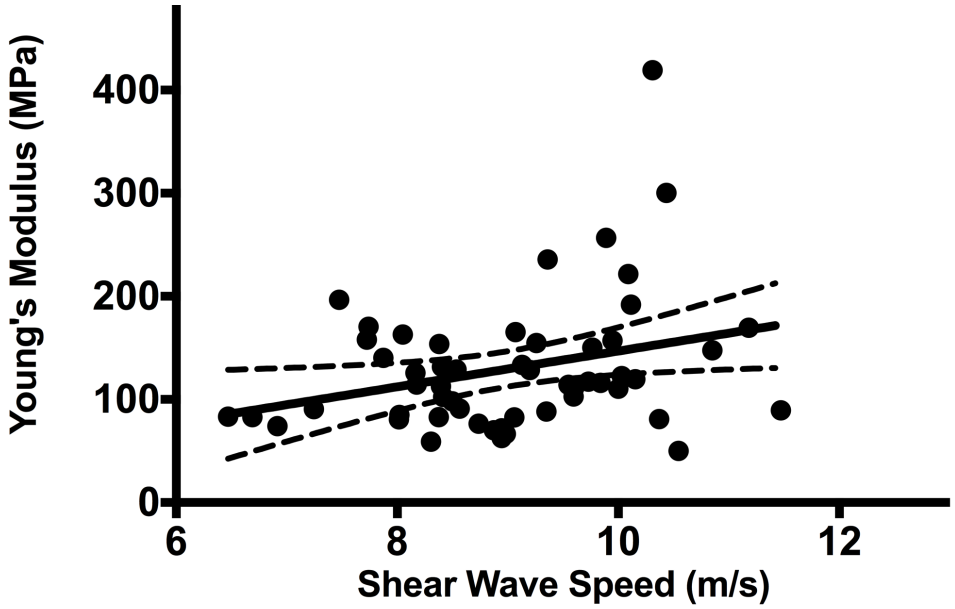

Figure 4.8.1D. XY scatter plot of Young's modulus and shear wave speed for the short term (4-week) groups. There was moderate correlation among the data (r=0.52, p<0.001.).). Bands denote 95% confidence intervals.

		Intact	Surgically Repaired	Combined
Young's Elastic Modulus	**Slope [MPa×m^{-1}s]**	51.6	43.3	54.8
	r	0.19	0.22	0.52
	p	0.09	0.08	0.00
Ultimate Stress	**Slope [MPa×m^{-1}s]**	6.17	4.64	7.09
	r	0.24	0.30	0.58
	p	0.04	0.03	0.00

Table 4.8.2A. Best fit slope, correlation and significance for relationship between SWI speeds, Young's modulus and ultimate stress for the cases of: intact tendons only, surgically repaired tendons only, and all tendons combined together.

4.8.3 SWI Sensitivity and Specificity

Of the metrics considered, the SWI determined ultimate stress data, based on extrapolation from the correlation between ultimate stress and SWI speeds, exhibited the greatest combination of sensitivity and specificity in distinguishing between damaged and intact tendons. The SWI speed determined Young's modulus data, based

on extrapolation from the correlation between Young's modulus and SWI speeds exhibited similar sensitivity to, but lower specificity than SWI determined ultimate stress. SWI speed information by itself was both less sensitive and less specific than any other SWI determined biomechanical parameter in identifying differences among the surgically repaired tendons (**Table 4.8.3A)**

	Young's Modulus	Ultimate Stress	Shear Wave Speed
Sensitivity	0.93	0.93	0.81
Specificity	0.79	0.88	0.64

Table 4.8.3A Sensitivity and specificity for SWI derived Young's Modulus, SWI derived ultimate stress and SWI speed alone as diagnostic tests for establishing tendon state (intact tendons vs. severed/repaired tendons).

4.8.4 SWI Speed Data

Evaluation of SWI speeds over all time periods (0, 2 and 4 weeks) **(Figures 4.8.4A, B, C),** demonstrated that changes in SWI speeds do occur. While there was a significant difference in one of the groups (HF/HV) at time 0, the significance of this is uncertain. As time progressed, more groups developed significant differences from the control suture (ZF/ZV), but not to such a degree that separation among each other was possible. While it is possible to differentiate protein-coated sutures from the control, there is some difficulty in distinguishing differences among the protein coated groups. An analysis was performed to evaluate the differences in SWI speeds over time for both the medial and lateral branches. At all time points, no significant differences were identified between the medial and lateral branches (p=0.88, **Figure 4.8.4D**).

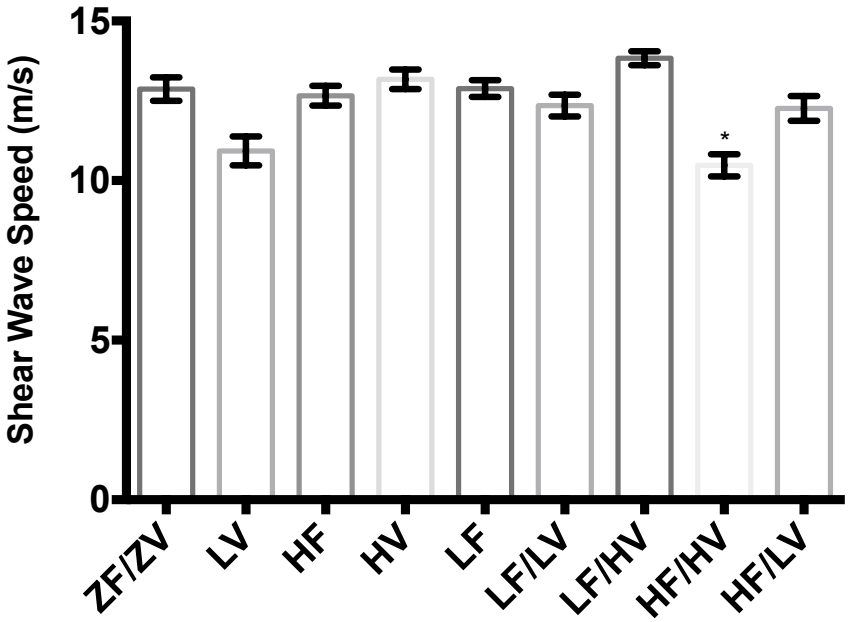

Figure 4.8.4A Bar chart of SWI speed evaluations, pre-surgery (0 weeks). Although no procedures had been performed, there was a significant difference (*) ($p<0.05$) for the HF/HV group to have slightly lower SWI speeds than the control ZF/ZV group. Data shown as mean ± SEM.

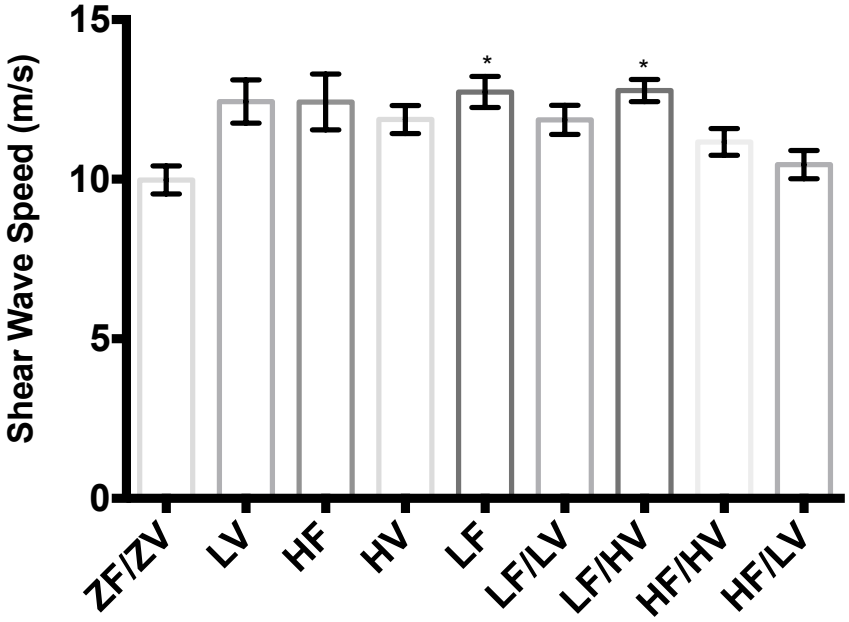

Figure 4.8.4B. Bar chart of shear wave speed evaluations, 2 weeks post surgery. Although there were no significant differences between several of the groups, the LF and LF/HV groups demonstrated significantly increased SWI speeds compared to control ZF/ZV. * denotes significant differences from the control ZF/ZV group. Data shown as mean ± SEM.

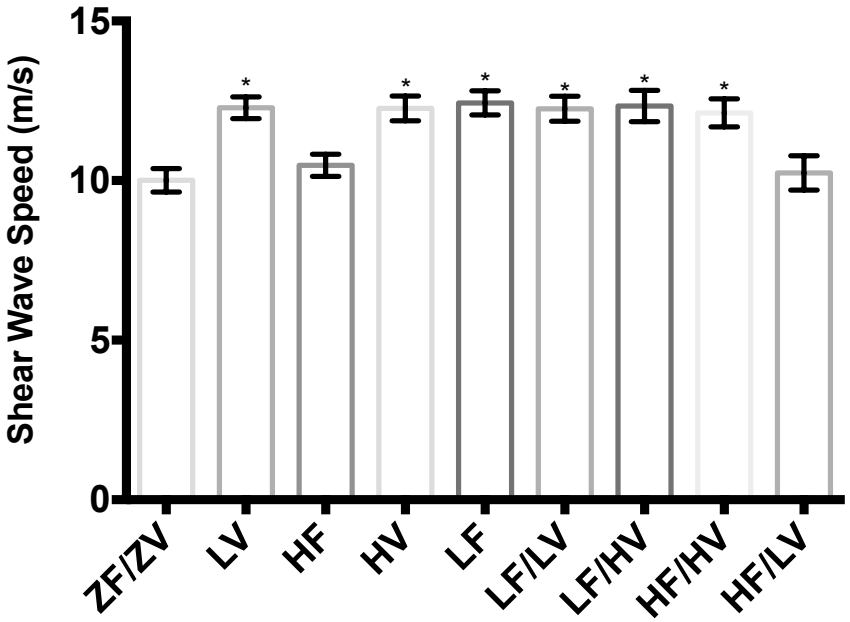

Figure 4.8.4C Bar chart of shear wave speed evaluations, 4 weeks post surgery. All groups with the exception of the HF and HF/LV groups are signficantrly different to the control ZF/ZV group. * denotes significant differences from the control ZF/ZV group. Data shown as mean ± SEM.

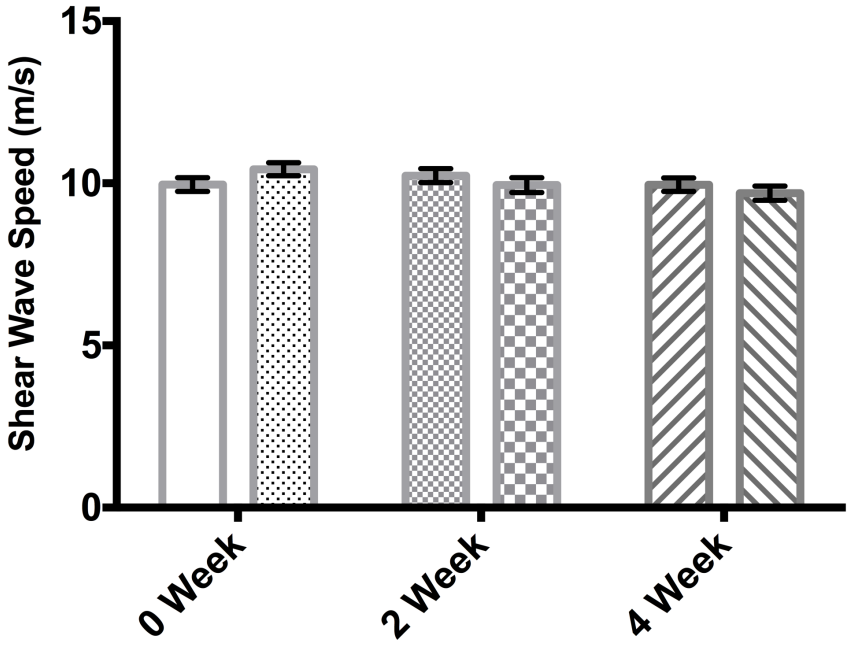

Table 4.8.4D Bar chart of shear wave speed evaluations at 0, 2 and 4 weeks post surgery. Left bars indicate medial tendons within each time period, and right bars indicate lateral tendon. There were no significant differences between the branches at any time point (p=0.88). Data shown as mean ± SEM.

4.8.5 AE Evaluation

Biomechanical properties were significantly and negatively correlated with the AE maximum pathology index (PI). AE maximum PI was negatively associated with ultimate tensile strength and stiffness values (r=0.43, p=0.0031, **Figure 4.8.5A**, r=0.44, p=0.0022, **Figure 4.8.5B**, respectively). There were no significant correlations identified for either stress or Young's modulus (r=0.17, p=0.25, **Figure 4.8.5C**, r=0.01, p=0.9, **Figure 4.8.5D**, respectively).

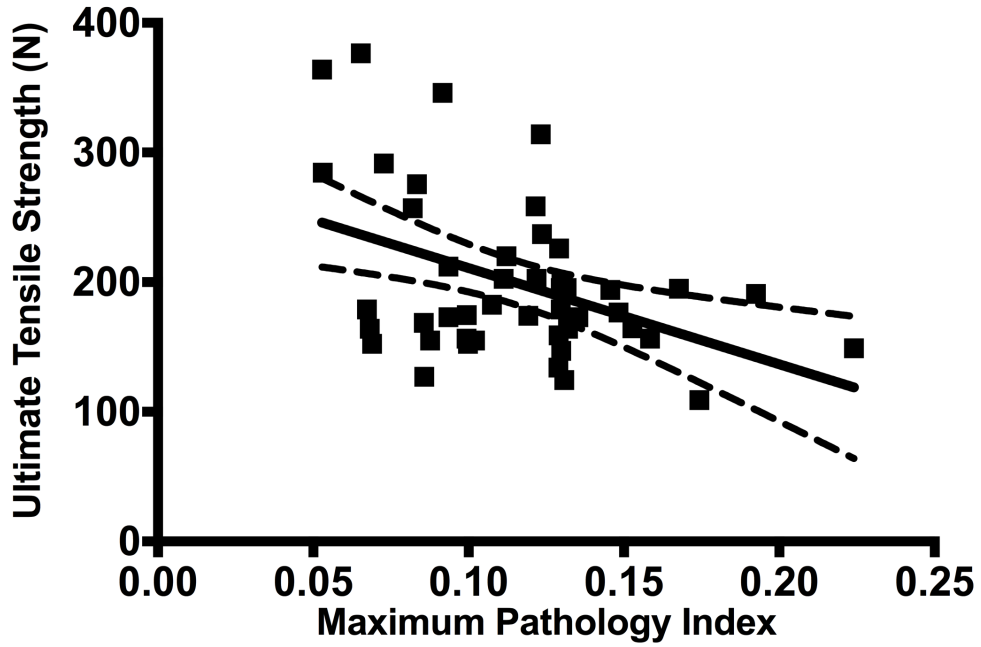

Figure 4.8.5A XY scatter plot of ultimate tensile strength and maximum pathology index for the short term (4-week) groups. There was moderate correlation among the data (r=0.43, p=0.0031). Bands denote 95% confidence intervals.

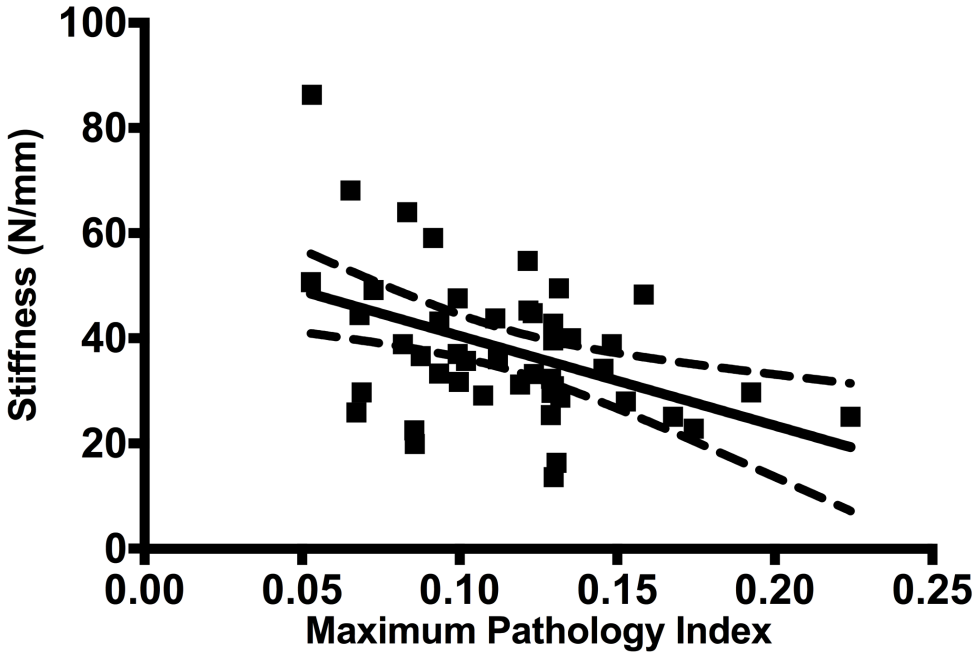

Figure 4.8.5B XY scatter plot of stiffness and maximum pathology index for the short term (4-week) groups. There was moderate correlation among the data (r=0.44, p=0.0022). Bands denote 95% confidence intervals.

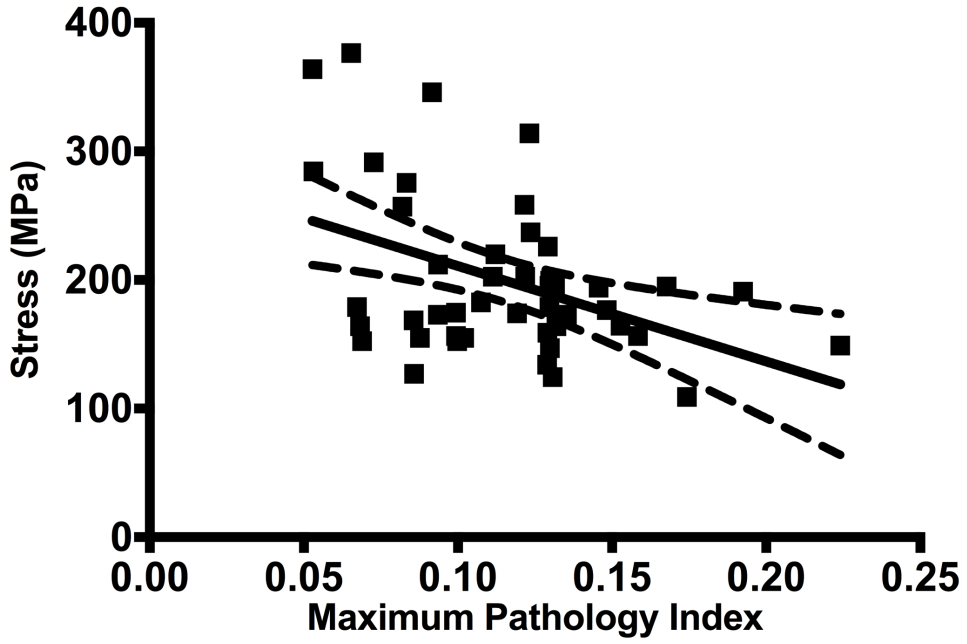

Figure 4.8.5C XY scatter plot of stress and maximum pathology index for the short term (4-week) groups. There was no correlation among the data (r=0.17, p=0.25). Bands denote 95% confidence intervals.

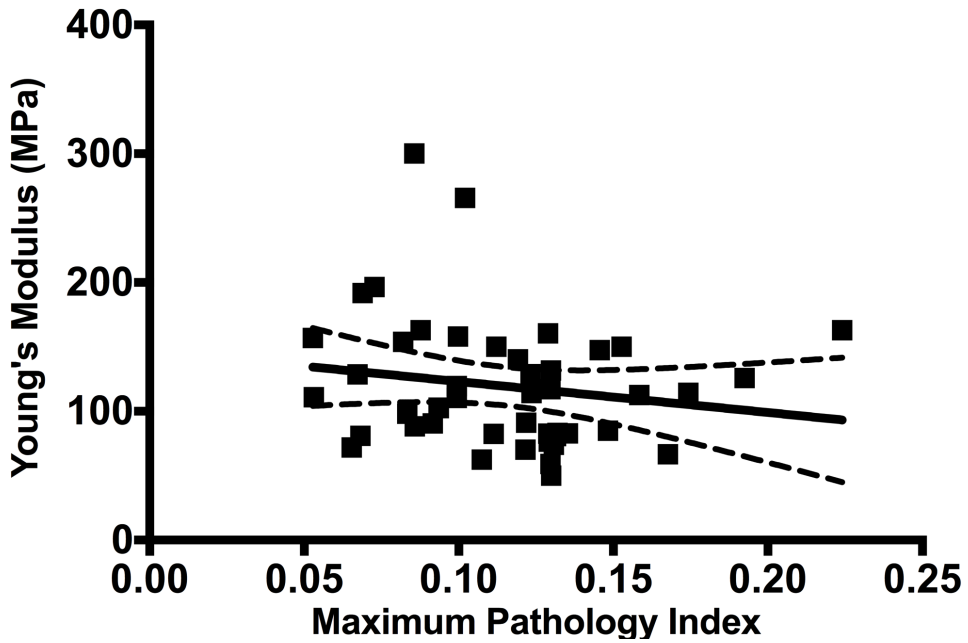

Figure 4.8.5D XY scatter plot of Young's modulus and maximum pathology index for the short term (4-week) groups. There was no correlation among the data (r=0.01, p=0.9). Bands denote 95% confidence intervals.

Evaluation of AE maximum PI over each group at the 0-week time period did not determine any significant differences among the protein and control groups (p=0.26, **Figure 4.8.5E**). At the 2-week time period, the control suture has a significantly higher maximum PI compared to all of the other groups (p=0.0009, **Figure 4.8.5F)**. At the 4-week time period, there are no longer any differences identified among the groups (p=0.1850, **Figure 4.8.5G**)

The mean maximum PI obtained for both medial and lateral branches for all groups prior to surgery (0-weeks) was 0.0623 ± 0.002. There was no significant difference between the lateral branch (0.0599 ±0.002) and the medial branch maximum PI at 0 weeks (0.0644 ± 0.003). For the lateral branch of the gastrocnemius tendon

there were no significant difference among the groups for maximum PI at 0-weeks ($p=0.26$, **Figure 4.8.5H**). There were significant differences identified between the lateral tendons over the time periods, with a significant increase in maximum PI between 0 and 2-weeks, followed by a lowering of maximum PI between 2 and 4-weeks. However, the medial tendons demonstrated a significant and steady increase in maximum PI between 0,2 and 4 weeks ($p<0.001$).

The mean maximum PI for both branches at 2-weeks post surgery was 0.123523 ± 0.008. There was a highly significant difference between the lateral branch (0.1600 ± 0.0150) and the medial branches maximum PI at 2-weeks post surgery (0.08844 ± 0.0032, $p<0.0001$). For the lateral branch of the gastrocnemius tendon, there were significant differences among the groups for maximum PI at 2-weeks post surgery ($p=0.0009$). The ZF/ZV group had significantly higher maximum PI values compared to the other groups at 2-weeks post surgery.

For both medial and lateral tendons, significant differences were identified over time among the 0,2 and 4-week data ($p<0.0001$). The maximum PI of the medial branch increased between 0 and 2 week and 4 weeks. However, the lateral branch significantly increased in maximum PI between 0 and 2-weeks, but reduced between 2 and 4-week post surgery.

The mean maximum pathology index for both branches at 4-weeks post surgery was 0.10801 ± 0.00402. At 4-weeks, there was a significant difference between the

lateral branch (0.1199 ± 0.0054) and the medial branch maximum PI (0.09607 ± 0.00616, $p<0.001$). For the lateral branch, there was no significant difference among the groups for maximum PI.

The changes in maximum PI that occur over time are demonstrated by cineloop data in **Figure 4.8.5l**.

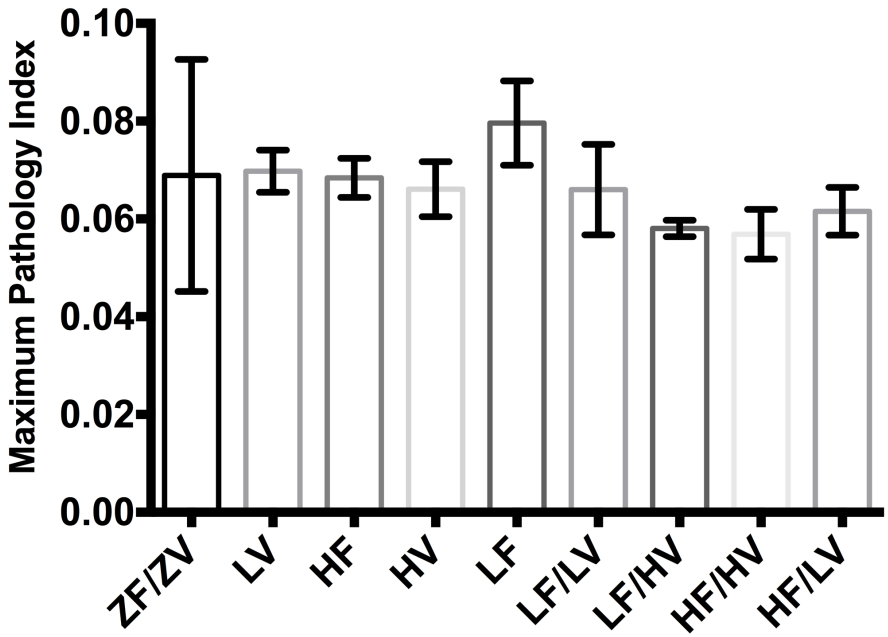

Figure 4.8.5E. Bar chart of maximum pathology index evaluations, pre-surgery (0 weeks) No significant differences were identified among the groups (p=0.2636). Data shown as mean ± SEM.

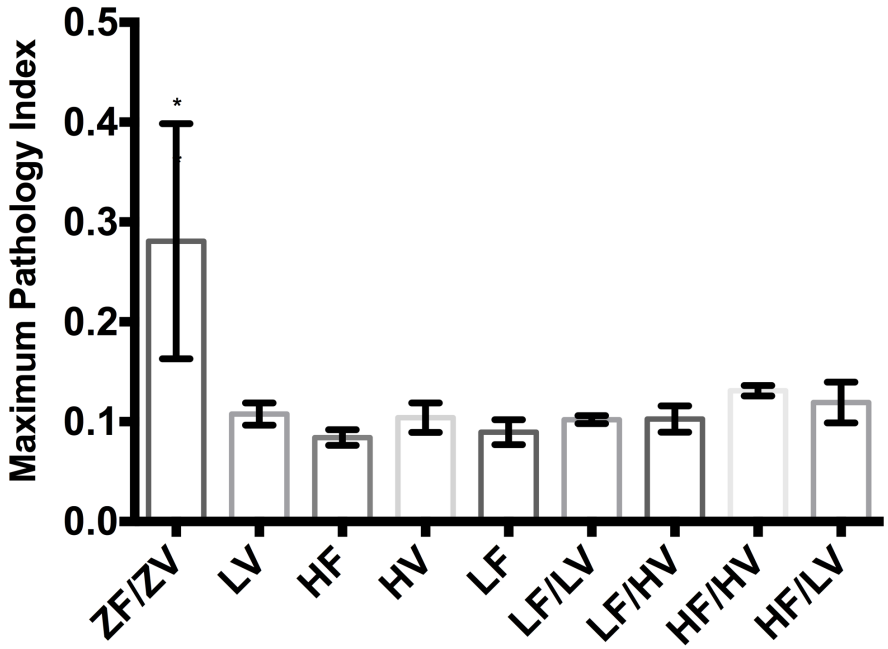

Figure 4.8.5F. Bar chart of maximum pathology index evaluations, 2-weeks post surgery. The ZF/ZV group was significantly (*) associated with higher PI values than all the other groups (p=0.0009). Data shown as mean ± SEM.

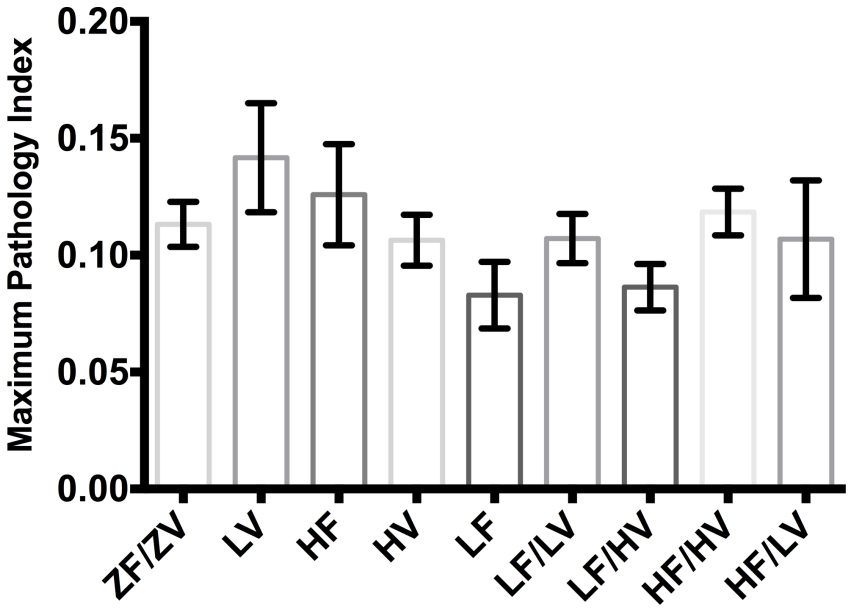

Figure 4.8.5G. Bar chart of maximum pathology index evaluations, 4-weeks post surgery. No significant differences were identified among the groups (p=0.1850) Data shown as mean ± SEM.

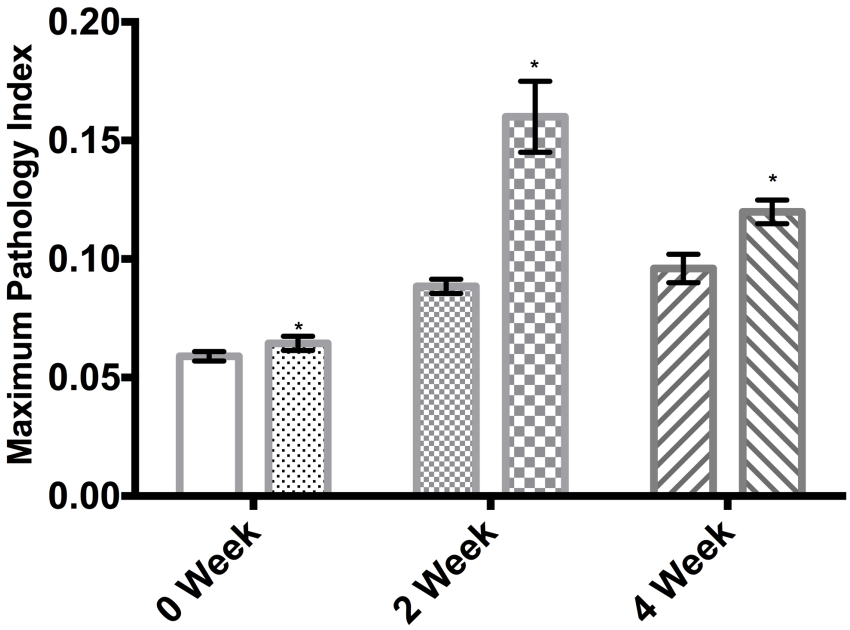

Figure 4.8.5H. Bar chart of maximum pathology index evaluations at 0, 2 and 4-weeks post surgery. Left bars indicate medial tendons within each time period, and right bars indicate lateral tendon. There was a significant and steady increase in pathology index values for the medial tendons between 0,2 and 4 weeks. In addition, there was a significant increase between 0-2 weeks, followed by a reduction in pathology index between 2-4 weeks in the lateral tendon (*)($p<0.001$). Data shown as mean ± SEM.

.

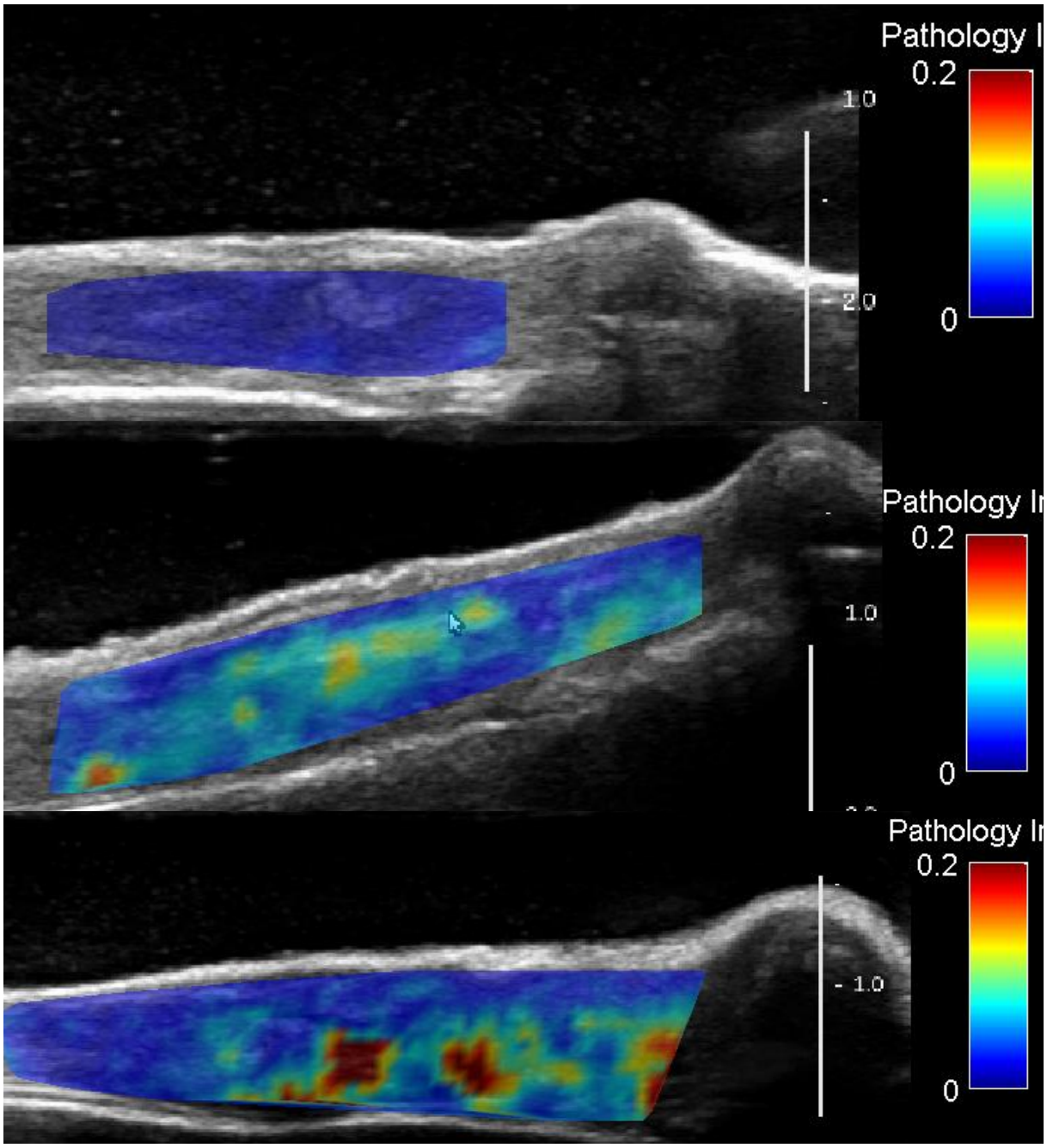

Figure 4.8.5l Cineloop data of maximum pathology index. (**Top**) Very quiescent tendon, low PI value (HF/HV group, 4-weeks). (**Middle**) Minor changes in PI score, intermediate value (HF group, 2-weeks). (**Bottom**) Significant changes, high PI scores (ZF/ZV-group, 2 weeks). Note how the majority of the high values (red) occur in the region of the surgical site.

4.8.6 SWI and AE Evaluation

In comparison of SWI speed and AE maximum PI, there was a significant and moderate negative correlation (r= 0.413, p=0.004, **Figure 4.8.6A**.).

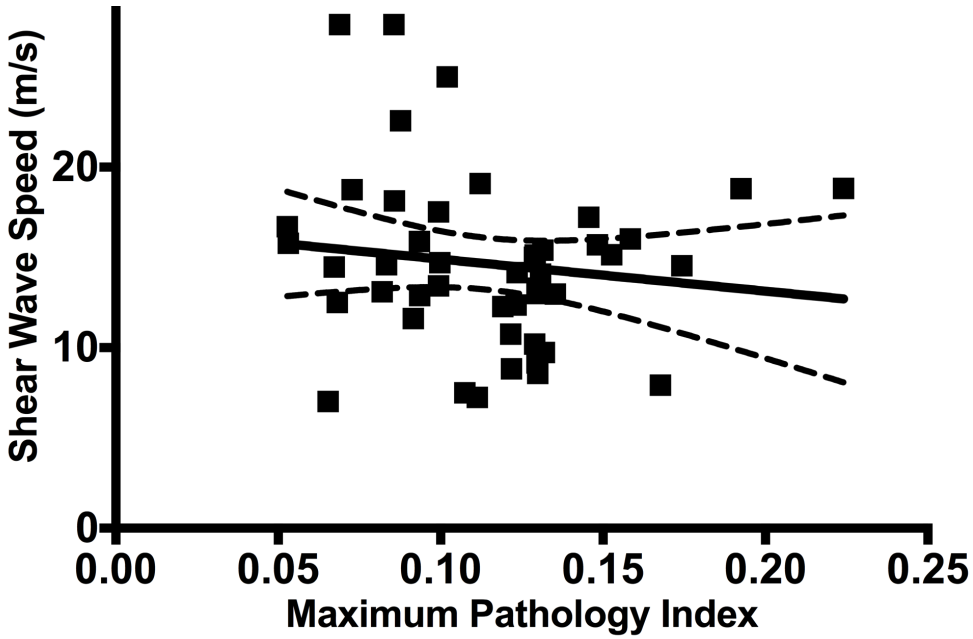

Figure 4.8.6A. XY scatter plot of shear wave speed and maximum pathology index. A moderate negative correlation exists between the two imaging parameters (r= 0.413, p=0.004). Bands represent 95% confidence intervals.

4.8.7 SWI and AE Modeling

A significant effect was identified for the regression of ultimate tensile strength on both SWI speed and AE maximum PI data, (p=0.0034). Using forward model selection, the model that explains the variability of ultimate tensile strength includes both the SWI speed and AE maximum PI values (adjusted r = 0.44). Both SWI speed (p=0.015) and maximum pathology index (p=0.0029) were significant variables in this model. Thus, a

potential model for optimal ultimate tensile strength evaluation includes both parameters and in this study, can be given by the formula:

$$UTS = 384.88 - 733.2 * (PI) - 11.42 * (SWI)$$

4.8.8 Microbubble Contrast Angiography

For the majority of 0-week cineloops, there was no significant uptake of MCA in the tendon. Therefore, from the computer processed data of the cineloops, a 10% above baseline and 85% of peak value could not be calculated in order to determine a mean pixel intensity value (MPV). Data representative of this scenario are depicted in **Figure 4.8.8A**. Thus any mean pixel value, which identified a change of 1.5 units or less, was deemed to have no contrast uptake.

Data were then analyzed using discrete variables. An animal was determined to have had contrast uptake if the 10% baseline – 85% peak difference exceeded an average distance of 1.5 MPV units. A change of 1.5 MPV's was chosen as a minimum registrable value from the data evaluated, which could be reliably interpreted as an increase in MPV.

There were no significant differences in MPV among the groups at 0-weeks ($p=0.83$, **Figure 4.8.8B**). At the 2-week time point, there was a significant difference in the number of animals with contrast uptake, in comparison to the 0-week time point

(P=0.002, **Figure 4.8.8C**). The LV, HF, LF/LV LF/HV and HF/HV groups had significantly more uptake than control suture (ZF/ZV) group.

At 4-weeks, there was a significant difference in the number of animals with contrast uptake among the groups (p=0.001, **Figure 4.8.8D**). While the ZF/ZV control suture group remained with few animals with MPV values greater than 1.5, the number of rabbits with uptake in the HF, HV, LF/LV groups increased. The number of animals with MPV greater than 1.5 continued to remain elevated or increased for all the other groups, which showed significant increases in vascularity compared to ZF/ZV control sutures group. Thus while it was not always possible to demonstrate differences among the groups, there was greater consistency in demonstrating increased vascularity compared to control sutures. Such an example of increased contrast uptake is demonstrated in **Figure 4.8.4E**.

Several adverse reactions were recorded with the use of MCA. Reactions were not predictable and occurred at all time points and were not confined to a specific group or sex. In total, six animals experience a reaction; symptoms included sudden reversal of anesthesia, urination and defecation, vocalization and while still under the influence of the anesthetic, apnea and tachycardia. No fatalities were recorded.

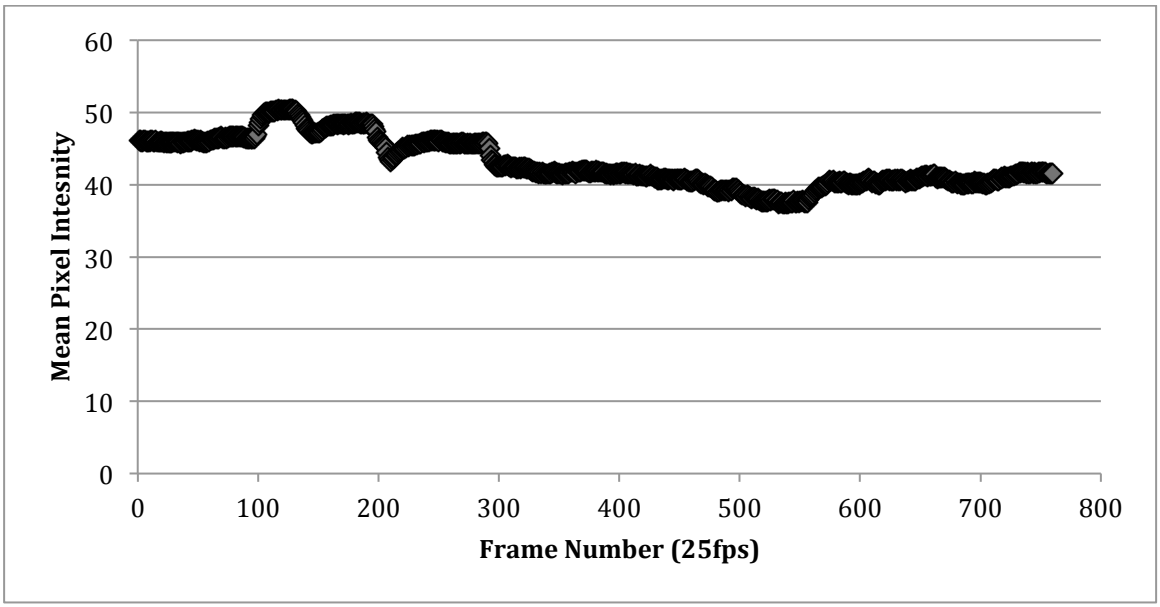

Figure 4.8.8A. Example of a noisy baseline setting (ZF/ZV group, 0-weeks). In this case, any form of calculation was impossible and the animal was determined to have no significant contrast uptake in the limb. Therefore, the graphs representing differences between groups demonstrate a small number of animals. Although a slight peak is indicated after 100 frames, the change in Mean pixel intensity is less than 1.5 after calculation of baseline +10% and 85% of peak values.

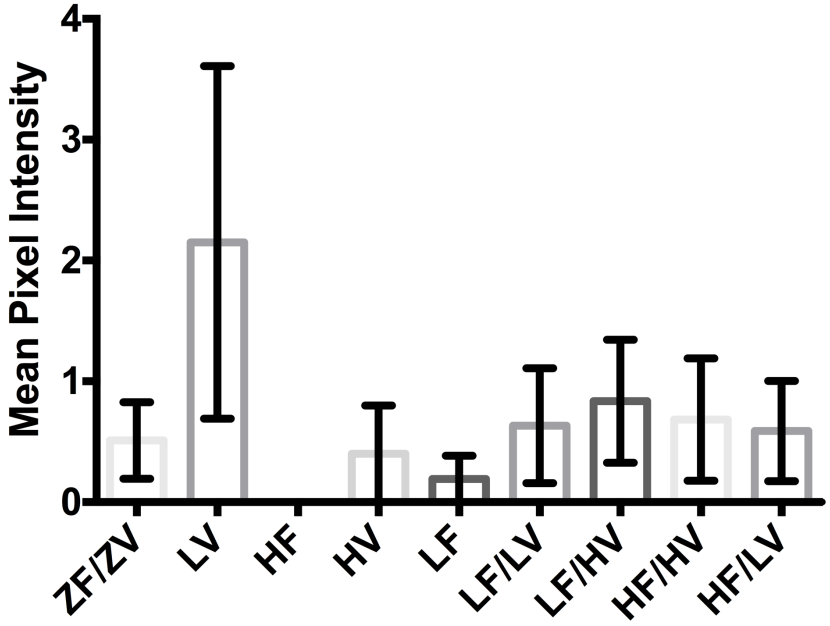

Figure 4.8.8B Bar chart of mean pixel intensity change, 0-weeks. Although some animals had significant contrast uptake at 0-weeks, the majority of animals possessed no uptake. There were no significant differences among the groups (p=0.8387) Data shown as mean ± SEM.

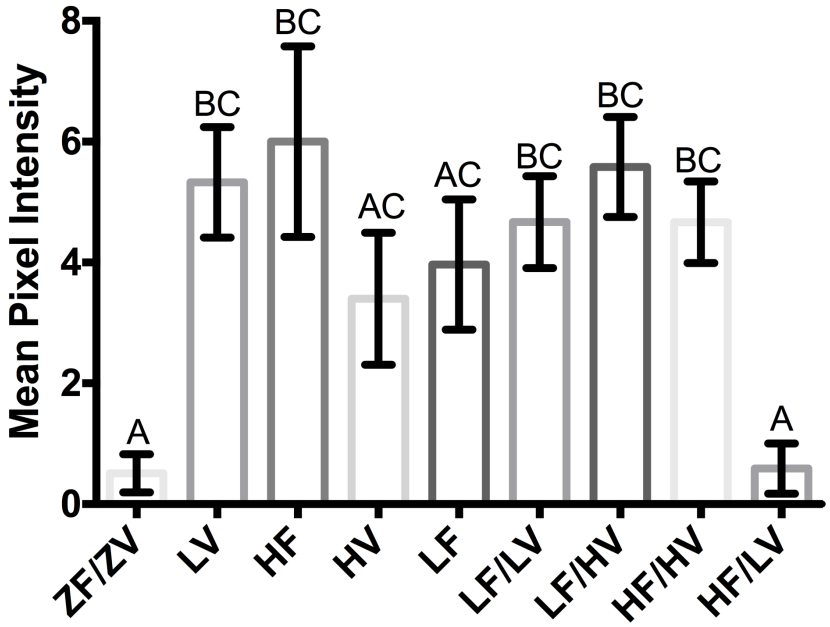

Figure 4.8.8C Bar chart of mean pixel intensity change, 2-weeks post surgery. Significantly (p=0.002) more rabbits at the 2-week time demonstrated contrast uptake in comparison to the 0 week time point. Although the majority of protein sutures had animals with contrast uptake, the ZF/ZV control group had more animals with lower contrast uptake. Differences among letters denote differences among groups at p<0.05. Data shown as mean ± SEM.

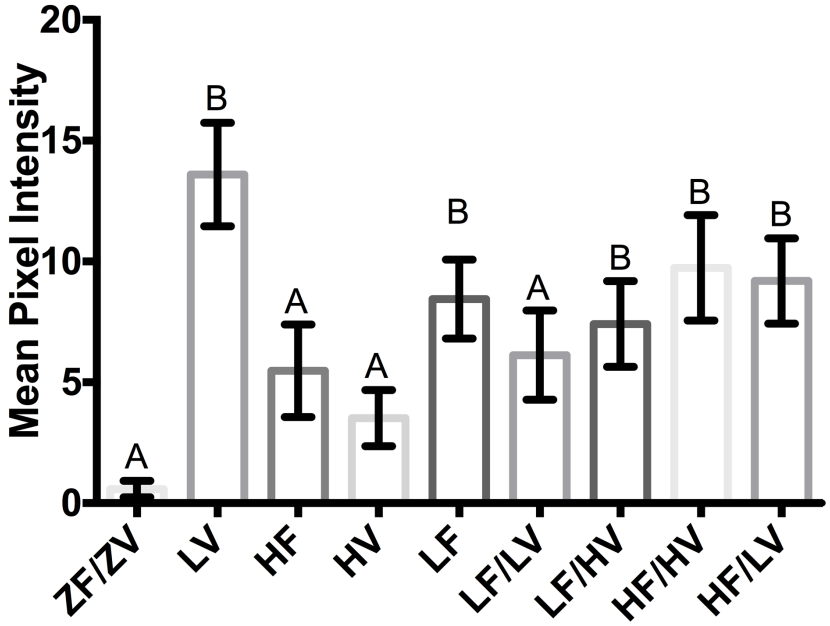

Figure 4.8.8D Bar chart of mean pixel intensity change, 4-weeks post surgery. Significantly (p=0.001) more animals at this time point demonstrated contrast uptake compared among either 0 week or 2-week data. Differences among letters denote differences among groups at p<0.05. The majority of protein sutures had animals with contrast uptake. The ZF/ZV control group had more animals with lower contrast uptake.

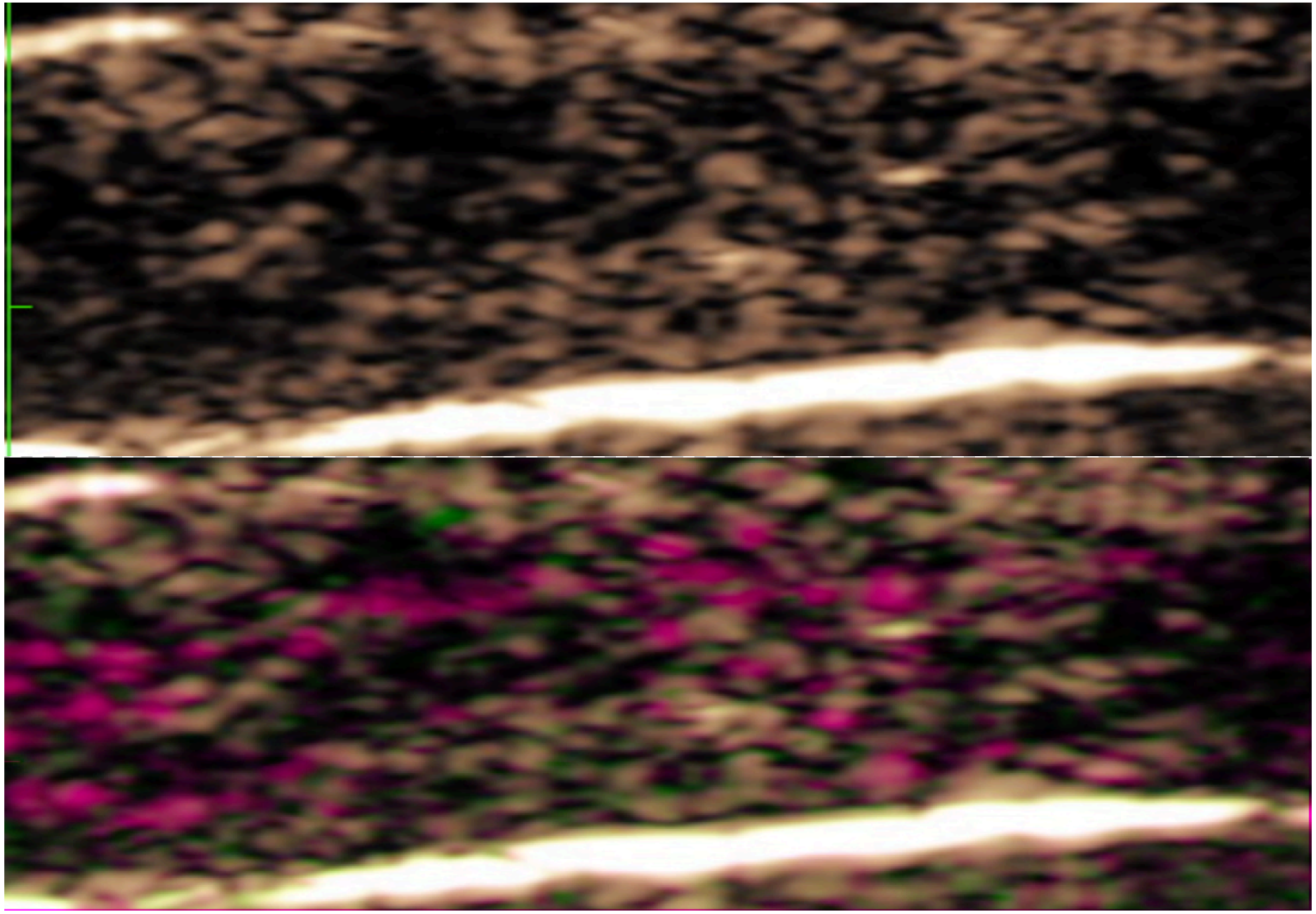

Figure 4.8.8E. Flow of contrast uptake through the tendon. Sequential images overlaid and MCA bubble enhancement highlighted via channel mixing, Adobe Photoshop. (**Top**). Quiescent tendon in cadence mode. (**Bottom**). Same section of tendon as in the top image. As MCA flows through the tendon, it is detected as changes in the pixel intensity, denoted in pink on the bottom image.

References

1 **Hamada, Y., et al.** Effects of monofilament nylon coated with basic fibroblast growth factor on endogenous intrasynovial flexor tendon healing. *J Hand Surg*, **31**, 530-540. (2006).

2 **Perrier, M., et al.** Acceleration of Second and Fourth Metatarsal Fracture Healing with Recombinant Human Bone Morphogenetic Protein 2/Calcium Phosphate Cement in Horses. *Vet Surg*, **37**, 648-655. (2008).

3 **Nakamura, Y., et al** Low dose fibroblast growth factor-2 (FGF-2) enhances bone morphogenetic protein-2 (BMP-2)-induced ectopic bone formation in mice. *Bone* **36**, 399-407. (2005).

4 **Zhang, F., et al.** Effect of vascular endothelial growth factor on rat Achilles tendon healing. *Plast Reconstr Surg* **112**, 1613-1619. (2003).

Chapter 5

Discussion

5.1 Discussion

This study was conducted to test several hypotheses and investigate the effects of two growth factors incorporated onto suture material in the surgical repair of transected lateral gastrocnemius tendon. One major aim was to evaluate if the combination of VEGF and FGF can result in superior repair at both 4-week and 9-weeks post surgery and how we may be able to noninvasively determine biomechanical information regarding the healing of tendon and its vascularity.

We were able to successfully generate suture material to release a calculated spatiotemporal mixture of the two growth factors. However, the HAP material is exceedingly brittle and it is not recommended to coat sutures in excess of 14 days due to premature loss of crystal during handling. Thus, alterations in the crystal composition or other methods to delay the dissolution of this layer would have to be employed in future studies. However, we were able to demonstrate that proteins can be incorporated at many layers and stages of the crystals, or then can be co-localized together, which provides data to support further studies.

The release experiments demonstrated the difference in adsorption rates for FGF and VEGF, despite similar incubation concentrations. It is apparent that FGF has a higher affinity to bind to the HAP crystal layer than VEGF and that absorbable sutures are more capable of being loaded with higher concentrations of protein. We identified that polyglactin 910 sutures dissolved between day-21 and day-28 after we initiated the

release experiment, when we expected the dissolution to occur at around day 40. Therefore, it is highly likely that the breakdown of the polyglactin 910 sutures had been initiated by hydrolysis at the time the incubation period was initiated. This is important in future studies, as polyglactin 910 sustains a 25% loss of tensile strength at day 14 and 50% at day 21.[1] Thus, after 10-day incubation period in mSBF, polyglactin 910 will retain only 50% of its tensile strength 11 days after implantation. Thus, biomechanical properties of the suture materials will need to carefully be considered.

We demonstrated the differences in release kinetics between superficial and deep layers of suture material. It was evident that a deeper layer provides a more gradual release, whereas a superficial layer provides a greater initial burst and then achieves a plateau at an earlier time point. Thus there is considerable coordination that can be achieved with careful engineering of the HAP layers. However, we encountered a significantly higher release when we took into account physiological mechanisms of suture use, namely passing the suture through tissue and applying a knot. This action results in shearing forces on the HAP layer, which increases the degree of initial burst. Furthermore, we encountered a secondary burst, often associated with the use of polyglactin 910 and its ultimate dissolution in our release experiments. Although a secondary burst phenomenon was also encountered with some nylon suture, this was often isolated to the tendon tissue and coincided with the time period the tendon tissue had dissolved by autolysis in our SBF solution, which would not occur *in vivo*. The nylon suture did not dissolve, thus the secondary burst cannot be attributed to suture dissolution in this case. Since autolysis would not occur *in vivo*, the results for the burst

phenomenon for the nylon suture are therefore limited to the *in vitro* application we performed in this study.

The concept that we applied protein solution in a laboratory setting, at various time points, followed by the drying and lyophilization and sterilization of the sutures in ethylene oxide lends significant credence to the notion that such a product may have viable commercial opportunities. We demonstrated the retention of bioactivity of the product in these experiments, although the exact reduction that occurs is unknown. It would also be interesting to determine if the reduction in bioactivity is greater for suture material in the superficial layer than the deep layer.

The idea that the addition of FGF or VEGF would increase cross sectional area was anticipated, since these have been shown to stimulate repair by the extra deposition of collagen. However, it was interesting to note that the cross sectional area increase due to surgical manipulation was not as significant as one might imagine as demonstrated by the control ZF/ZV group. Therefore, we noted that the addition of growth factors resulted in a significant enlargement of the repair site at the 4-week time period. Although one may have expected fibrous tissue deposited in this region to remain persistently, it is intriguing that the cross sectional area of the HF/HV group had returned to baseline values by the 9-week period. The ZF/ZV 9 week group cross sectional area had also returned to intact control baseline values, but were still larger than the HF/HV group, although this was not considered significant. The mechanisms

that therefore resulted in the reduction in cross sectional area in this time are intriguing to consider.

The addition of a variety of dose combinations of FGF and VEGF in tendon repair resulted in biomechanically superior properties in comparison to the ZF/ZV control suture. This information is not new and would have been expected. However, the identification that the HF/HV group more than doubled the ultimate tensile strength of the tendon in a 4-week time period is highly biologically relevant. One couples this with the fact that the ultimate strength attained surpassed even biological normal intact tendons, which was unexpected. The magnitude of the strength of the tendon was so great that it altered the failure mode for this group. Whereas most failures occurred at the site of repair, the majority of failures in HF/HV group occurred via avulsions of small pieces of bone off the proximal aspect of the calcaneus.

In terms of musculoskeletal components, it has not been previously reported that post injury, tissue regains its original biomechanical properties, let alone surpasses them. Bone is the only notable exception to this statement, and perhaps also the liver. Furthermore, there is an interesting parallel between the temporary formation of periosteal callus and resulting increase in bone cross sectional area while bone is healing, which temporarily provides increased biomechanical strength to the repair site and the increase in tendon cross sectional area observed in our study. We encountered significant differences for our cross sectional area, ultimate tensile strength and stiffness parameters of evaluation. High tensile strength tendons tended to have high cross

sectional areas. When we consider our calculations of Young's modulus, strain and stress, which takes into account the cross sectional area, there were fewer significant differences identified. Although there was a statistically significant difference among the groups in terms of Young's modulus, the majority of the protein groups were not significantly different among each other. The effect of the cross sectional area is therefore to normalize the Young's modulus throughout our data, which accounts for the differences in cross sectional area. This makes some biological sense, as Young's modulus is an intrinsic mechanical property of the tendon structure. A similar explanation can be used to describe variation in stress for all our groups.

From a biological and clinical perspective, these intrinsic parameters are of less value to a clinical case. The properties of the structure being examined, in this case stiffness and ultimate tensile strength, would be important to the patient with a healing tendon.

There appeared to be no significant effect of the suture material implanted in the lateral gastrocnemius tendon on the medial gastrocnemius tendon. For the most part, biomechanical testing parameters, although they became more variable in the post surgical period for the medial tendon, did not significantly differ from each other. This is encouraging by confirming that the major focus of protein action is local to the suture material delivery platform and not widespread with interactions at distant sites. During the surgical procedure, it was noted that during placement of the core suture, there was some flaking off of the HAP crystalline layer into the local environment. This primarily

occurred as tension was placed on the suture material to appose the tendon ends. Much less HAP was lost during placement of the paratenon suture, as there was no significant application of tension to this suture. The local action of the suture material was also confirmed via histological analysis, which demonstrated vasculature in close proximity to the suture material, but not in the core of the tendon. Thus the conclusion is that although some HAP and growth factors are lost during placement of the core suture, the main effect is local, although it is highly likely that the HAP crystals overlaying on the medial tendon contributed to the increase in variability for this structure in later evaluations.

One of the main hypotheses of this study was that the combination of FGF/VEGF would be synergistic. For the majority of the doses we used, the addition of another growth factor in low combination did not significantly affect any of the biomechanical parameters evaluated. It was only via the use of the HF/HV combination that a significant interaction and synergistic effect occurred. Thus, it is important to recognize that each species in which this technology may be translated, would require a similar dose-response evaluation.

As has been previously identified, we were able to determine a significant correlation between histology scores and biomechanical properties. This correlation was expected, as we identified that groups with multiple growth factors tended to have superior collagen fiber alignment and the presence of more spindle cells than the control or groups with a single coating of growth factor. Furthermore, we confirmed that

the use of the suture material coated with HAP resulted in only minor degrees of inflammation, as evidenced by some histological sections, but on the whole, suture integration into the tendon was accomplished successfully.

The main findings were therefore that the high combination group was the optimal suture group of all the combinations we evaluated for the repair of rabbit lateral gastrocnemius tendons. The HF/HV suture combination resulted in an increase in vascularity and superior histological organization as identified via histology and a significant increase in cross sectional area. The biomechanical properties of normal intact tendons are likely optimal for the daily activity of an individual, in this case a rabbit. Given that there is a reduction in cross sectional area, a reduction in biomechanical properties to physiological values and a superior histological organization by 9-weeks we conclude that sensing of biomechanical excess had occurred by some pathway and instigated the remodeling of the tendon, as occurs in Wolff's Law in bone. Excess mechanical properties above normal are not required so the tissue will remodel to return the tendon to intact normal biomechanical properties.

The introduction to this thesis mentioned the possibility of the role of macrophages in sensing the mechanotransduction signals, presumably regulated through the ECM of the tendon and tenocytes. Since parallels have already been drawn between callus formation and Wolff's Law in bone, one would be tempted to link the role of macrophages, which are of the same haematopoetic lineage as osteoclasts, with the regulation of tendon biomechanical properties. However, attempts to identify the

presence of macrophage using immunofluorescence were unsuccessful. Although there were instances were a single cell fluoresced with this antibody and the binding appeared specific to that cell, it is dubious if those cells are truly macrophage. It is difficult to envisage that the macrophage population in these tendons is limited to low single digits. Although the particular antibody we utilized has been used in rabbits previously[2] it is unknown why we were unable to detect a significant macrophage presence. Ideally, a positive control would have been used to verify our antibody in this model. Another potential candidate antibody we could have used would have been RAM 11, an antigen that labels rabbits macrophage but is so far uncharacterized. [3]

To evaluate why our macrophage binding was unsuccessful, we must identify the target of the MAC387 antibody. MAC387, L1, or Calprotectin molecule, is an intracytoplasmic antigen comprised of a 12 kDa alpha chain and a 14 kDa beta chain. The antigen is expressed by granulocytes, monocytes and tissue macrophages. It is related to the S100 family of proteins and has been detected on neutrophils, monocytes, invariably in endothelial and epithelial cells in addition to a soluble form. Furthermore, it is associated with activated macrophages and functions with an important role in inflammatory processes by regulating the adhesion of myeloid cells to endothelium and extracellular matrix.[4] The possibility exists that activated macrophages functioned in an immune response, probably during the first few days of this study, would have been identified via this antibody. Therefore, our results suggest that by the 4 or 9-week time point, there were no activated macrophages present in the tendon, which seems highly unlikely. An interesting possibility occurs if macrophages responsible for tendon

remodelling at the 4 or 9-week time point are differentiated further along the pathway and no longer express MAC387, such as with the expression of RANKL in osteoclasts. It is unclear if the transformation, if any, of macrophages would affect tissue resident macrophage or macrophage activated by the classical or alternative pathways. However, there may be other biomarkers for remodelling macrophage that are currently unidentified.

Due to its ease of use, ultrasound, SWI or AE could easily be adapted to clinical use for noninvasively and quantitatively tracking changes in SWI speed and PI following the treatment of a surgical repair of a transected tendon. The use of either SWI or AE metrics as biomarkers of tendon biomechanical properties are encouraging. We identified significant changes in both SWI and AE parameters observed after severing and surgically repairing a tendon, which may reflect a decrease in mechanical integrity of the damaged tissue.[5]

We found a correlation between SWI speed and both the ultimate stress and Young's modulus of tendons, supporting the use of SWI as a proxy measure of tendon mechanical properties, although it also correlated moderately with ultimate tensile strength and stiffness However, the use of SWI to track temporal changes during healing was not supported, since we found no significant increase in SWI between 2 and 4-weeks post-surgery. This latter result could mean that the time between 2 and 4-weeks post surgery were an insufficient for SWI speeds to significantly change with healing. Although we found changes between the ZF/ZV control suture and all the other

groups, separating differences among all of our test sutures was much more difficult. A curious result was obtained at the 0-week scan when a single group was found to have lower SWI speed than the rest. Although no outliers were identified in the data, this may simply be attributable to chance in this case and it is more likely that a type I error was made in this assessment. Another interesting point to note is how much the medial tendon SWI speed was affected by the transection of the lateral branch so much so that we were unable to identify any differences between the two branches at any time point using this modality. This may have occurred for several reasons. It may be that our positioning of the leg at 90 degrees of tarsal flexion was insufficient to tense the medial branch enough to fully evaluate changes in SWI speed in this structure. In future, a more acute tarsal angle may be more beneficial.

The positive relationship between SWI and mechanical measures is particularly encouraging given the small size of the rabbit tendon structures being imaged. Shear wavelengths are generally larger than tendon thickness, causing guided wave propagation along and across the tendon as the shear wave reflects off its boundaries.[6] The results from this study showed shear wave velocities of ~16 m /s and the frequency range used for the SWI technique (300–800 Hz), generates shear waves with a wavelength between 20-50 mm. These shear wave wavelengths are greater than the mean tendon cross sectional area of between ~6 mm for our intact normal tendons and ~19 mm for our HF/HV group. Such effects may be more pronounced in smaller tendons, such as the rabbit Achilles. There is also potential for interference from

adjacent tissues since spatial averaging is used to generate the SWI map. This may introduce error because tendon wave speeds are considerably higher than wave speeds in adjacent tissues such as muscle.[7] Both the wave guiding and spatial averaging effects on SWI errors would be lessened in larger tendons, such that there is potential for obtaining more reliable SWI measures in a larger animal model.

Our treatment group included rabbits undergoing repair using sutures coated with three levels of VEGF and FGF growth factors, which contributed to the variability in the elastic modulus and strengths measured for lateral tendons at sacrifice. We tested both repaired tendons and intact tendons so as to include distinct “injury states” in our analysis. It is encouraging that the SWI relationship to tendon mechanics was evident when examining individual groups. This suggests that SWI may serve as a proxy for mechanical properties irrespective of the state of the tendon or the specific treatment approach used on a torn tendon, which would clearly represent the case in clinical settings.

It is well understood that tendinous tissue is both nonlinearly elastic and anisotropic[8], which are important considerations when collecting and interpreting tendon SWI speeds. Our SWI speeds were measured at low tensions, in which tendon is known to exhibit nonlinear strain-stiffening behavior. The strain-stiffening effect would suggest an increase in shear wave speed with tendon stretch, a phenomenon that has been observed in both *in vivo*[9] and *ex vivo*[10] studies. In this study, we tried to control for the strain-stiffening effect by collecting all images at a set tarsal angle. There remains

the possibility that the slack length of the tendon is altered when severing the tendon, such that it is not guaranteed that the same posture results in the same loading and strain at the tissue level. In performing these studies, it is important to recognize that axial tendon strain can result in increases in shear wave speed that exceed the maximum tracking speed (16.3 m/s) of current commercial systems, such that it is necessary to restrict SWI speed measures to low loads at this time.

SWI speed is a function of shear modulus in both isotropic and transversely isotropic materials. In an isotropic, purely elastic material, there is an easily defined relationship between the shear and elastic moduli, such that the elastic modulus can be estimated based on the SWI speed. However, the relationship between the shear and elastic moduli in transversely isotropic tissues like tendon is more complex [11]raising interesting questions about how the more functionally relevant axial elastic modulus may be related to the shear modulus, and thus the shear wave speed. While not well understood for tendon, a strong linear correlation between shear modulus and axial Young's modulus has been observed in muscle[12], which is often also considered transversely isotropic.[13] Such a relationship would support the idea that SWI speed in transversely isotropic materials, being an indicator of shear modulus, may be at least a good correlate of elastic modulus as well. However, more experimental and modeling work is needed to understand this relationship in greater detail.

Our study was premised on the idea that tendon elasticity is related to tendon strength, as described in a meta-study by LaCroix et al[14]. One potential explanation for

this empirical observation is that failure is ultimately dependent on the strain the tissue can withstand, which can be estimated from the tissue elasticity. We indeed found a high correlation between SWI speeds, Young's modulus and ultimate stress ($r = 0.85$, $p < 0.001$), lending credibility to this idea. This relationship can also be seen in a previous rabbit Achilles regeneration study that showed similar percent increases in ultimate stress and Young's modulus during healing.[15]

When examining the effectiveness of ultrasound SWI as a diagnostic tool for tendon biomechanical inference, we found that there was only poor correlation with structural mechanical properties (stiffness or tensile strength) and moderate correlation with material properties, such as stiffness and Young's modulus. There was also some evidence to suggest that SWI and biomechanical data derived from SWI can be used to differentiate between fully intact (NT) and severed/repaired tendons. The benefit of SWI is that it is a noninvasive measurement technique, and thus can be used clinically. SWI showed reasonable sensitivity as an *in vivo* test (0.81), but poor specificity (0.64) when using Z score as differentiator (**Table 4.8.1G**). It should be noted that in this case, sensitivity is the more important of the two metrics, being that a false negative result would be more detrimental than a false positive result.

We noted a negative correlation between the AE maximum PI and ultimate tensile strength. There appeared to be good baseline values at the 0 week time period for both medial and lateral branches, indicating that repeatability of this technique is high. Although we were unable to use the maximum PI values to evaluate differences

among groups at the 2-week time point, we were able to identify that all treatment groups were superior to the control suture. Furthermore, the control suture group, at the 2-week time point, had the largest change in maximum PI values. At the four-week time point, we were unable to detect differences among the groups using maximum PI values. We did identify correlations between maximum PI values and ultimate tensile strength and stiffness. The correlation of maximum PI and material tendon properties (stress, Young's Modulus) were poor and not supported by this study.

It was also interesting to note that SWI and PI were moderately correlated with each other. This is encouraging since it supports the use of both parameters in tendon evaluation. Although SWI data appeared to have greater correlation with material tendon properties (Young's modulus and stress) AE PI assessment had greater correlation with structural tendon properties (ultimate tensile strength, stiffness). This raises the question which modality should we use? Unfortunately, the answer is not straightforward. From a clinical perspective, one would wish to identify the ultimate tensile strength of a tendon in order to promote or caution against a specific rehabilitation protocol. However, over time other parameters such as the intrinsic properties may become more important. When entering a mathematical model to calculate ultimate tensile strength, the greatest R-value was encountered when both maximum PI and SWI data were entered into the model, which was superior to the use of each modality alone. Thus, although they both provide different data, which are related, the combination of the two may prove to be the most successful in terms of accurate prediction of ultimate tensile strength, although it should be stressed that the

correlation using both these modalities was moderate and the results need to be interpreted with caution.

The MCA results were somewhat disappointing. It was expected that at the baseline time point, overall contrast uptake would be poor, representing the inherent lack of vascularity in a tendon. However, at the 2-week time period, we failed to detect any significant blood flow in 61% of the tendons examined. This may reflect the fact that the tendon transducer was not positioned in the correct location, or that some other technical error occurred during the data recording. Despite this detail, we were still able to identify differences among the groups. Similar to the SWI and AE data, significant differences between the test sutures and the controls sutures were often detected and such was the cases for the MCA at 2 weeks. Using our modified evaluation with a minimum mean pixel value change of 1.5 units, we were able to show that significantly more tendons had blood flow that was detected at the 2 and 4-week period than the control sutures. The combination groups LF/HV, HF/HV and HF/LV had the highest number of animals with an increased blood flow. It is interesting to note that these combination groups had the highest number of animals with detected blood flow, greater than the single growth factor groups which themselves were superior to the control suture. Thus, the combination of the two growth factors we used may have had a synergistic effect in promoting angiogenesis.

We did encounter several complications with the administration of the MCA. Several adverse anesthetic effects were noted, which were confined to the first injection

of the drug in that animal. The second injection for the contralateral side was asymptomatic. Reactions included sudden reversal of anesthesia, urination and defecation, vocalization while still under the influence of the anesthetic, apnea and tachycardia. No fatalities occurred as a MCA injection.

In conclusion, the results from this study support our original hypotheses. We identified that there was a synergistic interaction among the FGF and VEGF proteins when released in the manner described in this experiment. At the high concentration of both FGF and VEGF, the ultimate tensile strength of the tendon doubled at 4 weeks. This treatment, if proven in humans, would be significant. The benefits we encountered were not merely biomechanical, but also confirmed via superior tendon histological organization.

The imaging aspect of the project in essence advanced what is already known about the correlations between SWI and AE and biomechanical properties. Although these parameters can infer biomechanical data, they were most useful at differentiating test groups from controls and were less reliable among each other. We may have been limited in this regard by the size of our model. Further research is warranted in larger tendon structures.

Angiogenesis has also been implicated in tendon healing. Our histological evaluations, such as vascular scores and the histology imaging support the correlation of neovascularization and tendon healing. However, although angiogenesis is important

for healing, intact normal tendons and the HF/HV 9-week group demonstrated a lack of vascularity in the body of the tendon, implying vessels form, deliver nutrients for the tendon to heal and then regress. The exact time frame the blood vessels are required prior to regression is unknown. Imaging using MCA's is also of benefit to assess vascularity although we were again limited mainly to identifying differences between the control sutures and the protein groups.

Given the implications of a commercial product using this technology and the data generated in support of FGF and VEGF release in tendon healing, coupled with the supporting evidence generated by SWI, AE and MCA imaging, further studies targeting specific areas and questions generated in this discussion are warranted.

References

1 **Auer, J. A. & Stick, J. A**. *Equine surgery* (No. Ed. 4). WB Saunders. (2012)

2 **DeLeo III, M. J. et al.** Carotid Artery Brain Aneurysm Model: In Vivo Molecular Enzyme-specific MR Imaging of Active Inflammation in a Pilot Study 1. *Radiology*, **252**, 696-703. (2009).

3 **Zulli, A., Buxton, B. F., Black, M. J., & Hare, D. L.** CD34 Class III positive cells are present in atherosclerotic plaques of the rabbit model of atherosclerosis. *Histochem Cell Biol*, **124**, 517-522. (2005).

4 **Roth, J., Goebeler, M., Wrocklage, V., Van Den Bos, C. & Sorg, C.** Expression of the calcium-binding proteins MRP8 and MRP14 in monocytes is regulated by a calcium-induced suppressor mechanism. *Biochem J* **301**, 655-660 (1994).

5 **DeWall, R.J., Jiang, J., Wilson, J.J. & Lee, K.S.** Visualizing Tendon Elasticity in an *ex vivo* Partial Tear Model. *Ultrasound Med Biol* **40,** 158-167 (2014).

6 **Brum, J., Bernal, M., Gennisson, J-L. & Tanter, M.** *In vivo* evaluation of the elastic anisotropy of the human Achilles tendon using shear wave dispersion analysis. *Physics Med Biol*; **59,** 505-523 (2014).

7 **Chernak, L. A., DeWall, R. J., Lee, K. S., & Thelen, D. G.** Length and activation dependent variations in muscle shear wave speed. *Physiol Meas* **34**, 713-717 (2013).

8 **Elliott, D.H.** Structure and function of mammalian tendon. *Biol Reviews*, **40,** 392-421 (1965).

9 **Aubry, S et al.** Biomechanical properties of the calcaneal tendon *in vivo* assessed by transient shear wave elastography. *Skeletal Radiol* **42,** 143-1150 (2013).

10 **DeWall, R.J, Slane, L.C., Lee, K.S. & Thelen, D.G.** Spatial variations in Achilles tendon shear wave speed. *J Biomech* in press (2014).

11 **Royer, D., Gennisson, J.L., Deffieux,T., & Tanter, M**. On the elasticity of transverse isotropic soft tissues (L). *J Acoust Soc Am* **129,** 2757-2760 (2011).

12 **Eby, S.F. et al.** Validation of shear wave elastography in skeletal muscle. *J Biomech* **46,** 2381-2387 (2013).

13 **Gennisson, J.L. et al.** Viscoelastic and anisotropic mechanical properties of in vivo muscle tissue assessed by supersonic shear imaging. *Ultrasound Med Biol*, **36**, 789-801 (2010).

14 **LaCroix, A.S., Duenwald-Kuehl, S.E., Lakes, R.S. & Vanderby, R.** Relationship between tendon stiffness and failure: a metaanalysis. *J Appl Physiol* **115**, 43-51. (2013).

15 **Nagasawa, K., Noguchi, M., Ikoma, K. & Kubo, T**. Static and dynamic biomechanical properties of the regenerating rabbit Achilles tendon. *Clin Biomech* **233,** 832-838 2008).

Chapter 6

Limitations and Assumptions

6.1 Limitations

There are many limitations and assumptions in this study worth mentioning. Foremost, when comparisons to physiological values are being made, it is helpful to have more accurate population data. We were only able to obtain estimates of population data for the SWI data and some biomechanical properties. It would have been more appropriate to conduct the study on a group of completely naive animal in all modalities in order to generate reference values for these parameters. In our surgical model, our control suture was coated in HAP/BSA as we wanted to demonstrate that it was the presence of growth factors and not the HAP/BSA, which resulted in any changes, however, a second control group with uncoated suture would have been a welcome addition to the study. We felt that for the number of groups we used in this study, an n=6 per group was insufficient and may result in an underpowered study. However, although significance was identified in a variety of cases, with an n=6 per group the study was underpowered when no significant differences were demonstrated.

Given the data we obtained, we would suggest that if the study was repeated, an earlier time point should be considered. We managed to double the ultimate tensile strength of the tendon in a 4-week period. While this is remarkable, perhaps a 1 or 2-week time point would have been able to evaluate the healing cycle at more obvious time points. It is unclear if the peak ultimate tensile strength for each group is attained at 4 weeks. The FGF/VEGF interaction may result in changes in the not only the peak ultimate tensile strength, but also the rate at which the ultimate tensile strength is

attained. More time points would have given us a greater understanding of the temporal situation in regard to peak ultimate tensile strength.

The surgical model we utilized to model Achilles tendon repairs is not representative of the clinical scenario. We performed sharp transections that were immediately repaired. The clinical scenario is representative of a laceration with hemorrhage and trauma surrounding the tissues. Thus, extrapolation of these highly controlled results to a clinical situation needs to be interpreted with significant caution.

List of Abbreviations

AE	Acoustoelastography
AER	Axial Ectodermal Ridges
ARFI	Acoustic Radiation Force Impulse
bFGF	Basic Fibroblast Growth Factor (FGF-2)
bHLH	Basic Helix-Loop-Helix
BrdU	Bromodeoxyuridine
BSA	Bovine Serum Albumin
CDMP	Cartilage-derived morphogenetic protein
CEU	Contrast Enhanced Uptake
DAPI	4',6-diamidino-2-phenylindole
ECM	Extracellular Matrix
EDS	Energy Dispersive X-Ray Spectroscopy Analysis
EGF	Epidermal Growth Factor
ERK	Extracellular Signal-Regulated Kinase
FACIT	Fibril Associated Collagens With Interrupted Triple Helices
FGF	Fibroblast Growth Factor
FGFR	Fibroblast Growth Factor Receptor
GAG	Glycosaminoglycan
HAP	Hydroxyapatite
HF	High FGF
HF/HV	High FGF/ High VEGF
HF/LV	High FGF/ Low VEGF
HV	High VEGF
IFN-γ	Interferon - gamma
IL-1	Interleukin-1
LF	Low FGF
LF/HV	Low FGF/ High VEGF

LF/LV	Low FGF/ Low VEGF
LOX	Lysyl Oxidase
LT	Long Term (9-Week)
LV	Low VEGF
MAGP	Microfibril-Associated Glycoproteins
MCA	Microbubble Contrast Angiography
MPV	Mean Pixel Value
NT	Normal Tendons
PAMP	Pathogen Associated Molecular Patterns
PDGF	Platelet Derived Growth Factor
PI	Pathology Index
ROI	Region of Interest
SDFT	Superficial Digital Flexor Tendon
SDUV	Shear Wave Dispersion Vibrometry
SLRP	Small Leucine-Rich Proteoglycan
Smad	Small Mother Against Decapentaplegic
SMURF	Spatially Modulated Ultrasound Radiation Force
ST	Short Term (4-Week)
TGF- β	Transforming Growth Factor Beta
SWI	Shear Wave Imaging
TIEG	TGF beta inducible early gene
TLR	Toll Like Receptor
TNF- α	Tumor Necrosis Factor Alpha
TSPC	Tendon Stem/Progenitor Cell
uPA	Urokinase Plasminogen Activator
UTS	Ultimate Tensile Strength
VEGF	Vascular Endothelial Growth Factor
ZF/ZV	Zero FGF/ Zero VEGF